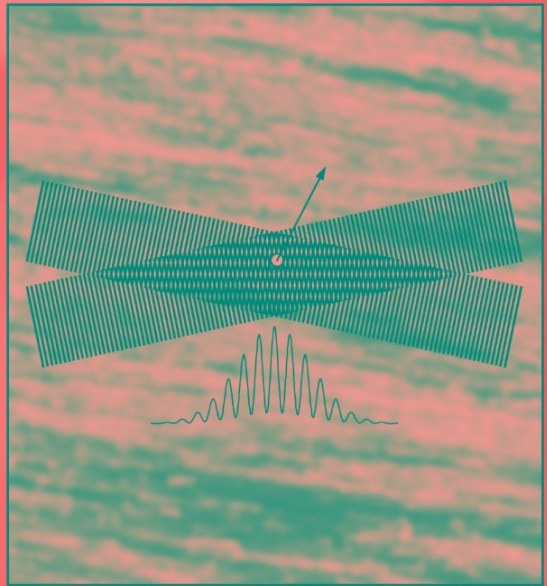


Zh. Zhang

LDA APPLICATION METHODS

Laser Doppler Anemometry
for Fluid Dynamics



 Springer

Experimental Fluid Mechanics

Series Editors

Wolfgang Merzkirch

Donald Rockwell

Cameron Tropea

For further volumes:

<http://www.springer.com/series/3837>

Zhengji Zhang

LDA Application Methods

Laser Doppler Anemometry
for Fluid Dynamics

 Springer

Zhengji Zhang
Oberhasli Hydroelectric Power Company
3862 Innertkirchen
Switzerland
zha@kwo.ch

ISBN 978-3-642-13513-2 e-ISBN 978-3-642-13514-9
DOI 10.1007/978-3-642-13514-9
Springer Heidelberg Dordrecht London New York

Library of Congress Control Number: 2010931104

© Springer-Verlag Berlin Heidelberg 2010

This work is subject to copyright. All rights are reserved, whether the whole or part of the material is concerned, specifically the rights of translation, reprinting, reuse of illustrations, recitation, broadcasting reproduction on microfilm or in any other way, and storage in data banks. Duplication of this publication or parts thereof is permitted only under the provisions of the German Copyright Law of September 9, 1965, in its current version, and permission for use must always be obtained from Springer. Violations are liable to prosecution under the German Copyright Law.

The use of general descriptive names, registered names, trademarks, etc. in this publication does not imply, even in the absence of a specific statement, that such names are exempt from the relevant protective laws and regulations and therefore free for general use.

Cover design: WMXDesign GmbH, Heidelberg

Printed on acid-free paper

Springer is part of Springer Science+Business Media (www.springer.com)

Preface

Experimental flow measurements, as the indispensable measure to investigate and improve engineering flows and flow processes, have been greatly advanced, as the laser methods have found applications in this area. Contrary to the traditional methods of using mechanical probes, the laser method obviously provides the most effective and accurate tools for non-intrusive flow measurements. Nowadays, the laser method for flow measurements has become very fashionable, mainly because of a lot of fashionable applications of laser techniques everywhere. The most widely applied laser methods for flow measurements are doubtlessly the laser Doppler anemometry (LDA), also known as the laser Doppler velocimetry (LDV), and particle image velocimetry (PIV). While the PIV method is suitable to quantitatively image the flow distribution, the LDA method is mostly applied to accurately diagnose and quantify all types of flows. The subject of treatment in the current book is the LDA method.

Since the first successful test of LDA principles, especially during the last 20 years, the LDA technique has been developed to be a high-level standard method for flow measurements. It has been acknowledged as being the most successful and widely applied measurement technique in both the scientific and engineering flow investigations. The advanced laser and computer technologies have greatly contributed to the development of advanced LDA technology. As a very effective and reliable measurement technique, the LDA method demonstrates its established significance not only in the field of mechanical engineering but also extensively in the fields of chemical and biological engineering, as well as in many other fields.

With regard to the uninterrupted developments of LDA technology up until now, it is worth noting that the majority of developments are mainly restricted to LDA principles under application of optics on one hand, and to improved soft- and hardware on the other hand. These developments lead to establishment of standard LDA instruments that have been commercial products and are easily obtainable for applications. Corresponding professional publications mostly concern the basic principle of the LDA method and the related developments named above. Only few investigations and developments have been conducted with regard to the integration of LDA optical facilities into flow mechanics. As has been perceived for a long time, it clearly lacks a supportive reference for LDA users in the practical applications.

The integration of LDA optical facilities into flow mechanics is designated as the LDA application methods. It stands for the methods to improve the optical conditions and to enhance the measurement accuracies. It also provides the guidelines for simplifying the measurements and correcting measurement errors as well as for clarifying the application limits and extending the application areas of LDA techniques. Based on corresponding developments in the last 15 years, the author of this book tries to summarize all important methods related to the aspects listed above and to make a useful reference for LDA users. As a practical reference, the book also contains all other basic knowledge of LDA technology. It is therefore suitable for all LDA users in universities, research institutes and industries. It also supports the further developments of both the hard- and software of LDA instrumentations.

The author highly esteems and thanks his lovely wife Nan for her great spiritual support and the great patient she has shown for many years. He also thanks Sulzer Markets & Technology Ltd for supporting the research works of applying LDA for flow measurements during the years 1990–2003.

Innertkirchen, Switzerland
March 2010

Dr.-Ing. Zhengji Zhang

Contents

1	Introduction	1
1.1	Flows and Flow Measurements	1
1.2	Traditional Methods of Flow Measurements	2
1.3	Laser Methods and Laser Doppler Anemometry (LDA)	2
1.3.1	Developments of LDA Fundamentals and Instrumentations	4
1.3.2	Developments of LDA Application Methods	5
1.4	Purposeful Flow Measurements and Rational Measurement Evaluations	8
1.5	Purposes of this Book	9
2	Specifications of Engineering Turbulent Flows	11
2.1	Turbulent Flow Properties	11
2.1.1	Statistical Views of Flow Turbulences	11
2.1.2	Isotropic and Anisotropic Turbulences	13
2.2	Reynolds Turbulent Stresses	15
3	LDA Principles and Laser Optics	19
3.1	Light Wave and Its Propagation	19
3.2	The Doppler Effect	22
3.3	Superposition of Two Plane Light Waves	24
3.4	LDA Principle	27
3.5	Fringe Model on the Light Interference	29
3.6	Frequency Shift Method to Resolve the Flow Direction	32
3.6.1	Fringe Shift Speed	34
3.7	Gaussian Beam Properties	35
3.7.1	Geometrical Specifications of the Gaussian Beam	35
3.7.2	Transmission Performance of the Gaussian Beam	38
3.8	Measurement Volume Size	39
4	LDA Systems	41
4.1	Hardware and Optical Components	41
4.2	Specification of LDA Measurement Volumes	44

5	Basic Data Processing Methods in LDA Measurements	47
5.1	Direct Data Processing for Mean Velocities and Velocity Fluctuations	47
5.2	Weighting Facilities of Mean Velocity and Fluctuations	51
6	Linear Transformation of Velocities and Turbulent Stresses	53
6.1	Orthogonal Linear Transformation	53
6.1.1	Velocity Transformation	53
6.1.2	Turbulent Stress Transformation	55
6.1.3	Directional Distribution of Turbulent Stresses	55
6.2	Non-orthogonal Transformation	61
6.2.1	Velocity Transformation	62
6.2.2	Turbulent Stress Transformation	63
6.3	Graphical Presentation of Turbulent Stresses	65
6.3.1	Ellipse Form of the Turbulence Distribution	65
6.3.2	Expressions of Turbulent Stresses in Mohr's Stress Circle	66
7	Tracer Particles and Particle Motion Equations	69
7.1	Effective Forces Exerted on the Particle in the Flow	70
7.1.1	Viscous Drag Force	70
7.1.2	Gravitational and Lift Forces	71
7.1.3	Pressure Force	72
7.1.4	Force from Added Mass	73
7.2	Particle Motion Equation	74
7.3	Particle Motion in the Straight Flow of Constant Velocity	75
7.4	Particle Motion in Nozzle and Diffuser Flows	76
7.4.1	Nozzle Flow	78
7.4.2	Diffuser Flow	80
7.5	Particle Motion in the Oscillation Flow	82
7.5.1	Particle Flows of Small Stokes Numbers	86
7.5.2	Particle Flows of Large Stokes Numbers	88
8	Zero Correlation Method (ZCM)	89
8.1	Shear Stress Measurements with Non-coincident LDA	89
8.2	Basics of ZCM	90
8.3	Extension of ZCM	93
8.3.1	Non-orthogonal Velocity Components	93
8.3.2	Three-Dimensional Flow Turbulence	93
8.4	Restriction and Validation of ZCM	94
9	Dual Measurement Method (DMM)	97
9.1	Possibility of Resolving the Secondary Flow	97
9.2	DMM in Basic Form	99
9.3	DMM with Coordinate Transformation	103

- 9.4 Extension of DMM 105
 - 9.4.1 Direct Component Measurements 106
 - 9.4.2 Method of Using Coordinate Transformation 109
- 10 Symmetrical Method of 3D-Velocity Measurements 113**
- 11 Non-stationary Turbulent Flows 117**
 - 11.1 Non-stationary Turbulent Flows in the Practice 117
 - 11.2 Time-Resolved Non-stationary Turbulent Flows 119
 - 11.2.1 Method of Linear Least Squares Fitting 119
 - 11.2.2 Linear Trend of the Velocity and the
Calculation Method 121
 - 11.2.3 Time-Dependent Flow Turbulences 123
 - 11.3 Phase-Resolved Non-stationary Turbulent Flows 126
 - 11.3.1 Method of Linear Least Squares Fitting 127
 - 11.3.2 Linear Trend of the Velocity and the
Calculation Method 128
 - 11.3.3 Phase-Dependent Flow Turbulences 130
- 12 Turbulent Flow with Spatial Velocity Gradient 133**
 - 12.1 Apparent Turbulence Intensity and Related Quantities 135
 - 12.2 Combined Velocity Bias Effect 140
 - 12.2.1 Mean Velocity 141
 - 12.2.2 Turbulent Normal Stress 142
 - 12.3 Method of Resolving the Non-uniform Velocity Distribution 145
- 13 Flow Measurements Behind the Plane Window: On-axis 147**
 - 13.1 Fringe Spacing 147
 - 13.2 Shift of the Measurement Volume 148
 - 13.3 Optical Dispersion and its Negligible Effect 149
- 14 Flow Measurements Behind the Plane Window: Off-axis 151**
 - 14.1 Off-axis Measurements and Velocity Transformation 152
 - 14.2 Fringe Spacing in Measurement Volume
and Velocity Corrections 153
 - 14.3 Refraction of Optical Axis and Orientation
of the Measurement Volume 155
 - 14.4 Two-Dimensional Shift of the Measurement Volume 156
 - 14.5 Astigmatism and its Presence in Transmitting Optics 159
 - 14.6 Astigmatism at the Focused Laser Beam Bundle 163
 - 14.6.1 One-time Refraction of a Focused Beam Bundle 163
 - 14.6.2 Multiple Refraction of a Focused Beam Bundle 169
 - 14.7 Measurement Volume and Its Distortion 170
 - 14.7.1 Single Refraction of Laser Beams 172
 - 14.7.2 Multiple Refractions of Laser Beams 173
 - 14.7.3 Astigmatism at the On-axis LDA Alignment 174

14.8	Signal Qualities and the Lens Dependence	175
14.8.1	Deterioration of Signal Qualities and Strengths	175
14.8.2	Lens Dependence of Signal Qualities and Strengths	176
14.9	Error Sensitivities in Forming the Measurement Volume	179
14.9.1	Beam Separation in the Test Medium	179
14.9.2	Beam Separation After Multiple Refractions	185
14.9.3	Possible Impact on PDA Measurements	185
14.10	Method for Compensation of Astigmatism	186
15	Flow Measurements in Circular Pipes	191
15.1	Measurements of Axial Velocities	193
15.2	Measurements of Tangential Velocities	197
15.2.1	Basic Geometrical Relationships	197
15.2.2	Simplifications of Calculations	198
15.2.3	Fringe Spacing and Velocity Corrections	199
15.3	Measurements of Radial Velocities	200
15.3.1	Accurate Positioning of the Measurement Volume	200
15.3.2	Laser Beam Intersection Angle	205
15.3.3	Fringe Spacing and Velocity Corrections	206
15.3.4	Orientation of the Measurement Volume	207
15.3.5	Determination of Radial Velocities	208
15.3.6	Remarks on the Method	208
15.4	Optical Aberrations and Measurement Volume Distortion	209
15.4.1	Optical Aberrations in Transmitting and Receiving Optics	210
15.4.2	Dislocation of Laser Beam Waists from the Measurement Volume	211
16	Fringe Distortion Effects	219
16.1	Linear Longitudinal Distribution of the Fringe Spacing	220
16.2	Fringe Distortion Number and the Apparent Mean Velocity	221
16.3	Overestimation of the Flow Turbulence	224
17	Velocity Bias Effects	227
17.1	Velocity Bias as a Flow Phenomenon	227
17.2	Velocity Bias and the Momentum Flow Rate	229
17.3	Velocity Bias in One-Dimensional Flow Fluctuations	231
17.4	Velocity Bias in Two- and Three-Dimensional Flow Fluctuations	235
17.4.1	Velocity Bias in Mean Velocities	236
17.4.2	Velocity Bias in Turbulent Normal Stresses	238
17.4.3	Velocity Bias in Turbulent Shear Stresses	241
18	LDA Application Examples	243
18.1	High Speed Water Jet Flow in a Pelton Turbine	243
18.2	Measurements of Warp Yarn Speed in a Weaving Machine	247
18.3	Verification of the Shift Frequency in the Laser Beam	249

- Appendix A Off-axis LDA Alignment and Measurement**
- Volume Displacement** 253
- A.1 Laser Beams in the Meridian Plane 254
- A.2 Laser Beams in the Sagittal Plane 255
- A.3 Combination 257
- Appendix B Laser Beam Orientation Under the Effect
of the Bias Angle δ** 259
- Appendix C Coordinate Transformation of the Reynolds
Stress Matrix** 263
- References** 267
- Index** 271

Symbols

Symbol	Unit	Description
a	m	Half length of the measurement volume
a	m/s^2	Acceleration (velocity gradient in the time domain)
a	m/s	Velocity gradient in the phase angle domain
a	$1/\text{s}$	Velocity gradient in the nozzle and diffuser flows
A	m^2	Area
A_f	m/s	Amplitude of the oscillation carrying flow
c	m/s	Light speed
c_D	–	Drag coefficient in viscous flow
d_{mv}	m	Measurement volume thickness
d	m	Window thickness
d_p	m	Particle diameter
E	–	Wave amplitude
f	m	Lens focal length
f_w	–	weighting factor
F	m^4/s^4	Flatness (velocity)
F	N	Forces
I	–	Light intensity
\dot{J}	N/m^2	Momentum flux
k	m^2/s^2	Turbulent kinetic energy
k	$1/\text{m}$	Angular wavenumber of light
k_m	$1/\text{m}$	Modulation wavenumber
k_{mv}	–	Measurement volume shift ratio
k_{vel}	–	Velocity correction factor concerning the fringe spacing
\vec{l}	–	Directional unit vector
m_p	kg	Particle mass
n	–	Refractive index
N	–	Sample size
N	–	Fringe number in measurement volume
N_S	–	Stokes number
p	Pa	Pressure
p	$1/(\text{m/s})$	Probability density function of velocity
\dot{Q}	m^3/s	Volumetric flow rate
r	–	Radial coordinate
\vec{r}	–	Unit vector
R	m	Circular pipe radius
R	m	Curvature radius of the wave front

Symbol	Unit	Description
R	–	Transformation matrix
R	–	Correlation coefficient
Re	–	Reynolds number
rms	m/s	Root mean square (velocity)
s	m	Distance
s_{tt}	s ²	Statistical quantities
s_{ut}	m	Statistical quantities
s_{uu}	m ² /s ²	Statistical quantities
s_{uv}	m ² /s ²	Statistical quantities
$s_{u\varphi}$	m/s	Statistical quantities
$s_{\varphi\varphi}$	–	Statistical quantities
S	m ³ /s ³	Skewness (velocity)
t	s	Time
tbd	s	Time between data
T	s	Period
Tu	–	Turbulence intensity
u	m/s	Velocity component
\bar{u}	m/s	Mean velocity
\hat{u}	m/s	Regression velocity
u'	m/s	Fluctuation velocity
\bar{u}_{app}	m/s	Apparent mean velocity
\bar{u}_{bias}	m/s	Biased mean velocity
\bar{u}_E	m/s	Mean velocity in energy flux
\bar{u}_J	m/s	Mean velocity in momentum flux
u_p	m/s	Particle velocity
u_{sh}	m/s	Shift speed of fringes in measurement volume
v	m/s	Velocity component
v_{sh}	m/s	Velocity shift arising from LDA alignment error
w	m/s	Velocity component
w	m	Half thickness of a Gaussian beam
w_0	m	Half thickness of the beam at the beam waist
x	–	Coordinate
y	–	Coordinate
z	–	Coordinate
z_R	m	Rayleigh length
α	deg	Half intersection angle between laser beams
α	deg	Angle between coordinates
α	–	Energy flux correction factor
β	deg	Angle between coordinates
β	–	Momentum flux correction factor
γ	deg	Angle between coordinates
γ	–	Fringe distortion number
δ	deg	Bias angle in LDA alignment
ε	deg	Incident and refraction angle
θ	deg	Divergence angle of the Gaussian beam
λ	m	Wavelength
μ	Pas	Dynamical viscosity
ν	Hz	Light wave frequency

Symbol	Unit	Description
ν	m^2/s	Kinematic viscosity
ν_D	Hz	Doppler frequency
ν_{sh}	Hz	Shift frequency
ξ	–	Coordinate
ρ	kg/m^3	Density
σ	m/s	Standard deviation of velocity
σ_{mn}	m^2/s^2	Reynolds stress components
σ_{11}	m^2/s^2	Normal stress in the main flow direction
σ_{22}	m^2/s^2	Normal stress perpendicular to the main flow
τ	deg	Bias angle (error parameter in DMM)
τ	s	Relaxation time
τ_{max}	m^2/s^2	Maximum shear stress
τ_{mn}	m^2/s^2	Shear stress component
φ	deg	Directional angle
$\bar{\varphi}$	deg	Mean flow angle
φ_{LDA}	deg	Off-axis angle of LDA head
φ_{m}	deg	Directional angle of the principal normal stress
ψ	deg	Bias angle in LDA alignment
ω	$1/\text{s}$	Angular frequency
$\bar{\omega}$	$1/\text{s}$	Mean angular frequency
ω_{m}	$1/\text{s}$	Modulation angular frequency
Δx	m	Fringe spacing
$\Delta x_{\text{m,s}}$	m	Astigmatic difference

Subscript

11	Normal stress in the main flow direction
22	Normal stress perpendicular to the main flow direction
a	Air
app	Apparent velocity and turbulence intensity
b	Biased velocity and turbulence intensity
D	Doppler frequency; drag force
E	Energy flux
f	Flow
g	Glass
J	Momentum flux
m	Meridian focal point; Modulation wavenumber
max	Maximum shear stress
mn	Reynolds stress component
m,s	Distance between meridian and sagittal focal points (astigmatic difference)
mv	Measurement volume
p	Particle
s	Sagittal focal point
sh	Shift frequency, velocity shift
tt	Variance of time series
ut	Covariance between velocity and time
uu	Variance of velocity component u
uv	Covariance between velocity components u and v
u φ	Covariance between velocity component u and phase angle φ
vel	Velocity correction factor
w	Water; Weighting factor

Chapter 1

Introduction

1.1 Flows and Flow Measurements

In industrial applications as well as in scientific research, fluid flows are often utilized to serve diverse functions. The associated physical processes such as those in thermal and fluid engineering, as well as in chemical and biological process controls, constantly require accurate quantifications and optimizations, especially as concerns flow dynamics. The complex flows encountered in diverse industrial applications usually comprise various varieties of turbulent flows, three-dimensional and non-stationary flows, flows with separation and relative eddies, multiphase flows and so forth. To some extent it even deals with non-Newtonian fluid flows. Depending on the application areas and process specifications, most flows are further specified by flow rate, Reynolds number, velocity distribution, turbulence intensity and other relevant flow dynamical parameters. For the flows in heat exchangers, for instance, both the Reynolds number and the related flow state are crucial for the thermal efficiency of the apparatus. In treating flows in aerodynamics the most relevant flow dynamical parameters are directly related to the turbulent boundary layers. Obviously each engineering flow has individual specifications with corresponding flow dynamical parameters. Amongst all of these flows, the flow turbulence acts as the most important and complex phenomenon.

Because of the complexities of most industrial and natural flows, theoretical flow analysis that relies on fluid mechanics mostly appears to be inefficient and unable to quantify the respective flows. This is the case even if simplifications are used. Although nowadays the method of computational fluid dynamics (CFD) has been found to be of wide application in evaluating complex flows and improving the flow processes, its general reliability and applicability still need to be enhanced, especially through experimental validations. Moreover, the CFD method is unable to provide the online analysis of the flow process of interest. For these reasons, experimental flow measurements have often been taken into account, aiming to investigate the flows and thus to optimise the related flow processes.

1.2 Traditional Methods of Flow Measurements

Traditional flow measurements in the field of flow dynamics basically include the measurements of velocity and pressure distributions in the flow. The most familiar methods for local flow measurements are using the Pitot tubes to measure total pressure and the Prandtl tubes to gauge dynamical pressure. Because such pressure probes all require insertion into the flow, the flow is disturbed. Both the Pitot and Prandtl tubes are usually restricted to stable or quasi stable flow measurements. They are generally not used for measuring flow turbulence or any high frequency flow fluctuations, mainly because of the delay of pressure signals in the pressure probes. This can happen due to the compressibility of the gaseous flow or other causes. Also, the associated velocity fluctuations cannot be calculated from the measured pressure fluctuations in a straightforward way. In addition, it should be kept in mind that the pressure probes are not applicable to the boundary layers nor to flows with streamline curvatures.

A much more appropriate method for turbulent flow measurements are the hot wire anemometers (HWA). This method makes use of the relationship between the heat transfer on the thin hot wire surface and the flow velocity. The hot wire is only a few micrometers in diameter and is usually made of platinum or tungsten. Such a thin hot wire ensures the rapid response of the hot wire temperature and hence of the electrical signals to the fluctuations in the local flow velocity. Thus the method can be well applied to measurements of most turbulent flows, including those in the turbulent boundary layers. The downside of the method is that the hot wire has to be calibrated prior to each application. The thin hot wire also demands that the flow does not contain any hard particles, which could damage the wire. Because of the considerable flow resistance exerted on the hot wire the method is not applicable to water flows of high velocity. In practice, the hot wire anemometer has found wide application in air flow measurement.

There are many other methods that are used in the practical flow measurements. Most of them require that the flow has to be arranged so that it is mechanically accessible for probe insertion. Another well-known method without flow disturbance is using ultrasonic waves. It has found wide application in pipe flows, where neither mechanical nor optical access to the flow is possible.

1.3 Laser Methods and Laser Doppler Anemometry (LDA)

Modern measurement techniques for flow investigations are doubtless marked by use of laser techniques. The laser method obviously provides the far and wide perspective of measuring flows both more accurately and informatively. On one side, traditional measurement methods (Sect. 1.2) will be replaced where high measurement accuracies are demanded and special flow parameters should be quantified. On the other side, the significant progress of making the laser method to be standard and hence to be easily handled has largely extended the application area of flow measurements. The well-known laser methods being extended in the

practical applications are Particle Image Velocimetry (PIV) for flow field measurements and the Laser Doppler Anemometry (LDA), also known as Laser Doppler Velocimetry (LDV), for measurements of local flow velocities. In principle, both methods complement each other.

The Particle Image Velocimetry (PIV) is a method of using a laser light sheet to illuminate particles that are seeded and suspended in the flow. Based on measurements of particle displacements in the image of the visualized flow, the flow distribution in the illuminated flow area can be quantitatively evaluated. This can be conducted by means of efficient evaluation software and high-speed computers, which have all reached a very high standard. The PIV method helps to identify the flow pattern which could comprise flow separation and relative eddies. In comparison with conventional methods of flow visualization for instance using smokes, the PIV method additionally provides quantitative flow information. Also to be mentioned is that this advanced property of PIV measurements has often been insufficiently put to use. As known, the flow measurement merely provides data for further analyses and hence behaves as the prerequisite of flow investigation. In many application examples, quantitative velocities measured by the PIV method are barely exploited to show the flow pattern. For the most part, no further intensive and extensive analyses have been or could be completed. Hence, the flow pattern that is outlined through PIV measurements does not provide any more useful flow information than that provided through the simple flow visualization, for instance by using smoke or color. This comparison implies that the flow investigation is not simply restricted to the stage of flow measurements. More about this aspect will be explained in Sect. 1.4.

The Laser Doppler Anemometry (LDA), of which the functionality and application methods constitute the subject of this book, is probably the most effective and widest applied non-intrusive method in experimental investigations of flows and flow dynamics. It represents an optical, state of the art method commonly with high measurement accuracy. Since the first application of the LDA method by Yeh and Cummins (1964), the method has been continuously developed and extended, so that it nowadays becomes a standard instrument for flow measurements in both industrial applications and model flow investigations. The fundamental development in LDA technology includes the progressive hard- and software developments, which are achieved mainly based on the progressive developments of laser and computer technologies. In general, the LDA technology can be categorized into two areas:

LDA fundamentals

LDA applications

In the aspect of LDA applications, significant achievements have been made since the nineties of the last century, as the LDA method had then found its wide application. In accordance with more and more LDA applications at that time and for the purpose of exchanging the application experiences, many local and global associations have been grounded like EALA (European Association for Laser Anemometry, no longer active) and GALA (German Association for Laser Anemometry).

1.3.1 Developments of LDA Fundamentals and Instrumentations

Since the first LDA measurement was successfully tested by Yeh and Cummins (1964), the method is undergoing continuous development. These developments are mainly restricted to the enhancement of opto-electronic performance of LDA system and the hard- and software improvements. Such developments have enabled the LDA nowadays to be a mature and important measurement instrument which is also commercially available. Within the framework of this book, it is not the purpose to make a historic review of LDA developments. For informative LDA developments, the readers are referred to the earlier work of Durst et al. (1981) as well as to the recent work of Albrecht et al. (2003).

Developments on LDA fundamentals also include investigations of diverse optical and flow-specific aspects that are tightly related to LDA applications and could considerably influence the measurement accuracies. Corresponding influencing factors are known, for instance, as the effect of fringe distortion in LDA measurement volumes, the velocity and angular bias effects, the effect of the time and spatial velocity gradients and so on. Because of their importance in LDA measurements, correspondingly extended investigations have been carried out at an earlier time. They are mentioned here, as follows:

- (A) *Velocity bias effect*: The velocity bias arises from the effect that the velocity sampling rate in LDA measurements is not time-equidistant but depends on the velocity itself. In concrete terms, high velocities are proportionally more frequently sampled than low velocities. This effect generally exists both in non-stationary flow and turbulent flow with velocity fluctuations. Because of its dependence on flow velocity, the velocity bias effect is indeed a flow phenomenon. It was firstly recognized by McLaughlin and Tiederman (1973) and later had been broadly investigated by a great number of researchers (for instance Buchhave 1975, Erdmann and Tropea 1981). Corresponding investigations are mainly restricted to the correction of the related measurement error. Based on numerical calculations the velocity bias errors were extensively characterized by Nobach (1998) for three-dimensional flow turbulence. Fully analytical specifications of velocity bias and their dependence on the turbulence intensity have been completely accomplished by Zhang (2000, 2002), for three-dimensional flow turbulence and the turbulence intensity covering the range from zero to infinity. It should be here remarked that the velocity bias does not always represent the measurement error. This viewpoint is completely described in Chap. 17 of this book.
- (B) *Fringe distortion*: As an optical phenomenon, the fringe distortion in the LDA measurement volume is mainly caused by improper optical layout or by irregular i.e. asymmetrical laser beam refractions on the medium interface. The fringe distortion in the measurement volume due to improper optical layout was carefully dimensioned by Hanson (1973, 1975). By use of a magnified image the distorted fringe pattern in the measurement volume was visualized for instance

by Miles and Witze (1994, 1996). The fringe distortion in the LDA measurement volume as a result of laser beam refractions was confirmed to be the effect of astigmatism by Zhang (1995) and Zhang and Eisele (1995a, b). It represents a particularly crucial phenomenon when the laser beam refraction takes place on the inclined plane surface or the surface of a circular pipe (Zhang 2004a, 2004b). The outcome of all types of fringe distortion in the LDA measurement volume is the deterioration of the measurement accuracy. Measurement errors, for instance, are mainly interpreted in the overestimation of all relevant turbulence quantities. For this reason the associated effect is also called the broadening effect in turbulence measurements (Hanson 1973). Quantitative evaluations of the fringe distortion effect on the flow measurement accuracy were performed by Zhang and Eisele (1997, 1998c) for the case of linear fringe distortion in the measurement volume. For other types of fringe distortion in the measurement volume, the respective effect cannot yet be well-estimated.

- (C) *Spatial velocity gradient effect*: For flows with spatial velocity gradient, such as the flows in the turbulent boundary layers, LDA measurements suffer from measurement errors in both mean and fluctuation velocities. The reason for these errors is the non-uniform velocity distribution within the length of the LDA measurement volume. Because the standard LDA optics is unable to resolve the velocity distribution within the measurement volume, both the mean velocity and especially turbulence quantities suffer from measurement errors. Corresponding investigations have been carried out by Durst et al. (1996, 1998). As a matter of fact, the existence of the spatial velocity gradient within the LDA measurement volume also leads to ambiguity in representing the measurement result because of the effect of the involved velocity bias.
- (D) *Non-stationary flow measurements*: In the enforced non-stationary turbulent flows, flow fluctuations comprise both the enforced velocity variation because of the flow periodicity, for instance, and the stochastic velocity fluctuations because of the flow turbulence. To evaluate such flows based on LDA measurements, the appropriate data processing has to be worked out. Usually it refers to the method of resolving the stochastic from composite fluctuations. Corresponding investigations on the evaluation method have been carried out by Zhang et al. (1996, 1997) as well as by Jakoby et al. (1996).

1.3.2 Developments of LDA Application Methods

As a result of fundamental developments and the developments of hard- and software, the LDA method has been established to be a very efficient optical technique for flow measurements, especially for investigations of complex turbulent flows. Correspondingly the LDA instrument has become a mature commercial product and found the widest applications. Because of this, the LDA technique has been commonly considered as an available tool, although complicated, for direct application in the flow measurements.

In reality and as experienced from applications, the knowledge of LDA fundamentals and the instrument functionalities does not ensure any fully-correct measurement of flows that are practically of countless varieties with respect to the flow itself, the flow arrangement and the related optical specifications. This viewpoint is objective and true, as it has been well-known for instance that the particle size, the velocity bias and the fringe distortions could largely influence the measurement accuracies. Although there have been countless LDA applications in almost all possible flows, only few attempts have been made to improve the optical conditions and enhance the measurement accuracies, to simplify the measurements and correct measurement errors as well as to clarify the application limits and extend the application areas of LDA techniques. Aside from the concerned velocity bias and fringe distortion, practical applications of LDA method in effect suffer from much more undesirable, partly unknown optical phenomena. The most significant disturbing factor in LDA applications is related with refractions of laser beams for internal flow measurements. In facing this situation and to suppress the occurrence of any optical aberration, the refractive index matching method has been occasionally applied. This method, however, acts only as a passive method and is actually not always applicable. The problem arising from the laser beam refractions will be enlarged, if the beam refractions take place on a curved surface like that of a circular pipe. Obviously the LDA technique with respect to its applications and application optimizations still needs to be developed.

- (A) *Optical aberration and astigmatism*: In LDA applications, the optical aberrations generally exist in each measurement of internal flows, where the laser beams must transmit through at least one optical window and hence undergo refractions. The most remarkable optical aberration was confirmed to be astigmatism which in worst cases would lead to total interruption of measurements (Zhang 1995, Zhang and Eisele 1995a, b). The phenomenon and the associated disturbances on both the signal quality and the signal rate become crucial, if the LDA optical axis is aligned off-axis i.e. not coincident with the normal of the optical window. Some LDA users might have experienced that at the mentioned optical configuration either no signal or very bad signals will be received. The reason for signal disappearance is the non-intersection of laser beams after refractions on the air-glass and glass-flow interfaces. The reason for bad signals is mostly the bad intersection between laser beams and the deterioration of receiving aperture of the receiving optics. Another issue of astigmatism is the fringe distortion in the measurement volume that could lead to measurement errors (Zhang and Eisele 1996b). Detailed descriptions of influences of astigmatism on LDA measurements and the guideline for correct measurements with correction method can be found in the mentioned references. To minimize the effect of astigmatism the method of configuring the receiving optics is described in Zhang and Eisele (1996a, 1998b).
- (B) *Three-component flow measurements in circular pipes*: Another most common case of LDA measurements is referred to flow measurements in circular pipes. In this case, the optical aberration associated with the laser beam refractions is

much more complex and serious than that at a plane surface. In reality, measurements could not run without any aid, either of matching the refractive index of the flow, or by the exact calculation of the laser beam intersection in the flow. Because the refractive index matching method is not available each time, direct measurements of pipe flows must often be carried out. Accordingly great difficulties in obtaining signals of high quality in such measurements would have been encountered by lots of LDA users. Some users tried a great deal to track the laser beams in both the pipe wall and the flow (Boadway and Karahan 1981). As a matter of fact, the optical aberrations in the receiving optics and the corresponding most serious influence on both the signal strength and quality have often been overlooked. As shown by Zhang (2004a, b) the optical performance of direct flow measurement can be greatly enhanced by making the outside surface of the circular pipe to be plane (Fig. 1.1). This contributes not only to the reduction of optical aberrations in both the transmitting and receiving optics, but also to the simplification of calculating the laser beam intersection in the flow for measurements of all three velocity components.

- (C) *Dual Measurement Method (DMM)*: As is known, LDA measurements are measurements of velocity components. Because of this property, there are sometimes difficulties in accurately resolving a component, say that one in the secondary flow, which is much smaller against the other components. Usually the direct measurement of such a small velocity component requires exact optical alignment, which is, however, often impossible or very complicated and time-consuming. A method which enables the lowest secondary flow to be exactly measured has been developed by Zhang (2005) and is denoted as the Dual Measurement Method (DMM). The method has been successfully applied to resolve the secondary flow structure in a high speed jet flow, see also Zhang and Parkinson (2001, 2002).
- (D) *Zero Correlation Method (ZCM)*: In measuring the turbulent flows, it is often required to measure both the mean velocity and the turbulence quantities such as the turbulence intensity and turbulent stresses in the Reynolds stress matrix. For measurements of turbulent shear stresses, usually two-component LDA system should be applied to enable the fluctuations in two velocity components

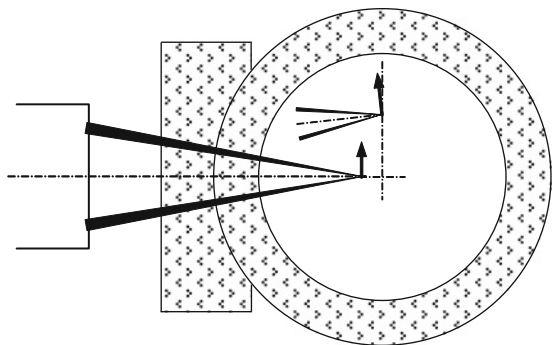


Fig. 1.1 Effective method for measurements of all three velocity components of the flow in a circular pipe (Zhang 2004a)

to be measured simultaneously. The corresponding technique is known as the two-component coincident measurement technique. Although most LDA systems are designed and equipped for doing such measurements, turbulence measurements can be simplified by accounting for the common randomness of velocity fluctuations. For stationary flows, this fluctuation randomness indicates that velocity fluctuations occur symmetrically around the mean flow direction. Based on such an assumption a special method that is called the Zero Correlation Method (ZCM) has been developed by Zhang (1999). The method enables the complete turbulence quantities to be simply measured without requiring the two-component coincident measurement technique.

As outlined above, LDA application methods represent an important category of LDA techniques and play a crucial role in correctly and efficiently carrying out the flow measurements. They form the main subject of this technical book.

1.4 Purposeful Flow Measurements and Rational Measurement Evaluations

Each flow encountered in the engineering applications is arranged to execute the given functions and thus specified by corresponding relevant parameters. It appears to be always important to LDA users to be aware of such parameters prior to starting each measurement. Although the LDA technique nowadays is greatly progressed and the LDA system becomes highly efficient and most convenient for use, it only serves as a useful application tool for flow measurements. In reality, flow investigations will just begin after the measurements have been carried out. For this reason, preliminary studies to specify and clarify the most relevant flow parameters should be made. Such preliminary studies also include how the interested flow quantities can be measured either directly or indirectly, and how accurate the measurement should be. They therefore provide the prerequisite for choosing the available measurement technique and the appropriate measurement method.

On the other hand, it is often a hard task for engineers and researchers to properly evaluate the measurement data. As indicated in Sect. 1.3 referring to the PIV method, the simple graphical mapping of the flow field directly from the PIV measurements, even quantitative, is often no more informative than the qualitative flow visualization. With the graphical mapping of the interested flow field, investigations should indeed just begin rather than just be finished. On one side, more deep studies and evaluations of measurement data require the knowledge of both the flow mechanics and the associated physical (thermal or chemical) processes. On the other side, the poor time-resolution of the achieved measurement data is obviously the significant shortage of the PIV method that prevents the user from further studying the flow. Against this shortage, the LDA method provides highly time-resolved measurements. It is therefore highly suitable for diagnosing the flow for instance by detecting the flow instability, turbulence intensity and exact flow profiles in the

region of boundary layers and so on. For this reason, the LDA method is sometimes considered to be comparable with the method of blood test in a clinical laboratory, while the PIV method is comparable with the x-ray method. That is why the LDA method as a diagnostic tool, which provides a lot of useful flow information, is widely applied in practice.

1.5 Purposes of this Book

Since the first LDA application and for a long time thereafter, developments in LDA technology are mainly restricted to LDA fundamentals and instrumentations, as stated in Sect. 1.3. Great advancements in this category of LDA technology enabled the LDA method to become the most favorite technique for flow measurements. The LDA method has thus found its widest applications in experimental flow investigations. As also stated in Sect. 1.3, unique intimate knowledge of LDA fundamentals and instrumentations does not fully ensure correct flow measurements. For LDA users in practical applications, the application methods appear to be as much important and helpful as LDA fundamentals.

The current book therefore tries to completely summarize knowledge that is available in the aspect of LDA application methods. For completeness, the basic fundamentals of LDA measurement techniques and many other relevant aspects like the particle dynamics and velocity transformation algorithm will also be shown. To certain optical aspects, like those in specifying the LDA measurement volume in the circular pipe flows, the mathematical calculations seem to be rather complex. They are nevertheless all crucial for clarifying the background of each optical aspect and for estimating the extent of corresponding influences in measurements. Moreover, they also serve as the basis for further investigations of related optical aspects.

Finally some special applications of LDA methods will be presented. It will also show that the LDA method is just as suitably applicable for solid mechanics as for flow mechanics.

This book with its main subject thus serves as an extended reference for guidance on the LDA applications to users who are attempting to optimize the optical conditions and to gain the maximum results from measurements. Because it is the first book dealing with LDA application methods, it would contribute to the further build-up of LDA technology. Although the book has its weight in the application methods which mainly addresses LDA users, it can also be referred to by developers and manufactures of LDA systems.

Chapter 2

Specifications of Engineering Turbulent Flows

Most flows encountered in the practical applications are turbulent viscous flows. Because of the randomness of flow fluctuations, the flow turbulence probably belongs to the most complex phenomenon in our natural world. It is almost only the flow turbulence that decisively influences the physical (e.g. thermal or chemical) processes in respective fluid flows. On one side, basic research works have been continuously and highly concentrated on the general properties of flow turbulence (Bradshaw 1978, Hinze 1975, Lumley et al. 1996). Efforts have also been made to establish the appropriate turbulence models, especially in the computational fluid dynamics (CFD). On the other side, countless experimental investigations of turbulent flows and their influences on respective flow processes in engineering applications have been carried out. Here the most often used parameter for quantitative characterization of the flow turbulence is simply the turbulence intensity as the outcome directly from statistical evaluation of flow fluctuations. It also represents the most easily obtainable turbulence quantity in experimental flow measurements.

In the aspect of flow dynamics, the significant features of flow turbulence are the time-dependent velocity fluctuations and their statistics regarding the time and spatial extent of fluctuations. With respect to these features of flow turbulence, the most appropriate measurement method is obviously the LDA method that enables the velocity fluctuations in a turbulent flow to be highly resolved and has already been widely applied in experimental flow investigations. For this reason only turbulence quantities will be considered here that are tightly and directly related with LDA measurements in engineering flows.

2.1 Turbulent Flow Properties

2.1.1 Statistical Views of Flow Turbulences

Turbulent flows are known as the flows with irregular fluctuations of fluid particles in motion. To describe the turbulent flow with velocity fluctuations, the flow velocity is usually split into a time-averaged mean and a fluctuation velocity. In regarding

the velocity component u for instance, the flow velocity with fluctuations is then expressed as

$$u(t) = \bar{u} + u'(t) \quad (2.1)$$

In accordance with this treatment of a turbulent flow, there is $\overline{u'(t)} = 0$ which means that the time-average of velocity fluctuations vanishes. In order to statistically quantify the extent of flow fluctuations, the standard deviation of the mean velocity of a stationary turbulent flow has always been applied, as it is calculated for the given velocity component by

$$\sigma_u = \sqrt{\frac{1}{T} \int_0^T u'^2 dt} \quad (2.2)$$

Velocity fluctuations around the mean velocity are of different magnitudes and take place to different magnitudes by different probabilities. While velocity events in velocity classes close to the mean velocity happen at high probabilities, velocity events far from the mean appear rather few. Mostly the probability distribution of fluctuation velocities is of a symmetrical bell form as shown in Fig. 2.1 for example from measurements of a stationary turbulent flow. In most cases dealing with stationary turbulent flows, flow fluctuations are stochastic and can be approximated by the Gaussian probability density function as given by

$$\text{pdf}_u = \frac{1}{\sqrt{2\pi} \sigma_u} e^{-\frac{(u-\bar{u})^2}{2\sigma_u^2}} \quad (2.3)$$

In this expression, σ_u in m/s is the standard deviation of the mean velocity \bar{u} and has been specified in Eq. (2.2). It represents the statistical variability of velocity and

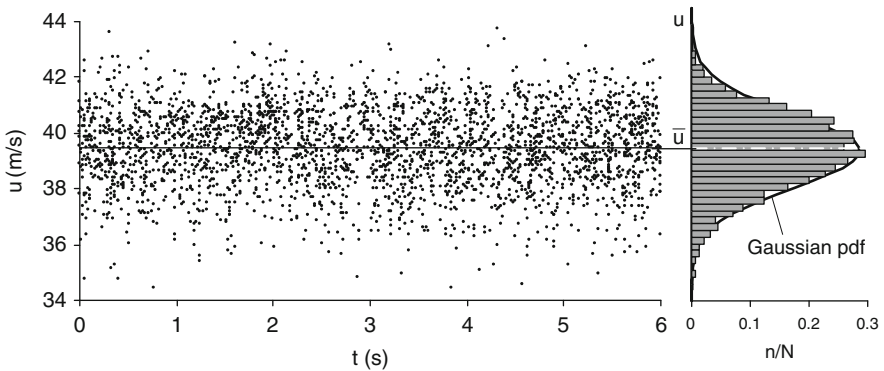
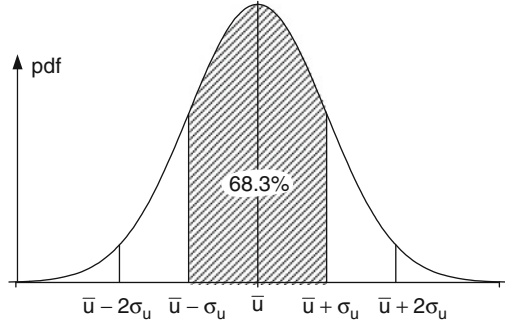


Fig. 2.1 Fluctuation velocity and its probability distribution in a high speed jet flow measured by LDA method

Fig. 2.2 Gaussian probability density function



specifies the most available range of flow fluctuations around the time-average of respective velocity components. In Fig. 2.2 the corresponding probability density function has been shown to approximate the distribution of fluctuation velocities. The probability of random velocities occurring in the range $u = \bar{u} \pm \sigma_u$ is calculated as

$$P(\sigma_u) = \int_{\bar{u}-\sigma_u}^{\bar{u}+\sigma_u} \text{pdf}_u du = \frac{2}{\sqrt{\pi}} \int_0^{1/\sqrt{2}} e^{-z^2} dz = \text{erf}\left(\frac{1}{\sqrt{2}}\right) \approx 68.3\% \quad (2.4)$$

Here the substitution of $z = \frac{u-\bar{u}}{\sqrt{2}\sigma_u}$ was applied. The term $\text{erf}(x)$ is the error function. It vanishes when $x = 0$ and approaches unity as x tends to infinity.

Furthermore, the probability of random velocities occurring in the range $u = \bar{u} \pm 2\sigma_u$ is given by

$$P(2\sigma_u) = \int_{\bar{u}-2\sigma_u}^{\bar{u}+2\sigma_u} \text{pdf}_u du = \frac{2}{\sqrt{\pi}} \int_0^{\sqrt{2}} e^{-z^2} dz = \text{erf}\left(\sqrt{2}\right) \approx 95.4\% \quad (2.5)$$

The standard deviation σ_u generally represents a statistical parameter that depicts the extent of non-uniformity in a data series as in the process fluctuations. In relating to LDA measurements of a stationary turbulent flow, the method of calculating the standard deviation σ_u will be shown in [Chap. 5](#).

2.1.2 Isotropic and Anisotropic Turbulences

Since velocity fluctuations in each turbulent flow are always three-dimensional, it distinguishes between isotropic and anisotropic turbulences, as illustrated in Fig. 2.3 in the general field coordinate system. Local isotropy of turbulence is given at large Reynolds numbers and conditions without remarkable influences of any boundaries.

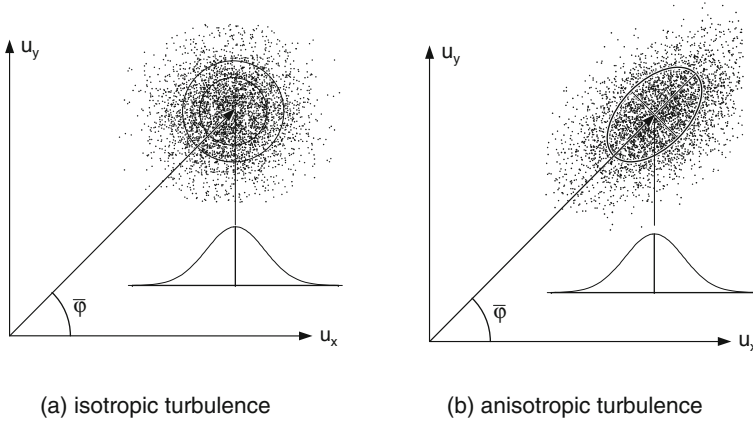


Fig. 2.3 Isotropic and anisotropic turbulences (two-dimensional), shown in the form of scatter diagrams of the fluctuation velocity measured by LDA method

In such a turbulent flow, velocity fluctuations in all spatial directions are of the same statistical level i.e. $\sigma_x = \sigma_y = \sigma_z = \sigma$ in terms of standard deviations. The standard deviation of the mean velocity can then be directly applied to calculate the turbulence intensity of the related turbulent flow:

$$Tu = \frac{\sigma}{\bar{u}} \quad (2.6)$$

with \bar{u} as the mean velocity in the main flow direction.

As a matter of fact, turbulence encountered in most practical flows is anisotropic, mainly because of reactions of existing boundaries on flow fluctuations. The turbulent flow with anisotropic turbulence as shown in Fig. 2.3b represents the most common case. It is characterised by two distinct aspects: the first aspect is that velocity fluctuations are confined to more or less symmetrical distribution on both sides of the mean velocity vector. This property of the flow turbulence simply arises from the randomness of velocity fluctuations. It can be made of use in order to simplify both the specification of the flow turbulence and the measurement of corresponding turbulence quantities, see Chap. 8. The second aspect is that the velocity fluctuation along the mean velocity vector is of maximum magnitude while it is of minimum magnitude perpendicular to the mean velocity vector. The turbulence with minimum fluctuation magnitude along the mean velocity vector is practically uncommon. Its mathematical treatment is equal to that of the common case. For this reason, as well as for simplicities of representing the measurement techniques, only the common case of anisotropic turbulences according to Fig. 2.3b will be further considered.

The asymmetrical distribution of velocity fluctuations around the mean velocity vector has usually been found in the flows where large velocity gradients are present. This type of velocity fluctuations can be confirmed for instance in the shear flow of turbulent boundary layers, as shown by Zhang and Zhang (2002). To some extent,

the approximation of symmetrical velocity fluctuations can be made in order to simplify both the measurements and data processing. In principle, it merely depends on the requirement of the measurement accuracy.

2.2 Reynolds Turbulent Stresses

The basic equations of describing the stationary turbulent viscous flows are momentum equations which are also called the Reynolds-averaged Navier–Stokes (RANS) or simply Reynolds equations. In the Cartesian coordinate system with u , v and w as three orthogonal velocity components at a local point in the flow, the Reynolds equations are given as

$$\rho \left(\bar{u} \frac{\partial \bar{u}}{\partial x} + \bar{v} \frac{\partial \bar{u}}{\partial y} + \bar{w} \frac{\partial \bar{u}}{\partial z} \right) = -\frac{\partial \bar{p}}{\partial x} + \mu \nabla^2 \bar{u} + \left(\frac{\partial \overline{\rho u' u'}}{\partial x} + \frac{\partial \overline{\rho u' v'}}{\partial y} + \frac{\partial \overline{\rho u' w'}}{\partial z} \right) \quad (2.7)$$

$$\rho \left(\bar{u} \frac{\partial \bar{v}}{\partial x} + \bar{v} \frac{\partial \bar{v}}{\partial y} + \bar{w} \frac{\partial \bar{v}}{\partial z} \right) = -\frac{\partial \bar{p}}{\partial y} + \mu \nabla^2 \bar{v} + \left(\frac{\partial \overline{\rho v' u'}}{\partial x} + \frac{\partial \overline{\rho v' v'}}{\partial y} + \frac{\partial \overline{\rho v' w'}}{\partial z} \right) \quad (2.8)$$

$$\rho \left(\bar{u} \frac{\partial \bar{w}}{\partial x} + \bar{v} \frac{\partial \bar{w}}{\partial y} + \bar{w} \frac{\partial \bar{w}}{\partial z} \right) = -\frac{\partial \bar{p}}{\partial z} + \mu \nabla^2 \bar{w} + \left(\frac{\partial \overline{\rho w' u'}}{\partial x} + \frac{\partial \overline{\rho w' v'}}{\partial y} + \frac{\partial \overline{\rho w' w'}}{\partial z} \right) \quad (2.9)$$

In these equations ∇^2 is the Laplace operator which operates for instance

$$\nabla^2 u = \frac{\partial^2 u}{\partial x^2} + \frac{\partial^2 u}{\partial y^2} + \frac{\partial^2 u}{\partial z^2} \quad (2.10)$$

Flow fluctuations in the turbulent flows represent the momentum exchange between fluid particles. Their statistical properties are given by local gradients of Reynolds turbulent stresses which are involved in above equations in terms of $\partial \overline{\rho u' u'} / \partial x$ and other similar terms. For simplicity and later convenience, constant density of fluid is assumed and the Reynolds stresses are represented by the variance and the covariance of respective velocity components. The Reynolds turbulent stresses are commonly expressed in the following matrix form

$$\sigma_{mn} = \begin{vmatrix} \sigma_{xx} & \tau_{xy} & \tau_{xz} \\ \tau_{yx} & \sigma_{yy} & \tau_{yz} \\ \tau_{zx} & \tau_{zy} & \sigma_{zz} \end{vmatrix} = \begin{vmatrix} \overline{u'^2} & \overline{u'v'} & \overline{u'w'} \\ \overline{v'u'} & \overline{v'^2} & \overline{v'w'} \\ \overline{w'u'} & \overline{w'v'} & \overline{w'^2} \end{vmatrix} \quad (2.11)$$

The turbulent stresses σ_{xx} , σ_{yy} and σ_{zz} in m^2/s^2 are called the Reynolds normal stresses. For flow fluctuations that approximately fulfill the Gaussian probability

distribution, each normal stress is equal to the square of the respective standard deviation that has been defined in Eq. (2.2) and shown for application in Eq. (2.3). Correspondingly, turbulent stresses τ_{mn} with $m \neq n$ are called the Reynolds shear stresses. Both turbulent normal and shear stresses are time-averages of velocity fluctuations in corresponding velocity components. According to the definition of Reynolds shear stresses in Eq. (2.11) there are simply

$$\tau_{xy} = \tau_{yx}, \tau_{xz} = \tau_{zx}, \tau_{yz} = \tau_{zy} \quad (2.12)$$

In addition, each turbulent shear stress can be positive and negative, depending on the flow fluctuations themselves and the used coordinate system. This is, however, only of mathematical relevance. It does not represent any difference in flow properties. As can also be recognized from Reynolds equations given above, it is not the Reynolds stresses themselves but their gradients which determine the flow states and the related flow dynamics. For this reason, only the absolute maximum value of the turbulent shear stress behaves as a flow parameter. Other relevant turbulent parameters are the principal normal stresses, as described below.

Turbulences with equal normal stresses i.e. $\sigma_{xx} = \sigma_{yy} = \sigma_{zz}$ are called isotropic turbulence, as already concerned in Fig. 2.3a. It also indicates that all turbulent shear stresses at the considered local point in the flow vanish automatically. This circumstance indeed represents a special case of the general anisotropic turbulence with $\sigma_{xx} \neq \sigma_{yy} \neq \sigma_{zz}$ which has been found in most practical turbulent flows.

The Reynolds stress matrix given in Eq. (2.11) is related to the Cartesian coordinate system $x - y - z$. According to the matrix algebra there exists an orthogonal coordinate system in which all related turbulent shear stresses vanish. The Reynolds stress matrix then takes the form

$$\sigma_{mn} = \begin{vmatrix} \sigma_{11} & 0 & 0 \\ 0 & \sigma_{22} & 0 \\ 0 & 0 & \sigma_{33} \end{vmatrix} \quad (2.13)$$

The remaining normal stresses are known as the principal normal stresses at the considered local point in the turbulent flow. They are ordered with respect to their values to σ_I, σ_{II} and σ_{III} , conventionally with $\sigma_I > \sigma_{II} > \sigma_{III}$.

The turbulence state in a turbulent flow can thus be described by all three normal stresses, which also determine the maximum of the absolute shear stress (Chap. 6). Another intrinsic property of the turbulence state at a local point in the flow is that the sum of all three normal stresses remains constant as given by $\sigma_I + \sigma_{II} + \sigma_{III} = \sigma_{xx} + \sigma_{yy} + \sigma_{zz}$, independent of the applied coordinate system. This constant sum is known as the first invariant of the matrix given by Eq. (2.11). It actually represents the mean value of the turbulent kinetic energy that is involved in the flow fluctuations and usually written as

$$k = \frac{1}{2} \rho \left(\overline{u^2} + \overline{v^2} + \overline{w^2} \right) \quad (2.14)$$

In using the first invariant of the Reynolds stress matrix, the local turbulence intensity of a turbulent flow is calculated by

$$\text{Tu} = \frac{1}{\sqrt{\overline{u'^2} + \overline{v'^2} + \overline{w'^2}}} \sqrt{\frac{1}{3} (\overline{u'^2} + \overline{v'^2} + \overline{w'^2})} \quad (2.15)$$

For isotropic turbulence with $\overline{u'^2} = \overline{v'^2} = \overline{w'^2}$ Eq. (2.15) reduces to Eq. (2.6).

It should be mentioned that the turbulence intensity actually behaves as a statistical parameter and does not signify any mechanical significance of the flow turbulence. The physical property of the flow turbulence is indeed always related to the turbulent kinetic energy i.e. in the proportional form of Tu^2 .

Chapter 3

LDA Principles and Laser Optics

The technique of Laser Doppler Anemometry (LDA), as the name stands for, is a technique of using the laser light and the Doppler effect for velocity measurements. It is an optical method and hence tightly related to both the physical and geometrical optics. In order to depict the functionality of the LDA method, some physical properties of the light and the light wave propagation in medium will firstly be considered.

3.1 Light Wave and Its Propagation

The light is the electromagnetic wave which is specified by its amplitude, the polarization and the wavelength λ . In the LDA technology regarding special laser light properties, the polarization of the laser light is less interesting, at least for LDA users. It will only be considered by splitting the laser beam into parts and transmitting them through single-mode fibers to the LDA head. In addition, it will also be taken into account if the change in the light intensity due to refraction has to be concerned based on Fresnel equations. For laser light refractions at not too large refraction angles, the effect of laser light polarization on the change in the laser light intensity has usually been neglected. By disregarding the light polarization the spatial propagation of a plane light wave of the amplitude E_0 in the positive x -direction can be expressed by

$$E = E_0 \cos(\omega t - kx) \tag{3.1}$$

The parameters $\omega = 2\pi/T$ and $k = 2\pi/\lambda$, respectively, represent the angular frequency and the angular wavenumber, or simply wavenumber of the light wave. They are coupled by the wave propagation speed i.e. the light speed in the medium in which the light propagates. As known, the wave propagation speed is expressed by the phase velocity that is determined by

$$\frac{d(\omega t - kx)}{dt} = 0 \tag{3.2}$$

The light speed is then obtained as

$$c = \frac{dx}{dt} = \frac{\omega}{k} \quad (3.3)$$

Because of the constant light speed in the homogeneous medium, this equation signifies that the light wave can be represented either by the angular frequency ω in the time domain or equivalently by the wavenumber k in the space. The light speed in Eq. (3.3) can also be expressed as $c = \nu\lambda$ with $\nu = 1/T$ as the oscillation frequency of the light wave. In the vacuum, the light speed is measured as $c = 2.99792458 \times 10^8$ m/s. In the dielectric or non-conducting medium, like water for instance, the light speed is less than that in the vacuum. The ratio between them is denoted by n and called the refractive index of the respective dielectric medium. For the case that the light propagates from one medium (n_1) into another (n_2), the light speed then changes from c_1 to c_2 according to the following relation

$$\frac{c_2}{c_1} = \frac{n_1}{n_2} \quad (3.4)$$

Since the light frequency does not change while the light is refracted at the interface between two mediums, Eq. (3.4) can further be written with respect to $c = \nu\lambda$ as

$$\frac{c_2}{c_1} = \frac{n_1}{n_2} = \frac{\lambda_2}{\lambda_1} \quad (3.5)$$

This means that the wavelength of the light in a medium is reciprocally proportional to the medium refractive index n .

The refractive index n is an optical and physical parameter of a dielectric medium. It is not only a function of the medium and the medium temperature, but also a function of the light wavelength (color). The latter phenomenon is known as the dispersion or the chromatic aberration. In LDA measurements, the optical dispersion is generally neglected without causing any significant measurement errors (Chap. 13).

The transmission of light from one medium into another is also related to the change in the direction of light propagation. This is described by the law of refraction (also known as Snell's law) according to Fig. 3.1:

$$n_1 \sin \varepsilon_1 = n_2 \sin \varepsilon_2 \quad (3.6)$$

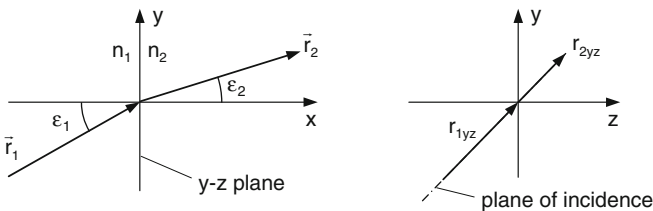


Fig. 3.1 Light ray refraction and the plane of incidence

In this equation, ε_1 and ε_2 represent the angles of incidence and refraction (or transmission), respectively. They are measured from the normal of the medium interface. Corresponding mediums are denoted as the incident and the refractive mediums.

The law of refraction given above can be generalized. According to Fig. 3.1 the x -axis agrees to the normal of the medium interface. The incident ray and the normal of the medium interface determine a plane that is known as the plane of incidence. The law of refraction also specifies that the refracted ray must also lie in the plane of incidence. For the purpose of performing extended calculations, the propagation directions of both the incident and the refracted rays are denoted by unit vectors \vec{r}_1 and \vec{r}_2 , respectively. Their projections onto the medium interface ($y - z$ plane) are also shown in Fig. 3.1. Corresponding vector components are given by r_{1yz} and r_{2yz} in the $y - z$ plane. Clearly, these two vector components are calculated by $\sin \varepsilon_1$ and $\sin \varepsilon_2$, respectively. Equation (3.6) is then expressed as

$$r_{2yz} = \frac{n_1}{n_2} r_{1yz} \quad (3.7)$$

Because two sub-vectors \vec{r}_{1yz} and \vec{r}_{2yz} are parallel vectors in the $y - z$ plane, following expressions can be immediately obtained

$$r_{2y} = \frac{n_1}{n_2} r_{1y} \quad (3.8)$$

$$r_{2z} = \frac{n_1}{n_2} r_{1z} \quad (3.9)$$

These expressions represent the law of refraction in the form of using vectors i.e. vector components. For later convenience of completing some special calculations, Eq. (3.6) is further considered in the form

$$1 - \frac{n_1^2}{n_2^2} = \frac{\sin^2 \varepsilon_1 - \sin^2 \varepsilon_2}{\sin^2 \varepsilon_1} = \frac{\cos^2 \varepsilon_2 - \cos^2 \varepsilon_1}{\sin^2 \varepsilon_1} \quad (3.10)$$

With respect to $r_{1x} = \cos \varepsilon_1$ and $r_{2x} = \cos \varepsilon_2$ it follows

$$1 - \frac{n_1^2}{n_2^2} = \frac{r_{2x}^2 - r_{1x}^2}{\sin^2 \varepsilon_1} = \frac{r_{1x}^2}{\sin^2 \varepsilon_1} \left(\frac{r_{2x}^2}{r_{1x}^2} - 1 \right) = \frac{1}{\tan^2 \varepsilon_1} \left(\frac{r_{2x}^2}{r_{1x}^2} - 1 \right) \quad (3.11)$$

from which one obtains

$$\frac{r_{2x}^2}{r_{1x}^2} - 1 = \left(1 - \frac{n_1^2}{n_2^2} \right) \tan^2 \varepsilon_1 \quad (3.12)$$

The law of refraction is thus interpreted in the form of unit vector components r_{1x} and r_{2x} . This equation will be applied in Chap. 14 to simplify the characterization of astigmatism which, as an optical aberration, is related to the refraction of a focused laser beam.

3.2 The Doppler Effect

The Doppler effect in optics is associated with the light propagation and accounts for the frequency shift when the light source is moving or light is reflected off a moving surface. Because there is no absolute motion according to the special theory of relativity, the Doppler effect must be described by the same mathematical formula, whether it is arising from the moving light source or the moving observer. This statement also relies on the physical reality that the light emitted from a moving light source is independent of the light source motion.

In Fig. 3.2, an optical interaction system with a moving light source and a fixed receiver has been shown. The initial distance between the light source and the receiver is given by s . The time used to transform the light through this distance is t , so that there is $s = ct$. For simplicity it is assumed that the light source emits the monochromatic light of wavelength λ_0 . In the first instance, the light source is assumed to be seated in the space. The number of waves on the path s is then given by $s/\lambda_0 = ct/\lambda_0$. In the second instance, the light source is assumed to move at a velocity equal to \vec{u}_s . Because the light velocity is independent of the motion of the light source, the time used for wave transmission through the path s is still equal to t . Within this time, the light source itself moves from the plane a to the plane b . The waves which were initially distributed on the path s are now squeezed into the path $ct - (\vec{u}_s \cdot \vec{l})t$. Because it deals with the same number of waves there is

$$\frac{ct}{\lambda_0} = \frac{ct - (\vec{u}_s \cdot \vec{l})t}{\lambda_1} \tag{3.13}$$

The wavelength of the light wave perceived at the receiver is then obtained as

$$\lambda_1 = \left(1 - \frac{\vec{u}_s \cdot \vec{l}}{c}\right) \lambda_0 \tag{3.14}$$

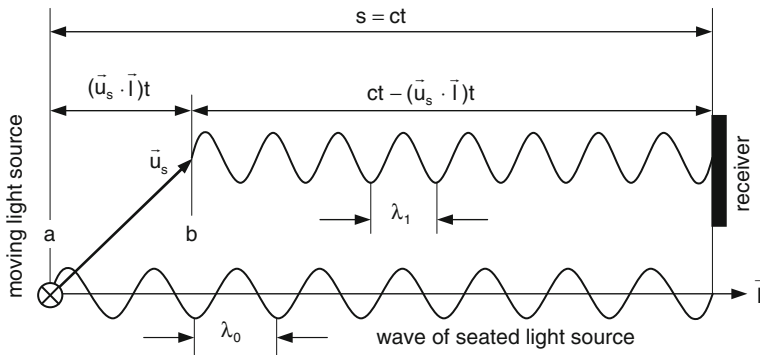


Fig. 3.2 Doppler effect in an optical system with moving light source

With respect to the constant light speed given by $\lambda_1 \nu_1 = \lambda_0 \nu_0 = c$, the frequency of the light wave is calculated as

$$\nu_1 = \frac{\nu_0}{1 - \vec{u}_s \cdot \vec{l}/c} \quad (3.15)$$

This frequency of the light wave perceived at the receiver is shifted against the frequency ν_0 of the light wave that is emitted by the light source. The associated phenomenon is called the Doppler effect. It depends on the relative motion between the light source and the receiver.

Because of $\vec{u}_s \cdot \vec{l}/c \ll 1$ the above equation is simplified to

$$\nu_1 = \nu_0 \left(1 + \frac{\vec{u}_s \cdot \vec{l}}{c} \right) \quad (3.16)$$

Equation (3.15) i.e. (3.16) is derived by assuming the moving light source and the fixed receiver. According to the special theory of relativity, such a system is totally equivalent to the system with a fixed light source and a moving receiver, when the moving velocity of the receiver is set by $\vec{u}_r = -\vec{u}_s$. Because of this total equivalence the frequency of the light wave received by the moving receiver is obtained directly from Eq. (3.16) as

$$\nu_1 = \nu_0 \left(1 - \frac{\vec{u}_r \cdot \vec{l}}{c} \right) \quad (3.17)$$

In relying on LDA principles, a scattering system is considered to consist of a fixed light source, a moving object (i.e. a small particle) and a fixed observer to receive the light scattered by the moving particle. The corresponding optical arrangement has been illustrated in Fig. 3.3. The particle moves at a velocity equal to \vec{u}_p . The light frequency from the light source is ν_0 . The frequency which is observed by the moving particle is ν_1 and can be calculated by Eq. (3.17) using substitutions $\vec{u}_p = \vec{u}_r$ and $\vec{l}_1 = \vec{l}$. The particle in its moving system scatters the incident light at the same frequency ν_1 . In a certain spatial direction (\vec{l}_2), the scattered light is then received as the light of another frequency ν_2 by the fixed receiver because of the Doppler effect.

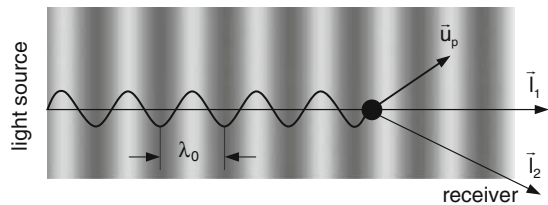


Fig. 3.3 Optical interaction system with a light source, a moving object and a receiver to explain the Doppler effect in LDA measurements

The relationship between the frequencies ν_1 and ν_2 is obtained from Eq. (3.16) by simply changing the indices

$$\nu_2 = \nu_1 \left(1 + \frac{\vec{u}_p \cdot \vec{l}_2}{c} \right) \quad (3.18)$$

Combining Eqs. (3.17) and (3.18) yields

$$\nu_2 = \nu_0 \left(1 - \frac{\vec{u}_p \cdot \vec{l}_1}{c} \right) \left(1 + \frac{\vec{u}_p \cdot \vec{l}_2}{c} \right) \quad (3.19)$$

This equation is found as the basic theory of the laser Doppler anemometry. The shifted frequency according to Eq. (3.19) is then a function of the particle velocity which is considered to be equal to the flow velocity. Because the flow velocity is always negligible against the light speed as given by $\vec{u}_p \cdot \vec{l}_1/c \ll 1$ and $\vec{u}_p \cdot \vec{l}_2/c \ll 1$, Eq. (3.19) is further simplified to

$$\nu_2 \approx \nu_0 \left(1 - \frac{\vec{u}_p \cdot \vec{l}_1}{c} + \frac{\vec{u}_p \cdot \vec{l}_2}{c} \right) \quad (3.20)$$

The shifted frequency ν_2 is in the order of ν_0 and therefore still too high to be measured by conventional devices that are found in usual laboratories. In order to make use of the Doppler effect for flow measurements, the dual beam configuration has been confirmed to be highly effective. In fact, the configuration of using two laser beams has been widely applied and comes to be the standard in LDA measurements. The physical background of this configuration is given in Sect. 3.4. The key technique in it is the superposition of two light waves with different frequencies, as described in the next section.

3.3 Superposition of Two Plane Light Waves

The dual beam configuration of LDA optics (see Sect. 3.4) relies upon the superposition of two light waves that are differently shifted by the Doppler effect. As known in general, light is the electromagnetic oscillation in the form of waves. The superposition of two light waves of different frequencies leads to the so-called optical interference. For simplicity only the plane waves are considered, which propagate in the x -direction. According to Fig. 3.4a and b two harmonic waves are assumed to have different amplitudes and frequencies, as given by

$$E_a = E_{a0} \cos(\omega_a t - k_a x) \quad (3.21)$$

$$E_b = E_{b0} \cos(\omega_b t - k_b x) \quad (3.22)$$

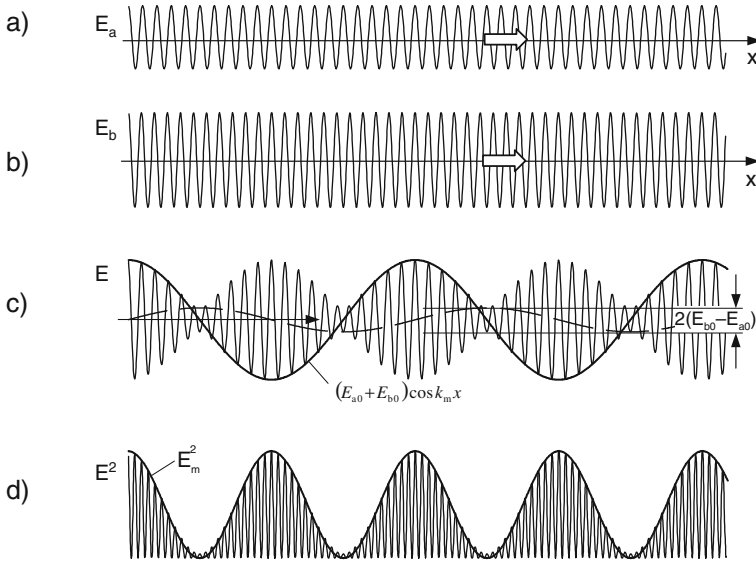


Fig. 3.4 Superposition of two light waves

Different amplitudes of two waves have been assumed, because in LDA measurements with the dual beam configuration the intensities of two chains of laser lights scattered by the particle are always different. This is true even if two laser beams are initially of equal light intensity.

The superposition of these two waves is simply given as

$$E = E_{a0} \cos(\omega_a t - k_a x) + E_{b0} \cos(\omega_b t - k_b x) \quad (3.23)$$

The spatial distribution of this superimposed wave can be obtained at a given time, as shown in Fig. 3.4c for the case $E_{b0} = 1.5E_{a0}$ and $\omega_b = 1.1\omega_a$ i.e. $k_b = 1.1k_a$. Obviously the superimposed wave possesses both a high frequency and a low modulation frequency. For calculating these two frequencies Eq. (3.23) is rearranged as

$$E = E_{a0} [\cos(\omega_a t - k_a x) + \cos(\omega_b t - k_b x)] + (E_{b0} - E_{a0}) \cos(\omega_b t - k_b x) \quad (3.24)$$

By applying the trigonometric identity

$$\cos \alpha + \cos \beta = 2 \cos \frac{1}{2}(\alpha + \beta) \cos \frac{1}{2}(\alpha - \beta) \quad (3.25)$$

to the first term on the r.h.s. of Eq. (3.24), then the following equation is obtained:

$$E = 2E_{a0} \cos\left(\frac{\omega_a + \omega_b}{2}t - \frac{k_a + k_b}{2}x\right) \cos\left(\frac{\omega_a - \omega_b}{2}t - \frac{k_a - k_b}{2}x\right) + (E_{b0} - E_{a0}) \cos(\omega_b t - k_b x) \quad (3.26)$$

For further calculations the following abbreviations are applied

$$\bar{\omega} = \frac{1}{2}(\omega_a + \omega_b), \quad \omega_m = \frac{1}{2}(\omega_a - \omega_b) \quad (3.27)$$

and

$$\bar{k} = \frac{1}{2}(k_a + k_b), \quad k_m = \frac{1}{2}(k_a - k_b) \quad (3.28)$$

Herein ω_m and k_m represent the modulation frequency and the modulation wavenumber, respectively.

To the cosine function $\cos(\omega_b t - k_b x)$ in Eq. (3.26), $\omega_b = \bar{\omega} - \omega_m$ and $k_b = \bar{k} - k_m$ are substituted so that

$$\cos(\omega_b t - k_b x) = \cos(\bar{\omega}t - \bar{k}x) \cos(\omega_m t - k_m x) + \sin(\bar{\omega}t - \bar{k}x) \sin(\omega_m t - k_m x) \quad (3.29)$$

Eq. (3.26) is then converted to

$$E = (E_{a0} + E_{b0}) \cos(\bar{\omega}t - \bar{k}x) \cdot \cos(\omega_m t - k_m x) + (E_{b0} - E_{a0}) \sin(\bar{\omega}t - \bar{k}x) \cdot \sin(\omega_m t - k_m x) \quad (3.30)$$

At the time $t = 0$, the superimposed wave represents a spatial wave distribution given by

$$E = (E_{a0} + E_{b0}) \cos(\bar{k}x) \cos(k_m x) + (E_{b0} - E_{a0}) \sin(\bar{k}x) \sin(k_m x) \quad (3.31)$$

In accordance with Fig. 3.4c, the first term on the r.h.s. of this equation represents the main form of the superimposed wave, whose maximum amplitude is given by $E_{a0} + E_{b0}$. Correspondingly the second term depicts an auxiliary wave with a maximum amplitude equal to $E_{b0} - E_{a0}$. It usually represents a negligible value and only disappears, if two plane waves of equal amplitude are superimposed.

The main form of the superimposed wave comprises the high angular frequency equal to $\bar{\omega}$ (i.e. \bar{k} in the spatial wave distribution) and the low modulation frequency equal to ω_m (k_m). The amplitude of the high frequency oscillation is given by the modulated wave

$$E_m = (E_{a0} + E_{b0}) \cos(\omega_m t - k_m x) \quad (3.32)$$

It indeed represents the envelope of the high frequency wave, as shown in Fig. 3.4c for $t=0$. Such a modulated wave form can be imagined to be obtainable by transmitting the wave given in Eq. (3.30) through a low pass filter.

The intensity of a light wave that is sensed by the human eyes or the photonic detectors such as photomultiplier tubes is given by the flux density that is proportional to the wave amplitude squared. From the superposition of two waves, as given by Eq. (3.30) and illustrated in Fig. 3.4c, the amplitude of the main wave oscillation has been confirmed to be the modulated wave and given in Eq. (3.32). Because of this the time and spatial distribution of intensities of the superimposed wave can thus be expressed by

$$E_m^2 = (E_{a0} + E_{b0})^2 \cos^2 (\omega_m t - k_m x) \quad (3.33)$$

or equivalently as

$$E_m^2 = \frac{1}{2} (E_{a0} + E_{b0})^2 [1 + \cos 2 (\omega_m t - k_m x)] \quad (3.34)$$

The flux density that is proportional to E_m^2 oscillates with an angular frequency of $2\omega_m = \omega_a - \omega_b$ which is known as the beat frequency. The corresponding spatial distribution of such an oscillation is shown in Fig. 3.4d for the considered example. It is evident that even in the applied example with large amplitude difference ($E_{b0} = 1.5E_{a0}$) the superimposed wave can be well approximated by its main part which is specified by Eq. (3.32) for the amplitude and by Eq. (3.34) for the light intensity.

At this moment it should be mentioned that in LDA measurement techniques the comparable beat frequency of the flux density oscillation is considered and measured to calculate the flow velocities. Because this frequency is many orders smaller than the light frequency (of about $6 \cdot 10^{14}$ Hz), it can be accurately measured by means of usual measurement devices.

3.4 LDA Principle

After the Doppler effect and the superposition of two light waves have been treated in foregoing sections, the optical configuration of an LDA-system and its functionality will be demonstrated. A standard one-component LDA system consists of two laser beams. For simplicity two laser beams (A and B) of equal frequencies (ν_0) are considered to intersect at an angle 2α (Fig. 3.5). The cross area of these two laser beams in the flow is called the measurement volume. A particle that is suspended in the flow is assumed to pass through the measurement volume and so scatters the lights of two laser beams simultaneously. Because of the different spatial layout of two laser beams, the moving particle of velocity \vec{u}_p perceives the different light frequencies resulted from different Doppler effects. A detector is spatially located along \vec{l}_2 for receiving the light that is scattered from the measurement volume. The considered system including the laser light source, a moving particle and a detector is completely comparable with the optical interaction system that has already been presented in Fig. 3.3 for explaining the Doppler effect. Hence according to

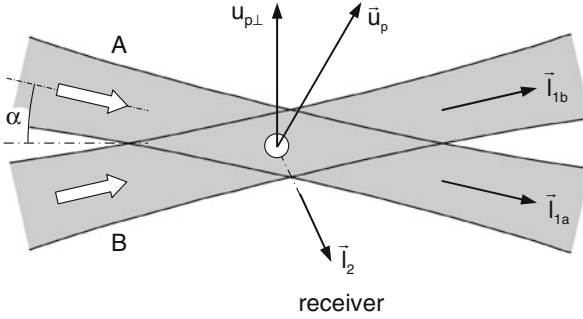


Fig. 3.5 Particle motion through the measurement volume

Eq. (3.20) the frequencies of two light waves received by the detector along \vec{l}_2 are given by

$$\nu_{2a} \approx \nu_0 \left(1 - \frac{\vec{u}_p \cdot \vec{l}_{1a}}{c} + \frac{\vec{u}_p \cdot \vec{l}_2}{c} \right) \quad (3.35)$$

and

$$\nu_{2b} \approx \nu_0 \left(1 - \frac{\vec{u}_p \cdot \vec{l}_{1b}}{c} + \frac{\vec{u}_p \cdot \vec{l}_2}{c} \right) \quad (3.36)$$

respectively.

While being received by the photodetector, the two light waves of frequencies ν_{2a} and ν_{2b} get to be superimposed. In accordance with Eq. (3.34), the flux density of the resultant light wave exhibits a low frequency that is known as the beat frequency and equal to twice the modulation frequency ($2\omega_m = \omega_a - \omega_b$). It indeed deals with a low frequency that can be easily measured by means of conventional measurement devices. In the terminology of LDA measurement techniques, this low frequency is called the Doppler frequency. It is calculated from Eqs. (3.35) and (3.36) by

$$\nu_D = |\nu_{2a} - \nu_{2b}| = \frac{\nu_0}{c} \left| \vec{u}_p \cdot (\vec{l}_{1b} - \vec{l}_{1a}) \right| \quad (3.37)$$

Because of $c/\nu_0 = \lambda_0$ and $\left| \vec{u}_p \cdot (\vec{l}_{1b} - \vec{l}_{1a}) \right| = 2u_{p\perp} \sin \alpha$ with $u_{p\perp}$ as the component of the particle velocity perpendicular to the bisector of the two laser beams, the above equation becomes

$$\nu_D = 2 \frac{u_{p\perp}}{\lambda_0} \sin \alpha \quad (3.38)$$

The Doppler frequency is directly proportional to the velocity component $u_{p\perp}$ of the particle motion, however, independent of the particle motion direction. In assuming the particle velocity to be equal to the velocity of the fluid flow, the corresponding flow velocity component can be obtained by measuring the Doppler frequency. It yields then from Eq. (3.38)

$$u_{\perp} = \frac{\lambda_0}{2 \sin \alpha} \nu_D \quad (3.39)$$

The factor that is multiplied to the Doppler frequency is a physical and geometrical constant. This circumstance implies that the LDA method for flow measurements is a method without system calibration. In addition, as seen from Eq. (3.38), the Doppler frequency detected in the scattered light is independent of the spatial position of the detector. This property enables the detector to be freely positioned for measurements. By using the separate detector, however, it is always time-consuming to align the detector optics to be focused onto the measurement volume. For this reason, most LDA systems are configured as the backscattering system in which the detector unit is integrated into the transmitting unit, see Chap. 4.

Because the Doppler frequency is always positive, independent of the particle flow direction, the velocity component u_{\perp} that is calculated from Eq. (3.39) only corresponds to its absolute value. It is yet impossible to determine the sign of this velocity component i.e. the flow direction. A method to remove the ambiguity of the flow direction is the use of a Bragg cell to shift the frequency in one of two laser beams. This method has come to be a standard in most LDA optics.

Detailed descriptions of an LDA system including photodetectors (photomultiplier) and the use of Bragg cells will be given in Sect. 3.6.

3.5 Fringe Model on the Light Interference

The Doppler frequency in the light scattered by the particle while passing through the measurement volume, as given in Eq. (3.38), can also be calculated by accounting for the interference of laser lights in the measurement volume. The associated calculation method is known as the fringe model. As a matter of fact, the fringe model has most often been applied to explain the principle of LDA method in flow measurements because of its illustrative capability for easy understanding.

Two plane light waves of equal amplitudes (E_0) and frequencies (ω) are postulated to propagate in the directions of \vec{k}_a and \vec{k}_b , respectively, and intersect at an angle 2α , as shown in Fig. 3.6. Because of equal angular frequencies and thus equal wavelengths of two plane waves, equal wavenumbers are given as $k = |\vec{k}_a| = |\vec{k}_b| = 2\pi/\lambda_0$. For the convenience of analysis, the two-dimensional $z-x$ coordinate system is applied with z as the optical axis which coincides with

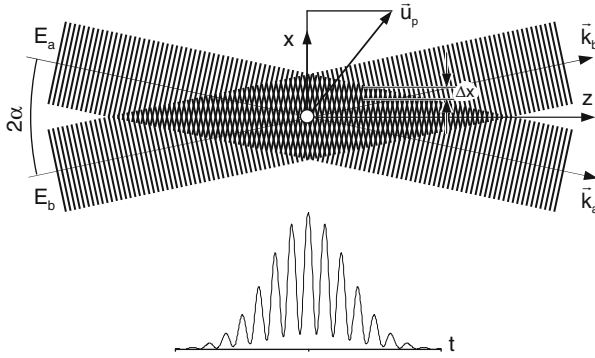


Fig. 3.6 Fringe model of LDA principle and the burst signal

the bisector of two wave vectors \vec{k}_a and \vec{k}_b . In the field of the plane wave E_a for instance, the electromagnetic wave at $\vec{r} = (z, x)$ is given by

$$E_a = E_0 \cos(\omega t - \vec{k}_a \cdot \vec{r}) \quad (3.40)$$

Let us remember, the case of the vector \vec{r} coinciding with the wave vector \vec{k} has already been treated and given in Eq. (3.21).

With respect to the wavenumber $\vec{k}_a = (k \cos \alpha, -k \sin \alpha)$ in the $z-x$ plane Eq. (3.40) becomes

$$E_a = E_0 \cos[\omega t - k(z \cos \alpha - x \sin \alpha)] \quad (3.41)$$

Similarly, the electromagnetic wave at the same point, however, in the field of the plane wave E_b can be obtained. The wavenumber in this case is given as $\vec{k}_b = (k \cos \alpha, k \sin \alpha)$, so that

$$E_b = E_0 \cos[\omega t - k(z \cos \alpha + x \sin \alpha)] \quad (3.42)$$

The superposition of these two plane waves at the point $\vec{r} = (z, x)$ in the $z-x$ plane is obtained by again applying the trigonometric identity according to Eq. (3.25)

$$E = E_a + E_b = 2E_0 \cos(kx \sin \alpha) \cdot \cos(\omega t - kz \cos \alpha) \quad (3.43)$$

Obviously the resultant wave at the given point $\vec{r} = (z, x)$ shows the high angular frequency equal to ω . The amplitude of this wave oscillation is $2E_0 \cos(kx \sin \alpha)$ that is a constant and geometrically only a function of the coordinate x . The light intensity that is proportional to the square of the wave amplitude is calculated by

$$E_m^2 = 4E_0^2 \cos^2(kx \sin \alpha) = 2E_0^2 [1 + \cos 2(kx \sin \alpha)] \quad (3.44)$$

With respect to $k = 2\pi/\lambda_0$ this equation is again written as

$$E_m^2 = 2E_0^2 \left[1 + \cos 2\pi \left(\frac{2 \sin \alpha}{\lambda_0} x \right) \right] = 2E_0^2 \left[1 + \cos \left(2\pi \frac{x}{\Delta x} \right) \right] \quad (3.45)$$

In the direction perpendicular to the optical axis i.e. parallel to the x -axis, the light intensity alternates with a distance equal to

$$\Delta x = \frac{\lambda_0}{2 \sin \alpha} \quad (3.46)$$

This distance is known as the fringe spacing in the measurement volume. It is resulting from the interference of two light waves that takes place by overlapping them. To show the dimension of the fringe spacing in the measurement volume, two laser beams of equal wavelength $\lambda_0 = 514.5 \text{ nm}$ are considered to intersect at an half intersection angle $\alpha = 3^\circ$. From the above equation the fringe spacing is calculated as $\Delta x = 5 \mu\text{m}$. Obviously it deals with a quite small value. By use of a magnified image, the fringe pattern i.e. the light intensity distribution in the measurement volume could be visualized for instance by Miles and Witze (1994, 1996).

In comparing with Eq. (3.39), the velocity component of a particle passing through the measurement volume is calculated by

$$u_{\perp} = \Delta x \cdot \nu_D \quad (3.47)$$

This equation points out that the Doppler frequency can be considered to be the alternating frequency in the intensity of light that is scattered out by a particle passing through the measurement volume. The corresponding light signal has also been shown in Fig. 3.6. In the terminology of LDA measurements, such a signal is called the Doppler burst. Because the laser beams used in LDA measurements have a Gaussian distribution in the intensity (see Sect. 3.7), the Doppler burst shows its maximum amplitude, as the particle is found in the centre of the measurement volume.

The fringe model presented above is a very useful tool to understand the LDA measurement principle. It also represents a very convenient means to make further studies of diverse optical phenomena influencing the measurement accuracy. To be mentioned here are for instance the change in the fringe spacing at flow measurements in the circular pipes, the fringe distortion caused by either improper optical layout or astigmatism arising from laser beam refractions, and the signal properties in measurements of particle size using Phase Doppler Anemometry (PDA). All of these points excluding that in PDA measurements can be found in the corresponding chapters of this book.

3.6 Frequency Shift Method to Resolve the Flow Direction

The LDA method is based on the evaluation of the burst signals that are generated by particles passing through the measurement volume. An ambiguity to the flow direction of the particle, however, exists because a positive and a negative velocity of the same magnitude will cause the same Doppler frequency. The burst signals thus only involve the magnitude but not the signs of respective velocities. In order to resolve the flow direction from each Doppler burst, the technique of using Bragg cells to slightly shift the frequency in one or both of two laser beams in each laser beam pair has become a standard. The physical principle of the Bragg cell can be found for instance in Albrecht et al. (2003). The purpose of shifting the light frequency is to create the moving fringes in the measurement volume in a predefined direction. The principle of using the frequency shift method to resolve the flow direction is explained here.

According to Fig. 3.7 the light wave frequency of the laser beam A is assumed to be shifted up by ν_{sh} , so that $\nu_{a0} = \nu_0 + \nu_{sh}$. Two laser beams thus show different frequencies. Correspondingly, the light frequencies perceived at the detector in the direction \vec{l}_2 can be directly obtained from Eqs. (3.35) and (3.36) as

$$\nu_{2a} = (\nu_0 + \nu_{sh}) \left(1 - \frac{\vec{u} \cdot \vec{l}_{1a}}{c} + \frac{\vec{u} \cdot \vec{l}_2}{c} \right) \quad (3.48)$$

and

$$\nu_{2b} = \nu_0 \left(1 - \frac{\vec{u} \cdot \vec{l}_{1b}}{c} + \frac{\vec{u} \cdot \vec{l}_2}{c} \right) \quad (3.49)$$

respectively. Herein both \vec{l}_1 and \vec{l}_2 are unit vectors.

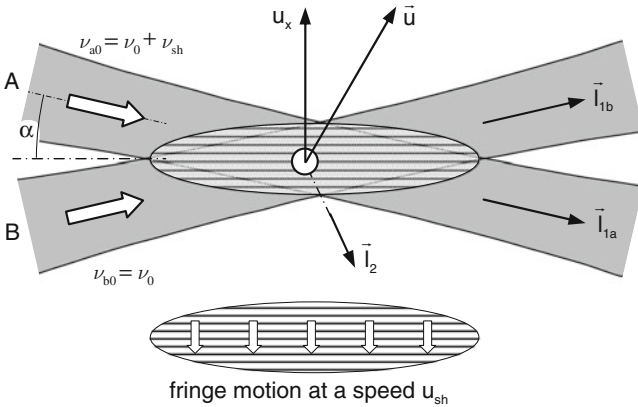


Fig. 3.7 Frequency shift at the laser beam A and the resultant fringe motion in the measurement volume with a shift speed u_{sh}

In the practical application, the shift frequency ν_{sh} is selected in the order of megahertz. It is much lower against the light frequency, however, sufficiently high in comparison to the Doppler frequency caused by the maximum flow velocity. Indeed, the value of the shift frequency should ensure that the difference $\nu_{2a} - \nu_{2b}$ is constantly positive. Under this condition the effective frequency of light signals measured by the receiving unit like the photomultiplier (PM) is simply

$$\nu_{PM} = \nu_{2a} - \nu_{2b} = \nu_{sh} + \frac{\nu_0}{c} \vec{u} \cdot (\vec{l}_{1b} - \vec{l}_{1a}) + \frac{\nu_{sh}}{c} \vec{u} \cdot (\vec{l}_2 - \vec{l}_{1a}) \quad (3.50)$$

The third term on the r.h.s. of above equation is negligible against the second term because of $\nu_{sh} \ll \nu_0$.

With respect to the definition of the positive sign of the velocity component u_x according to Fig. 3.7, the vector difference $\vec{l}_{1b} - \vec{l}_{1a}$ coincides with the positive x -axis. Because of $\vec{u} \cdot (\vec{l}_{1b} - \vec{l}_{1a}) = 2u_x \sin \alpha$ Eq. (3.50) is then simplified to

$$\nu_{PM} = \nu_{sh} + 2\nu_0 \frac{u_x}{c} \sin \alpha \quad (3.51)$$

The second term on the r.h.s. of this equation represents the Doppler frequency caused by the flow velocity. With respect to $c = \lambda_0 \nu_0$ and in using the fringe model according to Eq. (3.46), Eq. (3.51) is then rewritten as

$$\nu_{PM} = \nu_{sh} + \nu_D = \nu_{sh} + \frac{u_x}{\Delta x} \quad (3.52)$$

The velocity component u_x is then resolved as

$$u_x = \Delta x (\nu_{PM} - \nu_{sh}) \quad (3.53)$$

Thus from direct comparison between the frequency ν_{PM} which is detected at the photomultiplier and the preset shift frequency ν_{sh} both the value and the sign of the velocity component u_x can be exactly determined. According to Eq. (3.53) there is $u_x > 0$ from $\nu_{PM} > \nu_{sh}$. In particular, the zero velocity of the flow i.e. a particle seated in the measurement volume can also be measured. In this case, there is $\nu_{PM} - \nu_{sh} = 0$.

The technique of using the shift frequency to detect the flow direction is to generate the moving fringe pattern in the measurement volume. According to Eq. (3.52) the detected frequency is simply given as the superposition of the Doppler frequency and the shift frequency. By rewriting Eq. (3.52) to be $\nu_{PM} = (\nu_{sh} \Delta x + u_x) / \Delta x$ it is evident that the detected frequency results from the superposition of the particle velocity and a velocity equal to $\nu_{sh} \Delta x$. This implies that fringes in the measurement volume move in the negative x -direction at the constant speed equal to $u_{sh} = -\nu_{sh} \Delta x$ which is called fringe shift speed. The postulated fringe motion in the measurement volume can be demonstrated in the following way.

3.6.1 Fringe Shift Speed

According to Fig. 3.7 the angular frequency of two laser beams are assumed to be $\omega_a = 2\pi\nu_a$ and $\omega_b = 2\pi\nu_b$, respectively. The corresponding wave equations can be obtained from Eqs. (3.41) and (3.42). For simplicity, the fringe distribution along the x -axis will be considered. This means that $z = 0$ has to be applied, so that

$$E_a = E_0 \cos(\omega_a t + k_a x \sin \alpha) \quad (3.54)$$

$$E_b = E_0 \cos(\omega_b t - k_b x \sin \alpha) \quad (3.55)$$

The superposition of these two plane waves is obtained by again applying the trigonometric identity according to Eq. (3.25)

$$E = E_a + E_b = 2E_0 \cos(\omega_m t + \bar{k}x \sin \alpha) \cdot \cos(\bar{\omega}t + k_m x \sin \alpha) \quad (3.56)$$

with $\bar{\omega} = \frac{1}{2}(\omega_a + \omega_b)$, $\omega_m = \frac{1}{2}(\omega_a - \omega_b)$, $\bar{k} = \frac{1}{2}(k_a + k_b)$ and $k_m = \frac{1}{2}(k_a - k_b)$.

The resultant light wave at the given x shows the high angular frequency equal to $\bar{\omega}$. The amplitude of this wave oscillation is again the modulated wave $2E_0 \cos(\omega_m t + \bar{k}x \sin \alpha)$ with the low frequency ω_m . The light intensity that is proportional to the square of the wave amplitude is calculated by

$$E_m^2 = 4E_0^2 \cos^2(kx \sin \alpha) = 2E_0^2 [1 + \cos 2(\omega_m t + \bar{k}x \sin \alpha)] \quad (3.57)$$

In the current calculation with respect to the shift frequency, there are $\omega_a = \omega_0 + \omega_{sh}$ and $\omega_b = \omega_0$, so that $\omega_m = \omega_{sh}/2 = \pi\nu_{sh}$. Correspondingly there is $\bar{k} = \frac{1}{2}(k_a + k_b) \approx 2\pi/\lambda_0$ because of $\nu_{sh} \ll \nu_0$. With such simplifications as well as with respect to $\Delta x = \lambda_0/(2 \sin \alpha)$ from Eq. (3.46) one obtains from Eq. (3.57)

$$E_m^2 = 2E_0^2 \left[1 + \cos 2\pi \left(\nu_{sh} t + \frac{x}{\Delta x} \right) \right] \quad (3.58)$$

It represents an apparent harmonic wave that would move in the negative x -direction. In reality, it only signifies the unsteadiness of the fringe pattern as if this is rolling at a constant speed. It does not indicate any energy transport. For $\nu_{sh} = 0$ one obtains Eq. (3.45).

The speed with which the fringe pattern rolls is determined from the condition

$$\nu_{sh} t + \frac{x}{\Delta x} = \text{const} \quad (3.59)$$

to

$$u_{sh} = \frac{dx}{dt} = -\nu_{sh} \Delta x \quad (3.60)$$

This speed is denoted as the fringe shift speed and has been postulated before based on Eq. (3.52).

The shift frequency, created by means of Bragg cells, is for instance 40 MHz in some LDA applications. With respect to a fringe spacing $\Delta x = 5\mu\text{m}$, see Sect. 3.5, the shift speed of fringes in the measurement volume is calculated to $u_{\text{sh}} = -200\text{ m/s}$. Because this speed is sufficiently higher than all possible fluctuation velocities in most flows, the sign of each measured velocity component u_x in a turbulent flow can be determined without ambiguity.

Some LDA users would sometimes like to check the accuracy of the shift frequency preset in the LDA system. A simple and accurate method for performing this task is presented in Chap. 18.

3.7 Gaussian Beam Properties

3.7.1 Geometrical Specifications of the Gaussian Beam

The laser beams that are applied in LDA techniques are generally single-mode laser beams. The intensity distribution in the cross section of such a laser beam can be approximated by the Gaussian distribution as given by

$$I(r) = I_0 e^{-2(r/w)^2} \tag{3.61}$$

The light intensity on the beam axis is denoted by I_0 . The thickness of a Gaussian beam is confirmed to be equal to $2w$. At $r = w$ the light intensity falls down to a level of about $e^{-2} = 13.5\%$ of the light intensity on the beam axis ($r = 0$), as shown in Fig. 3.8.

The light intensity represents the time rate of flow of radiant energy i.e. the radiant flux density. The total power involved in a light beam is obtained by integrating the light intensity distribution across the light beam section, yielding

$$P = 2\pi I_0 \int_0^\infty e^{-2(r/w)^2} r dr = \frac{1}{2} \pi w^2 I_0 \tag{3.62}$$

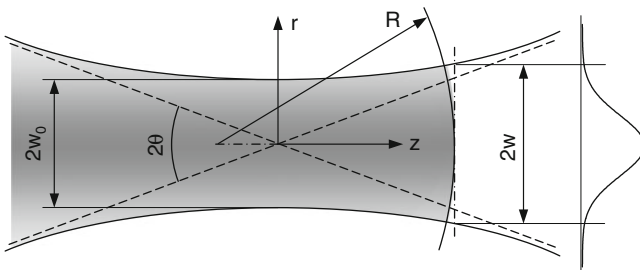


Fig. 3.8 Geometrical and optical specifications of the Gaussian beam

Light beams with the Gaussian distribution always comprise a well-defined beam waist. This property indicates that the Gaussian beam is a focused beam. In fact, such a light beam is geometrically completely describable by merely using the beam waist diameter. According to Fig. 3.8 the geometrical feature of a Gaussian beam mainly includes the curvature radius R of the wave front and the beam thickness $2w$ representing the beam divergence. The wave front is considered as a surface on which the phase is constant. From the wave optics the curvature radius of the front surface of a Gaussian beam and the beam thickness at the distance z from the beam waist are given by

$$R = z \left[1 + \left(\frac{\pi w_0^2}{\lambda z} \right)^2 \right] \quad (3.63)$$

and

$$w = w_0 \sqrt{1 + \left(\frac{\lambda z}{\pi w_0^2} \right)^2} \quad (3.64)$$

respectively.

For large values of the distance z the thickness of the light beam linearly increases with the distance.

Obviously the beam thickness at the beam waist, given by $2w_0$, is the most essential parameter that determines all geometrical features of a Gaussian beam. According to Eq. (3.63) the curvature radii of the beam front, both at the beam waist ($z = 0$) and at the large distance ($z = \infty$), are infinite. The beam can thus be considered as the plane wave beam. The position that the Gaussian beam possesses the smallest curvature radius (R_{\min}) is obtained from Eq. (3.63) under the condition

$$\frac{dR}{dz} = 0 \quad (3.65)$$

to

$$z_R = \frac{\pi \cdot w_0^2}{\lambda} \quad (3.66)$$

This distance from the beam waist is called the Rayleigh length. It is again a function of the beam waist thickness. The smallest curvature radius in a Gaussian beam is then obtained from Eq. (3.63)

$$R_{\min} = 2z_R = \frac{2\pi \cdot w_0^2}{\lambda} \quad (3.67)$$

This smallest curvature radius in the wave front is relevant when evaluating the uniformity of the fringe pattern in the LDA measurement volume. In the case that

the measurement volume does not coincide with the waists of two laser beams, non-uniform fringe in the measurement volume will be created. The largest fringe distortion occurs when the measurement volume is formed by laser beam crossing on the Rayleigh length of both laser beams. More about this property and the influence of the fringe distortion on the measurement accuracy will be described in Chap. 16.

In using the Rayleigh length as a characteristic parameter, both the curvature radius of the front surface and the thickness of a Gaussian beam at a distance z from the beam waist are expressed by

$$R = z \left[1 + \left(\frac{z_R}{z} \right)^2 \right] \quad (3.68)$$

and

$$w = w_0 \sqrt{1 + \left(\frac{z}{z_R} \right)^2} \quad (3.69)$$

respectively.

Especially at the Rayleigh length there is

$$w_R = \sqrt{2} w_0 \quad (3.70)$$

At great distance it yields from Eq. (3.68) with $z \gg z_R$

$$R = z \quad (3.71)$$

This last equation signifies that the front surface of a Gaussian beam is a circular surface which has its centre at the beam waist.

The light intensity in the Gaussian beam at the Rayleigh length can be calculated from Eq. (3.62). Because the total power in the beam remains constant, the light intensity in the center of the beam, if compared to the center light intensity at the beam waist, is given by

$$\frac{I_{0R}}{I_{0w}} = \frac{w_0^2}{w_R^2} = \frac{1}{2} \quad (3.72)$$

The divergence of a Gaussian beam can be expressed by the corresponding divergence angle 2θ under the condition $z \rightarrow \infty$. This can be obtained by accounting for $\tan \theta = dw/dz$ and carrying out the corresponding calculation from Eq. (3.69). Because it usually deals with a very small angle, the approximation $\tan \theta \approx \theta$ can be applied. The half divergence angle of a Gaussian beam is then obtained as

$$\theta = \frac{w_0}{z_R} \quad (3.73)$$

With regard to the Rayleigh length given in Eq. (3.66) this divergence angle of a Gaussian beam is again expressed as

$$\theta = \frac{\lambda}{\pi w_0} \quad (3.74)$$

Obviously laser beams that have large diameters at the beam waist show the negligible divergence angle. For instance for a laser beam of $\lambda = 500 \text{ nm}$ and $w_0 = 1 \text{ mm}$, the divergence angle is only about 0.009° .

3.7.2 Transmission Performance of the Gaussian Beam

The transmission performance of a Gaussian beam through a lens of the focal length f is considered here according to Fig. 3.9. The Gaussian beam considered is assumed to have a beam waist thickness $2w'_0$. The corresponding Rayleigh length is given by z'_R . Based on lens optics the following geometrical relationships concerning the Gaussian beam prior to and after the lens are available

$$w_0 = \frac{f}{\sqrt{(s' - f)^2 + z_R'^2}} w'_0 \quad (3.75)$$

$$s = f + \frac{f^2 (s' - f)}{(s' - f)^2 + z_R'^2} \quad (3.76)$$

In most cases and for simplicity, a Gaussian beam after passing through a lens can be still considered as a Gaussian beam. All geometrical specifications of a Gaussian beam, as presented in Sect. 3.7.1, remain unchanged.

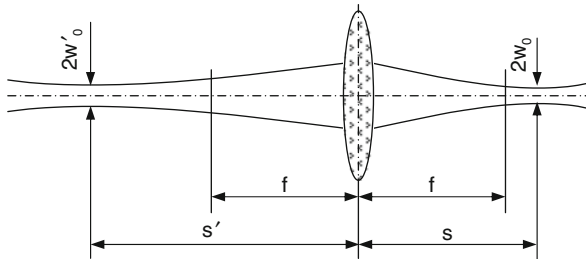


Fig. 3.9 Transmission performance of the Gaussian beam

3.8 Measurement Volume Size

On the optical side of LDA techniques, the measurement volume behaves as the key element in system operations. Both the measurement volume size and the specified optical performance determine the quality of flow measurements. In general, the measurement volume should always be created by arranging the intersection of two laser beams on their waists respectively. On one side, this requirement facilitates the high light intensity in the measurement volume, as this is necessary for detecting small particles passing through the measurement volume. On the other side, the plane wave front at the laser beam waist enables one to create uniform fringes in the measurement volume and hence to enhance the reliability and accuracy of measurements. Otherwise fringe distortion in the measurement volume will occur and lead to measurement errors (see Chap. 16).

For this reason and in general, the measurement volume is created at the waists of two laser beams. The form of the measurement volume can be approximated to be an ellipsoid, as illustrated in Fig. 3.10. The thickness i.e. the diameter of the measurement volume is given by the laser beam thickness at the beam waist

$$d_{mv} = \frac{2w_0}{\cos \alpha} \quad (3.77)$$

with α as the half intersection angle between two laser beams.

The thickness of the measurement volume is proportional to the laser beam thickness. It depends therefore on the optical arrangement of laser beams regarding the focal length of the used optical lens because of Eq. (3.75). More about this dependence will be presented in Chap. 4 on the optical configuration of a concrete LDA system. In general, the thickness of the measurement volume is in the order of about 0.05–0.1 mm.

With regard to the fringe spacing in the measurement volume, as given in Eq. (3.46), the number of fringes in the measurement volume is then calculated as

$$N = \frac{d_{mv}}{\Delta x} = 4 \frac{w_0}{\lambda_0} \tan \alpha \quad (3.78)$$

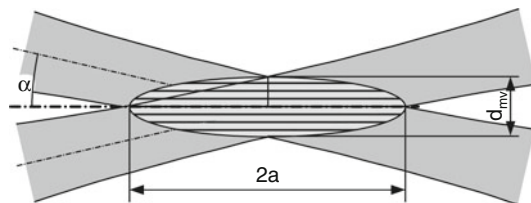


Fig. 3.10 Specification of the measurement volume size

The length of the measurement volume depends, for the same reason, both on the laser beam waist thickness and the crossing angle between two laser beams. According to Fig. 3.10 it is calculated as

$$2a = \frac{d_{mv}}{\tan \alpha} = \frac{2w_0}{\sin \alpha} \quad (3.79)$$

In comparison with the thickness of the measurement volume, the measurement volume has usually a finite length of about 0.5–3 mm, again depending on the optical arrangement of laser beams.

The geometrical dimension of the measurement volume is defined here independent of the particle size. In reality, the calculated measurement volume size is applicable to small particles of diameters that are comparable to or smaller than the fringe spacing. For large particles that could still scatter the laser light and hence be detected even if the particle center is outside of the measurement volume, the effective detection volume is larger than the independent geometrical measurement volume. Such a dependence of the detection volume size on the particle size is especially crucial in the particle size and mass flux measurements (Zhang et al. 1998, Zhang and Ziada 2000) by means of the Phase Doppler Anemometry (PDA), which is an extended method of LDA, see Albrecht et al. (2003).

Chapter 4

LDA Systems

4.1 Hardware and Optical Components

Based on advanced development of laser and computer technologies as well as on extended requirements in high quality flow measurements, LDA systems have become commercially well available and state of the art products. The hardware of an LDA system consists of transmitting and receiving units. The optical component in the transmitting unit commonly counts the laser, the laser beam transmitter including the Bragg cells and splitters, the fiber and the LDA-head, as shown in Fig. 4.1a for a system of Dantec Dynamics. The laser that is mostly used in LDA measurements is the argon-ion laser that basically provides three selectable wavelengths of 514.5, 488 and 476.5 nm. An LDA system is usually configured to use the laser light of the wavelength 514.5 (green) and 488 (blue) nanometers. After getting into the transmitter, the laser is separated and split into a pair of green and a pair of blue beams. For the purpose of resolving velocity directions, the light frequencies respectively in one green and one blue beams are shifted by Bragg cells, typically for 40 MHz. In some optical configurations, the Bragg cell also serves as the beam splitter. Four laser beams are then conducted into four fibers that are bundled and connected to the LDA head. A two-component LDA head is usually configured such that the plane of two green beams is perpendicular to the plane of two blue beams. This arrangement ensures the measurements of two perpendicular velocity components. The front lens on the LDA head enables all four laser beams to be focused at a unique point for forming the LDA measurement volume. By changing this front lens for different focal lengths the distance of the measurement volume to the LDA head can be changed. Corresponding geometrical and optical properties of the measurement volume in using the lens of different focal lengths will be described in Sect. 4.2.

Because of the use of fiber techniques, LDA optics is sometimes also called the fiber-optic LDA.

The receiving unit of a LDA system commonly includes the components such as the receiving optics, photodetectors like photomultipliers (PM), the signal processor and a computer for both controlling measurements and evaluating measurement data. In the act of using two pair of laser beams, the backward scattered laser light

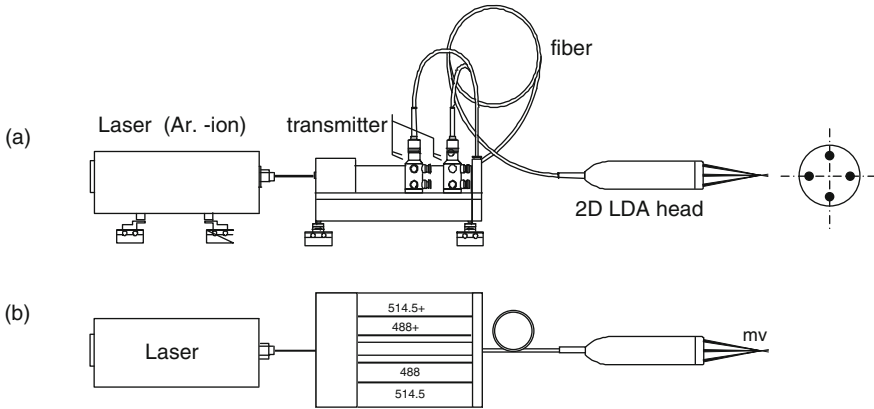


Fig. 4.1 Transmitting optics of an LDA system (Dantec Dynamics)

contains two sequences of light signals and hence is informative of two-component flow velocities. As shown in Fig. 4.2 for the most common case, the LDA head with the corresponding front lens also serves as the receiving unit. The scattered laser light is collected and focused onto the plane end of a supplementary fiber. At another end of the fiber which is usually integrated into the transmitter, the light is firstly separated into two parts of wavelengths 514.5 and 488 nm. These are then guided to respective photomultipliers which convert the light signals into electronic signals. The signal processor and the computer finally work out signals involving the flow velocities and the velocity-time relations.

The LDA system, as shown in Fig. 4.2, is called the backward scattering system. The most relevant advantage of such a system is the consistency of the optical alignment between the transmitting and the receiving units. The LDA head can thus be placed mobile for flow measurements, without realignment each time. In contrast, the forward scattering system necessitates a separate optical receiver for receiving the forward scattered laser light. The background of sometimes configuring such

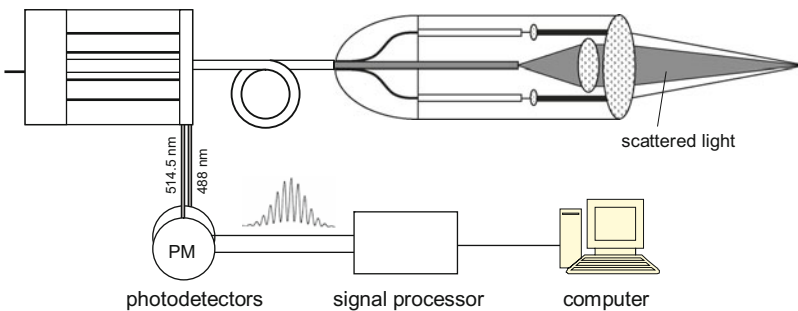


Fig. 4.2 Receiving optics of a backward scattering LDA system

a system is the utilization of high intensity of the forward scattered laser light. Because of the separation between the transmitting and the receiving units an optical realignment is usually always indispensable when the measurement point i.e. the measurement volume in the flow is changed. The realignment of the measurement volume will be very time-consuming, if it deals with measurements of internal flows. All refractions of both the transmitting light beams and the scattering light on diverse medium interfaces (as air-glass and glass-flow) have to be concerned.

LDA systems that use other laser lights (e.g. diode laser) rather than the argon-ion lasers have also been found in the practical applications.

In some few other applications with special optical configurations, coincident measurements of three particular velocity components have been carried out (Hüttmann et al. 2007, Richter and Leder 2006). In these applications, the additional laser light of the wavelength of 476.5 nm has usually been used. As demonstrated in Fig. 4.3 for instance, usually it deals with the measurements of non-orthogonal velocity components. The complete flow information including all three velocity components and the turbulence quantities in the Cartesian coordinate system can be obtained through the appropriate coordinate transformation. More about this technique will be presented in Chap. 6.

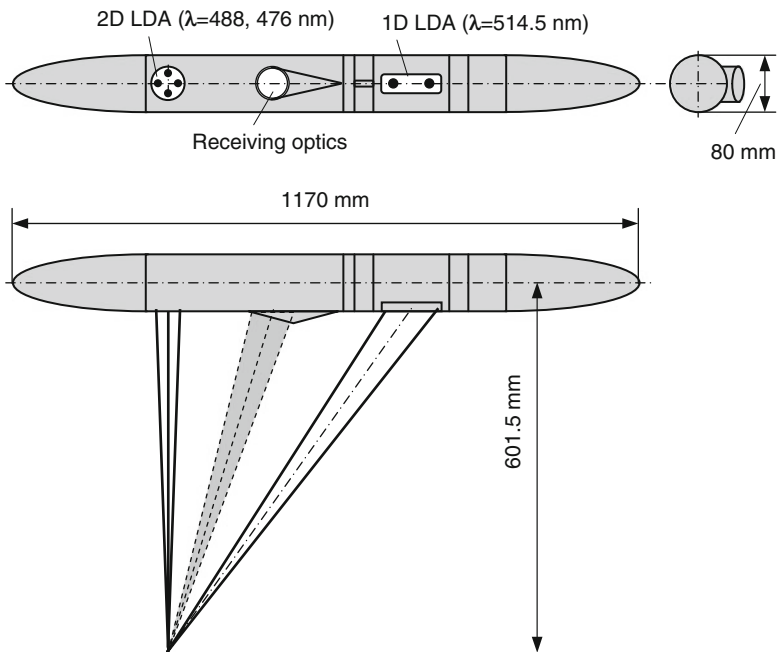


Fig. 4.3 Integrated three-component LDA head, applied for in-water measurements (Richter and Leder 2006)

4.2 Specification of LDA Measurement Volumes

It has been indicated in Sect. 3.8 that the measurement volume size depends on the optical configuration and the used optical lens which determines both the beam crossing angle and the waist thickness of each laser beam. In all LDA configurations, the laser beam crossing is achieved by the lens on the LDA head. Usually each laser beam prior to the lens is configured to be a nearly parallel light bundle. The diameter of such a light bundle is of about $2w'_0 = 1 \sim 2$ mm. By considering this thickness as the waist diameter of a light bundle and according to Eq. (3.74) for the laser light with a wavelength $\lambda = 500$ nm, the divergence angle of the light bundle of a diameter $2w'_0 = 2$ mm is only about 0.009° . Correspondingly the Rayleigh length is calculated from Eq. (3.66) to be $z'_R = 6283$ mm. In all commercial LDA systems, the laser beam thickness $2w'_0$ prior to the lens is configured to be a fixed value. Another fixed value is the distance $2d$ between two laser beams of a beam pair (Fig. 4.4). By changing the lens on the LDA head, both the geometrical dimensions and the optical properties (brightness, fringe spacing etc.) of the measurement volume will get updated. Applying Eq. (3.76) with respect to $f \ll z'_R$ i.e. $f/z'_R \ll 1$ yields

$$s = f \quad (4.1)$$

The waist of the laser beam thus coincides with the focal point of the lens on the LDA head. The crossing of two laser beams in a beam pair at the beam waists has been thus ensured.

The waist thickness of each laser beam at the beam crossing point (measurement volume) can be calculated from Eq. (3.75) with respect to $(s' - f)/z'_R \ll 1$ as

$$w_0 = \frac{f}{z'_R} w'_0 \quad (4.2)$$

It is thus directly proportional to the focal length of the lens used on the LDA head. The corresponding thickness of the measurement volume is then given from Eq. (3.77) as

$$d_{mv} = \frac{2f}{z'_R \cos \alpha} w'_0 \quad (4.3)$$

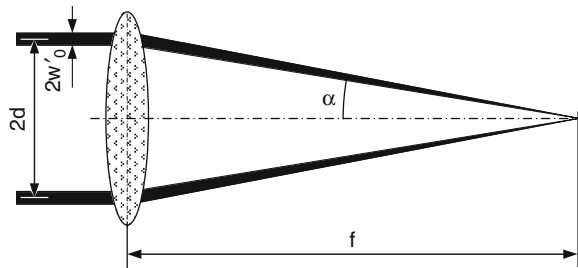


Fig. 4.4 Creation of LDA measurement volume and basic parameters determining the measurement volume size

In using the lens with a small focal length, for instance, small thickness and thus high brightness of the measurement volume can be achieved. This could be very meaningful for LDA measurements at which small natural particles in the flow should be used.

Furthermore, the focal length of the lens simply determines the crossing angle between two laser beams and thus the fringe spacing in the measurement volume. This determination relation is given from Eq. (3.46) as

$$\Delta x = \frac{\lambda_0}{2 \sin \alpha} = \frac{\lambda_0}{2} \sqrt{1 + \frac{f^2}{d^2}} \quad (4.4)$$

The number of fringes in the measurement volume can be calculated by Eq. (3.78). As it can be confirmed with respect to $\tan \alpha = d/f$ and Eq. (4.2), the number of fringes remains unchanged while changing the lens for another focal length:

$$N = 4 \frac{w_0}{\lambda_0} \frac{d}{f} = 4 \frac{d}{\lambda_0} \frac{w'_0}{z'_R} \quad (4.5)$$

The length of the measurement volume, according to Eq. (3.79) with respect to Eq. (4.2), is calculated as

$$2a = \frac{2f}{\sin \alpha} \frac{w'_0}{z'_R} = 2f \frac{w'_0}{z'_R} \sqrt{1 + \frac{f^2}{d^2}} \quad (4.6)$$

It largely depends on the focal length of used front lens on the LDA head.

In Table 4.1 considering the optical configuration of a standard LDA head manufactured by Dantec Dynamics, calculation examples of geometrical properties of the measurement volume have been shown. While the thickness of the measurement volume is usually in the order of about 0.1 mm, the measurement volume length varies between 0.5 and 5 mm. It should be mentioned that the use of the lens with a long focal length will reduce both the brightness of the measurement volume and the spatial resolution in velocity measurements. In addition, the effective aperture of the receiving optics to the measurement volume decreases too, leading to weakening of signals to be detected.

Table 4.1 Optical configurations and geometrical properties of the measurement volume, example of a standard LDA head $\phi 60$ of Dantec Dynamics

$\lambda_0 = 514.5 \text{ nm}$, $2w'_0 = 2.2 \text{ mm}$, $2d = 38 \text{ mm}$				
Focal length of the lens f	mm	160	400	600
Beam intersection angle $2\alpha_0$	deg	13.54	5.44	3.63
Beam waist radius w_0	mm	0.024	0.060	0.089
Measurement volume diameter d_{mv}	mm	0.05	0.12	0.18
Measurement volume length $2a$	mm	0.40	2.51	5.65
Fringe spacing Δx	μm	2.18	5.42	8.13
Number of fringes N	–	22	22	22

Chapter 5

Basic Data Processing Methods in LDA Measurements

Most flows encountered in nature and in practical applications are turbulent flows which are specified by high rate velocity fluctuations. In stationary flows, flow fluctuations are merely originated from flow turbulence and hence are completely of randomness. Depending upon the environmental flow conditions, the fluctuation frequency may reach the level of thousands of hertz. For measurements of turbulent flows with such a high velocity fluctuation rate, the LDA method probably provides a most efficient tool. It is non-intrusive, highly accurate and able to highly resolve the flow both in the time and spatial extensions.

LDA measurements basically provide the time series of velocities, to be accurate, the velocity components (see Fig. 2.1). The data processing from LDA measurements finally depends on the specification parameters of respective flow processes and thus on the purpose of conducting flow measurements. The simplest case is probably the measurement of the velocity profile in a channel flow, from which the volumetric flow rate can be calculated. In many other cases, the flow turbulence and its effect on the associated flow processes could be much more relevant. Especially in dealing with non-stationary or periodic flows, corresponding data processing methods have to be worked out, with which all process-relevant flow parameters and dimensionless numbers can be obtained from the time series of measured velocities. In addition, even in the case of dealing with the mean flow velocity and because of the effect of velocity bias, the arithmetic mean from LDA measurements could be insufficient for the required measurement accuracy. Special data processing will then be needed, see Chaps. 11, 12 and 17.

In this chapter, only the general methods of data processing will be described.

5.1 Direct Data Processing for Mean Velocities and Velocity Fluctuations

The stationary turbulent flow is described by the mean velocity and the flow fluctuations, as expressed by Eq. (2.1) with respect to the velocity component u . Based on LDA measurements, the arithmetic mean i.e. the sample mean of the velocity component u , for instance, is calculated as

$$\bar{u} = \frac{1}{N} \sum_{i=1}^N u_i \quad (5.1)$$

with N as the total number of velocity samples.

In assuming the known distribution of measurement data like that in Eq. (2.3) or in Fig. 2.1, the sample mean in the above equation can also be expressed by

$$\bar{u} = \int_{-\infty}^{\infty} p_u u du \quad (5.2)$$

Herein p_u simply represents the probability density function of velocity distribution from the measurement. It is related to the velocity component u and is not necessarily of the symmetrical form.

Velocity fluctuations involved in the corresponding velocity component can be described, in the statistical specification, by the standard deviation of the mean velocity, as presented in Eq. (2.2). As a statistical measure the so-called root mean square (rms) is calculated by

$$rms_u = \sqrt{u'^2} = \sqrt{\frac{1}{N} \sum_{i=1}^N (u_i - \bar{u})^2} \quad (5.3)$$

Basically, the standard deviation differs from the root mean square in the above equation in that it is calculated from the same statistics as in Eq. (5.3), however, with $1/(N-1)$ in place of $1/N$. Because of large sample size (N) in all LDA measurements, the difference between two statistical quantities is negligibly small, so that there is usually no need to make any distinction between them. The standard deviation σ_u in the mean velocity of a velocity component can thus be represented by the root mean square. In using $\sigma_u = rms_u$ it is further calculated from above equation

$$\sigma_u^2 = \frac{1}{N} \sum_{i=1}^N (u_i - \bar{u})^2 = \frac{1}{N} \sum_{i=1}^N u_i^2 - \frac{2}{N} \sum_{i=1}^N u_i \bar{u} + \frac{1}{N} \sum_{i=1}^N \bar{u}^2 \quad (5.4)$$

Because of $\frac{1}{N} \sum u_i \bar{u} = \bar{u}^2$ and $\frac{1}{N} \sum \bar{u}^2 = \bar{u}^2$ one obtains

$$\sigma_u^2 = \overline{u^2} - \bar{u}^2 \quad (5.5)$$

This relationship will be used in Chap. 17 for estimating the effect of velocity bias on the measurement accuracy.

The square of the standard deviation, as given in Eq. (5.5), is also called the variance. It represents the normal turbulent stress related to the respective velocity

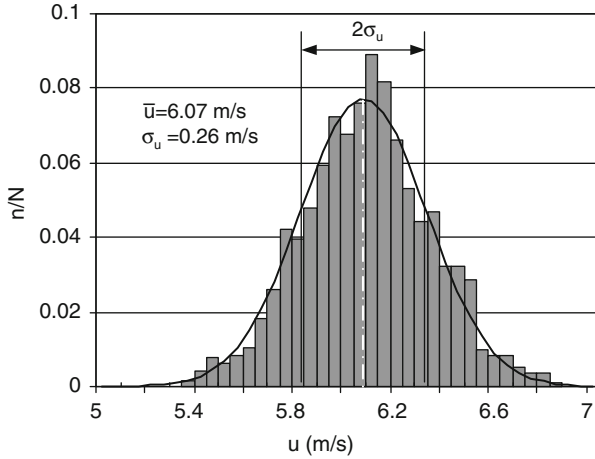


Fig. 5.1 Normalized histogram of velocities and the related Gaussian distribution

component. Both the mean velocity and the standard deviation can be graphically represented by the so-called histogram, as shown in Fig. 5.1 for example of an LDA measurement. This histogram is calculated in such a way that the number of velocity events in each bin is normalized by the total number N of velocity samples. Because of the randomness of velocity fluctuations around the mean velocity, the histogram is generally of symmetrical form and can be well approximated by the Gaussian probability density function as given by Eq. (2.3). In Fig. 5.1 with calculated Gaussian distribution, the mean velocity is confirmed to have the maximum probability in the histogram. The standard deviation measures the variability of velocities. In detail, in the velocity spread of $2\sigma_u$, the fluctuation velocity occurs with a probability of 68.3%, see Fig. 2.2.

It should be mentioned that because of the effect of velocity bias (Chap. 17) the symmetry of the histogram constructed from LDA measurements is always more or less disturbed.

In relying on LDA measurements, from which the root mean square is calculated by Eq. (5.3), the turbulence intensity of the considered turbulent flow with three-dimensional velocity fluctuations is represented by

$$Tu = \frac{1}{\sqrt{\bar{u}^2 + \bar{v}^2 + \bar{w}^2}} \sqrt{\frac{1}{3}(rms_u^2 + rms_v^2 + rms_w^2)} \quad (5.6)$$

Another statistical parameter that can be obtained from measurements is the covariance that is related to two orthogonal velocity components. Like Eq. (5.4) and in considering the velocity components u and v , this is calculated as

$$\overline{u'v'} = \frac{1}{N} \sum_{i=1}^N (u_i - \bar{u})(v_i - \bar{v}) \quad (5.7)$$

In the similar way of calculating Eq. (5.5), one obtains

$$\overline{u'v'} = \overline{uv} - \bar{u}\bar{v} \quad (5.8)$$

This parameter from the statistical evaluation of the flow turbulence actually represents one shear stress in the Reynolds stress matrix that has been shown in Eq. (2.11). It also represents the anisotropy of flow turbulence because it usually does not vanish. According to the calculation algorithm that is shown in Eq. (5.8), the value of the turbulent shear stress may be positive and negative, depending on both the velocity of fluctuations themselves and the choice of the coordinate system. For this reason, an anisotropic turbulence could only be completely described by considering all components of the turbulent shear stress in the respective Reynolds stress matrix.

As can be confirmed from above calculations, determinations of basic turbulence quantities such as $\overline{u'v'}$ clearly require synchronized i.e. coincident measurements of two velocity components. More about the related measurement technique is outlined in Chaps. 6 and 8.

Based on the graphical presentation of turbulent flows in the form of histogram i.e. the probability distribution of flow velocities according to Fig. 5.1, the form of the distribution is sometimes representative for comparing different turbulence properties in internal flows (Durst et al. 1992, 1996). There are two parameters that are often used to describe the form of velocity distributions: the skewness and flatness. The skewness of the probability distribution of the velocity component u is defined by

$$S = \overline{u'^3} = \frac{1}{N} \sum_{i=1}^N (u_i - \bar{u})^3 \quad (5.9)$$

It depicts the scale of the asymmetry of the probability distribution of the velocity component u around its mean value. In most stationary turbulent flows, random velocity fluctuations occur symmetrically around the respective means. The skewness is then close to zero.

The flatness of the probability distribution of a velocity component is defined by

$$F = \overline{u'^4} = \frac{1}{N} \sum_{i=1}^N (u_i - \bar{u})^4 \quad (5.10)$$

In reality and like the standard deviation, the flatness as a statistical parameter represents the variability of the velocity that is considered. In order to show that this flatness is equivalent to, as well as related with the standard deviation, the Gaussian probability distribution given at Eq. (2.3) is considered as a reference. Corresponding flatness is calculated as

$$F_{\text{Gauss}} = \int_{-\infty}^{\infty} \text{pdf}_u(u - \bar{u})^4 du = 3\sigma_u^4 \quad (5.11)$$

It is simply proportional to the fourth power of the standard deviation. Because of this, the flatness generally does not provide any more about the extent of flow fluctuations than the standard deviation. In addition, it has hardly any physical and mechanical significance, while the standard deviation squared (σ_u^2) represents the turbulent kinetic energy.

From the derived equation for the flatness of a Gaussian probability distribution, the so-called flatness factor, also known as the kurtosis factor, is given as

$$K_{\text{Gauss}} = \frac{F}{\sigma_u^4} = 3 \quad (5.12)$$

5.2 Weighting Facilities of Mean Velocity and Fluctuations

Statistical calculations given in Eqs. (5.1), (5.2), (5.3), (5.4), (5.5), (5.6), and (5.7) are simply calculations of respective arithmetical means. Because data acquisitions in all LDA measurements are not time-equidistant, results from above calculations do not exactly represent the corresponding time-averages of respective flow parameters. The apparent deviations of the sample means from those of time-averages are called the bias. Among many sources leading to bias in velocity measurements, velocity fluctuations have been concerned to play a primary role. This type of bias is known as velocity bias. It arises from the mechanism that the high velocities will be more frequently sampled than the low velocities, provided tracer particles in the flow are distributed homogeneously and uniformly. Consequently, the sample mean of velocities from the measurement shifts towards the upper value. This phenomenon was firstly confirmed by McLaughlin and Tiederman (1973) and has been ever since widely investigated with respect to its estimations and corrections. In all traditional considerations, the velocity bias has been uniquely categorized to be an error that is involved in LDA measurements. Because the appearance of velocity bias is directly related to the non-uniformity of flow velocities, the velocity bias is indeed a flow rather than an optical phenomenon. In addition, the biased mean velocity exactly represents a characteristic mean, which should be applied to calculate the momentum flux in the flow. For more details about this concept, see Chap. 17.

With respect to the background of velocity bias, different correction methods have been developed and implemented. The most common method is to use a weighting factor f_w in calculating arithmetical means of respective flow parameters. The mean velocity, its standard deviation and the covariance will then be calculated as

$$\bar{u} = \sum_{i=1}^N f_{w,i} u_i \quad (5.13)$$

$$rms_u = \sqrt{\sum_{i=1}^N f_{w,i} (u_i - \bar{u})^2} \quad (5.14)$$

$$\overline{u'v'} = \sum_{i=1}^N f_{w,i} (u_i - \bar{u})(v_i - \bar{v}) \quad (5.15)$$

The weighting factor in dimensionless form is used here for instance to compensate for the effect of irregularity in sampling velocities. For this purpose, McLaughlin and Tiederman (1973) suggested the use of the reciprocal of each individual velocity, related to a total sum, as the weighing factor in the above equations. Theoretically it should be the reciprocal of the magnitude of each velocity vector, which is usually not available because of the lack of three-component LDA measurements.

Another more available weighting factor used to correct the effect of velocity bias is the transit time of each particle while passing through the LDA measurement volume. This correction method is indeed comparable to that of using inverted magnitude of velocity vectors simply because of the proportionality between them by assuming the constant measurement volume thickness. The measurement of the transit time of each particle, however, is in principle much more convenient than that of each velocity vector. Also to be mentioned are measurement uncertainties that might result from both the non-uniformity of fringe spacing in the measurement volume (Chap. 16) and the use of non-monodisperse particles. Large particles, for instance, lead to the existence of long transit time while passing through the measurement volume (i.e. the detection volume in the present aspect).

Besides the use of waiting factors, another method to suppress the effect of velocity bias is to sample flow velocities by controlling LDA detection unit for time-equidistant signals. This method, however, has nowadays not found any practical applications.

Actually, the most important thing concerning the effect of velocity bias is the estimation of the maximal possible extent of influences rather than the correction of it by means of complex data processing or expensive measurement techniques with hard- and software modifications. In the case where the resultant inaccuracy does not exceed the limit that is specified by measurements, no correction of velocity bias is necessary. In addition, velocity bias that is involved in the sample mean of velocities, for instance, does not imply any error, if the momentum flux (instead of the volumetric flux) in the area of measurement volume should be calculated. Based on these viewpoints it appears to be indispensable to quantify the effect of velocity bias first. Because the velocity bias is actually a flow phenomenon and thus can be considered to be related with a turbulence parameter like the turbulence intensity, its accurate quantification can be conducted anyway. Based on this conception, complete calculations for quantifying the effect of velocity bias in turbulent flows with three-dimensional velocity fluctuations have been carried out by Zhang (2002), as this will be shown in Chap. 17 for details.

Chapter 6

Linear Transformation of Velocities and Turbulent Stresses

LDA measurements are known as measurements of velocity components, as has been demonstrated by Eq. (3.39). Because these velocity components are found in the LDA coordinate system, it is always necessary to transform them into the flow field system. This transformation applies not only to the mean velocities, but also to the turbulence quantities. Very often it deals with the two-dimensional orthogonal transformation because usually two orthogonal velocity components are directly obtainable from LDA measurements. Exceptions will be encountered if for instance the third velocity component does not agree to the perpendicular of the other two. In this chapter, both the orthogonal and the non-orthogonal velocity transformations between the LDA and the flow field systems will be presented. It mainly takes account of the two-dimensional coordinate transformation, as this is of great practical relevance. For three-dimensional coordinate transformation concerning the turbulence quantities the readers are referred to Appendix C.

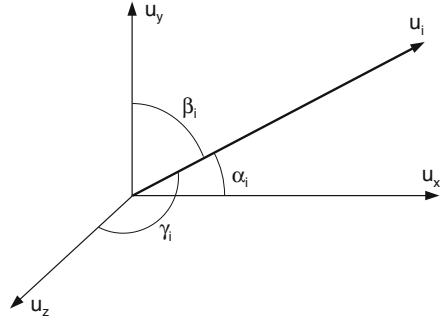
6.1 Orthogonal Linear Transformation

6.1.1 Velocity Transformation

Velocity components in the LDA optical system are denoted by u_1 , u_2 and u_3 that are assumed to be perpendicular to each other. The flow field is usually given in the Cartesian coordinate system (x, y, z) that may not agree with the LDA optical system. The velocity transformation between these two coordinate systems is the simplest orthogonal transformation. It is assumed that LDA components u_i ($i = 1, 2, 3$) lie at angles α_i , β_i and γ_i respectively to the flow field coordinates x , y and z , as shown in Fig. 6.1. Then the following velocity transformation is available

$$\begin{bmatrix} u_1 \\ u_2 \\ u_3 \end{bmatrix} = \begin{bmatrix} \cos \alpha_1 & \cos \beta_1 & \cos \gamma_1 \\ \cos \alpha_2 & \cos \beta_2 & \cos \gamma_2 \\ \cos \alpha_3 & \cos \beta_3 & \cos \gamma_3 \end{bmatrix} \begin{bmatrix} u_x \\ u_y \\ u_z \end{bmatrix} = R \begin{bmatrix} u_x \\ u_y \\ u_z \end{bmatrix} \quad (6.1)$$

Fig. 6.1 Relationship between velocity components in both the LDA system with orthogonal coordinates and the Cartesian field coordinate system (x, y, z)



In this equation, R represents the orthogonal transformation matrix. Its inverse is simply equal to its transpose, as given by

$$R^{-1} = R' \tag{6.2}$$

Eq. (6.1) is given to generally transform velocities between two coordinate systems. In a two-dimensional $x - y$ plane, as shown in Fig. 6.2 with redefined angles ($\alpha_1 = \varphi, \alpha_2 = 90 + \varphi, \beta_1 = 90 - \varphi$ and $\beta_2 = \varphi$ in degree), the transformation matrix is simplified to

$$R = \begin{bmatrix} \cos \varphi & \sin \varphi \\ -\sin \varphi & \cos \varphi \end{bmatrix} \tag{6.3}$$

With substitutions of $u_1=u$ and $u_2=v$, corresponding velocity transformations are given by

$$u = u_x \cos \varphi + u_y \sin \varphi \tag{6.4}$$

$$v = -u_x \sin \varphi + u_y \cos \varphi \tag{6.5}$$

as well as in the reverse form

$$u_x = u \cos \varphi - v \sin \varphi \tag{6.6}$$

$$u_y = u \sin \varphi + v \cos \varphi \tag{6.7}$$

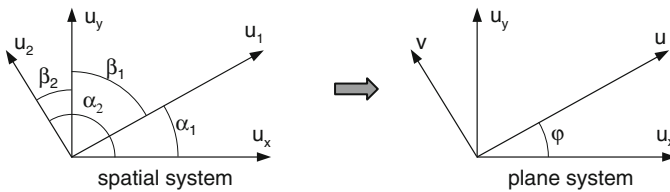


Fig. 6.2 Simplification of expressing velocity components in the plane coordinate system

These transformations of velocity components can be directly applied to both the mean and fluctuation velocities. For the transformation of turbulent stresses which are components of a Reynolds stress matrix, corresponding calculations will be shown in the following section.

6.1.2 Turbulent Stress Transformation

In Chap. 2 with respect to Fig. 2.3, it has been distinguished between isotropic and anisotropic turbulences. Because isotropic turbulence is characterised by turbulent normal stresses that are independent of the coordinate system, it will not be further considered.

The transformation of anisotropic turbulence quantities that are generally represented by the Reynolds stress matrix according to Eq. (2.11) again follows the matrix algebra. It is assumed that in the LDA coordinate system the stress tensor is given by σ_{ij} . The turbulent stresses in the flow system ($x - y - z$) can then be obtained from the following linear transformation

$$\sigma_{mn} = \begin{bmatrix} \sigma_{xx} & \tau_{xy} & \tau_{xz} \\ \tau_{yx} & \sigma_{yy} & \tau_{yz} \\ \tau_{zx} & \tau_{zy} & \sigma_{zz} \end{bmatrix} = R' \sigma_{ij} R \quad (6.8)$$

In again considering the turbulent stress distribution in the $x - y$ plane (Fig. 6.2), the Reynolds turbulent stresses related to the velocity components u_x and u_y are then derived from Eq. (6.8) as

$$\sigma_{xx} = \sigma_{uu} \cos^2 \varphi + \sigma_{vv} \sin^2 \varphi - \tau_{uv} \sin 2\varphi \quad (6.9)$$

$$\sigma_{yy} = \sigma_{uu} \sin^2 \varphi + \sigma_{vv} \cos^2 \varphi + \tau_{uv} \sin 2\varphi \quad (6.10)$$

$$\tau_{xy} = \frac{1}{2}(\sigma_{uu} - \sigma_{vv}) \sin 2\varphi + \tau_{uv} \cos 2\varphi \quad (6.11)$$

These equations describe the orthogonal transformation of two-dimensional turbulent stresses between two coordinate systems, which are in the same two-dimensional plane and of a difference φ in the rotation angle. In reality, such a coordinate transformation also represents a way to calculate the plane distribution of respective turbulence quantities, as shown below.

6.1.3 Directional Distribution of Turbulent Stresses

6.1.3.1 On the Basic Parameters σ_{xx} , σ_{yy} and τ_{xy}

The anisotropic turbulence is characterized by the directional dependence of intensities of velocity fluctuations (Fig. 2.3b). In many cases, this directional dependence

i.e. the directional distribution of flow fluctuations is interesting because from it the maximum of both the turbulent normal and shear stresses can be determined. In general, the calculation of directional distribution of turbulent stresses is simply the transformation of respective turbulent stresses from given values in a basic coordinate system. This can be demonstrated by again considering Eq. (6.8) for velocity components in the $x - y$ plane (Fig. 6.2). The inverse calculation of Eq. (6.8) is given as follows

$$\sigma_{ij} = \begin{vmatrix} \sigma_{uu} & \tau_{uv} \\ \tau_{vu} & \sigma_{vv} \end{vmatrix} = R\sigma_{mn}R' \quad (6.12)$$

The component σ_{uu} , which is found by φ in the $x - y$ coordinate system (measured from the x -axis counter clockwise, Fig. 6.3) will be denoted by $\sigma_{\varphi\varphi}$. Thus one obtains from the above equation with substitutions of $\sigma_{\varphi\varphi} = \sigma_{uu}$ and in like manner $\tau_{\varphi,\varphi+90^\circ} = \tau_{uv}$

$$\sigma_{\varphi\varphi} = \sigma_{xx} \cos^2 \varphi + \sigma_{yy} \sin^2 \varphi + \tau_{xy} \sin 2\varphi \quad (6.13)$$

$$\tau_{\varphi,\varphi+90^\circ} = -\frac{1}{2}(\sigma_{xx} - \sigma_{yy}) \sin 2\varphi + \tau_{xy} \cos 2\varphi \quad (6.14)$$

Eq. (6.13) for instance shows the directional distribution of the turbulent normal stress in the $x - y$ plane based on given quantities σ_{xx} , σ_{yy} and τ_{xy} . As will be shown in Sect. 6.3, the square root of this normal stress and its directional distribution is precisely described by an ellipse function.

From the directional distribution of Reynolds turbulent stresses and according to Eq. (2.13) there exist in the two-dimensional $x - y$ plane two principal normal stresses with corresponding vanishing shear stresses. The orientation of two orthogonal principal normal stresses (σ_{11} and σ_{22}) are found from Eq. (6.13) by setting $d\sigma_{\varphi\varphi}/d\varphi = 0$ which leads to

$$\tan 2\varphi_m = \frac{2\tau_{xy}}{\sigma_{xx} - \sigma_{yy}} \quad (6.15)$$

Obviously two angles $\varphi_{m1} = \varphi_m$ and $\varphi_{m2} = \varphi_m + 90^\circ$ satisfy this condition. For the common reason $0 \leq \varphi_m < 90$ is agreed on in further calculations. For the anisotropic turbulence as shown in Fig. 2.3b, where the main orientation of velocity fluctuations is given by $\varphi_m \approx \bar{\varphi}$ as in most cases (see Chap. 8), there is $\tau_{xy} > 0$.

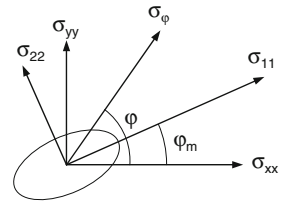


Fig. 6.3 Plane distribution of the turbulent normal stress with the first principal normal stress at φ_m

The principal normal stress that is found at φ_m is denoted by σ_{11} . It is calculated from Eq. (6.13) firstly as

$$\sigma_{11} = \sigma_{xx} \frac{1 + \cos 2\varphi_m}{2} + \sigma_{yy} \frac{1 - \cos 2\varphi_m}{2} + \tau_{xy} \sin 2\varphi_m \quad (6.16)$$

and further to

$$\sigma_{11} = \frac{1}{2}(\sigma_{xx} + \sigma_{yy}) + \frac{1}{2}(\sigma_{xx} - \sigma_{yy}) \cos 2\varphi_m + \tau_{xy} \sin 2\varphi_m \quad (6.17)$$

With respect to $\tau_{xy} > 0$ the principal normal stress σ_{11} in Eq. (6.16) represents the first principal of normal stress as $\sigma_I = \sigma_{11}$. Correspondingly, there is $\sigma_{II} = \sigma_{22}$ for the second principal of normal stress. As in the common case, it is $\sigma_I > \sigma_{II}$.

Inserting τ_{xy} from Eq. (6.15) into Eq. (6.17) yields

$$\sigma_{11} = \frac{1}{2}(\sigma_{xx} + \sigma_{yy}) + \frac{1}{2 \cos 2\varphi_m}(\sigma_{xx} - \sigma_{yy}) \quad (6.18)$$

To make further calculations, Eq. (6.15) is written, with respect to $\tau_{xy} > 0$, as

$$\cos 2\varphi_m = \frac{\sigma_{xx} - \sigma_{yy}}{\sqrt{(\sigma_{xx} - \sigma_{yy})^2 + 4\tau_{xy}^2}} \quad (6.19)$$

Eq. (6.18) then becomes

$$\sigma_{11} = \frac{1}{2}(\sigma_{xx} + \sigma_{yy}) + \sqrt{\frac{1}{4}(\sigma_{xx} - \sigma_{yy})^2 + \tau_{xy}^2} \quad (6.20)$$

The second principal of normal stress is found at $\varphi_{m2} = \varphi_m + 90^\circ$, as shown in Fig. 6.3. With the substitution of angle φ_{m2} in Eq. (6.18) one obtains immediately

$$\sigma_{22} = \frac{1}{2}(\sigma_{xx} + \sigma_{yy}) - \sqrt{\frac{1}{4}(\sigma_{xx} - \sigma_{yy})^2 + \tau_{xy}^2} \quad (6.21)$$

The corresponding Reynolds stress matrix is then given by

$$\sigma_{I,II} = \begin{bmatrix} \sigma_{11} & 0 \\ 0 & \sigma_{22} \end{bmatrix} \quad (6.22)$$

One of the most important properties of the stress matrix is that the sum of all three normal stresses is independent of the coordinate system used to represent the turbulent stresses, see Eq. (2.14). In a two-dimensional plane, the so-called first invariant of the matrix is thus expressed by

$$I_1 = \sigma_{11} + \sigma_{22} = \sigma_{xx} + \sigma_{yy} \quad (6.23)$$

As pointed out in Sect. 2.2 in the context of Eq. (2.12), only the absolute maximum value of the turbulent shear stress is representative for the flow state and can be considered as a parameter of the turbulent flow. In the similar way of getting φ_m for the maximum normal stress in the $x - y$ plane, the maximum value of the absolute turbulent shear stress is obtained from Eq. (6.14) to be given at the angle φ_τ which satisfies the condition

$$\tan 2\varphi_\tau = -\frac{\sigma_{xx} - \sigma_{yy}}{2\tau_{xy}} = -\frac{1}{\tan 2\varphi_m} \quad (6.24)$$

The relationship between φ_τ and φ_m in this equation also means $\varphi_\tau = \varphi_m \pm 45^\circ$. Because each turbulent shear stress is always related to the flow fluctuations in two orthogonal velocity components, the two velocity components are commonly assumed to be found counter clockwise at $\varphi_{\tau,1} = \varphi_m - 45$ and $\varphi_{\tau,2} = \varphi_m + 45$, respectively. For simplicity $\varphi_\tau = \varphi_{\tau,1}$ is applied in further calculations, in which $\varphi_\tau < 45$ and thus $2\varphi_\tau < 90$ are available because of $\varphi_m < 90^\circ$.

With respect to Eq. (6.24) the maximum shear stress is then derived from Eq. (6.14) to

$$\tau_{\max} = \left[1 + \frac{(\sigma_{xx} - \sigma_{yy})^2}{4\tau_{xy}^2} \right] \tau_{xy} \cos 2\varphi_\tau \quad (6.25)$$

With respect to $\cos 2\varphi_\tau = \sqrt{1/(1 + \tan^2 2\varphi_\tau)}$ one obtains

$$\tau_{\max} = \sqrt{\left(\frac{\sigma_{xx} - \sigma_{yy}}{2} \right)^2 + \tau_{xy}^2} \quad (6.26)$$

The maximum turbulent shear stress has been shown to be a function of parameters σ_{xx} , σ_{yy} and τ_{xy} . As seen in Eq. (6.14), these parameters are also used to represent the directional distribution of the turbulent shear stress. In actual fact, the interested distribution can also be shown to be a function of the maximum shear stress τ_{\max} only. For this reason the maximum shear stress is calculated from Eq. (6.14) firstly as

$$\tau_{\max} = -\frac{1}{2}(\sigma_{xx} - \sigma_{yy}) \sin 2\varphi_\tau + \tau_{xy} \cos 2\varphi_\tau \quad (6.27)$$

and then with respect to $\varphi_\tau = \varphi_m - 45^\circ$ as

$$\tau_{\max} = \frac{1}{2}(\sigma_{xx} - \sigma_{yy}) \cos 2\varphi_m + \tau_{xy} \sin 2\varphi_m \quad (6.28)$$

Combining this equation with Eq. (6.14) yields

$$\frac{\tau_{\varphi, \varphi+90^\circ}}{\tau_{\max}} = \frac{\sin 2\varphi - \frac{2\tau_{xy}}{\sigma_{xx} - \sigma_{yy}} \cos 2\varphi}{-\cos 2\varphi_m - \frac{2\tau_{xy}}{\sigma_{xx} - \sigma_{yy}} \sin 2\varphi_m} \quad (6.29)$$

The expression $2\tau_{xy}/(\sigma_{xx} - \sigma_{yy})$ in this equation will be replaced by Eq. (6.15). After a short rearrangement one obtains

$$\tau_{\varphi, \varphi+90^\circ} = \tau_{\max} \sin 2(\varphi_m - \varphi) \quad (6.30)$$

The directional distribution of the turbulent shear stress has been shown to be a sine function that has an amplitude equal to τ_{\max} . At the angle $\varphi = \varphi_m$, at which the maximum normal stress is found, the shear stress vanishes as $\tau(\varphi_m) = 0$.

The turbulent shear stress according to Eq. (6.30) may be positive and negative. This is only of mathematical significance, which must be considered while carrying out the coordinate transformation of the Reynolds stress matrix. By only considering the absolute value of the turbulent shear stress and its spatial distribution, Eq. (6.30) represents a polar rose curve in polar coordinates, as shown in Fig. 6.4 for $\varphi_m = 30^\circ$ and $\varphi_m = 0^\circ$, respectively.

Another special case is given for $\varphi = 0$. From Eq. (6.30) one obtains then

$$\tau_{xy} = \tau_{\max} \sin 2\varphi_m \quad (6.31)$$

The maximum shear stress clearly behaves as a key parameter with which other dependent turbulence quantities can be shown in the simple form. Combining Eq. (6.31) with Eq. (6.15) for instance yields

$$\sigma_{xx} - \sigma_{yy} = 2\tau_{\max} \cos 2\varphi_m \quad (6.32)$$

With respect to Eq. (6.26) for $\tau_{\max} > 0$ Eq. (6.20) is written as

$$\sigma_{11} = \frac{1}{2} (\sigma_{xx} + \sigma_{yy}) + \tau_{\max} \quad (6.33)$$

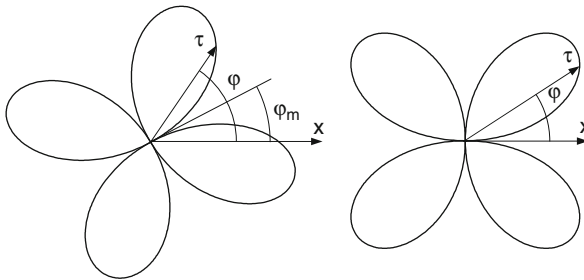


Fig. 6.4 Directional dependence of the turbulent shear stress in the polar coordinate system

This relationship can be well confirmed in the graphical Mohr's stress circle, see Sect. 6.3.2.

There are also some other relations which, however, appear not to be of much relevance and therefore are not shown here.

6.1.3.2 On the Basic Parameters σ_{11} and σ_{22}

In Eqs. (6.13) and (6.14), the directional distributions of both the normal and shear stresses have been shown in the function of given parameters σ_{xx} , σ_{yy} and τ_{xy} . On the other side, these distributions can also be shown as the function of two principal normal stresses σ_{11} and σ_{22} . According to Fig. 6.3 and in accounting for σ_{11} and σ_{22} as independent parameters, the normal stress in Eq. (6.13) is directly written, by changing indices and with respect to $\tau_{12} = 0$ at φ_m , as

$$\sigma_{\varphi\varphi} = \sigma_{11} \cos^2(\varphi - \varphi_m) + \sigma_{22} \sin^2(\varphi - \varphi_m) \quad (6.34)$$

Similarly there is from Eq. (6.14)

$$\tau_{\varphi, \varphi+90^\circ} = -\frac{1}{2}(\sigma_{11} - \sigma_{22}) \sin 2(\varphi - \varphi_m) \quad (6.35)$$

From these two general expressions of directional distributions of turbulent stresses some basic relationships can be obtained. For $\varphi = 0$ and $\varphi = 90^\circ$ for instance, one obtains

$$\sigma_{xx} = \sigma_{11} \cos^2 \varphi_m + \sigma_{22} \sin^2 \varphi_m \quad (6.36)$$

and

$$\sigma_{yy} = \sigma_{11} \sin^2 \varphi_m + \sigma_{22} \cos^2 \varphi_m \quad (6.37)$$

respectively.

In addition, it results from Eq. (6.35) for $\varphi = 0$

$$\tau_{xy} = -\frac{1}{2}(\sigma_{11} - \sigma_{22}) \sin(-2\varphi_m) = \frac{1}{2}(\sigma_{11} - \sigma_{22}) \sin 2\varphi_m \quad (6.38)$$

In comparing with Eq. (6.31), one obtains

$$\tau_{\max} = \frac{\sigma_{11} - \sigma_{22}}{2} \quad (6.39)$$

This relationship can also be obtained when comparing Eq. (6.35) with Eq. (6.30).

6.1.3.3 Approximation $\varphi_m \approx \bar{\varphi}$ and Simplifications

In above calculations, the angle φ_m for principal normal stress has often been applied to represent the directional distribution of the turbulent normal and shear stresses. An approximation to this angle should be noted. In a great deal of turbulent flows, the principal normal stress σ_{11} which is found at φ_m approximately coincides with the main flow direction $\bar{\varphi}$, as already illustrated in Fig. 2.3b. This approximation enables the angle φ_m to be determined merely from two velocity components in the form $\tan \varphi_m = \bar{u}_y / \bar{u}_x$. If compared with Eq. (6.15) it is evident that the approximation $\varphi_m \approx \bar{\varphi}$ much contributes to the simplification of treating turbulence quantities. In particular, experimental estimations of all related turbulence quantities can be considerably simplified, as will be fully described in Chap. 8.

6.2 Non-orthogonal Transformation

In most LDA applications, the LDA optics is designed for coincident measurements of two orthogonal velocity components in a two-dimensional plane. Based on these measurements, velocity components including the flow fluctuations and turbulence quantities in the flow field coordinate system can be obtained by orthogonal coordinate transformations, as treated in Sect. 6.1. The very different case will be encountered for instance at measurements of all three velocity components according to Fig. 4.3, in which the third velocity component is usually not perpendicular to the other two. Also in more frequent cases dealing with indirect measurements of the third velocity component through an additional one-component measurement, as illustrated in Fig. 6.5, non-orthogonal velocity components are again encountered.

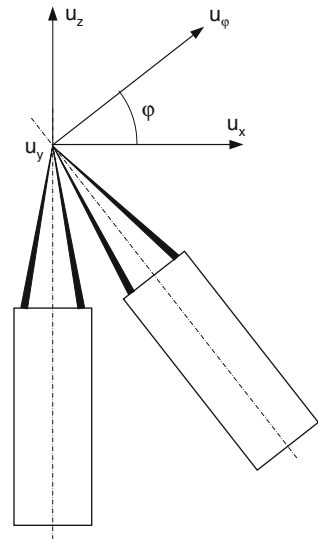


Fig. 6.5 Indirect measurement of the third velocity component u_z

In such situations and with regard to the coordinates given in Fig. 6.5, the third velocity component u_z is obtained from measurements of u_x and u_φ by

$$u_z = \frac{1}{\sin \varphi} (u_\varphi - u_x \cos \varphi) \quad (6.40)$$

This velocity transformation is usually applicable only to the mean velocity. It could, however, not be supposed to be able to transform each flow fluctuation. That is to say that the fluctuation velocity u'_z could not be determined from the fluctuation velocities u'_x and u'_φ , if these are not in coincidence. This circumstance of non-coincident measurements, however, does not restrict the determination of interested turbulence quantities based on statistical evaluations of flow fluctuations. Corresponding methods will be shown in Sect. 6.2.2.

6.2.1 Velocity Transformation

The case that is shown in Fig. 6.5 can be generalized to that of in Fig. 6.6 where velocity transformation between LDA and flow field system should be conducted. Obviously both velocity components u and v can be written as

$$u = u_x \cos \varphi_u + u_y \sin \varphi_u \quad (6.41)$$

and

$$v = u_x \cos \varphi_v + u_y \sin \varphi_v \quad (6.42)$$

respectively.

For mathematical convenience such a velocity transformation is again described by the matrix form as

$$\begin{bmatrix} u \\ v \end{bmatrix} = \begin{bmatrix} \cos \varphi_u & \sin \varphi_u \\ \cos \varphi_v & \sin \varphi_v \end{bmatrix} \begin{bmatrix} u_x \\ u_y \end{bmatrix} = R \begin{bmatrix} u_x \\ u_y \end{bmatrix} \quad (6.43)$$

It is yet the purpose of the current section to calculate velocity components u_x and u_y in the flow system from velocity components u and v as measured by LDA.

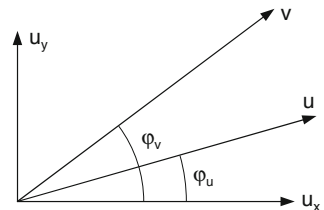


Fig. 6.6 Method of transforming velocity components u and v from LDA measurements into the field velocities u_x and u_y

Thus Eq. (6.43) is written in its inverse form as

$$\begin{bmatrix} u_x \\ u_y \end{bmatrix} = R^{-1} \begin{bmatrix} u \\ v \end{bmatrix} \quad (6.44)$$

with

$$R^{-1} = \frac{1}{\sin(\varphi_v - \varphi_u)} \begin{bmatrix} \sin \varphi_v & -\sin \varphi_u \\ -\cos \varphi_v & \cos \varphi_u \end{bmatrix} \quad (6.45)$$

Both the transformation matrix R and R^{-1} are no longer orthogonal matrixes as that in Eq. (6.3) and therefore there is $R^{-1} \neq R'$. Only for $\varphi_v - \varphi_u = 90^\circ$ the orthogonal transformation is again in effect.

For the special case of $\varphi_u = 0$ and in concerning the mean velocity components, one obtains from Eq. (6.44) besides $\bar{u}_x = \bar{u}$ also

$$\bar{u}_y = \frac{1}{\sin \varphi_v} (\bar{v} - \bar{u} \cos \varphi_v) \quad (6.46)$$

It completely agrees with Eq. (6.40) for the third velocity component.

6.2.2 Turbulent Stress Transformation

The measurement arrangement shown in Fig. 6.6 does not directly provide turbulent stresses as given in Reynolds stress matrix. In order to establish relationships between turbulent stresses in LDA and flow field coordinate systems, it will firstly be assumed that coincident measurements of velocity components u and v enables the covariance $\overline{u'v'}$ to be calculated. This means that the related turbulent shear stress τ_{uv} is assumed to be known. This assumption is only of mathematical reasoning. As soon as all relationships have been established, it will be clear how the parameter τ_{uv} can be eliminated. Based on the rule of matrix calculations, the Reynolds stress matrix in the flow field system with Cartesian coordinates is calculated by

$$\sigma_{mn} = \begin{bmatrix} \sigma_{xx} & \tau_{xy} \\ \tau_{yx} & \sigma_{yy} \end{bmatrix} = R^{-1} \sigma_{ij} (R^{-1})' \quad (6.47)$$

Herein the Reynolds stresses relating to velocity components u and v are given by σ_{uu} , σ_{vv} and τ_{uv} with $\tau_{uv} = \tau_{vu}$. The transformation matrix $(R^{-1})'$ is the transpose of the matrix R^{-1} which is given by Eq. (6.45).

From Eq. (6.47) one obtains¹

¹Another possibility to transform the turbulent stresses from the non-orthogonal into the orthogonal coordinate system will be presented here based on Fig. 6.6. In applying Eq. (6.41) and (6.42) to velocity fluctuations in respective velocity components, one obtains

$$\begin{aligned} u' &= u'_x \cos \varphi_u + u'_y \sin \varphi_u \\ v' &= u'_x \cos \varphi_v + u'_y \sin \varphi_v \end{aligned}$$

$$\sigma_{xx} = \frac{\sigma_{uu} \sin^2 \varphi_v + \sigma_{vv} \sin^2 \varphi_u - 2\tau_{uv} \sin \varphi_u \sin \varphi_v}{\sin^2 (\varphi_v - \varphi_u)} \quad (6.48)$$

$$\sigma_{yy} = \frac{\sigma_{uu} \cos^2 \varphi_v + \sigma_{vv} \cos^2 \varphi_u - 2\tau_{uv} \cos \varphi_u \cos \varphi_v}{\sin^2 (\varphi_v - \varphi_u)} \quad (6.49)$$

$$\tau_{xy} = -\frac{\sigma_{uu} \sin 2\varphi_v + \sigma_{vv} \sin 2\varphi_u - 2\tau_{uv} \sin (\varphi_u + \varphi_v)}{2 \sin^2 (\varphi_v - \varphi_u)} \quad (6.50)$$

Like for Eq. (6.46), simplifications for special case of $\varphi_u = 0$ can be made. Corresponding results are then applicable to the case that has been shown in Fig. 6.5. Especially for $\varphi_v - \varphi_u = 90^\circ$ the above equations are simplified to Eqs. (6.9), (6.10), and (6.11).

The above calculations that lead to Eqs. (6.48), (6.49), and (6.50) assumed the known turbulent stresses σ_{uu} , σ_{vv} and τ_{uv} . In effect, the turbulent shear stress τ_{uv} is usually not available because of restrictions in the respective measurement technique and the environmental conditions. To eliminate the parameter τ_{uv} , there are two ways for it to be applied. Firstly, an additional measurement is required, for instance the measurement of velocity component u_x . Together with measurements of velocity components u and v (Fig. 6.6) all turbulence quantities can be obtained theoretically. For the special case of $\varphi_u + \varphi_v = 0$ this can be well realized, as demonstrated below. Secondly, the approximation of $\varphi_m \approx \bar{\varphi}$, whose meaning has been explained at the end of Sect. 6.1, can be applied. This leads to the launch of the so-called Zero-Correlation Method (ZCM) that will be outlined in detail in Chap. 8.

Special case with $\varphi_u + \varphi_v = 0$:

A special arrangement of measurements with $\varphi_u + \varphi_v = 0$ i.e. $\varphi_v = -\varphi_u = -\varphi$ is considered here. It corresponds to two measurements which lie symmetrically to the x -axis, as shown in Fig. 6.7. For this special case Eqs. (6.48), (6.49), and (6.50) are then simplified as

$$\sigma_{xx} = \frac{\sigma_{uu} + \sigma_{vv} + 2\tau_{uv}}{4 \cos^2 \varphi} \quad (6.51)$$

Consequently there is

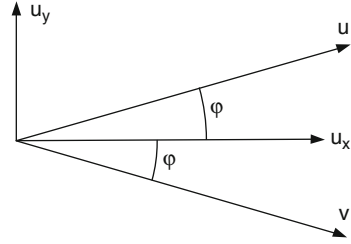
$$u'v' = u_x'^2 \cos \varphi_u \cos \varphi_v + u_y'^2 \sin \varphi_u \sin \varphi_v + u_x' u_y' \sin (\varphi_u + \varphi_v)$$

The sample means of corresponding fluctuations are calculated as

$$\begin{aligned} \sigma_{uu} &= \overline{u'^2} = \sigma_{xx} \cos^2 \varphi_u + \sigma_{yy} \sin^2 \varphi_u + \tau_{xy} \sin 2\varphi_u \\ \sigma_{vv} &= \overline{v'^2} = \sigma_{xx} \cos^2 \varphi_v + \sigma_{yy} \sin^2 \varphi_v + \tau_{xy} \sin 2\varphi_v \\ \tau_{uv} &= \sigma_{xx} \cos \varphi_u \cos \varphi_v + \sigma_{yy} \sin \varphi_u \sin \varphi_v + \tau_{xy} \sin (\varphi_u + \varphi_v) \end{aligned}$$

From these three equations with σ_{uu} , σ_{vv} and τ_{uv} as given quantities, the turbulent stresses σ_{xx} , σ_{yy} and τ_{xy} can be resolved. The same results as given in Eqs. (6.48), (6.49), and (6.50) are obtained.

Fig. 6.7 Special arrangement of LDA measurements to resolve the turbulent stress $\overline{u_y^2}$ through the measurements of velocity components u , v and u_x



$$\sigma_{yy} = \frac{\sigma_{uu} + \sigma_{vv} - 2\tau_{uv}}{4 \sin^2 \varphi} \quad (6.52)$$

$$\tau_{xy} = \frac{\sigma_{uu} - \sigma_{vv}}{2 \sin 2\varphi} \quad (6.53)$$

From Eq. (6.51) and (6.52) one obtains, by eliminating the term τ_{uv}

$$\sigma_{yy} = \frac{\sigma_{uu} + \sigma_{vv} - 2\sigma_{xx} \cos^2 \varphi}{2 \sin^2 \varphi} \quad (6.54)$$

This equation signifies that, from the additional measurement of velocity component u_x with the available normal stress σ_{xx} , the normal stress σ_{yy} can be obtained. Together with the shear stress from Eq. (6.53) the complete two-dimensional state of flow turbulence becomes available. Corresponding applications of Eqs. (6.53) and (6.54) can be found in Tropea (1983).

The measurement technique presented here supposes three independent measurements of σ_{uu} , σ_{vv} and σ_{xx} . It is simply based on statistical evaluation of flow fluctuations without any simplification. Therefore it generally applies not only to LDA but also to other measurement methods. The method, however, appears sometimes too expensive, because for obtaining the mean velocity distribution in the $x - y$ plane basically two single measurements are sufficient, see Eq. (6.46) for instance. An approximation method to simplify the turbulence measurements will be presented in Chap. 8.

6.3 Graphical Presentation of Turbulent Stresses

6.3.1 Ellipse Form of the Turbulence Distribution

It has been confirmed in Sect. 6.1.3 that at φ_m the turbulent shear stress vanishes and the corresponding stress matrix is given by Eq. (6.22). In the function of two principal normal stresses σ_{11} and σ_{22} , the normal stress distribution in the $x - y$ plane has been shown by Eq. (6.34). In order to graphically show the related turbulence

quantities in the velocity diagram, substitutions of $\hat{\varphi} = \varphi - \varphi_m$, $r_{\hat{\varphi}}^2 = \sigma_{\hat{\varphi}\hat{\varphi}}$, $a^2 = \sigma_{11}$ and $b^2 = \sigma_{22}$ will be applied. Based on the definition of respective turbulent stresses given in Eq. (2.11), the new parameters $r_{\hat{\varphi}}$, a and b all have the unit m/s. They represent the standard deviations of respective mean velocities i.e. the root mean square (*rms*) of flow fluctuations in relying on Eq. (5.3). Equation (6.34) is then rewritten as

$$r_{\hat{\varphi}}^2 = a^2 \cos^2 \hat{\varphi} + b^2 \sin^2 \hat{\varphi} \quad (6.55)$$

This equation can be considered to be originated from following two equations:

$$r_{\hat{\varphi},x} = a \cos \hat{\varphi} \quad (6.56)$$

$$r_{\hat{\varphi},y} = b \sin \hat{\varphi} \quad (6.57)$$

with $r_{\hat{\varphi},x}$ and $r_{\hat{\varphi},y}$ as two components of $r_{\hat{\varphi}}$. Clearly $r_{\hat{\varphi}}$ precisely represents the radial coordinate (radius) of an ellipse in the polar coordinate system. Both axes of the ellipse are given by a and b , respectively, see Fig. 6.8. The case shown in Fig. 6.8a with corresponding ellipse orientation is often encountered in the practical flows.

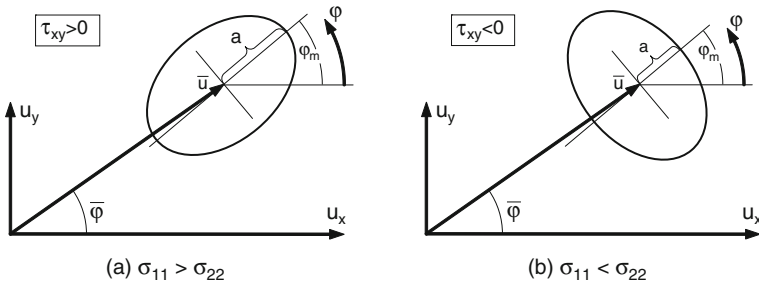


Fig. 6.8 Ellipse form of the turbulence distribution in a two-dimensional plane

6.3.2 Expressions of Turbulent Stresses in Mohr's Stress Circle

Flow turbulences in a two-dimensional $x - y$ plane are again considered here. In using the trigonometric identity $\cos 2\varphi = 2 \cos^2 \varphi - 1 = 1 - 2 \sin^2 \varphi$, Eq. (6.13) is rewritten as

$$\sigma_{\varphi\varphi} - \frac{1}{2} (\sigma_{xx} + \sigma_{yy}) = \frac{1}{2} (\sigma_{xx} - \sigma_{yy}) \cos 2\varphi + \tau_{xy} \sin 2\varphi \quad (6.58)$$

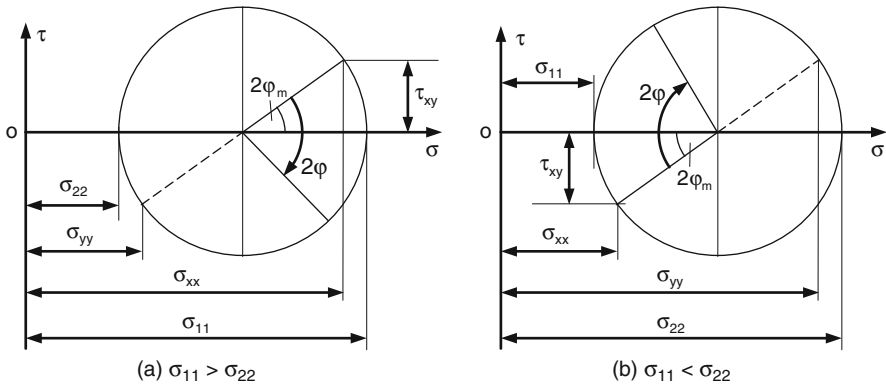


Fig. 6.9 Two-dimensional turbulent stresses expressed in the Mohr's stress circle

Squaring this equation and adding it to the square of Eq. (6.14) yields

$$\left(\sigma_{\varphi\varphi} - \frac{\sigma_{xx} + \sigma_{yy}}{2}\right)^2 + \tau_{\varphi,\varphi+90^\circ}^2 = \left(\frac{\sigma_{xx} - \sigma_{yy}}{2}\right)^2 + \tau_{xy}^2 \quad (6.59)$$

This equation precisely represents a circle in the coordinate system with normal and shear stresses as two orthogonal coordinates, as shown in Fig. 6.9. The centre of the circle is given by $\sigma = (\sigma_{xx} + \sigma_{yy})/2$ and $\tau = 0$ and the radius by

$$R = \sqrt{\left(\frac{\sigma_{xx} - \sigma_{yy}}{2}\right)^2 + \tau_{xy}^2}.$$

To show the angle φ_m at which the normal stress σ_{11} is present, Fig. 6.9 concerned two cases respectively for $\sigma_{11} > \sigma_{22}$ and $\sigma_{11} < \sigma_{22}$. Correspondingly there are $\tau_{xy} > 0$ in Fig. 6.9a and $\tau_{xy} < 0$ in Fig. 6.9b. In both cases, there is $\sigma_{\varphi\varphi} = \sigma_{11}$ at $2\varphi = 2\varphi_m$.

The graphical presentation of the turbulent stresses is similar to the graphical presentation of the mechanical stresses in the technical mechanics, where the stress circle is called Mohr's stress circle. The difference has to be mentioned: in the flow dynamics, all turbulent normal stresses are always positive, while mechanical stresses in the technical mechanics may be negative, depending on the external loads.

Chapter 7

Tracer Particles and Particle Motion Equations

Flow measurements by means of LDA technique always require particles being suspended in the flow to scatter the laser light. Because the measured particle velocity is used to represent the flow velocity, particles have to be able to follow the flow, especially flow fluctuations. Such a capability of particles is determined by both the particle size and the particle density. In general, a particle in the flow does not behave as a fluid particle because of the difference in their densities. In measuring non-stationary flows or the flows with large velocity fluctuations for instance, particles may have different velocities as the flow. This velocity difference is again the source of diverse forces exerted on the particle. The capability of particles of tracking the flow fluctuations should thus be accounted for with respect to both the particle size and the density of the particle substance.

The motion of a particle in the flow is governed by the dynamical equilibrium between effective forces acting on the particle and the inertial force of the particle. Amongst diverse effective forces, the drag force arising from the viscosity of the flow is usually decisive. Because this force is generally proportional to the particle surface while the particle inertial force is a function of the particle volume and the density of the particle substance, small particles always possess higher capabilities of tracking the flows than large particles. In details, it concerns the particle capabilities of tracking the flow fluctuations and the velocity changes along the streamlines, which may also be curved as a result of the flow arrangement. Since most practical flows are turbulent flows that are specified by the pressure fluctuation and the fluctuation of flow velocities, the particle in the flow also suffers from the pressure force and other force effects. In the straight flow with velocity fluctuations for instance, all force effects on the particle motion are finally found in the amplitude and phase difference of the particle motion in response to the flow fluctuations. This can be well demonstrated, for instance by calculating the particle motion in an oscillation flow.

The capability of particles of tracking the curved streamlines represents a further aspect of greater complexity. As we know, the streamline curvature in the flow is always related to a pressure gradient perpendicular to the streamlines. Such a transverse pressure gradient leads to deviation of the particle motion from streamlines

of the flow. The possibility of making sure whether a particle is able to follow the streamline curvature depends on how the deviation of the particle motion from the curved streamline can be specified. This is unfortunately not straightforward as that for particles in the flow with straight streamlines.

The effective forces exerted on a moving particle in the practical flows are of different mechanisms and therefore different extent and importance. The most significant forces are the viscous drag force, the pressure force and the forces associated with the particle acceleration.

Although in many cases the natural particles in the flow (e.g. water flow) are sufficiently able to scatter the laser light and thus can be made use of for LDA measurements, as the author of this book has often experienced, it is nevertheless indispensable to make the quantitative reference regarding the capability of seeded particles of tracking the flows. For this reason, diverse flow forces and the respective significances in diverse flows will be considered in this chapter.

7.1 Effective Forces Exerted on the Particle in the Flow

7.1.1 Viscous Drag Force

The drag force exerted on a particle arises from the fluid viscosity and the velocity difference between the particle and the viscous fluid. Since the velocity difference is a vector quantity, the drag force as a vector quantity has its direction coinciding with the difference of two velocity vectors. In assuming the spherical particle of the diameter d_p , the viscous drag force exerted on the particle is calculated by

$$\vec{F}_D = c_D \frac{1}{4} \pi d_p^2 \cdot \frac{1}{2} \rho_f |\vec{u}_f - \vec{u}_p| (\vec{u}_f - \vec{u}_p) \quad (7.1)$$

In this determination equation, the drag coefficient c_D is a function of the Reynolds number and can be given, for quasi-stationary flow around the particle, as

$$c_D = \frac{24}{\text{Re}} \quad (\text{Re} < 1) \quad (7.2)$$

$$c_D = \frac{24}{\text{Re}} \left(1 + 0.15 \text{Re}^{0.687} \right) \quad (1 < \text{Re} < 1000) \quad (7.3)$$

Equation (7.2) is known as the Stokes law. In concerning the particle motion in the fluid flow, the Reynolds number in above equations is calculated with the relative velocity between the particle and the flow. Because for LDA measurements always small particles are available, the Reynolds number applied to such small particles is usually small. For a particle of diameter $d_p = 0.02$ mm in the water flow ($\nu = 1.0 \cdot 10^{-6} \text{m}^2/\text{s}$) with a relative velocity of $u_f - u_p = 0.1 \text{m/s}$, for instance, the Reynolds number is calculated as $\text{Re} = 2$. The drag coefficient, if calculated by

Eq. (7.3), is 15, which is about 25% larger than that calculated by Eq. (7.2). Because of its simplicity the Stokes law given by Eq. (7.2) is often applied to theoretically investigate the dynamical feature of a small particle in the flow. The flow for instance can be assumed to be a sinusoidal function of the time. By choosing high oscillation frequency in the assumed flow, the flow turbulence could be simulated. The fact that the drag coefficient for $Re > 1$ according to Eq. (7.3) is greater than that from Eq. (7.2) clearly indicates that the real capability of a particle of tracking the flow is higher than that calculated by regarding Eq. (7.2). More about the particle dynamics in diverse types of flows will be shown in Sects. 7.2, 7.3, 7.4, and 7.5.

For particle motion in the same direction as the flow and in using the Stokes flow resistance law, the viscous drag force exerted on the particle is calculated from Eq. (7.1) as

$$F_D = 3\pi\mu d_p \cdot (u_f - u_p) \quad (7.4)$$

Herein $\mu = \rho_f \nu$ denotes the dynamical viscosity of the fluid. The drag force is directly proportional to the particle size and the velocity difference. It obviously represents the most significant force exerted on a particle. The drag force is effective, as long as the velocity difference between the particle and the flow exists.

In the general flows with velocity fluctuations or instability, there are also other forces which are proportional to the third power of the particle diameter (such as the pressure force and the force due to added mass, see following sections). The drag force with its linear dependence on the particle diameter clearly dominates in influencing the particle motion in the flow when the particle is sufficiently small.

7.1.2 Gravitational and Lift Forces

The motion of tracer particles in the flow undergoes the influence of the gravity. The associated gravitational force is given by $F_{\text{gravity}} = m_p g$ with m_p as the particle mass and g the gravitational acceleration. On the other side, there exists a lift force exerted on the particle in the counter direction of the gravitational force. The difference between them is given by

$$F_{\text{gravity}} - F_{\text{lift}} = \frac{1}{6}\pi d_p^3 \rho_p g - \frac{1}{6}\pi d_p^3 \rho_f g = \frac{1}{6}\pi d_p^3 g (\rho_p - \rho_f) \quad (7.5)$$

For particles of density that does not much differ from the density of the fluid, the total effect of the gravitational and lift forces can be neglected. Usually the choice of appropriate particles for water flow measurements is not difficult. On the contrary, in dealing with the measurements of air flows that has a density of about 1.2 kg/m^3 , there is much restricted possibility in selecting the appropriate particles. Available particles may be the hollow solid particles or liquid particles generated by atomizers. In common cases, the large density difference between the flow and particles can be

neglected as long as the particles are sufficiently small. This can be demonstrated by comparing the gravitational force with the drag force arising from the fluid viscosity. The ratio of the gravitational force to the drag force is given by

$$\frac{\text{gravitational force}}{\text{drag force}} \sim \frac{d_p^3}{d_p} = d_p^2 \quad (7.6)$$

Because for small particles the volumetric force including gravitational and lift forces are negligible against the drag force, the corresponding influence on the particle motion can be neglected. For this reason very fine particles such as aerosols of 1 μm in diameter should always be applied for air flow measurements.

7.1.3 Pressure Force

The pressure force exerted on the particle arises from the local pressure gradient in the flow, that may be caused for instance by flow fluctuations in association with both the flow turbulence and the flow periodicity, by the change of velocities along the streamlines as well as by the gravity. For simplicity, only the velocity variation along the straight streamlines i.e. one-dimensional flows and the turbulent flow fluctuations are considered. According to the Euler equation for incompressible flows along the x -direction, the pressure gradient along the streamline is given by

$$-\frac{1}{\rho_f} \frac{\partial p}{\partial x} = \frac{du_f}{dt} = \frac{\partial u_f}{\partial t} + u_f \frac{\partial u_f}{\partial x} \quad (7.7)$$

The first term on the r.h.s. of this equation represents the effect of the temporal flow fluctuations, while the second term accounts for the flow acceleration along the streamlines. For flows without velocity fluctuations ($\partial u_f / \partial t = 0$) the above equation can also be derived from the Bernoulli equation when applied to a stationary flow.

Within the longitudinal region around a small particle, a linear pressure distribution can be assumed. By integrating all infinitesimal pressure forces exerted normally on the spherical particle surface, the resultant pressure force is calculated as

$$F_p = -\frac{\pi}{6} d_p^3 \frac{\partial p}{\partial x} = \frac{\pi}{6} d_p^3 \rho_f \left(\frac{\partial u_f}{\partial t} + u_f \frac{\partial u_f}{\partial x} \right) \quad (7.8)$$

The calculation of this force is just comparable to that of the lift force of a particle in a flow, see Eq. (7.5). Such a similarity is obvious because the lift force indeed arises in the same way from the pressure gradient $dp/dz = \rho_f g$, which is caused by the gravitation.

In general, the pressure gradient that is related with the velocity acceleration $u_f du_f/dx$ along the streamlines can be of the same order as or much greater than

the pressure gradient caused by the gravity. For the flow through a nozzle of circular section for instance, the pressure gradient can be calculated by applying the Bernoulli equation with respect to the volumetric flow rate $\dot{Q} = Au_f = \text{const}$

$$\frac{dp}{dx} = -\frac{1}{2}\rho_f u_f^2 \frac{8}{d} \tan \varphi \quad (7.9)$$

Herein d and φ denote the local diameter and the half contraction angle of the nozzle, respectively. For a large flow velocity u_f through a nozzle of small diameter, the pressure gradient dp/dx may be many times larger than the pressure gradient $\rho_f g$ that is caused by the gravity. On the other hand, the resultant pressure force exerted on the particle impels the particle to be accelerated. According to the Newton's second law of motion, the corresponding acceleration of the particle is related with the pressure force by $F_p = m_p du_p/dt$ with m_p as the particle mass. Combining this force with the corresponding term in Eq. (7.8) for stationary flow and with respect to $du_p/dt = u_p du_p/dx$ yields

$$\frac{du_p}{dx} = \frac{\rho_f}{\rho_p} \frac{u_f}{u_p} \frac{du_f}{dx} \quad (7.10)$$

The particle acceleration, because of the pressure force, is independent of the particle size, but depends on the density of used particles. This result can be well demonstrated by observing air bubbles rising in water. Air bubbles of different sizes (although not spherical) show nearly equal rising velocity. It has to be mentioned that in the real flow the particle undergoes the combined effect of pressure force, viscous drag force, the force arising from the added mass, etc. This will be shown in Sects. 7.4 and 7.5.

7.1.4 Force from Added Mass

When dealing with the motion of a spherical particle at a constant velocity in a fluid at rest, the resistance received by the particle is described by the Stokes flow resistance which accounts for the regular change of the fluid around the particle and thus the constant momentum exchange between the particle and the fluid. In the special case as in the non-viscous potential flow, a spherical particle at the constant velocity does not undergo any resistance from the fluid, which is known as the d'Alembert's paradox. The regular and stationary flow structure around the particle, however, could not be maintained when the free particle in the fluid undergoes the acceleration, for instance, because of the force of gravity or as a result of the Stokes resistance. In association with the acceleration of the particle, more fluid around the particle will be set in motion. This precisely implies that additional momentum exchange between the particle and the fluid takes place. The particle motion thus suffers from an additional resistance, even in the non-viscous fluid. On the other

hand, the particle receives an additional force which opposes the particle motion, when it is decelerated in the fluid.

The mass that is additionally displaced by the particle because of the particle acceleration is called added mass or the virtual mass. From the theory for potential flow and as concerns the added mass being equally accelerated as the particle, the added mass is equal to the half mass of the fluid that the particle displaces. For the general case of the particle motion in the flow of a velocity u_f and on the same streamline as the flow, the associated force exerted on the particle is given as

$$F_{\text{add}} = -\frac{1}{2} \frac{\pi}{6} d_p^3 \rho_f \frac{d(u_p - u_f)}{dt} \quad (7.11)$$

Because of the added mass the associated force acts as a negative force and counteracts the change of the velocity difference.

7.2 Particle Motion Equation

The motion of a particle in the flow is determined by the equilibrium of diverse forces exerted on the particle. Because this force equilibrium is usually concerned with the flow direction, the vertical gravitational and lift forces will be neglected for simplicity. In fact, the force of gravity and the lift force counteract each other and the remaining effect is negligible if the particle density does not much differ from the fluid density. Some other forces that are associated with the unsteady motion of the particle and are only of less significance will not be considered here.

As effective forces exerted on the particle, the frictional Stokes drag force for $Re < 1$, the pressure force and the force associated with the added mass will be taken into account. From the Newton's second law of motion the equation of the particle motion in the straight flow is given by

$$\frac{\pi}{6} d_p^3 \rho_p \frac{du_p}{dt} = 3\pi \mu d_p (u_f - u_p) + \frac{\pi}{6} d_p^3 \rho_f \frac{du_f}{dt} - \frac{1}{2} \frac{\pi}{6} d_p^3 \rho_f \frac{d(u_p - u_f)}{dt} \quad (7.12)$$

In this equation, the Stokes drag force according to Eq. (7.2) for small Reynolds number i.e. $Re < 1$ has been applied. The condition of $Re < 1$ is indeed only satisfied when particles in the flow are sufficiently undersized or the relative velocity between the particle and the flow is sufficiently small. For the particle flow with $Re > 1$, Eq. (7.3) should be applied in which an additional term regarding the viscous drag force is of concern. Because of this feature Eq. (7.12) in assuming $Re < 1$ indeed represent the worst case with respect to the applicability of tracer particles in the flow.

Equation (7.12) will be applied to some special flows to reveal the capability of particles of following the flow variations.

7.3 Particle Motion in the Straight Flow of Constant Velocity

A very common case encountered in the practical flows with particles is the one-dimensional stationary carrying flow. Particles that are seeded into the flow have their initial velocities which are usually not equal to the flow velocity. Under the effect of diverse forces a particle of given diameter and initial velocity will be accelerated or decelerated, until the constant velocity equal to the flow velocity is reached.

For simplicity the particle motion is assumed to be merely influenced by the drag force and the force from the added mass. This means that it deals with a flow field of constant pressure. The particle will be accelerated or slowed down because of the velocity difference between the particle and the flow. From Eq. (7.12) one obtains the particle motion equation rearranged as

$$\left(1 + \frac{1}{2} \frac{\rho_f}{\rho_p}\right) \frac{du_p}{dt} = \frac{18\mu}{\rho_p d_p^2} (u_f - u_p) = \frac{1}{\tau} (u_f - u_p) \quad (7.13)$$

In this equation, the time scale is defined by

$$\tau = \frac{\rho_p d_p^2}{18\mu} \quad (7.14)$$

It is called the relaxation time and is a constant representing the particle and flow properties. For a particle of diameter $d_p = 0.01\text{mm}$ and density $\rho_p = 1.5\text{ gr/cm}^3$ in the water flow ($\mu = 1.0 \cdot 10^{-3}\text{Pas}$) for instance, the relaxation time is calculated to $\tau = 8.3 \cdot 10^{-6}\text{s}$.

To the carrying flow of constant velocity $u_f = \text{const}$, the initial velocity difference between the particle and the flow is assumed to be $u_f - u_{p0}$. Integrating Eq. (7.13) yields

$$\frac{u_p - u_{p0}}{u_f - u_{p0}} = 1 - e^{-t/A\tau} \quad (7.15)$$

Herein $A = 1 + \frac{1}{2} \rho_f/\rho_p$ is a constant that regards the density ratio between the particle substance and the carrying flow.

Figure 7.1, as a calculation example for a particle ($d_p = 0.02\text{mm}$) of different density ratios, represents the development of the particle velocity relative to the constant flow velocity. Regarding the particle with $\rho_p/\rho_f = 2$ (i.e. $A = 1.25$) for instance, the particle will reach a velocity of at least 86.5% ($1 - e^{-2} = 0.865$) of the stationary flow velocity after a period of $t = 2A\tau = 1.1 \cdot 10^{-4}\text{s}$. Because it generally deals with a very short time, the particle of the given diameter could be considered to be able to well follow the flow, despite initially large velocity difference.

From Eq. (7.15) the relaxation time τ can be used as a useful parameter to evaluate the capability of a particle following the flow. It is only a function of the particle and fluid properties but not of the flow properties (e.g. Reynolds number). Whether

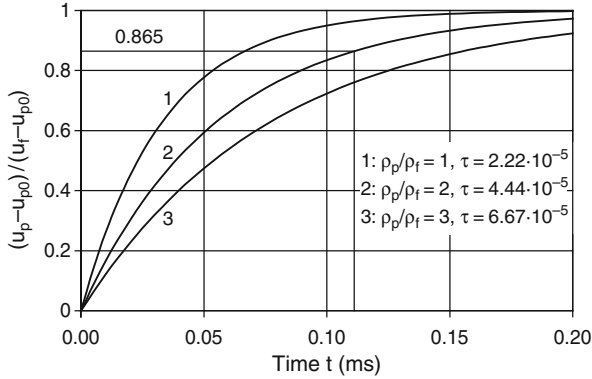


Fig. 7.1 Development of the particle motion velocity relative to the constant flow velocity for $d_p = 0.02$ mm, $\rho_f = 1000\text{kg/m}^3$ and $\mu = 0.001$ Pas

a particle of a certain relaxation time can be applied as the tracer particle for LDA measurements depends on each individual flow and the requirement of the measurement accuracy. In any case, the relaxation time has been widely used to evaluate the applicability of particles for measurements, also in other types of flows. To be mentioned is that the result shown in Eq. (7.15) is derived for $\text{Re} < 1$. This is in any case reasonable, when the particle velocity reaches a value which is close to the velocity of the carrying flow.

7.4 Particle Motion in Nozzle and Diffuser Flows

The particle motion in the flow depends on the state of the fluid flow. Basically the particle motion can be considered to be along the streamlines, when the flow does not rapidly change its direction. Because the velocity of fluid along a streamline is usually not constant, the particle motion will generally differ from the fluid flow. As a result of the difference in the density, the particle will respond to the velocity change along the streamline always with a time delay. The simplest flow with changeable velocity along the streamlines is probably the flow in the nozzle or the diffuser, where the flow along the streamlines is either accelerated or decelerated, with resultant pressure gradients. As already indicated in Sect. 7.1.3, the contribution of the pressure force exerted on the particle to the particle acceleration is independent of the particle size. Additional forces are obviously the viscous drag force and the force because of the added mass. It is interesting to determine the particle motion in such practical flows. For simplicity, the fluid flow is assumed to linearly change along the axis of the nozzle or diffuser, as given by

$$u_f = ax + u_{f0} \quad (7.16)$$

For the flow in the nozzle there is $a > 0$, while in the diffuser flow it is $a < 0$. At the entrance of the nozzle and the diffuser, both the particle and the flow have equal velocities $u_{p0} = u_{f0} = u_0$. With respect to $du_f/dt = u_p du_f/dx \approx u_f du_f/dx$ and $du_p/dt \approx u_f du_p/dx$ as well as the relaxation time according to Eq. (7.14), one obtains from Eq. (7.12)

$$\frac{du_p}{dx} = \frac{1}{\tau} \left(1 - \frac{u_p}{u_f} \right) + \frac{\rho_f}{\rho_p} \frac{du_f}{dx} - \frac{1}{2} \frac{\rho_f}{\rho_p} \frac{d(u_p - u_f)}{dx} \quad (7.17)$$

In accounting for $du_f/dx = a$ and thus $dx = du_f/a$, the above equation becomes

$$\left(1 + \frac{1}{2} \frac{\rho_f}{\rho_p} \right) \frac{du_p}{du_f} = -\frac{1}{a\tau} \frac{u_p}{u_f} + \left(\frac{3}{2} \frac{\rho_f}{\rho_p} + \frac{1}{a\tau} \right) \quad (7.18)$$

The combined influence of the particle size and the density, the dynamical viscosity and the flow acceleration in the nozzle on the particle motion is confirmed to be given only by the product $a\tau$, which is dimensionless.

For further calculations the following abbreviations are applied:

$$A = 1 + \frac{1}{2} \frac{\rho_f}{\rho_p}, \quad B = \frac{1}{a\tau}, \quad C = \frac{3}{2} \frac{\rho_f}{\rho_p} + \frac{1}{a\tau} \quad (7.19)$$

In using the parameter substitution of $\frac{u_p}{u_f} = \bar{u}_p$ from which $\frac{du_p}{du_f} = u_f \frac{d\bar{u}_p}{du_f} + \bar{u}_p$ is obtained, Eq. (7.18) is further written as

$$\frac{d\bar{u}_p}{du_f} = \frac{C - (A + B)\bar{u}_p}{A u_f} \quad (7.20)$$

This equation with A, B and C as constants represents the particle motion in responding to the velocity change in the straight nozzle or diffuser flows. Because the parameters \bar{u}_p and u_f have been separated, Eq. (7.20) can be integrated, firstly leading to

$$\ln \frac{C - (A + B)\bar{u}_p}{C - (A + B)\bar{u}_{p0}} = \frac{A + B}{A} \ln \frac{u_{f0}}{u_f} \quad (7.21)$$

With respect to $\bar{u}_{p0} = 1$ at $t = 0$ i.e. $x = 0$ the particle velocity can then be resolved as

$$\bar{u}_p = \left(1 - \frac{C}{A + B} \right) \left(\frac{u_{f0}}{u_f} \right)^{1+B/A} + \frac{C}{A + B} \quad (7.22)$$

Of concern is that Eq. (7.22) is applicable to both the straight nozzle and diffuser flows. For nozzle flows there is $a > 0$ according to Eq. (7.16), while for diffuser flows it is $a < 0$. It should be mentioned that the purpose of current calculations is to evaluate the particle capability of responding to the change in the flow velocity. The

assumption of linear dependence of flow velocity on the flow path in both the nozzle and the diffuser contributes to the simplification of calculations. In the practice, this linearity in the flow velocity requires the non-linear design of nozzle or diffuser with respect to the constant volumetric flow rate $\dot{Q} = u_f A_f$, with A_f as the flow section area.

7.4.1 Nozzle Flow

The linear change of the flow velocity in the straight nozzle is given by Eq. (7.16) with $a > 0$. Based on the assumption that at the nozzle entrance the particle and the fluid flow have equal velocities, the particle velocity along the particle streamline has been derived and shown in Eq. (7.22). To a certain nozzle flow with $a = 20$ (m/s)/m for example, Fig. 7.2 shows the ratio of the particle velocity to the flow velocity along the flow path for different particle densities. At the inlet of the nozzle, every particle suffers from a delay in the acceleration against the flow acceleration, so that there is $\bar{u}_p < 1$. The particle acceleration relative to the flow acceleration just at the nozzle inlet, at which $u_{f0} = u_0$ and $\bar{u}_{p0} = 1$ are available, can be directly obtained from Eq. (7.20) as

$$\left(\frac{d\bar{u}_p}{du_f} \right)_{x=0} = \frac{1}{u_{f0}} \frac{C - (A + B)}{A} \quad (7.23)$$

Further, because of $\bar{u}_p = u_p/u_f$ the above equation is rewritten as

$$\left(\frac{du_p}{du_f} \right)_{x=0} - \frac{u_{p0}}{u_{f0}} = \frac{C - (A + B)}{A} \quad (7.24)$$

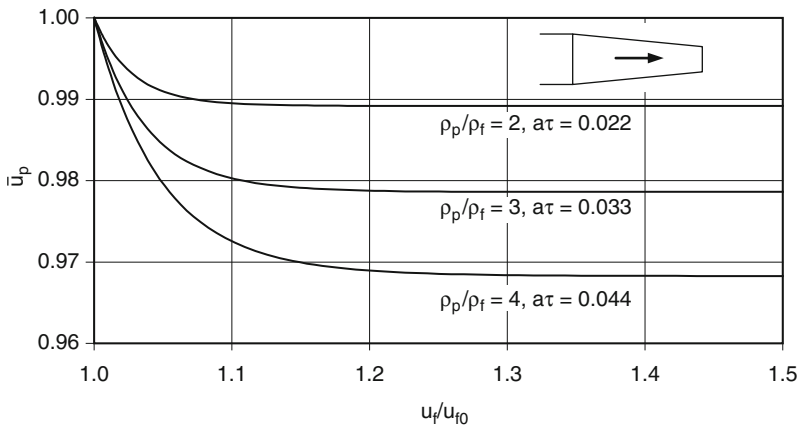


Fig. 7.2 Capability of tracer particles of diameter $d_p = 0.1$ mm of following the water flow ($\mu = 0.001$ Pas) in a nozzle with the flow acceleration equal to $a = 20$ (m/s)/m

With respect to $u_{p0}/u_{f0} = 1$ at the nozzle inlet one obtains

$$\left(\frac{du_p}{du_f}\right)_{x=0} = \frac{C - B}{A} = \frac{3}{1 + 2\rho_p/\rho_f} \tag{7.25}$$

It is a function of the relative density of the particle only and is independent of the particle size and the viscosity of the flow. Such a result indeed can also be expected from Eq. (7.17). Because at the nozzle entrance the velocity difference between the particle and the flow is zero, the viscous drag force vanishes. Thus with the reject of the first term on the r.h.s. of Eq. (7.17), the particle motion is determined merely by the density ratio ρ_p/ρ_f .

For tracer particles with the density ratio $\rho_p/\rho_f < 2$ in the considered example as shown in Fig. 7.2, the final particle velocity is merely about 1% less than the flow velocity. This difference seems to be really negligible for most applications.

As it can also be further confirmed from Fig. 7.2 for the given example, the ratio of particle to flow velocities tends to be constant after a short time at which the flow velocity reaches a value of about $u_f/u_{f0} \approx 1.1 \sim 1.2$. The related constant velocity ratio can be obtained from Eq. (7.22) by setting $u_{f,\infty} = \infty$ to be given as

$$\bar{u}_{p,\infty} = \frac{C}{A + B} \tag{7.26}$$

This final particle velocity can be considered as a measure of the applicability of tracer particles used in LDA measurements. Because of Eq. (7.19), the final particle velocity is obviously a function of the density ratio ρ_p/ρ_f and the product $a\tau$. Corresponding relationships have been show in Fig. 7.3. The almost linear dependence of the final particle velocity on the parameter $a\tau$ can be made use of to

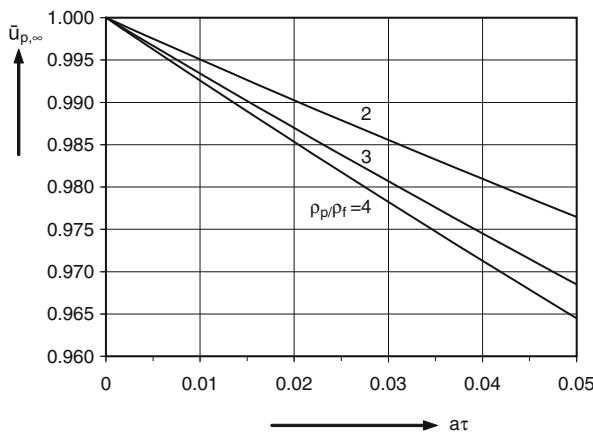


Fig. 7.3 Final reachable ratio of particle to flow velocities in the nozzle flow, in the function of the particle density and the combined parameter $a\tau$

explicitly simplify Eq. (7.26). Because for $a\tau = 0$ there is $\bar{u}_{p,\infty} = 1$, the linearization of Eq. (7.26) will be performed at $a\tau = 0$. With respect to Eq. (7.19) it yields from Eq. (7.26)

$$\left. \frac{d\bar{u}_{p,\infty}}{d(a\tau)} \right|_{a\tau=0} = - \left(1 - \frac{\rho_f}{\rho_p} \right) \quad (7.27)$$

The linearization of Eq. (7.26) is then obtained as

$$\bar{u}_{p,\infty} = 1 - \left(1 - \frac{\rho_f}{\rho_p} \right) a\tau \quad (7.28)$$

This relationship serves for rapidly evaluating the applicability of interested tracer particles to be used in LDA measurements of nozzle flows. The relaxation time τ of the particle is calculated by Eq. (7.14). The flow acceleration a in the nozzle flow depends not only on the nozzle geometry but also on the flow velocity itself. From the constant volumetric flow rate $\dot{Q} = u_f A_f$ through the nozzle the flow acceleration in the nozzle is calculated as

$$a = \frac{du_f}{dx} = - \frac{u_f}{A_f} \frac{dA_f}{dx} \quad (7.29)$$

In general, the flow in a nozzle of small dimension undergoes the greater acceleration than the flow in a large geometrically analogous nozzle.

7.4.2 Diffuser Flow

The diffuser flow in the present context is given by Eq. (7.16) with $a < 0$. Under the assumption of equal particle and flow velocities at the diffuser entrance, the particle motion in such a diffuser flow is described by Eq. (7.22). To a certain diffuser flow with $a = -20(\text{m/s})/\text{m}$ for example, Fig. 7.4 shows the ratio of the particle velocity to the flow velocity along the flow path for different particle density ratios. Because the particle velocity is less slowed down than the flow velocity, there is $\bar{u}_p > 1$. At the diffuser inlet, the ratio of the particle deceleration to the flow deceleration is again given by Eq. (7.25).

For the considered example and for tracer particles with the density ratio $\rho_p/\rho_f < 2$ the final particle velocity is merely about 1% more than the flow velocity. This difference seems to be really negligible in most applications.

According to Fig. 7.4 the state of the particle flow i.e. the ratio of the particle velocity to the flow velocity tends to be constant after a short time. The related constant velocity ratio can be obtained from Eq. (7.22) with respect to $1 + B/A < 0$ and $u_{f,\infty} = 0$

$$\bar{u}_{p,\infty} = \frac{C}{A + B} \quad (7.30)$$

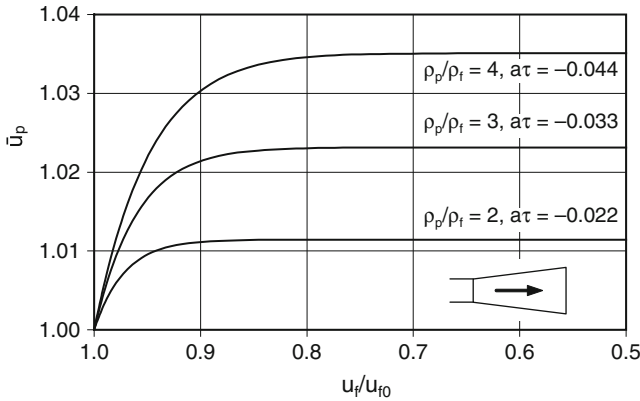


Fig. 7.4 Capability of tracer particles of diameter $d_p = 0.1$ mm of following the water flow ($\mu = 0.001$ Pas) in a diffuser with the flow deceleration equal to $a = -20$ (m/s)/m

It is formally equal to Eq. (7.26). The constant A, B and C are again calculated from Eq. (7.19), however, with $a\tau < 0$ for diffuser flows. Figure 7.5 shows corresponding relationships calculated from the above equation. The almost linear dependence of the final particle velocity on the parameter $a\tau$ can be again utilized to simplify Eq. (7.30). Like calculations leading to Eq. (7.28) for $a\tau \ll 1$, corresponding calculations are summarized as follows

$$\left. \frac{d\bar{u}_{p,\infty}}{d(-a\tau)} \right|_{a\tau=0} = 1 - \frac{\rho_f}{\rho_p} \tag{7.31}$$

$$\bar{u}_{p,\infty} = 1 - \left(1 - \frac{\rho_f}{\rho_p} \right) a\tau \tag{7.32}$$

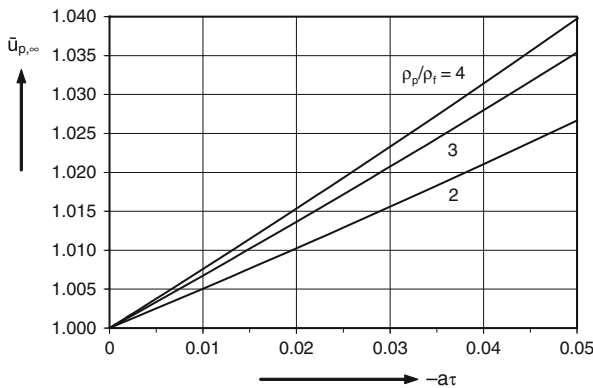


Fig. 7.5 Final reachable ratio of particle to flow velocities in the diffuser flow, in the function of the particle density and the combined parameter $a\tau$

This last relationship has the same form as Eq. (7.28). Because of $a\tau < 0$ for diffuser flows there is $\bar{u}_{p,\infty} > 1$. Thus a rapid and direct method of evaluating the applicability of interested tracer particles in diffuser flow measurements by means of LDA method is available.

7.5 Particle Motion in the Oscillation Flow

One of the most important aspects dealing with tracer particles for LDA measurements is the particle capability of following velocity fluctuations in a turbulent flow. Because of the high frequency of velocity fluctuations commonly up to thousands hertz it is reasonable to make sure what type of tracer particles should be applied, in order to resolve the true velocity fluctuations in each interested flow. The reaction behavior of a particle to the flow fluctuations can be estimated basically by accounting for a spatially uniform fluctuation flow. The most simple case is to assume the flow fluctuation to be a sinusoidal function with the mean velocity u_0 , the angular frequency ω and the amplitude A_f as follows

$$u_f = u_0 + A_f \sin \omega t \quad (7.33)$$

The assumption of spatially uniform flow is for the present consideration necessary, because then the spatial pressure distribution in function of $\partial u_f / \partial x$ in Eq. (7.8) disappears. The introduction of the sinusoidal flow model aims to simulate the non-steadiness of the flow in function of $\partial u_f / \partial t \neq 0$, to which the pressure force exerted on the particle is directly related. It should be mentioned that around the particle the local pressure gradient $\partial p / \partial x$ arising from the fluctuation velocity $\partial u_f / \partial t$ according to Eq. (7.8) can be assumed to be constant, as long as the particle size is sufficiently small against the turbulent structures.

By inserting Eq. (7.33) into Eq. (7.12) one obtains the rearranged particle motion equation as

$$\frac{d(u_p - u_0)}{dt} + a(u_p - u_0) = b \sin \omega t + c \cos \omega t \quad (7.34)$$

with corresponding particle and fluid constants

$$a = \frac{36\mu}{d_p^2(2\rho_p + \rho_f)}, \quad b = \frac{36\mu A_f}{d_p^2(2\rho_p + \rho_f)} \quad \text{and} \quad c = \frac{3\rho_f \omega A_f}{2\rho_p + \rho_f} \quad (7.35)$$

Integrating Eq. (7.34) then yields

$$u_p - u_0 = \frac{(ab + c\omega) \sin \omega t + (ac - b\omega) \cos \omega t}{a^2 + \omega^2} + C \cdot e^{-at} \quad (7.36)$$

Herein C is the integration constant.

It is again especially interesting to know the final state of the particle oscillation in the assumed oscillation flow according to Eq. (7.33). This is obtained from Eq. (7.36) by setting $t \rightarrow \infty$, so that the last term on the r.h.s. of the equation disappears. The particle oscillation in the flow is then independent of the initial velocity difference between the flow and the particle and is described by

$$u_p - u_0 = \frac{(ab + c\omega) \sin \omega t + (ac - b\omega) \cos \omega t}{a^2 + \omega^2} \quad (7.37)$$

Obviously the particle motion has been shown to be a pure oscillation. To further simplify this equation, the relationship $(ab + c\omega)^2 + (ac - b\omega)^2 = (a^2 + \omega^2)(b^2 + c^2)$ is applied, so that the following substitutions can be applied

$$\frac{ab + c\omega}{\sqrt{(a^2 + \omega^2)(b^2 + c^2)}} = \cos \varphi_p, \quad \frac{b\omega - ac}{\sqrt{(a^2 + \omega^2)(b^2 + c^2)}} = \sin \varphi_p \quad (7.38)$$

Eq. (7.37) then becomes

$$u_p - u_0 = \sqrt{\frac{b^2 + c^2}{a^2 + \omega^2}} (\sin \omega t \cos \varphi_p - \cos \omega t \sin \varphi_p) = A_p \sin(\omega t - \varphi_p) \quad (7.39)$$

As can be seen, it deals with an oscillation of the particle at the same oscillation frequency as the fluid flow, however with an amplitude modification and a phase difference. The amplitude A_p of the particle oscillation is calculated, with respect to Eq. (7.35), as

$$A_p = \sqrt{\frac{b^2 + c^2}{a^2 + \omega^2}} = \sqrt{\frac{1 + \frac{1}{12^2} \left(\frac{\omega d_p^2}{\nu}\right)^2}{1 + \frac{1}{36^2} \left(1 + 2\frac{\rho_p}{\rho_f}\right)^2 \left(\frac{\omega d_p^2}{\nu}\right)^2}} \cdot A_f \quad (7.40)$$

or

$$\frac{A_p}{A_f} = \sqrt{\frac{1 + \frac{1}{12^2} N_S^4}{1 + \frac{1}{36^2} \left(1 + 2\frac{\rho_p}{\rho_f}\right)^2 N_S^4}} \quad (7.41)$$

Herein the Stokes number is applied which is defined by

$$N_S = \sqrt{\frac{\omega d_p^2}{\nu}} \quad (7.42)$$

with ν as the kinematic viscosity of the flow.

Correspondingly, the phase difference in Eq. (7.39) is calculated as

$$\tan \varphi_p = \frac{b\omega - ac}{ab + c\omega} = \frac{24(\rho_p/\rho_f - 1)N_S^2}{432 + (2\rho_p/\rho_f + 1)N_S^4} \quad (7.43)$$

The Stokes number combines the influences of the flow fluctuation frequency, the particle size and the kinematic viscosity of the fluid on the particle motion in the flow. Its values in usual flows with tracer particles can be estimated. The flow fluctuation rate is assumed for instance to be 1000 hertz. For a particle of diameter $d_p = 0.1$ mm and the flow of kinematic viscosity $\nu = 1.0 \cdot 10^{-6}$ m²/s (water at $p = 1$ bar and $T = 20^\circ\text{C}$), the Stokes number is calculated to $N_S \approx 8$. This value can be considered to be the upper value of tracer particles usually applied in LDA flow measurements. Table 7.1 shows the variation range of the Stokes numbers in diverse situations in the water flow ($\nu = 1.0 \cdot 10^{-6}$).

In using the Stokes number, as defined in Eq. (7.42), the influences of the particle size and the particle density on the oscillation amplitude of the particle in the flow has been separated. This clearly shows the great advantage against the use of the relaxation time, which is defined in Eq. (7.14) and is basically available for stationary rather than the oscillation carrying flows.

The amplitude ratio given in Eq. (7.41) as a function of the density ratio ρ_p/ρ_f and the Stokes number is shown in Fig. 7.6 for a wide range of the Stokes number. In general, particles with the density ratio $\rho_p/\rho_f < 1.2$ could well follow the flow oscillation, even at high oscillation frequency and for large particles. The maximum diminishment of the oscillation amplitude is about 10%. For $\rho_p = \rho_f$ there are both $A_p = A_f$ and $\varphi_p = 0$. The particle will follow the flow exactly regardless of size. It indeed deals with a fluid particle.

As the Stokes number increases, the amplitude ratio A_p/A_f tends to be a constant that is only a function of the density ratio. This can be easily confirmed, as for very large Stokes numbers it results from Eq. (7.41)

$$\frac{A_p}{A_f} = \frac{3}{1 + 2\rho_p/\rho_f} \quad (7.44)$$

For particles with $\rho_p/\rho_f = 1.2$ for instance there is $A_p/A_f = 0.88$.

Table 7.1 Stokes number in the water flow in function of the particle size and the fluctuation rate (frequency) of the flow

Frequency (Hz)	Particle diameters (mm)				
	$d_p = 0.02$	$d_p = 0.04$	$d_p = 0.06$	$d_p = 0.08$	$d_p = 0.1$
100	0.5	1.0	1.5	2.0	2.5
200	0.7	1.4	2.1	2.8	3.5
500	1.1	2.2	3.4	4.5	5.6
1000	1.6	3.2	4.8	6.3	7.9

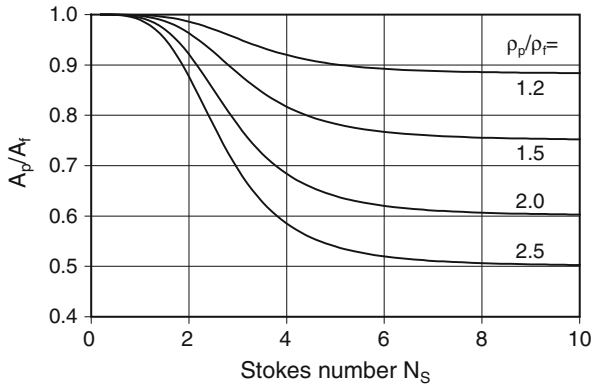


Fig. 7.6 Amplitude of the particle oscillation in the oscillation carrying flow in the function of the Stokes number for different particle density ratios

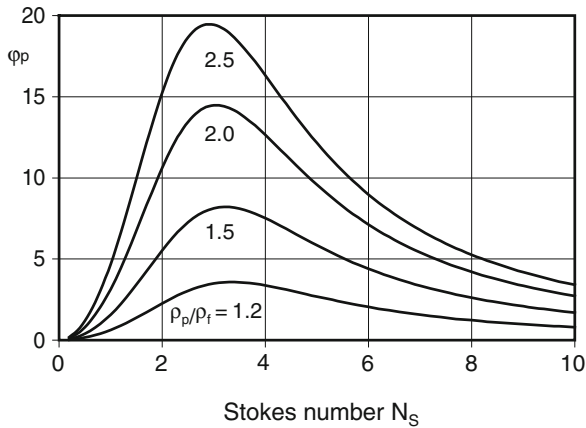
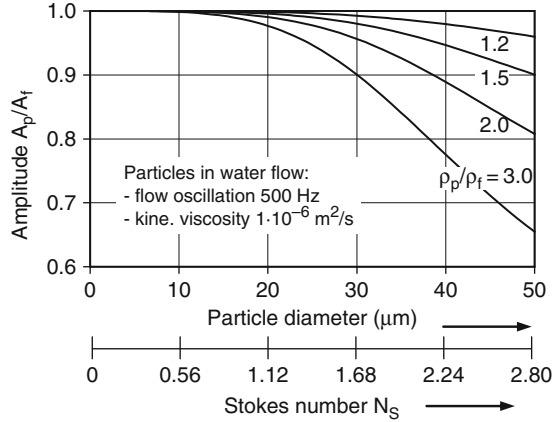


Fig. 7.7 Phase difference of the particle oscillation in the oscillation carrying flow in the function of the Stokes number for different particle density ratio

In Fig. 7.7, the phase difference between the particle and the flow oscillations has been shown. For particles with a density ratio $\rho_p/\rho_f < 1.2$ the phase difference could be kept within 3.5° . It should be mentioned that for measurements of turbulent flows the phase difference is actually irrelevant. Also the existence of a maximum phase difference for each given particle density ratio ρ_p/ρ_f appears to be less interesting.

From above considerations with an oscillation flow model both the capability of particles of following the flow fluctuations and its limitation could be well demonstrated. The calculation results can be applied to simulate the particle behaviors in turbulent flows by considering Eq. (7.33). On one hand, the turbulence intensity of a flow, that is given by $|u'|/\bar{u}$, can be simulated in terms of the amplitude ratio A_f/u_0 of a sinusoidal fluctuation. On the other hand, the frequency of the turbulent flows

Fig. 7.8 Amplitude ratio of the particle to the water flow oscillations in the function of the particle size for different particle density ratios



that commonly takes hundreds to thousands of hertz, can be simulated by the angular frequency ω . For each particle of a given size, the related Stokes number can be calculated according to Eq. (7.42). From Eq. (7.41) then the amplitude ratio of the particle to the flow fluctuations can be further determined. Fig. 7.8 represents such a calculation example for different particles in a turbulent water flow, in which the frequency of velocity fluctuations is assumed to be 500 Hz. For particles with a density ratio below 2.0 (for glass sphere it is about 2.4) and diameters of less than $30 \mu\text{m}$, the amplitude ratio of the particle oscillation to the flow fluctuations is calculated to be greater than 95%. For most engineering flows and the flow evaluation, such a level of measurement accuracy is well acceptable.

With respect to the calculated particle motion in the oscillation flow there are two special aspects that should be accounted for. Firstly, for very small particles the particle motion in the flow is governed by the viscous drag force, as this has already been indicated in Sect. 7.1. Secondly, for large particles i.e. at large Stokes numbers the volumetric forces dominate in the particle dynamics. These two special cases will be treated below.

7.5.1 Particle Flows of Small Stokes Numbers

For LDA measurements, small particles are in favor to be used because of their high capabilities of following the flows and the flow fluctuations. In general, small particles are specified by small Stokes numbers. For $N_s < 1$ Eq. (7.41) is simplified by neglecting the high order term as N_s^8 in the Taylor series expansion to

$$\frac{A_p}{A_f} = 1 - \frac{1}{288} \left[\frac{1}{9} \left(1 + 2 \frac{\rho_p}{\rho_f} \right)^2 - 1 \right] N_s^4 \quad (7.45)$$

On the other side, as mentioned before, the viscous drag force dominates in influencing the particle motion when particles are sufficiently small. In order to quantify this circumstance, only the viscous drag force in Eq. (7.12) is considered. By again assuming the same sinusoidal flow oscillation as Eq. (7.33), the corresponding amplitude ratio can be calculated from the same calculation procedure, leading to

$$\frac{A_p}{A_f} = \frac{1}{\sqrt{1 + \frac{1}{18^2} \frac{\rho_p^2}{\rho_f^2} N_S^4}} \approx 1 - \frac{1}{648} \frac{\rho_p^2}{\rho_f^2} N_S^4 \quad (7.46)$$

Also to be mentioned is that in using the relaxation time according to Eq. (7.14), the expression at square root in above equation can also be written as $\sqrt{1 + \omega^2 \tau^2}$. The corresponding expression for A_p/A_f can be found in some earlier publications as cited in Carter et al. (2001).

The comparison between Eqs. (7.45) and (7.46) has been shown in Fig. 7.9. It clearly demonstrates that for small particles the viscous drag force dominates. Since in deriving Eq. (7.46) both the pressure force arising from the flow fluctuation $\partial u_f / \partial t$ according to Eq. (7.7) and the force owing to the added mass were neglected, the amplitude ratio A_p/A_f will not be in unity, even for the density ratio $\rho_p/\rho_f = 1$. For this reason Eq. (7.45) is more precise than Eq. (7.46) and could be considered to be resulted only from the viscous drag force.

Correspondingly the phase difference that is given in Eq. (7.43) is simplified for $N_S < 1$ as

$$\tan \varphi_p \approx \frac{1}{18} \left(\frac{\rho_p}{\rho_f} - 1 \right) N_S^2 \quad (7.47)$$

For $N_S \ll 1$ there are $A_p = A_f$ and $\varphi_p = 0$, as expected.

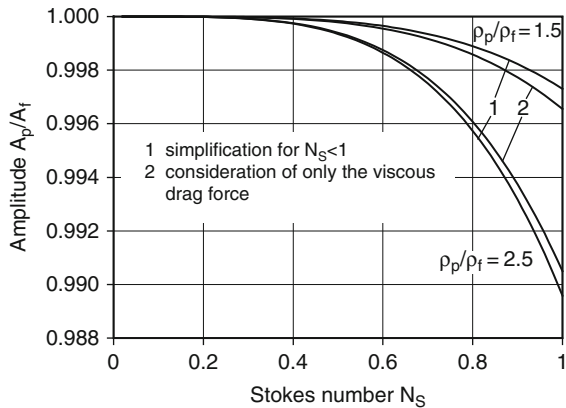


Fig. 7.9 Comparison of calculation results respectively from the simplification for small Stokes numbers and from the consideration of only the viscous drag force

7.5.2 Particle Flows of Large Stokes Numbers

In addition to the viscous drag force, the other effective forces exerted on the particle in the spatially uniform flow are the pressure force arising from the local flow fluctuation rate $\partial u_f / \partial t$ and the force because of the added mass. As it has been shown in Sect. 7.1, these last two forces are proportional to the third power of the particle diameter. Such a particle dynamical property implies that at large particles both volume forces dominate in influencing the particle motion against the viscous drag force which becomes negligible. This circumstance has already been confirmed in Fig. 7.6, as for large Stokes numbers ($N_S > 10$) the particle oscillation amplitude is independent of the Stokes number i.e., according to Eq. (7.42), independent of the fluid viscosity. The corresponding calculation result has been given in Eq. (7.44). In effect, the same result can also be obtained from Eq. (7.34) by directly neglecting the viscous drag force, that means to set $a = 0$ and $b = 0$. Because the particle motion is independent of the particle size, Eq. (7.44) can also be used to explain why the rising velocity of air bubbles in water is independent of the bubble size, as mentioned in Sect. 7.1.3.

Chapter 8

Zero Correlation Method (ZCM)

8.1 Shear Stress Measurements with Non-coincident LDA

The most significant turbulence parameters of a turbulent flow are specified by corresponding Reynolds stresses that are given in the matrix form at Eq. (2.11). The knowledge about the turbulent shear stresses for instance τ_{uv} basically demands, according to Eq. (5.7), coincident measurements of two velocity components u and v . For such measurements a two-component LDA-system has usually to be applied and optically arranged for direct measurements of u and v (Chap. 4). This is well available because most LDA systems are designed so. The different case, however, will be encountered in measurements of all three velocity components. In such a case, the third i.e. on-axis velocity component has usually to be separately measured by off-axis alignment of the LDA head. This can be achieved either directly by the method according to Fig. 8.1a, or indirectly according to Fig. 8.1b. In the case of indirect measurements, the on-axis velocity component is calculated by transforming the velocity components u_x and u_φ

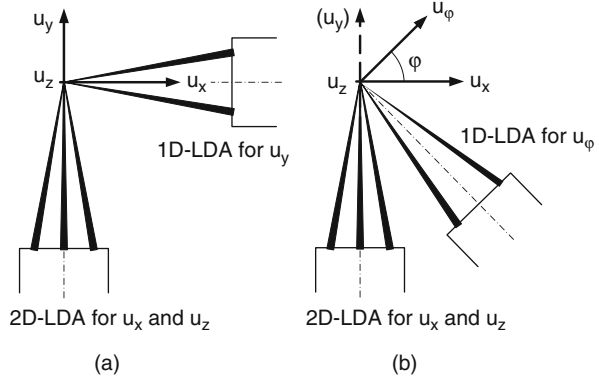
$$u_y = \frac{u_\varphi - u_x \cos \varphi}{\sin \varphi} \quad (8.1)$$

This equation has already been given by Eq. (6.40).

Because it deals here with non-coincident measurements of velocity components u_x and u_y , the turbulent shear stress $\overline{u'_x u'_y}$ could not be directly obtained by regarding Eq. (5.7). For indirectly obtaining any turbulent shear stress, the Reynolds stress matrix shown in Eq. (2.11) is considered again. Because of equalities $\tau_{xy} = \tau_{yx}$, $\tau_{xz} = \tau_{zx}$ and $\tau_{yz} = \tau_{zy}$ there are indeed altogether six independent Reynolds turbulent stresses. According to the statement given by Durst et al. (1981) and for the most general case of non-coincident LDA measurements, six single measurements are needed for resolving all six Reynolds stresses in a three-dimensional space. In the case of considering the flow in a two-dimensional plane, then three single measurements are necessary. The corresponding measurement method has already been shown in Sect. 6.2 with respect to Fig. 6.7.

Measurements of complete turbulent stresses in a two-dimensional plane within a flow field, however, can be simplified by making use of a highly reasonable

Fig. 8.1 Separate measurement of the on-axis velocity component u_y by relocating the LDA head; The velocity component u_z is perpendicular to the drawing plane (a) direct measurement of the velocity component u_y ; (b) indirect measurement of the velocity component u_y



assumption to the turbulent flow. The so-called Zero Correlation Method (ZCM) (Zhang and Eisele 1998a, Zhang 1999) enables the complete stress components in a two-dimensional plane to be determined by just carrying out two single measurements. The method thus does not provide any more expenses, because two measurements are necessary anyway for obtaining both the magnitude and the direction of the mean velocity. This method will be presented in below.

8.2 Basics of ZCM

The significant attribute of a turbulent flow is the stochastic velocity fluctuations. In dealing with a stationary turbulent flow, flow fluctuations basically comprise the fluctuations of both the magnitude and the direction of the velocity vector, as illustrated in Fig. 8.2 for a turbulent flow which was measured by the LDA method. Because of the stochastic feature of flow fluctuations, the fluctuation of the velocity direction in the $x - y$ plane can be considered to symmetrically lie on both sides of the mean velocity vector that has its direction at $\bar{\varphi}$. For further consideration, the velocity component along the mean velocity vector is denoted by u_1 .

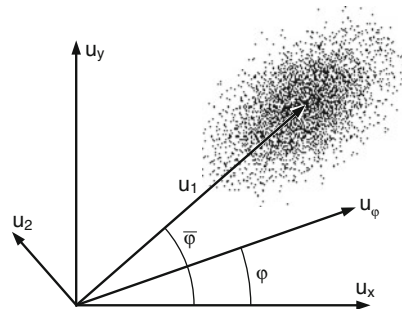


Fig. 8.2 Turbulent flow and velocity fluctuations measured by LDA

In its perpendicular, the velocity component is u_2 . Clearly there is $\bar{u}_2 = 0$. The symmetrical distribution of velocity fluctuations around the mean velocity vector is mathematically expressed by the zero correlation between flow fluctuations in velocity components u_1 and, u_2 as given by

$$C = \overline{u'_1 u'_2} = 0 \quad (8.2)$$

From velocity components u_1 and u_2 the velocity components u_x and u_y can be obtained from the orthogonal coordinate transformation that has already been outlined in Sect. 6.1. The same transformation is also applicable to the flow fluctuations. In effect, Eqs. (6.6) and (6.7) can be directly applied to represent the fluctuation velocities in the present case as

$$u'_x = u'_1 \cos \bar{\varphi} - u'_2 \sin \bar{\varphi} \quad (8.3)$$

$$u'_y = u'_1 \sin \bar{\varphi} + u'_2 \cos \bar{\varphi} \quad (8.4)$$

In these equations, the mean flow direction is denoted by angle $\bar{\varphi}$ that is calculated by

$$\tan \bar{\varphi} = \frac{\bar{u}_y}{\bar{u}_x} \quad (8.5)$$

For later convenience this equation is also represented as

$$\tan 2\bar{\varphi} = \frac{2 \tan \bar{\varphi}}{1 - \tan^2 \bar{\varphi}} = \frac{2\bar{u}_x \bar{u}_y}{\bar{u}_x^2 - \bar{u}_y^2} \quad (8.6)$$

The statistical turbulence properties including the Reynolds normal and shear stresses can be calculated from the velocity fluctuations u'_x and u'_y given above. With respect to the zero correlation condition given by Eq. (8.2), the following relationships are obtained

$$\overline{u_x'^2} = \overline{u_1'^2} \cos^2 \bar{\varphi} + \overline{u_2'^2} \sin^2 \bar{\varphi} \quad (8.7)$$

$$\overline{u_y'^2} = \overline{u_1'^2} \sin^2 \bar{\varphi} + \overline{u_2'^2} \cos^2 \bar{\varphi} \quad (8.8)$$

$$\overline{u'_x u'_y} = \frac{1}{2} (\overline{u_1'^2} - \overline{u_2'^2}) \sin 2\bar{\varphi} \quad (8.9)$$

Also to be mentioned is that these three equations can also be directly obtained from Eqs. (6.9), (6.10), and (6.11). The velocity components u and v there need to be considered to be the components on the main flow direction $\bar{\varphi}$ and its perpendicular, respectively. Because of predefined zero correlation condition by Eq. (8.2) $\tau_{uv} = 0$ should be applied.

Based on similar calculations, the turbulence properties related to any other components u_φ , according to Fig. 8.2, are given by

$$\overline{u_\varphi'^2} = \overline{u_1'^2} \cos^2(\varphi - \overline{\varphi}) + \overline{u_2'^2} \sin^2(\varphi - \overline{\varphi}) \quad (8.10)$$

$$\overline{u_\varphi' u_{\varphi+90}'} = -\frac{1}{2} (\overline{u_1'^2} - \overline{u_2'^2}) \sin 2(\varphi - \overline{\varphi}) \quad (8.11)$$

Because both normal stresses $\overline{u_1'^2}$ and $\overline{u_2'^2}$ are positive, the normal stress $\overline{u_\varphi'^2}$ is positive in all directions. In fact, $\overline{u_1'^2}$ and $\overline{u_2'^2}$ represent two principal normal stresses and $\overline{u_\varphi'^2}$ lies between them. From Eqs. (8.7) and (8.8) two principal normal stresses can be resolved as

$$\overline{u_1'^2} = \frac{1}{2} (\overline{u_x'^2} + \overline{u_y'^2}) + \frac{1}{2 \cos 2\overline{\varphi}} (\overline{u_x'^2} - \overline{u_y'^2}) \quad (8.12)$$

$$\overline{u_2'^2} = \frac{1}{2} (\overline{u_x'^2} + \overline{u_y'^2}) - \frac{1}{2 \cos 2\overline{\varphi}} (\overline{u_x'^2} - \overline{u_y'^2}) \quad (8.13)$$

Eq. (8.12) is indeed equal to Eq. (6.18) that represents the principal normal stress at the angle φ_m in the $x - y$ plane, see also Fig. 6.3. Obviously the zero correlation condition given by Eq. (8.2) assumes the angle φ_m for the principal normal stress to be equal to the main flow direction.

The above two equations are subsequently inserted into Eqs. (8.10) and (8.11), respectively. The following expressions are then obtained

$$\overline{u_\varphi'^2} = \frac{1}{2} (\overline{u_x'^2} + \overline{u_y'^2}) + \frac{\cos 2(\varphi - \overline{\varphi})}{2 \cos 2\overline{\varphi}} (\overline{u_x'^2} - \overline{u_y'^2}) \quad (8.14)$$

$$\overline{u_\varphi' u_{\varphi+90}'} = -\frac{\sin 2(\varphi - \overline{\varphi})}{2 \cos 2\overline{\varphi}} (\overline{u_x'^2} - \overline{u_y'^2}) \quad (8.15)$$

These last two equations indicate that the complete Reynolds stresses in the $x - y$ plane can be well resolved from two independent i.e. non-coincident measurements ($\overline{u_x'^2}$ and $\overline{u_y'^2}$). In comparison with the method of three measurements, as presented in Sect. 6.2 with respect to Fig. 6.7, the method presented here clearly shows advantages in the simplification of turbulence measurements. This accessibility is simply based on the assumption of zero correlation condition $\overline{u_1' u_2'} = 0$ as specified in Eq. (8.2). For this reason the method shown above is called Zero Correlation Method (ZCM).

The turbulent shear stress $\overline{u_x' u_y'}$ is obtained by setting $\varphi = 0$ in Eq. (8.15), which results in

$$\overline{u_x' u_y'} = \frac{1}{2} \tan 2\overline{\varphi} (\overline{u_x'^2} - \overline{u_y'^2}) \quad (8.16)$$

and because of Eq. (8.6)

$$\overline{u'_x u'_y} = \frac{\bar{u}_x \bar{u}_y}{\bar{u}_x^2 - \bar{u}_y^2} \left(\overline{u_x^2} - \overline{u_y^2} \right) \quad (8.17)$$

Eq. (8.16) is comparable to Eq. (6.15). It can be directly applied to Fig. 8.1a.

8.3 Extension of ZCM

8.3.1 Non-orthogonal Velocity Components

The Zero Correlation Method (ZCM) introduced in the last section applies to the orthogonal velocity components like u_x and u_y in a two-dimensional plane, as shown in Fig. 8.1a. Because LDA arrangement like that in Fig. 8.1b is also often available, the ZCM must be modified to extend its applications.

From Eq. (8.14) the turbulent normal stress $\overline{u_y'^2}$ is resolved as

$$\overline{u_y'^2} = \frac{\cos \varphi \cos(2\bar{\varphi} - \varphi) \overline{u_x^2} - \cos 2\bar{\varphi} \overline{u_\varphi^2}}{\sin \varphi \sin(2\bar{\varphi} - \varphi)} \quad (8.18)$$

This equation signifies that from measurements of two non-orthogonal turbulence components $\overline{u_x^2}$ and $\overline{u_\varphi^2}$ in a two-dimensional plane the turbulence component $\overline{u_y^2}$ in the same plane can be determined as well. One has again the case of orthogonal normal stresses. All results achieved in Sect. 8.2, especially Eq. (8.16), can be applied. The mean flow angle $\bar{\varphi}$ is calculated by Eq. (8.5), where the mean velocity component \bar{u}_y is obtained from Eq. (8.1).

8.3.2 Three-Dimensional Flow Turbulence

Calculations presented above are performed for turbulence properties in a two-dimensional plane. For purposes of applying the ZCM to three-dimensional turbulent flows in the Cartesian coordinate system, Eq. (8.17) is taken into account as the reference for other components. The completeness of turbulent stresses can be expressed in a matrix as given by

$$\overline{u'_i u'_j} = \begin{vmatrix} \overline{u_x^2} & \frac{\bar{u}_x \bar{u}_y}{\bar{u}_x^2 - \bar{u}_y^2} \left(\overline{u_x^2} - \overline{u_y^2} \right) & \frac{\bar{u}_x \bar{u}_z}{\bar{u}_x^2 - \bar{u}_z^2} \left(\overline{u_x^2} - \overline{u_z^2} \right) \\ \frac{\bar{u}_x \bar{u}_y}{\bar{u}_x^2 - \bar{u}_y^2} \left(\overline{u_x^2} - \overline{u_y^2} \right) & \overline{u_y^2} & \frac{\bar{u}_y \bar{u}_z}{\bar{u}_y^2 - \bar{u}_z^2} \left(\overline{u_y^2} - \overline{u_z^2} \right) \\ \frac{\bar{u}_x \bar{u}_z}{\bar{u}_x^2 - \bar{u}_z^2} \left(\overline{u_x^2} - \overline{u_z^2} \right) & \frac{\bar{u}_y \bar{u}_z}{\bar{u}_y^2 - \bar{u}_z^2} \left(\overline{u_y^2} - \overline{u_z^2} \right) & \overline{u_z^2} \end{vmatrix} \quad (8.19)$$

Obviously three non-coincident measurements, from which both the mean velocities ($\overline{u_x}$, $\overline{u_y}$ and $\overline{u_z}$) and the turbulence components ($\overline{u_x'^2}$, $\overline{u_y'^2}$ and $\overline{u_z'^2}$) at a fixed point in the flow are obtainable, are sufficient to complete the Reynolds stress matrix with nine elements. The advantage of the ZCM has been thus again demonstrated.

8.4 Restriction and Validation of ZCM

The zero correlation method is indeed an approximation method that is introduced to simplify the turbulence measurements. Respective application restrictions and accuracies must be considered. From Eqs. (8.14) and (8.15), it is evident that the main flow angle $\overline{\varphi}$ in the used coordinate system should not be equal or very close to 45° . This limitation could also be confirmed from Eq. (8.16) when measurements of u_x and u_y should be accomplished. It is therefore recommended to arrange the appropriate $x - y$ coordinate system for measurements. At best the x -axis is set to closely agree with the main flow direction.

The extent of errors resulting from the ZCM depends on the homogeneity of turbulence in the respective flow to be measured. In actual fact, the method does work accurately as long as the zero correlation condition according to Eq. (8.2) is highly satisfied. This is always the case when the local flow does not sensitively affected by the rigid surface or boundaries in the flow. An experimental verification of the method was conducted once through measurements in a turbulent channel flow (Zhang and Eisele 1998a, Zhang 1999). In this validation measurement, a two-component coincident LDA system was applied, so that turbulent stresses $\overline{u_x'^2}$, $\overline{u_y'^2}$ and $\overline{u_x' u_y'}$ were directly obtained. Based on such measurements the validation of the ZCM could be well accomplished by following calculations:

- (1) From the coincident measurements of velocity components u_x and u_y other velocity components u_φ and $u_{\varphi+90^\circ}$ for each given angle φ can be calculated via coordinate transformation according to Eq. (6.4) as

$$u_\varphi = u_x \cos \varphi + u_y \sin \varphi \quad (8.20)$$

$$u_{\varphi+90^\circ} = -u_x \sin \varphi + u_y \cos \varphi \quad (8.21)$$

Subsequently the covariance i.e. the correlation between velocity fluctuations u'_φ and $u'_{\varphi+90^\circ}$ is calculated by

$$\overline{u'_\varphi u'_{\varphi+90^\circ}} = \sum_{i=1}^N (u_\varphi - \overline{u_\varphi}) (u_{\varphi+90^\circ} - \overline{u_{\varphi+90^\circ}}) \quad (8.22)$$

This covariance indeed represents the turbulent shear stress and is a function of angle φ .

- (2) On the other side the covariance $\overline{u'_\varphi u'_{\varphi+90^\circ}}$ for each given angle φ can also be directly calculated from two normal stresses $\overline{u_x'^2}$ and $\overline{u_y'^2}$ by using Eq. (8.15). Because of the use of this equation as a result of the ZCM, the calculation results must be considered to be approximate.
- (3) Calculation results from calculations in (1) and (2), respectively, will be compared.

This validation procedure was applied to the validation measurements (Zhang and Eisele 1998a, Zhang 1999). Figure 8.3a shows the comparison of respective calculations in function of each given angle φ . Obviously the ZCM provides satisfactory measurement results.

The same validation can be completed by concerning the turbulence component $\overline{u_\varphi'^2}$. On one side, this component can be calculated from velocity data that are obtained by Eq. (8.20), leading to accurate values of variance. On the other side, it can also be calculated directly from $\overline{u_x'^2}$ and $\overline{u_y'^2}$ by means of Eq. (8.14), leading to approximated values. The comparison between two calculations in relying on the mentioned validation measurement is shown in Fig. 8.3b. The same satisfactory results were obtained.

Strictly, the zero correlation condition according to Eq. (8.2) is not satisfied if applied to the turbulent boundary layer. With respect to the main flow direction $u_1 = u_x$ and to the perpendicular $u_2 = u_y$, the covariance $\overline{u'_1 u'_2}$ i.e. $\overline{u'_x u'_y}$ in the turbulent boundary layer is indeed a function of the distance to the wall surface and therefore does not disappear as it is assumed in the ZCM. The error arising from

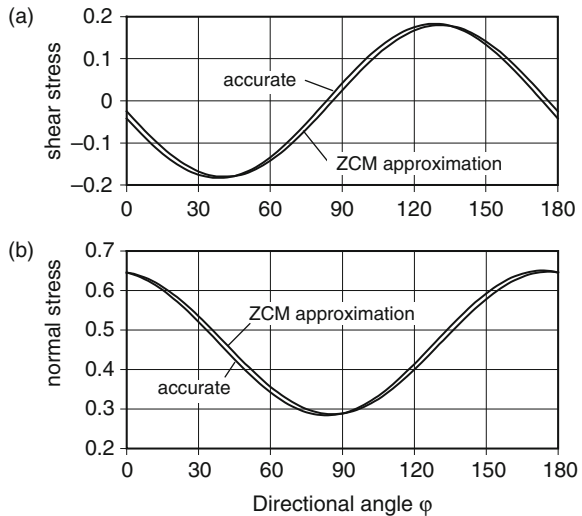
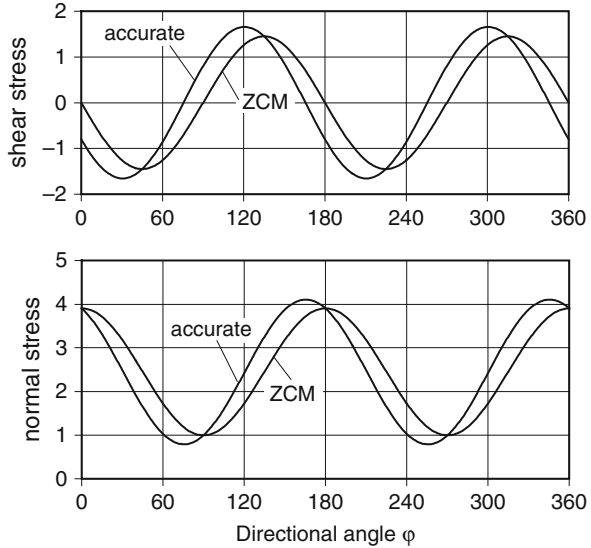


Fig. 8.3 Experimental validations of the ZCM by comparing the accurate turbulent stress in directional distribution with that calculated by the ZCM (Zhang and Eisele 1998a)

Fig. 8.4 Comparison of accurate turbulent stress in directional distribution with that calculated by ZCM for the flow in the turbulent boundary layer at $y^+ = 90$ (Zhang and Zhang 2002)



the assumption $\overline{u'_x u'_y} = 0$, when applied to the turbulent boundary layer, has been analyzed by Zhang and Zhang (2002). With known turbulent stresses $\overline{u'^2_x}$, $\overline{u'^2_y}$ and $\overline{u'_x u'_y}$ at a certain wall distance y^+ the directional distributions of the normal and shear stresses can be calculated by Eqs. (6.13) and (6.14), respectively. On the other hand, these distributions can also be calculated by assuming $\overline{u'_x u'_y} = 0$ which in effect simulates the application of ZCM. Figure 8.4 represents the comparison of respective calculations to the turbulent state at $y^+ = 90$ in the turbulent boundary layer. With certain reservation the ZCM in this application provides quite satisfactory result. This obviously arises from the fact that the amplitudes of both the normal and shear stresses in their trigonometric functions are mainly determined by the normal stresses $\overline{u'^2_x}$ and $\overline{u'^2_y}$. The assumption of $\overline{u'_x u'_y} = 0$ in the ZCM merely results in a shift in the directional distribution of respective turbulent stresses. In practical applications, it is indeed a matter of the application requirement, whether the resultant error could be accepted or not.

Chapter 9

Dual Measurement Method (DMM)

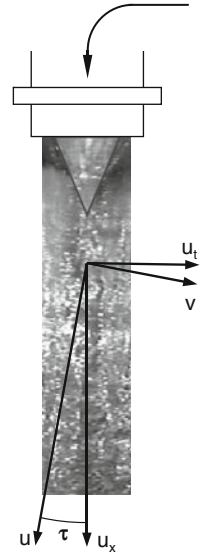
9.1 Possibility of Resolving the Secondary Flow

LDA measurements are component measurements. This means that the measured velocity components are always referred to as coordinates in the LDA optical system. For direct measurements of velocity components in the flow field coordinate system, LDA coordinates have to be arranged to agree with the flow field coordinates. In other cases, all interested velocity components in the flow field can be obtained from coordinate transformation, as described in [Chap. 6](#). Correspondingly, LDA users in practical applications always try to make sure either the accurate coincidence between two coordinate systems or an accurate rotation by a given angle. The alignment error has mostly been assumed to be small and hence is often neglected. This is generally allowed in most flow measurements at which the flow field could still be truly represented from the measurements despite the measurement errors. In contrast, however, there are cases at which a small error in LDA alignment to the flow field coordinates could lead to total misinterpretation of the actual flow field. Such a case has been for instance encountered by Zhang and Parkinson (2001, 2002) while trying to measure the very weak but very important secondary flow structure in a high speed water jet of a Pelton turbine (Fig. 9.1) In principle, it is generally impossible to align LDA velocity components u and v to be exactly coincident with velocity components u_x (axial) and u_t (tangential) of the jet flow. An inevitable small alignment error $\tau \neq 0$ simply means that the measured velocity component v additionally comprises a part of the axial velocity component, as given by

$$v = u_t \cos \tau + u_x \sin \tau \tag{9.1}$$

Although the bias angle τ as an error parameter is usually very small, the term $u_x \sin \tau$ in the above equation, however, could be still very large because of high values of the axial velocity component u_x in the high speed jet flow. In the case that this term is comparable to or larger than the term $u_t \cos \tau \approx u_t$, the secondary flow pattern represented by u_t would be sensitively and totally misinterpreted from measurements. For this reason the mentioned secondary flow in a cross section of the high speed jet flow could be measured neither directly nor indirectly through coordinate transformation.

Fig. 9.1 Possible inaccurate LDA alignment to a high speed jet flow and the associated problem of resolving the secondary flow structure in the jet cross section



Such a problem arising from inaccurate LDA alignment could be basically solved, when the alignment error i.e. the bias angle τ could be accurately identified and then the appropriate correction calculation of measurement data is implemented. In the mentioned measurement of the secondary flow structure in the high speed water jet, a method that is known as the Dual Measurement Method (DMM) was developed and applied to accurately identify the geometrical deviation in the LDA alignment to the jet flow. After finding out the alignment error, measurement data could be correctly evaluated. It dealt with a quite interesting flow phenomenon which could be detected by DMM.

The background of the dual measurement method is the two-measurement principle which is sometimes also called two-step method. The most famous example of using this principle is the Michelson-Morley experiment (Hecht 1990) that was constructed, by subsequently rotating the apparatus horizontally for 90° , to be able to measure the difference of light speeds in different directions, provided that this difference would exist. Another example that is directly related to LDA techniques is to exactly check the constant shift frequency generated in one of two laser beams of a laser beam pair, as it will be shown in Chap. 18.

In this chapter, the dual measurement method will be firstly presented in the version of its initial application to the high speed jet flow with complex secondary flow structures (Zhang and Parkinson 2001, 2002). Then the extended form of DMM (Zhang 2005) will be shown that can be applied to other special cases.

The readers would probably be interested in how the laser beams could enter into the jet that has a turbulent and hence opaque surface. The corresponding measurement technique of using an optical wedge can be found in Chap. 18 showing application examples.

9.2 DMM in Basic Form

The dual measurement method was initially developed to accurately resolve the secondary flow structure in the high speed jet flow of a Pelton turbine. The jet was generated by an injector which was connected to a bend, as shown in Fig. 9.2a. Because of the bend effect and the resultant change in the flow state, the flow after passing through the bend is characterised by the existence of a secondary flow structure across the pipe section, as shown in Fig. 9.2b based on LDA measurements of tangential velocity components. It deals with a typical secondary flow pattern that clearly demonstrates two identical areas with flow rotations. This flow structure remains while passing through the injector, as it was measured and has been shown in Fig. 9.2c, provisionally without mentioning how this secondary flow structure could be measured. Although it deals with a small scale secondary flow structure, it represents the main reason for the jet instability. One of the most serious disturbances on the jet because of related secondary flows is the generation of a chain of droplets on the jet surface, as indicated in Fig. 9.2a. The measurement of the secondary flow structure in the mentioned high speed water jet represents a highly difficult task and could only be conducted by means of DMM.

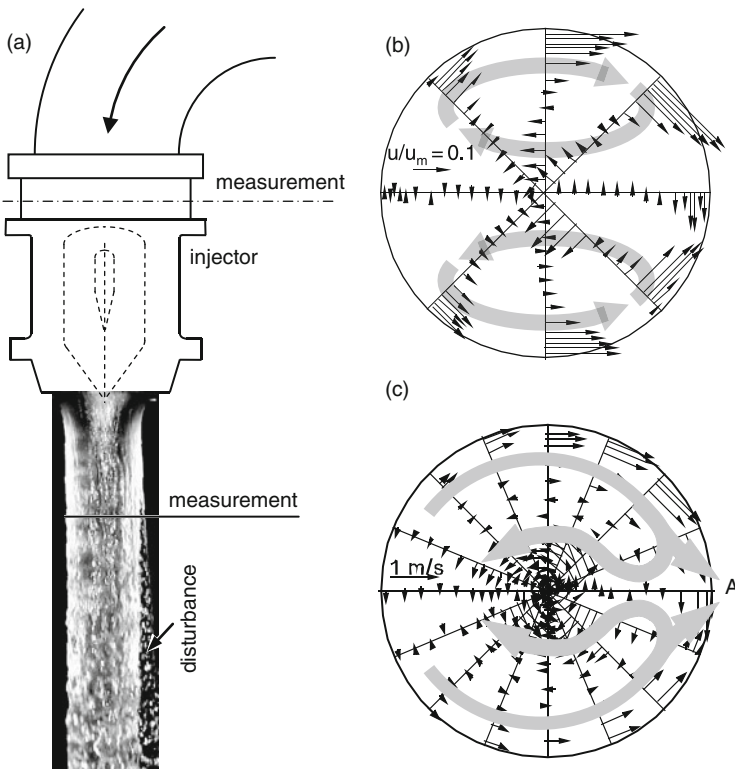


Fig. 9.2 Application example of the Dual Measurement Method (DMM) for accurately resolving the secondary flow in the high speed jet of a Pelton turbine (Zhang 2009)

The jet flow was made accessible for LDA measurements from all directions around the jet axis, as shown in Fig. 9.3a where a support platform for LDA head was installed. The LDA head is mounted on the traversing board of the support device that enables a velocity profile in the jet to be measured. For the measurement technique of getting the laser beams into the jet with turbulent and rough surface the readers are referred to Chap. 18.

The LDA optics was aligned for direct measurements of the tangential velocity component without using coordinate transformation. In assuming an alignment error i.e. a bias angle $\tau \neq 0$ as shown in Fig. 9.3b, the measured velocity component v takes

$$v_0 = u_t \cos \tau + u_x \sin \tau \quad (9.2)$$

In this equation the positive bias angle is defined as it is shown in Fig. 9.3.

The dual measurement method is constructed so as to arrange an additional flow measurement by simply rotating the LDA head around the jet axis by 180° (Fig. 9.3c). While rotating the measurement system the alignment error i.e. the bias angle τ can be assumed to be constant. The measured velocity component v this time at the same point in the jet flow is then given by

$$v_1 = -u_t \cos \tau + u_x \sin \tau \quad (9.3)$$

The second term on the r.h.s. of the above equation is the part arising from the axial velocity component u_x . For exact LDA arrangement with $\tau = 0$ there is

$$v_1 = -v_0 \quad (9.4)$$

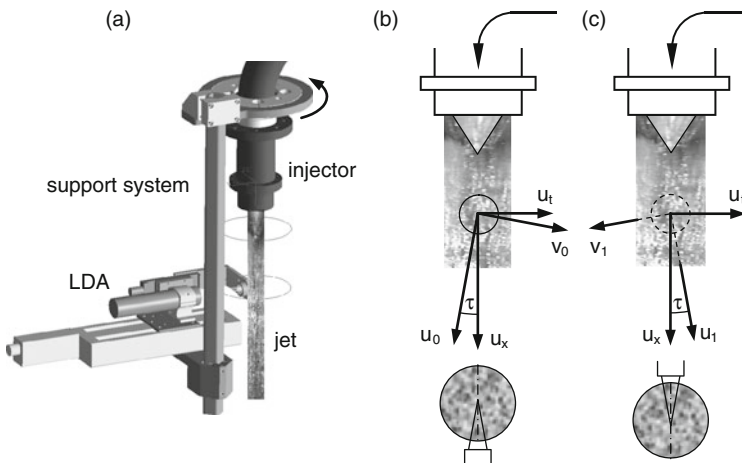


Fig. 9.3 DMM principle for accurately resolving the secondary flow structure in the high speed jet of a Pelton turbine

This equation represents a criterion of the faultless LDA alignment for direct measurement of velocity component u_t . Both values (v_1 and v_0) act as mirrored about $v = 0$. This ideal “mirrored view” of two velocity components v_1 and v_0 will be more or less disturbed by errors with $\tau \neq 0$ in LDA alignment. It can be concluded that any deviation from Eq. (9.4) is quantitatively related to the bias angle τ . Since this bias angle τ is actually a geometrical or mechanical arrangement error, it basically causes a systematic error which, according to Eqs. (9.2) and (9.3), takes $u_x \sin \tau$. This systematic error in the velocity measurement is called velocity shift because it acts as an additive quantity in both Eqs. (9.2) and (9.3).

From Eqs. (9.2) and (9.3) one obtains

$$v_{\text{sh}} = u_x \sin \tau = \frac{v_0 + v_1}{2} \quad (9.5)$$

as well as for $\tau \ll 1$

$$u_t = \frac{v_0 - v_1}{2} = v_0 - v_{\text{sh}} \quad (9.6)$$

It is now clear that through twice measurements of the same flow the velocity shift as the outcome of the LDA alignment error can be exactly identified. This dual deal of the jet flow measurement leads to direct determination of the tangential velocity component that otherwise could not be accurately measured. Because of this, the applied method is called the Dual Measurement Method (DMM).

With regard to the assumption that the velocity shift v_{sh} is a kind of systematic error involved in the LDA arrangement, it needs only to be determined one time at a fixed point in the flow by means of DMM. It can then be directly applied, according to Eq. (9.6), to correct the measurement results that are achieved at other points in the flow.

In the above mentioned example, the dual measurement method was applied to identify the bias angle τ and the associated velocity shift. The completed two measurements of the same velocity profile across the jet have been shown in Fig. 9.4a. Because it deals with the same velocity profile, the “mirrored view” of two-time measurements would have been expected. That is to say that two velocity profiles should have symmetrically lain on both sides of the neutral line with $v = 0$, if the bias angle τ would be zero. The measured deviation of the symmetry line from $v = 0$, as shown in Fig. 9.4a, just corresponds to the velocity shift calculated by Eq. (9.5). In this measurement example, the velocity shift reads at 0.4 m/s. It corresponds to a bias angle of $\tau = 0.92^\circ$ (for $u_x = 25$ m/s). Obviously this is a quite small angle. The associated velocity shift, however, is of the same order as the existing velocity component itself or even higher. With respect to the velocity shift determined from Fig. 9.4a measurement results could be immediately corrected, as shown in Fig. 9.4b. Both measurements after correction then behave as mirrored at $v = 0$, as expected.

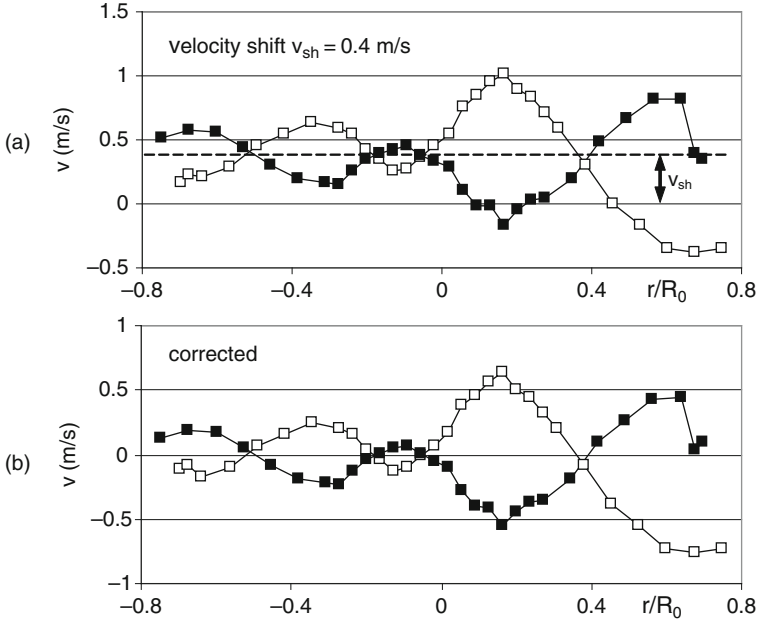


Fig. 9.4 Determination of the velocity shift by means of DMM and correction of the measurement results across the jet flow

With respect to the constant systematic error of $v_{sh} = 0.4$ in the installed system the complete secondary flow structure in a jet section has been measured and corrected, as already shown in Fig. 9.2c. Obviously the secondary flow that contains two counter-rotating vortices exhibits the similar flow structure as in the pipe ahead of the injector. At the point A both streams from two flow areas come together. Because of the absence of any rigid boundaries that could guide the jet flow, the fluid tends to escape from the jet. As the consequence a chain of water droplets comes about, as this has often been observed in hydro power plants with Pelton turbines since more than half century (Zhang 2009).

The comparison between Fig. 9.4a and Fig. 9.4b points out that a small bias angle τ could lead to total misinterpretation of the flow. In fact, none of the two measurements in Fig. 9.4a represents the real flow. While the real flow pattern in the jet section involves the swirling flow structures (Fig. 9.2c), each uncorrected measurement (Fig. 9.4a) simply shows a transversal motion of the fluid almost with $v > 0$.

Basically it is sufficient to apply the DMM to a single point in the flow to determine the bias angle τ and hence the systematic error in form of the velocity shift v_{sh} . In the presented example as shown in Fig. 9.4, the dual measurement method has been applied to a survey across the jet. This could be well realized by the constructed measurement system according to Fig. 9.3. The constant velocity shift across the jet straightforwardly demonstrates the reliability of DMM. The velocity shift as the systematic error involved in measurements has been thus verified.

It should be emphasized that the velocity shift could only be assumed as a constant systematic error, when the bias angle τ is kept constant while rotating the LDA support system. The consistency of the bias angle τ thus represents the prerequisite for applying the DMM.

9.3 DMM with Coordinate Transformation

In the last section, the direct dual measurement method has been presented. It is known as the direct method because in the applied example the LDA coordinates were initially set to be coincident with the flow coordinates by $u = u_x, v = u_y$ and $w = u_z$. Sometimes it is advantageous to rotate the LDA coordinate system by an angle α against the flow system, so that a coordinate transformation matrix $R(\alpha)$ generally exists between two coordinate systems (Chap. 6).

Because the angle of rotation of one coordinate system against another is by no means exact, its real value has to be assumed to involve a small LDA alignment error i.e. bias angle τ ($\ll 1$) and hence takes $\alpha + \tau$ according to Fig. 9.5 As for the general case, the velocity component to be measured in the secondary flow is denoted by u_y , instead of u_t that is used for the example in Sect. 9.2.

The alignment of a two-component LDA head according to Fig. 9.5a enables the measurements of velocity components u_0 and v_0 . The velocity component u_x and u_y in the flow system are then simply obtained by

$$u_x = u_0 \cos(\alpha + \tau) + v_0 \sin(\alpha + \tau) \tag{9.7}$$

$$u_y = -u_0 \sin(\alpha + \tau) + v_0 \cos(\alpha + \tau) \tag{9.8}$$

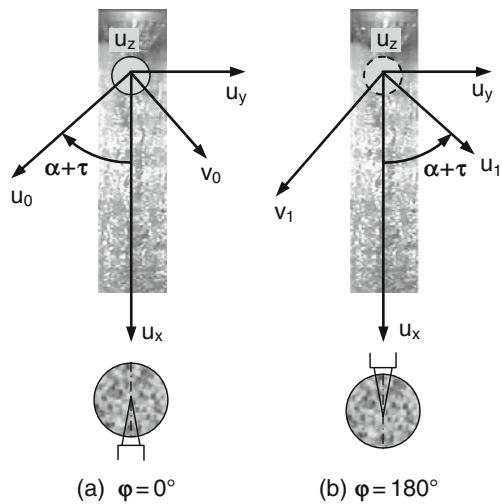


Fig. 9.5 DMM principle for accurately resolving the secondary flow structure in a high speed jet flow

Since the small alignment error τ only causes the negligible relative change in the axial velocity component u_x , so $\tau = 0$ can be applied to Eq. (9.7). Thus u_x acts as a component that is not affected by the alignment error τ . To Eq. (9.8) the approximations $\sin(\alpha + \tau) \approx \sin \alpha + \tau \cos \alpha$ and $\cos(\alpha + \tau) \approx \cos \alpha - \tau \sin \alpha$ because of $\tau \ll 1$ will be applied. This leads to

$$u_y = (-u_0 \sin \alpha + v_0 \cos \alpha) - u_x \tau \quad (9.9)$$

and further with the velocity shift $v_{sh} = u_x \tau$

$$u_y = (-u_0 \sin \alpha + v_0 \cos \alpha) - v_{sh} \quad (9.10)$$

Like in Eq. (9.5) the velocity shift appears again in the form of $v_{sh} = u_x \sin \tau$ i.e. $v_{sh} \approx u_x \tau$ because of $\tau \ll 1$. In addition, it has been again confirmed as an error that shifts the measurement results. Basically the velocity component u_y is intended to be determined by the first term on the r.h.s. of Eq. (9.10). This will be only true if $\tau = 0$ is true. The existence of the velocity shift v_{sh} as the consequence of the alignment error τ could significantly influence the determination of velocity component u_y , as already shown in the last section.

In order to examine the velocity shift existing in Eq. (9.10), the dual measurement method is again applied. This means that the LDA set-up needs to be turned around the x -axis by 180° , as shown in Fig. 9.5b. Attention has to be paid so that the bias angle τ as a systematic error has to remain constant.

From Fig. 9.5b and in analogy to Eq. (9.8), the velocity component u_y is directly written as

$$u_y = u_1 \sin(\alpha + \tau) - v_1 \cos(\alpha + \tau) \quad (9.11)$$

Based on similar calculation as that leading to Eq. (9.10) and newly with $u_x = u_1 \cos \alpha + v_1 \sin \alpha$ one obtains from the above equation

$$u_y = (u_1 \sin \alpha - v_1 \cos \alpha) + v_{sh} \quad (9.12)$$

Eq. (9.10) and (9.12) are found as basic equations to resolve both the velocity shift and the velocity component u_y . It yields

$$v_{sh} = u_x \tau = \frac{v_0 + v_1}{2} \cos \alpha - \frac{u_0 + u_1}{2} \sin \alpha \quad (9.13)$$

$$u_y = \frac{u_1 - u_0}{2} \sin \alpha + \frac{v_0 - v_1}{2} \cos \alpha \quad (9.14)$$

For $\alpha = 0$ one obtains Eq. (9.5) and (9.6), respectively.

Basically, the application of DMM in this case with coordinate transformation is completed. Although the velocity component u_y in Eq. (9.14) seems to be directly obtained from the dual measurements without via the calculation of the velocity shift, the velocity shift, however, gives a clear indication about the inaccuracy in

the LDA alignment. It will also be used, according to Eq. (9.10), to directly correct measurements at other measurement points in the flow with the same LDA setup. In practical applications, one can estimate the possible velocity shift according to $v_{\text{sh}} = u_x \tau$ by assuming the possible alignment error τ before carrying out the LDA measurement. When the estimated velocity shift is negligible against the velocity component u_y to be measured, then the dual measurement would not be necessary.

Sometimes it may be convenient to conduct calculations by using the velocity component u_x which is often assumed to be known. For this purpose, two cases in Fig. 9.5 are again considered. The velocity component v in LDA system can be expressed by

$$v_0 = u_x \sin(\alpha + \tau) + u_y \cos(\alpha + \tau) \quad (9.15)$$

$$v_1 = u_x \sin(\alpha + \tau) - u_y \cos(\alpha + \tau) \quad (9.16)$$

From these two equations and with respect to $\sin(\alpha + \tau) \approx \sin \alpha + \tau \cos \alpha$ it follows

$$\frac{v_0 + v_1}{2} = u_x \sin(\alpha + \tau) = u_x \sin \alpha + u_x \tau \cos \alpha \quad (9.17)$$

The velocity shift can thus be resolved as

$$v_{\text{sh}} = u_x \tau = \frac{v_0 + v_1}{2 \cos \alpha} - u_x \tan \alpha \quad (9.18)$$

It is completely equivalent to Eq. (9.13).

Especially it follows from (9.15) and (9.16) directly

$$u_y = \frac{v_0 - v_1}{2 \cos(\alpha + \tau)} \approx \frac{v_0 - v_1}{2 \cos \alpha} \quad (9.19)$$

This equation is completely equivalent to Eq. (9.14). Further for $\alpha = 0$, Eq. (9.6) is again obtained.

9.4 Extension of DMM

The Dual Measurement Method (DMM) has been constructed based on the “mirrored view” of two measurements. Through the direct comparison between two measurements of the same velocity component, the alignment error in LDA optics and the associated velocity shift can be exactly determined. However, it often comes about that the positioning of the LDA head at 180° for the second measurement is impossible. This will limit the application of DMM in such a way that by positioning the LDA head at another angle the measurement cannot be compared with the first measurement, because it deals with the measurements of two different velocity

components. This means that two measurements are generally not sufficient to identify the alignment error and the associated velocity shift. As an extension of DMM, a method of carrying out three arbitrary measurements at a fixed point in the flow from three different azimuth angles φ has been developed and also experimentally validated by Zhang (2005). The concept was that at a fixed point in the flow, any three velocity components measured at three different azimuth angles have to lie in a same plane and thus are related to a unique plane vector, when the LDA optics is aligned to the flow without any alignment error. Otherwise a unique plane vector would not exist, when the LDA system is aligned to the flow system with an error $\tau \neq 0$. Indeed, this concept has been clearly shown in Fig. 9.3. Because of the alignment error $\tau \neq 0$ the two measured velocity components v_0 and v_1 do not lie in the plane perpendicular to the jet axis.

9.4.1 Direct Component Measurements

The flow is given in the flow coordinate system by $\vec{u}_{\text{flow}} = (u_x, u_y, u_z)$. Herein u_x represents the component in the main flow direction. As an example, the jet flow with the axial component u_x has been shown in Fig. 9.3. The velocity components related to LDA are involved in the velocity vector $\vec{u}_{\text{LDA}} = (u, v, w)$. Usually a two-component LDA system is applied and the measured velocity components are denoted by u and v , respectively. The theoretically exact coincidence between the LDA and the flow systems is assumed to be given by $u = u_x$ and $v = u_y$. The corresponding arrangement of the LDA head to the flow (Fig. 9.6a, b) is denoted as the basic arrangement. Deviations from this basic arrangement are confirmed by

- (1) bias angle $\tau \neq 0$. It is unknown and should be identified through measurements. Here τ is like in Fig. 9.3 the angle between velocity components u and u_x ;
- (2) rotation of the LDA head about the x -axis for further carrying out two measurements at two other azimuth angles (Fig. 9.6c, $\varphi = \varphi_1$ and $\varphi = \varphi_2$).

With respect to these two deviations, specified by angles τ and φ , the general relationship between velocity components in two coordinate systems should be established. The velocity shift is expected to appear again in the form $v_{\text{sh}} = u_x \tau$. For the reason of mathematical simplicity the LDA alignment with τ and φ as parameters is assumed to be achieved by successively getting φ and τ from the basic arrangement with $u = u_x$ and $v = u_y$ (Fig. 9.6a). In the first step, when the LDA head has rotated about the x -axis by φ (Fig. 9.6c), the relationship between velocity components in LDA and flow systems is given by

$$u' = u_x \quad (9.20)$$

$$v' = u_y \cos \varphi - u_z \sin \varphi \quad (9.21)$$

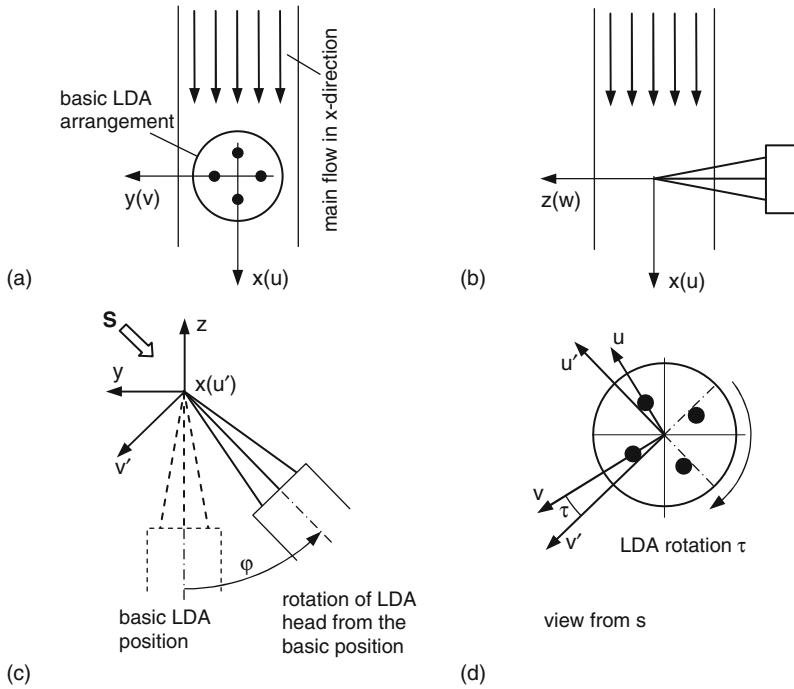


Fig. 9.6 Explanation of extended Dual Measurement Method

or in the form of matrix

$$\begin{bmatrix} u' \\ v' \end{bmatrix} = R' \begin{bmatrix} u_x \\ u_y \\ u_z \end{bmatrix} = \begin{bmatrix} 1 & 0 & 0 \\ 0 & \cos \varphi & -\sin \varphi \end{bmatrix} \begin{bmatrix} u_x \\ u_y \\ u_z \end{bmatrix} \quad (9.22)$$

The LDA head is subsequently turned about its axis by τ (Fig. 9.6d). Corresponding relationship between velocity components is given by

$$\begin{bmatrix} u \\ v \end{bmatrix} = R'' \begin{bmatrix} u' \\ v' \end{bmatrix} = \begin{bmatrix} \cos \tau & -\sin \tau \\ \sin \tau & \cos \tau \end{bmatrix} \begin{bmatrix} u' \\ v' \end{bmatrix} \quad (9.23)$$

From Eqs. (9.22) and (9.23), the general relationship between velocity components in two coordinate systems with τ and φ as parameters is obtained as

$$\begin{bmatrix} u \\ v \end{bmatrix} = R \begin{bmatrix} u_x \\ u_y \\ u_z \end{bmatrix} = \begin{bmatrix} \cos \tau - \cos \varphi \sin \tau & \sin \varphi \sin \tau \\ \sin \tau & \cos \varphi \cos \tau - \sin \varphi \cos \tau \end{bmatrix} \begin{bmatrix} u_x \\ u_y \\ u_z \end{bmatrix} \quad (9.24)$$

with $R = R''R'$

Equation (9.24) represents the background for both the basic DMM, as described in Sect. 9.2, and the extended DMM. In fact, for $\varphi_0 = 0$ and $\varphi_1 = 180^\circ$ both v_0 and v_1 are obtained which are equal to Eqs. (9.2) and (9.3), respectively. Correspondingly Eqs. (9.5) and (9.6) will also be obtained.

As mentioned at the beginning of this section, three single measurements at a fixed point in the flow would be necessary to determine the velocity shift, if the positioning of the LDA head at $\varphi_1 = 180^\circ$ is ineffectual. This can be achieved for instance by positioning the measurement volume on the x -axis ($y = 0, z = 0$) and the LDA optics to three azimuth angles $\varphi = 0, \varphi_1$ and φ_2 . The following relationships between velocity components from measurements and in the actual flow field can be obtained from Eq. (9.24):

$$v_0 = u_x \sin \tau + u_y \cos \tau \quad (9.25)$$

$$v_1 = u_x \sin \tau + u_y \cos \varphi_1 \cos \tau - u_z \sin \varphi_1 \cos \tau \quad (9.26)$$

$$v_2 = u_x \sin \tau + u_y \cos \varphi_2 \cos \tau - u_z \sin \varphi_2 \cos \tau \quad (9.27)$$

These three velocity components represent those which are measured by LDA method at a fixed point in the flow from three different azimuth directions. They will be used to determine the LDA alignment error and the associated velocity shift, in order to finally accurately determine the velocity component u_y .

By eliminating $u_z \cos \tau$ in Eqs. (9.26) and (9.27) one obtains

$$v_1 \sin \varphi_2 - v_2 \sin \varphi_1 = u_x \sin \tau (\sin \varphi_2 - \sin \varphi_1) + u_y \cos \tau \sin(\varphi_2 - \varphi_1) \quad (9.28)$$

The term $u_y \cos \tau$ in this equation will be replaced by that from Eq. (9.25). The velocity shift is finally resolved as

$$v_{\text{sh}} = u_x \sin \tau = \frac{(v_1 \sin \varphi_2 - v_2 \sin \varphi_1) - v_0 \sin(\varphi_2 - \varphi_1)}{(\sin \varphi_2 - \sin \varphi_1) - \sin(\varphi_2 - \varphi_1)} \quad (9.29)$$

The actual velocity component u_y then results from Eq. (9.25) with $\cos \tau \approx 1$

$$u_y = v_0 - \sin \tau \cdot u_x = v_0 - v_{\text{sh}} \quad (9.30)$$

Eq. (9.29) represents the extended DMM in determining the velocity shift by three single measurements. As long as the velocity shift is obtained through this way, it can be applied to Eq. (9.30) to determine the velocity component u_y , which is simply the same as that in Eq. (9.6) and represents the velocity component in the secondary flow. The prerequisite of the applicability of the method is to maintain the bias angle τ as the constant systematic error in the measurement system. This can be ensured for instance by an appropriate mechanical system like that is shown in Fig. 9.3a.

For recognising the LDA arrangement error and the associated velocity shift in such an application, it is recommended that one locates the LDA measurement volume on the x -axis. This enables the LDA users to merely rotate the LDA support system, without having to realign the measurement volume.

The reliability of Eq. (9.29) could be successively verified by making use of the measurement results which have been shown in Fig. 9.2c. As shown, the flow on the jet axis was measured eight times. According to Eq. (9.29) any combination of three initial measurements is sufficient for calculating the velocity shift as a systematic error. Corresponding calculations (altogether 56 combinations) showed the satisfactory consistency of the velocity shift with a maximum uncertainty of about 14% around $v_{sh} = 0.4$ m/s.

In addition, Eq. (9.29) also points out that for the purpose of determining the velocity shift only measurements of the v -component are required. In other words, the one-component LDA instrument can be applied.

Finally, the velocity component u_z at the measuring point can also be derived. From Eq. (9.26) for instance this velocity component is calculated as

$$u_z = \frac{u_x \sin \tau + u_y \cos \varphi_1 \cos \tau - v_1}{\sin \varphi_1 \cos \tau} \quad (9.31)$$

With respect to $v_{sh} = u_x \sin \tau$ and u_y from Eq. (9.30) as well as $\tau \ll 1$ leading to $\cos \tau \approx 1$, the above equation becomes

$$u_z = \frac{(v_0 - v_{sh}) \cos \varphi_1 - (v_1 - v_{sh})}{\sin \varphi_1} \quad (9.32)$$

Correspondingly this velocity component can also be calculated from Eq. (9.27) as

$$u_z = \frac{(v_0 - v_{sh}) \cos \varphi_2 - (v_2 - v_{sh})}{\sin \varphi_2} \quad (9.33)$$

Combining Eq. (9.32) and (9.33) to eliminate v_0 yields

$$u_z = \frac{(v_1 - v_{sh}) \cos \varphi_2 - (v_2 - v_{sh}) \cos \varphi_1}{\sin(\varphi_2 - \varphi_1)} \quad (9.34)$$

These last three equations are fully equivalent.

9.4.2 Method of Using Coordinate Transformation

In Sect. 9.2, DMM was applied to the case at which the LDA coordinate system is rotated against the flow system by the angle $\alpha + \tau$ (see Fig. 9.5) inclusive the unknown alignment error τ . Based on the “mirrored view” of two velocities and the

direct comparison between them, the velocity shift as a systematic error can be identified. Restriction of the “mirrored view” may be encountered if the positioning of the LDA head at $\varphi = 180^\circ$ is impossible. Like in the case treated in the last section, three measurements at a single point in the flow are required in order to determine the velocity shift that is resulted from the alignment error. Clearly, the LDA head with rotation by an angle $\alpha + \tau$ (Fig. 9.5a) has to be positioned at $\varphi = 0, \varphi_1$ and φ_2 , successively. To establish the relationship between velocity components in LDA and flow field systems, Eq. (9.24) that is available for $\alpha = 0$ can be made of use. Because the angle α always appears in the form $\alpha + \tau$, Eq. (9.24) is directly taken over for the present use by substituting the bias angle τ through $\alpha + \tau$. In accordance with Eqs. (9.25) to (9.27) the following relationships between measurements and the actual flow are obtained:

$$v_0 = u_x \sin(\alpha + \tau) + u_y \cos(\alpha + \tau) \quad (9.35)$$

$$v_1 = u_x \sin(\alpha + \tau) + u_y \cos \varphi_1 \cos(\alpha + \tau) - u_z \sin \varphi_1 \cos(\alpha + \tau) \quad (9.36)$$

$$v_2 = u_x \sin(\alpha + \tau) + u_y \cos \varphi_2 \cos(\alpha + \tau) - u_z \sin \varphi_2 \cos(\alpha + \tau) \quad (9.37)$$

They are velocity components which are measured by LDA method at a fixed point in the flow from three different azimuth directions.

Equations (9.36) and (9.37) are combined to eliminate $u_z \cos(\alpha + \tau)$. This results in, similar to Eq. (9.28)

$$v_1 \sin \varphi_2 - v_2 \sin \varphi_1 = u_x \sin(\alpha + \tau)(\sin \varphi_2 - \sin \varphi_1) + u_y \cos(\alpha + \tau) \sin(\varphi_2 - \varphi_1) \quad (9.38)$$

The term $u_y \cos(\alpha + \tau)$ in this equation will be replaced by that from Eq. (9.35), leading to

$$u_x \sin(\alpha + \tau) = \frac{v_1 \sin \varphi_2 - v_2 \sin \varphi_1 - v_0 \sin(\varphi_2 - \varphi_1)}{\sin \varphi_2 - \sin \varphi_1 - \sin(\varphi_2 - \varphi_1)} \quad (9.39)$$

With respect to $\tau \ll 1$ and thus $\sin(\alpha + \tau) \approx \sin \alpha + \tau \cos \alpha$ the velocity shift is finally resolved as

$$v_{sh} = u_x \tau = \frac{1}{\cos \alpha} \cdot \frac{(v_1 \sin \varphi_2 - v_2 \sin \varphi_1) - v_0 \sin(\varphi_2 - \varphi_1)}{(\sin \varphi_2 - \sin \varphi_1) - \sin(\varphi_2 - \varphi_1)} - u_x \tan \alpha \quad (9.40)$$

For $\alpha = 0$ this equation is simplified to Eq. (9.29). Further for the positioning of the LDA head at $\varphi_1 = 180^\circ$ the above equation becomes the same as Eq. (9.5) which represents the basic form of DMM.

After the velocity shift has been determined through Eq. (9.40), the velocity component u_y can then be determined from Eq. (9.35). With respect to $\tau \ll 1$ and thus $\sin(\alpha + \tau) \approx \sin \alpha + \tau \cos \alpha$ and $\cos(\alpha + \tau) \approx \cos \alpha$ one obtains

$$u_y = \frac{1}{\cos \alpha} (v_0 - u_x \sin \alpha) - v_{\text{sh}} \quad (9.41)$$

For $\alpha = 0$ this equation is simplified to Eq. (9.30).

Because the velocity component u_x appears in both Eqs. (9.40) and (9.41), the two-component LDA system is required for the current case with $\alpha \neq 0$.

Chapter 10

Symmetrical Method of 3D-Velocity Measurements

Most LDA measurement systems are two-component systems. In the case where all three velocity components need to be measured, then two separate measurements must be carried out with the necessary realignment of LDA optics between the measurement series. Such measurements with the optical realignment always lead to more expenses and are also time-consuming. They are especially not applicable when the flow measurements should be completed within a short time as demanded by special flow processes. Basically, it seems to be unreliable to directly measure all three velocity components by using a two-component LDA system without realignment. There are cases, however, in which the symmetrical flow distribution can be utilized to cleverly succeed such a flow measurement. It actually deals with a method of simply carrying out the two-component measurements and afterwards making an appropriate evaluation of measurement data.

The simplest case is obviously the axial symmetrical flow like the swirling flow out of a burner for instance. According to Fig. 10.1 measurements of all three velocity components by using a two-component LDA optics can be accomplished by positioning the LDA head firstly along the z -axis for measurements of both the axial and radial velocity components and then along the y -axis for the tangential velocity component. The entire measurements have been thus completed without the optical realignment. As a special case for direct measurements of all three velocity components in this example there is no need to reprocess measurement data.

In reality, such a possibility exists in any type of symmetrical flows that can be encountered in lots of practical applications. Figure 10.2 shows a practical water atomization process flow, at which the flow in the atomization region is clearly three-dimensional, however, symmetrical about the $x - z$ plane. In this example (Zhang et al. 1998, Zhang and Eisele 1999, Zhang and Ziada 2000), it dealt with the measurements of water droplet distribution in the atomization region by means of the Phase Doppler Anemometry (PDA) which is an extension of the LDA method. For quantitative evaluation of the related atomization process the local mass flux of droplets is an extraordinarily important quantity. Its measurements, however, presumes the measurements of all three velocity components at each point in the flow. The method of using two-component LDA system to measure all three velocity

Fig. 10.1 Axial symmetrical flow and the method for measurements of all three velocity components

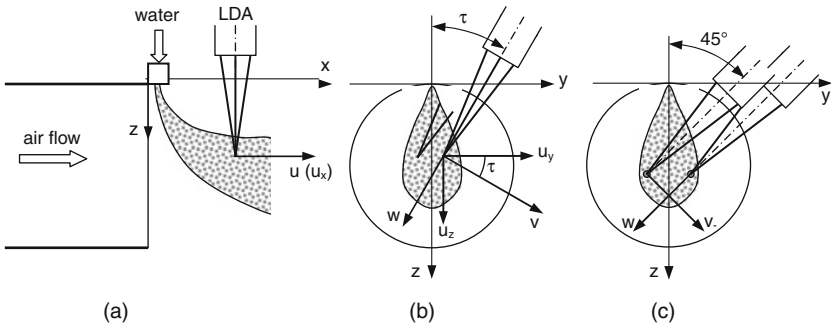
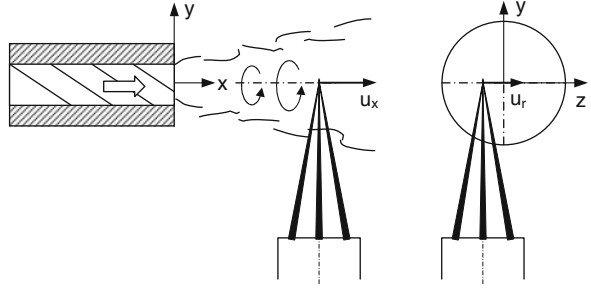


Fig. 10.2 Symmetrical atomization flow and the method for measurements of all three velocity components

components without rearranging the LDA optics was applied there. The main thing to do in this special application is the arrangement of measurements and the measurement data processing. This appears somewhat more complex than in the case that has been shown in Fig. 10.1.

In order to represent the universal applicability of this measurement method, the measurement example shown in Fig. 10.2 will be considered. For other cases and at other optical arrangements the LDA users have to probably find out respective relations for post-processing the measurement data.

According to Fig. 10.2 the flow is symmetrical about the $x - z$ plane. The two-component LDA head is aligned so that the optical axis is inclined by an angle τ in the $y - z$ plane. The two laser beam pairs are arranged to measure the velocity component u which is parallel to the x -axis and the component v which lies in the plane parallel to the $y - z$ plane. Two coordinate systems have been shown in Fig. 10.2: In the LDA-coordinate system, the velocity components are represented by u, v and w ; And in the flow coordinate system, they are symbolized by u_x, u_y and u_z . Obviously there is $u_x = u$. In the flow coordinate system, there are additionally $u_x(+y) = u_x(-y)$, $u_y(+y) = -u_y(-y)$ and $u_z(+y) = u_z(-y)$ because of the symmetry of the flow distribution about the $x - z$ plane.

The measurements are arranged by positioning the measurement volume sequentially and symmetrically in flow areas with positive and negative y -values

(Fig. 10.2b). This can be easily achieved by means of a traversing system on which the LDA head is mounted.

While the velocity component u_x in the flow coordinate system is directly measured because of $u_x = u$, the other two components u_y and u_z should be resolved from the measurements of velocity component v alone. In general, the velocity component v in the LDA coordinate system can be expressed by velocity components in the flow coordinate system. Depending on whether this v -component is measured in the positive (+) or negative (-) region of y , the velocity transformation is given by

$$v_+ = u_y (+y) \cdot \cos \tau + u_z \sin \tau \quad (10.1)$$

and

$$v_- = u_y (-y) \cdot \cos \tau + u_z \sin \tau \quad (10.2)$$

respectively.

With regard to the symmetry condition $u_y (+y) = -u_y (-y) = u_y$ these are two equations from which both the velocity component u_y and the component u_z can be resolved. By subtracting Eq. (10.2) from Eq. (10.1) as well as adding Eq. (10.1) to Eq. (10.2) one obtains

$$u_y = \frac{v_+ - v_-}{2 \cos \tau} \quad (10.3)$$

$$u_z = \frac{v_+ + v_-}{2 \sin \tau} \quad (10.4)$$

Together with $u_x = u$, these equations fully describe the three-dimensional flow state at the measurement point in the flow region $y > 0$. It refers to the flow region $y > 0$ because of the specification $u_y = u_y (+y)$. The velocity component v_- in above equations refers to the conjugate measurement point in the flow region $y < 0$. As a result of the symmetry of the flow distribution about the $x - z$ plane, corresponding three-dimensional flow states in the flow region $y < 0$ can be obtained immediately.

In the LDA coordinate system according to Fig. 10.2b, the third velocity component can be calculated by (for $y > 0$)

$$w = u_z \cdot \cos \tau - u_y \cdot \sin \tau = \frac{v_+ + v_-}{2 \tan \tau} - \frac{v_+ - v_-}{2} \tan \tau \quad (10.5)$$

It is indeed the on-axis velocity component. The restriction of the method is that the inclination angle of the LDA head could not be set at $\tau = 0$ or $\tau = 90^\circ$. The ideal inclination angle is obviously around $\tau = 45^\circ$ (Fig. 10.2c). At $\tau = 45^\circ$ it yields from Eq. (10.5)

$$w = v_- \quad (10.6)$$

It signifies that the velocity component v which is measured in the flow region $y < 0$ is equal to the velocity component w i.e. the on-axis component in the flow region $y > 0$. This results by all means because of the symmetry of the flow field and the LDA inclination at $\tau = 45^\circ$.

The method outlined above demonstrates that at least in the presented LDA alignment, measurements of all three velocity components are very well possible. Obviously data processing and calculation algorithms depend on used coordinate systems for both LDA optics and the flow. The calculation will be complex when for instance the u component in LDA-system does not coincide with the u_x component in the flow system. The calculation made above is obviously the simplest one. For other cases dealing with measurements of symmetrical flows, LDA users have to make their own calculations according to their LDA configurations.

Chapter 11

Non-stationary Turbulent Flows

11.1 Non-stationary Turbulent Flows in the Practice

Non-stationary turbulent flows are often encountered while starting or stopping a flow process. There are also designed non-stationary flow processes like the periodic flows in a reciprocating engine (also known as the piston engine) and the pulsatile flow through an prosthetic heart valve (Hirt et al.1994). Even in a stationary flow system, the local flow unsteadiness could occur. This can be encountered for instance in the alternating vortex flow from the trailing edge of a wing or in the flow at the exit of the impeller of a centrifugal pump (Fig. 11.1). The non-stationary flows are thus expressed either as the time- or phase-dependent flows. As in most cases, the non-stationary flows are usually also turbulent flows. Hence they are usually considered to be composed of the built-in i.e. enforced flow instability and the flow instability because of the flow turbulence. Mostly, as in the case of starting and stopping a flow process and even in the flow with local instabilities (Fig. 11.1), the flow turbulence can be considered as the small-scale flow fluctuations against the enforced flow state changes. The latter and their dependence on the time have been usually of much interest while evaluating a non-stationary flow process. For a general non-stationary turbulent flow, as presented in Fig. 11.2 for instance, the flow at a local point in the flow field can be expressed by the corresponding velocity component:

$$u(t) = \hat{u}(t) + u'(t) \tag{11.1}$$

The enforced non-stationary flow velocity $\hat{u}(t)$ is thus superimposed by the random flow fluctuation that is quantified by deviations of velocities from the enforced velocity profile. From measurements by means of LDA method that enables the rapid change of velocities in the non-stationary flow to be highly resolved and provides a time series of flow velocities, the enforced non-stationary flow $\hat{u}(t)$ can be well reconstructed i.e. regressed by the method of least squares fitting. This method has been widely applied in data analyses commonly based on experimental measurements.

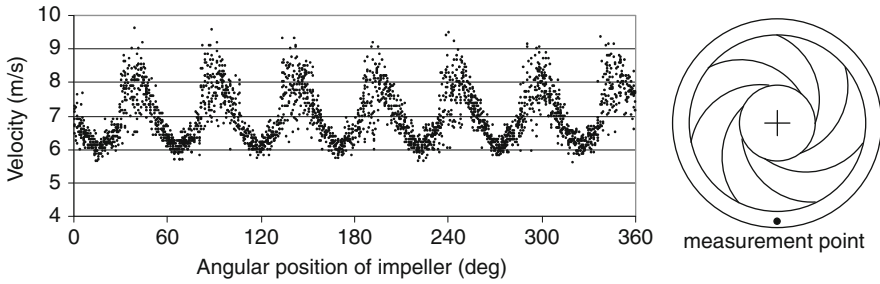
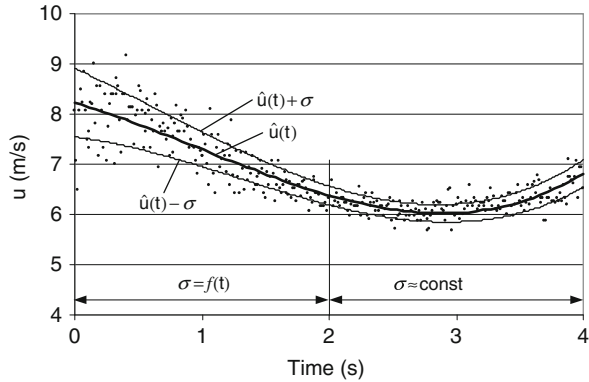


Fig. 11.1 Non-stationary flow at the exit of the impeller of a centrifugal pump, measured by LDA and rearranged to be the function of the angular position of the impeller

Fig. 11.2 Non-stationary turbulent flow and the method of data processing



Measurement data that do not lie on the fitted curve correspond to velocity fluctuations $u'(t)$ and can be considered, because of randomness, as resulted from the flow turbulence. In dealing with non-stationary flows, it is of most interest how the flow turbulence can be statistically evaluated. With regard to the time-dependent behavior of flow fluctuations, it is to distinguish between two fluctuation forms:

- nearly constant intensity of velocity fluctuations and
- variable intensity of velocity fluctuations in the function of time.

The first form of velocity fluctuations is characterized by the fact that the bandwidth of the flow fluctuation around the regressed curve is approximately constant. This can be confirmed for instance at Fig. 11.2 by considering the flow in the time period from 2 to 4 s. A unique value representing this bandwidth is representative for this form of flow turbulence. As the unique value the so-called standard deviation σ of the mean velocity (Chap. 2) has often been used. The second form of the turbulence distribution can be confirmed at Fig. 11.2 for instance by considering the flow in the time period from 0 to 2 s. A unique value representing the statistics of flow turbulence, however, does not exist in this case. Neither the turbulent normal

nor the shear stresses can be clearly represented by use of respective mean values. On the other hand, it is usually not clear what does the flow turbulence in such non-stationary flows actually mean for the related flow process (could be thermal or chemical for instance). Without knowing this, any complicated data processing would generally be of less value and could not be made of use. It is therefore always necessary to carry out the preliminary study and to carefully clarify the significance of respective turbulence quantities. In the case of dealing with turbulence models in computational fluid dynamics (CFD), for instance, the turbulent kinetic energy and hence the complete Reynolds turbulent stresses are known as the most important turbulence quantities. In the example shown in Fig. 11.2 with non-constant turbulence intensities, one can basically calculate the bandwidth of standard deviations of velocities in the function of time. The calculation indeed merely provides the precondition for further evaluations of measurement data with regard to the related physical and engineering flow processes.

The non-stationary flows encountered in the engineering practices can be divided into two categories. The first category is related to the start or stop of the flow process, so that the flow state is purely a function of the time. The second category of non-stationary flows is related to the enforced periodic flow that can be rearranged in function of the phase angle, like that as already shown in Fig. 11.1, for example.

11.2 Time-Resolved Non-stationary Turbulent Flows

11.2.1 Method of Linear Least Squares Fitting

In accounting for a non-stationary turbulent flow, it is in the first place interesting to know the time dependence of the enforced flow part. Based on LDA measurements, such a time-dependent flow can be well reconstructed by the curve fitting methods. Amongst lots of available mathematical functions used to approach the measurement data, the method of linear least squares fitting behaves as the basic form. As long as the linear trend of flow velocities measured in the interested time range is evident (e.g. at Fig. 11.2 in the time range from 0 to 2 s), the method can be applied to approximate the non-stationary turbulent flow. The linear regression function of the enforced flow is expressed as

$$\hat{u}(t) = at + b \quad (11.2)$$

Eq. (11.1) then becomes

$$u(t) = (at + b) + u'(t) \quad (11.3)$$

In order to perform the linear least squares fitting of measurement data, the sample means of both the time as the independent variable and the velocity as the dependent variable will be firstly calculated as

$$\bar{t} = \frac{1}{N} \sum_{i=1}^N t_i, \quad \bar{u} = \frac{1}{N} \sum_{i=1}^N u_i \quad (11.4)$$

Other quantities that are required are

$$s_{tt} = \frac{1}{N} \sum_{i=1}^N (t_i - \bar{t})^2, \quad s_{uu} = \frac{1}{N} \sum_{i=1}^N (u_i - \bar{u})^2, \quad s_{ut} = \frac{1}{N} \sum_{i=1}^N (u_i - \bar{u})(t_i - \bar{t}) \quad (11.5)$$

In all these calculations, no weighting factor has been used. The calculations hence suffer from certain inaccuracies which for instance are arising from the effect of velocity bias (Chap. 17). In particular, there is strictly $\bar{t} \neq (t_1 + t_N)/2$ because of velocity bias or other reasons and consecutively of non-constant data sampling rate during LDA measurements. For simplicity and also because of its negligible effect, the velocity bias is not considered here.

In LDA measurements, the time that is related to each velocity event is the independent variable and should be considered as accurate. The method of least squares fitting is formulated as

$$\sum_{i=1}^N (u_i - \hat{u}_i)^2 \rightarrow \min \quad (11.6)$$

In performing such a calculation with respect to \hat{u} as defined in Eq. (11.2), both constants a and b are determined as

$$a = \frac{s_{ut}}{s_{tt}}, \quad b = \bar{u} - a\bar{t} \quad (11.7)$$

The enforced non-stationary flow has been thus calculated based on the linear least squares fitting in the period $t_N - t_1$ containing N velocity events. The pure mathematical calculation additionally provides the knowledge about the degree of linearity between dependent and independent variables, given by the correlation coefficient

$$R = \frac{s_{ut}}{\sqrt{s_{uu}s_{tt}}} \quad (11.8)$$

The special case of $R = 1$ is obtained in that all measurement data lie on the fitted curve $\hat{u}(t) = at + b$. This implies the negligible random fluctuations of flow velocities. As will be shown in the next section, the correlation coefficient that is always less than unity actually involves the information about the mean flow turbulence in the time period $t_N - t_1$.

Because the velocity gradient that is given by a may be positive and negative, the correlation coefficient R in Eq. (11.8) may be so. In some applications like those of using a spreadsheet, the correlation coefficient is simply given in the form R^2 .

11.2.2 Linear Trend of the Velocity and the Calculation Method

The random velocity fluctuation in the non-stationary flow is denoted by $u'(t)$ for the given velocity component. The associated kinetic energy is represented by the turbulent normal stress or equivalently by the variance $\overline{u'^2}$ as a statistical parameter. In considering the measurement within the time period $t_N - t_1$, it is then calculated according to Eq. (11.3) and with respect to $b = \bar{u} - a\bar{t}$ as

$$\overline{u'^2} = \frac{1}{N} \sum_{i=1}^N [(u_i - \bar{u}) - a(t_i - \bar{t})]^2 \quad (11.9)$$

The calculation is given here simply as the arithmetic mean. Because of the use of $b = \bar{u} - a\bar{t}$ it is actually only applicable to the flow process with linear trend of velocity in the time period $t_N - t_1$.

Eq. (11.9) is then further written as

$$\overline{u'^2} = \frac{1}{N} \sum_{i=1}^N (u_i - \bar{u})^2 - \frac{2a}{N} \sum_{i=1}^N (u_i - \bar{u})(t_i - \bar{t}) + \frac{a^2}{N} \sum_{i=1}^N (t_i - \bar{t})^2 \quad (11.10)$$

and because of Eq. (11.5) also as

$$\overline{u'^2} = s_{uu} - 2as_{ut} + a^2s_{tt} \quad (11.11)$$

For the second term on the r.h.s. of this equation there is $as_{ut} = a^2s_{tt}$ because of Eq. (11.7). Equation (11.11) then becomes

$$\overline{u'^2} = s_{uu} - a^2s_{tt} \quad (11.12)$$

The regular data distribution i.e. the regular distribution of velocity events in the period $t_N - t_1$ will be assumed. This simply means $\bar{t} \approx (t_N + t_1)/2$. Then s_{tt} can be further calculated by converting the summation into the integral calculation as

$$s_{tt} = \frac{1}{N} \sum_{i=1}^N (t_i - \bar{t})^2 = \frac{1}{t_N - t_1} \int_{t_1}^{t_N} (t - \bar{t})^2 dt = \frac{(t_N - \bar{t})^3 - (t_1 - \bar{t})^3}{3(t_N - t_1)} \quad (11.13)$$

Because of $\bar{t} \approx (t_N + t_1)/2$ there is

$$s_{tt} = \frac{1}{12}(t_N - t_1)^2 \quad (11.14)$$

and from Eq. (11.7)

$$s_{ut} = as_{tt} = \frac{a}{12}(t_N - t_1)^2 \quad (11.15)$$

Eq. (11.12) is then rewritten as

$$\overline{u'^2} = s_{uu} - a^2 \frac{1}{12} (t_N - t_1)^2 \quad (11.16)$$

with s_{uu} as given in Eq. (11.5).

Furthermore, because of $\Delta \hat{u} = \hat{u}_N - \hat{u}_1 = a(t_N - t_1)$ from Eq. (11.2) the above equation is also written as

$$\overline{u'^2} = \frac{1}{N} \sum_{i=1}^N (u_i - \bar{u})^2 - \frac{1}{12} (\hat{u}_N - \hat{u}_1)^2 \quad (11.17)$$

The second term on the r.h.s. of this equation behaves as the correction term to the first term in calculating the turbulent normal stress in a non-stationary turbulent flow. Also to be mentioned is that the relationship given in Eq. (11.17) is obtained based on the assumption of linear trend of velocity in the time period $t_N - t_1$.

Following the similar calculations based on linear least squares fitting, the covariance of two orthogonal velocity components (u and v), that represents the turbulent shear stress, can be calculated as

$$\overline{u'v'} = s_{uv} - \frac{a_u a_v}{12} (t_N - t_1)^2 \quad (11.18)$$

Herein s_{uv} is calculated by the corresponding arithmetic mean as given by

$$s_{uv} = \frac{1}{N} \sum_{i=1}^N (u_i - \bar{u})(v_i - \bar{v}) \quad (11.19)$$

The second term on the r.h.s. of Eq. (11.18) is again the correction term. Both the constant a_u and a_v are equivalent to the constant a in Eq. (11.2). They are related to the velocity components u and v , respectively, and are calculated as

$$a_u = \frac{s_{ut}}{s_{tt}} \quad \text{and} \quad a_v = \frac{s_{vt}}{s_{tt}} \quad (11.20)$$

Because of relationships $\hat{u}_N - \hat{u}_1 = a_u(t_N - t_1)$ and $\hat{v}_N - \hat{v}_1 = a_v(t_N - t_1)$ Eq. (11.18) can then be written as

$$\overline{u'v'} = s_{uv} - \frac{1}{12} (\hat{u}_N - \hat{u}_1)(\hat{v}_N - \hat{v}_1) \quad (11.21)$$

In the last section, the correlation coefficient has been calculated and given in Eq. (11.8). Usually this correlation coefficient is directly accessible while carrying out the linear least squares fitting, for instance by applying a graphical tool with spreadsheet functions. As a matter of fact, the obtained correlation coefficient also contains information about the variance $\overline{u'^2}$ within the time interval $t_N - t_1$ and

therefore can be applied to determine the turbulent normal stress. With respect to s_{tt} from Eq. (11.14) and s_{uu} from Eq. (11.16) as well as $s_{ut} = as_{tt}$ from Eq. (11.7), Eq. (11.8) is expressed as

$$R^2 = \frac{s_{ut}^2}{s_{uu}s_{tt}} = \frac{a^2}{12} \cdot \frac{(t_N - t_1)^2}{u'^2 + \frac{a^2}{12}(t_N - t_1)^2} \quad (11.22)$$

The variance is then resolved as

$$\overline{u'^2} = \frac{a^2}{12} \left(\frac{1}{R^2} - 1 \right) (t_N - t_1)^2 \quad (11.23)$$

Because for linear data fitting there is $\hat{u}_N - \hat{u}_1 = a(t_N - t_1)$ Eq. (11.23) is also written as

$$\overline{u'^2} = \frac{1}{12} \left(\frac{1}{R^2} - 1 \right) (\hat{u}_N - \hat{u}_1)^2 \quad (11.24)$$

These last two equations can be applied to estimate the variance of each interested velocity component directly from the correlation coefficient R which is obtained from linear data fitting. Obviously the correlation coefficient R represents its mechanical significance always in the form R^2 . Also to be mentioned is that it cannot be concluded from Eq. (11.23) that for $a = 0$ there would be $\overline{u'^2} = 0$. This is because for $a = 0$ there is also $s_{ut} = 0$ and further $R = 0$.

Similarly the covariance of two orthogonal velocity components which are measured in the same time series can be obtained immediately when Eq. (8.16) is concerned:

$$\overline{u'v'} = \frac{1}{24} \tan 2\bar{\varphi} \left[\left(\frac{1}{R_u^2} - 1 \right) (\hat{u}_N - \hat{u}_1)^2 - \left(\frac{1}{R_v^2} - 1 \right) (\hat{v}_N - \hat{v}_1)^2 \right] \quad (11.25)$$

This equation is actually only applicable, if the enforced flow direction i.e. the flow angle $\bar{\varphi}$ in the plane of velocity components u and v remains constant despite of the flow instability. Otherwise the above equation is not valid.

Calculations given above based on the method of linear least squares fitting. In many other cases dealing with non-stationary flows, the enforced non-stationary flow can be, however, better approximated by other mathematical functions. Calculations presented in this section are then not applicable.

11.2.3 Time-Dependent Flow Turbulences

In the last section, the linear regression method in data processing has been presented. The method is applicable to each interested non-stationary flow in that in the time interval $t_N - t_1$, it can be approximated by the linear velocity distribution. Within this time interval, each turbulence quantity can be represented by its average,

like the turbulent normal stress by Eq. (11.9). This treatment has commonly found its wide practical applications.

In association with the determination of turbulence quantities in non-stationary turbulent flows there are generally two cases that limit the application of the presented method:

- The non-stationary flow could not be reconstructed through the linear or other approximations of measurement data within the interested time interval (Fig. 11.2).
- The turbulence is highly time-dependent and appreciably changes along the regressed curve in function of the time (Fig. 11.2 in the time interval 0–2 s). The flow turbulence in this case should be resolved in time and not be simply approximated by an average.

For both cases dealing with time-dependent turbulence quantities, an appropriate data processing method has to be worked out. Usually the data processing of non-stationary turbulent flows requires the classification of measurement data in the time series with predefined time steps which are also called time-averaging windows (Fig. 11.3). Inside each small sized time window, the flow could be roughly considered to be quasi-stationary. This treatment, however, is only valid if no appreciable change in the flow state within the time window is confirmed. This condition can be generally ensured by setting the time window Δt to be sufficiently small. Otherwise the variable flow within the time window has to be concerned. Because it deals now with a small sized window, the variable flow within it can be well approximated by the linear velocity distribution. In any case, either of quasi-steady or of variable flow state in each time window Δt , one has to make sure that sufficient measurement data are included for reliable statistical calculations of interested flow parameters.

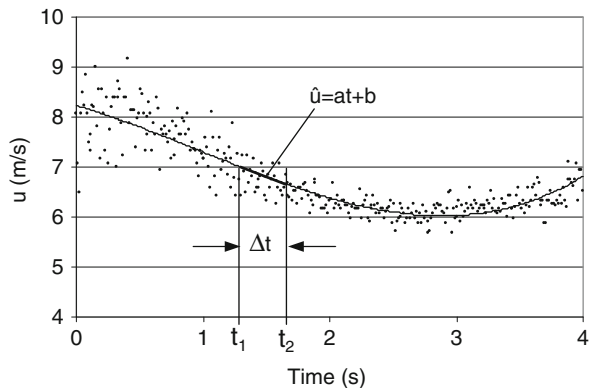


Fig. 11.3 Method of evaluating the non-stationary turbulent flows by specifying the appropriate time-averaging window size

The mean velocity inside the time window Δt in which n velocity events are included is obtained by the sample mean as

$$\bar{u} = \frac{1}{n} \sum_{i=1}^n u_i \quad (11.26)$$

As a matter of fact, this mean velocity is approximately equal to the middle value of \hat{u} in the time window Δt . It is thus independent of the slope of linear velocity distributions and further almost non-sensitive to the window size Δt . In contrast, the determination of turbulence quantities in the respective time window strongly depends on both the flow distribution in it and the window size itself. For simplicity, the general case of linear velocity distribution with regular velocity fluctuations in the time window Δt is considered. Calculations executed in Sect. 11.2.2 using the linear least squares fitting method in the time interval $t_N - t_1$ can then be directly applied to the present case with small sized time window $\Delta t = t_n - t_1$. From Eqs. (11.16) and (11.18) one obtains by substituting $\Delta t = t_n - t_1$ immediately the Reynolds normal and shear stresses being averaged in the time window

$$\overline{u'^2} = \frac{1}{n} \sum_{i=1}^n (u_i - \bar{u})^2 - \frac{a_u^2}{12} (\Delta t)^2 \quad (11.27)$$

$$\overline{u'v'} = \frac{1}{n} \sum_{i=1}^n (u_i - \bar{u})(v_i - \bar{v}) - \frac{a_u a_v}{12} (\Delta t)^2 \quad (11.28)$$

The temporal gradients of velocities inside the time window are denoted by a_u and a_v , respectively for velocity components u and v . In both equations, the second terms on the r.h.s. behave as the correction terms. Obviously the actual Reynolds stresses within the time window Δt are not simply equal to those from respective arithmetic average in the summation form of using $(u_i - \bar{u})$ and $(v_i - \bar{v})$ in above equations. Both first terms on the r.h.s. of equations given above are therefore called pseudo or apparent turbulent stresses. The apparent turbulent normal stress plainly implies the overestimation of flow turbulence. Hence turbulent stresses from arithmetic average should generally be corrected by respective terms like $a_u^2/12 \cdot \Delta t^2$ for the normal stress. It is, however, evident that for sufficiently small window all correction terms disappear. On the other hand, the time window of small size usually also implies few or insufficient data that are included in each time window for reliable statistical calculations. For this reason, the time window should be sufficiently large so that the real turbulence quantities can be accurately determined by accounting for respective correction terms in above equations. For stationary turbulent flow there is $a_u = 0$ and $a_v = 0$.

It should be mentioned that the necessity of accounting for the respective correction terms in Eqs. (11.27) and (11.28) depends on the requirement of calculation accuracies and therefore on the engineering application purposes of respective turbulence quantities. With regard to Eq. (11.28) for instance, it is possible that

the apparent shear stress (the first term on the r.h.s. of the equation) in the used coordinate system is equal or close to zero and hence the correction term dominates. The correction term, however, can still be neglected if it is sufficiently small against the normal stress in Eq. (11.27). This is grounded in that the relevant turbulence behavior in a turbulent flow is the directional dependence of respective turbulence quantities rather than that in a given spatial direction, see Figs. 8.3 and 8.4. In other words, the directional dependence of the turbulent stresses is mainly determined by the turbulent normal stresses.

11.3 Phase-Resolved Non-stationary Turbulent Flows

The most often encountered non-stationary flows in the engineering applications are periodic flows. As an example of this type of non-stationary flows the fluctuation velocity at the impeller exit of a centrifugal pump has been already shown in Fig. 11.1. The velocity data used in the diagram were achieved by LDA measurements and rearranged to be phase-resolved i.e. in the function of the angular

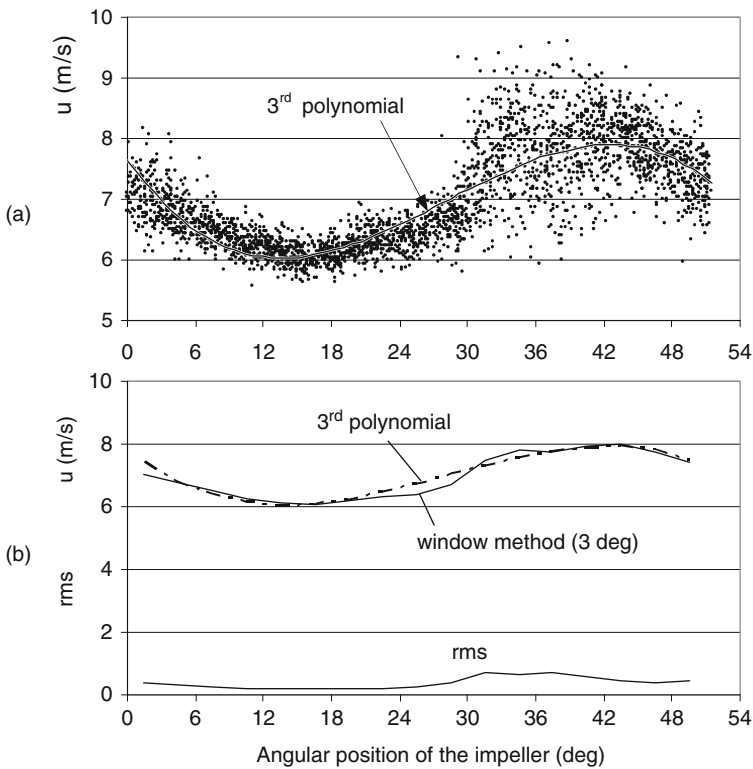


Fig. 11.4 Method of data processing by means of the small-sized phase averaging window (3°) without overlap, (a) Rearrangement of data from Fig. 11.1 to a sub-period of 51.4° ($360/7$), (b) Curve fitting and window method

position of the impeller. Obviously the enforced periodic flow is superimposed by the random flow fluctuations. The main objective of evaluating and processing such measurement data is to resolve both the periodicity of the flow and the turbulent flow fluctuations. In the example shown in Fig. 11.1, the flow repeated seven times in each pump rotation, corresponding to the flows in seven channels of the pump impeller. Because flows in all seven channels are primitively identical, the measurement data could also be rearranged to a sub-period which is specified by the phase angle range from 0 to 51.4° see Fig. 11.4a. The data rearrangement in this way greatly contributes to the simplification of further data processing. In order to resolve the phase-dependent mean velocity, usually appropriate data regression that is not necessarily linear can be calculated. In the example shown in Fig. 11.4a, an approach with a polynomial of 3rd order has been applied.

In principle, any deviation of velocities from the fitted velocity distribution should be considered to be from the random flow fluctuations. However, this deviation may actually also come from errors in the flow repeatability from circle to circle and thus is not of the randomness of velocity fluctuations as a result of the flow turbulence. The outcome of this situation, however, should only be considered at flows with low turbulence intensities, when the errors in the flow repeatability could not be simply accepted as the turbulent flow fluctuations.

On the side of measurement techniques, each periodic flow like that in the rotating machinery has to be resolved by the phase angle. This can be easily achieved by applying a rotary encoder that is mounted on the rotor shaft for instance and connected to the data acquisition unit.

11.3.1 Method of Linear Least Squares Fitting

As stated before with respect to Fig. 11.4a, the enforced velocity distribution of a non-stationary turbulent flow within an entire period can be well approximated by the regression of measurement data in accordance with an appropriate polynomial of at least second order. In order to utilize the advantages of linear least squares fitting to evaluate the phase-dependent flow turbulence, the periodic flow of interest can be approached by dividing a period into partial lengths and subsequently by assuming the linear distribution of velocities in form $\hat{u}(\varphi) = a\varphi + b$ in each of them. This approach is comparable with that described in Sect. 11.2.1 and applied in Sect. 11.2.2. For the purpose of direct application, similar calculations are presented here, as shown below.

In assuming the linear distribution of the enforced flow in the partial length $\varphi_N - \varphi_1$, the velocity component u for instance with fluctuations can be expressed as

$$u(\varphi) = (a\varphi + b) + u'(\varphi) \quad (11.29)$$

Like that shown in Sect. 11.2.1 both constant a and b are calculated respectively by

$$a = \frac{s_{u\varphi}}{s_{\varphi\varphi}} \text{ and } b = \bar{u} - a\bar{\varphi} \quad (11.30)$$

In the second equation, \bar{u} and $\bar{\varphi}$ are sample means of N velocity events that are involved in the considered phase interval i.e. partial length $\varphi_N - \varphi_1$ and calculated by

$$\bar{u} = \frac{1}{N} \sum_{i=1}^N u_i \text{ and } \bar{\varphi} = \frac{1}{N} \sum_{i=1}^N \varphi_i \quad (11.31)$$

Other available arithmetic means are

$$s_{\varphi\varphi} = \frac{1}{N} \sum_{i=1}^N (\varphi_i - \bar{\varphi})^2, \quad s_{uu} = \frac{1}{N} \sum_{i=1}^N (u_i - \bar{u})^2, \quad s_{u\varphi} = \frac{1}{N} \sum_{i=1}^N (u_i - \bar{u})(\varphi_i - \bar{\varphi}) \quad (11.32)$$

While performing the data regression, the correlation coefficient that represents the degree of linearity between dependent and independent variables is given as

$$R = \frac{s_{u\varphi}}{\sqrt{s_{uu}s_{\varphi\varphi}}} \quad (11.33)$$

It specifies a statistical quantity that most computational tools like the spreadsheet can provide with, usually in the form R^2 . It also represents a quantity that involves the information about the averaged flow turbulence within the phase interval $\varphi_N - \varphi_1$, see Sect. 11.3.2 below.

All the above equations can be further simplified when regular data distribution within the phase interval $\varphi_N - \varphi_1$ is assumed. The assumption simply implies the approximation $\bar{\varphi} \approx (\varphi_N + \varphi_1)/2$. Following the similar calculations as those in Sect. 11.2.2, one obtains

$$s_{\varphi\varphi} = \frac{1}{12} (\varphi_N - \varphi_1)^2 \quad (11.34)$$

$$s_{uu} = \overline{u'^2} + \frac{a^2}{12} (\varphi_N - \varphi_1)^2 \quad (11.35)$$

$$s_{u\varphi} = as_{\varphi\varphi} = \frac{a}{12} (\varphi_N - \varphi_1)^2 \quad (11.36)$$

In all these calculations, accurate angle measurements (φ) have been assumed. Also to be mentioned is that Eq. (11.35) actually represents the determination equation of the turbulent normal stress $\overline{u'^2}$.

11.3.2 Linear Trend of the Velocity and the Calculation Method

In order to calculate respective turbulence quantities in the interested phase interval $\varphi_N - \varphi_1$, the random flow fluctuation $u'(\varphi)$ should be basically resolved from Eq. (11.29). In likeness to Sect. 11.2.2 or directly from Eq. (11.35), the turbulent normal stress in the phase interval $\varphi_N - \varphi_1$ is calculated as

$$\overline{u'^2} = \frac{1}{N} \sum_{i=1}^N (u_i - \bar{u})^2 - \frac{a^2}{12} (\varphi_N - \varphi_1)^2 \quad (11.37)$$

And because of $\hat{u}_N - \hat{u}_1 = a (\varphi_N - \varphi_1)$ it is also written as

$$\overline{u'^2} = \frac{1}{N} \sum_{i=1}^N (u_i - \bar{u})^2 - \frac{1}{12} (\hat{u}_N - \hat{u}_1)^2 \quad (11.38)$$

Herein \hat{u}_1 and \hat{u}_N represent the linearized velocities at $\varphi = \varphi_1$ and $\varphi = \varphi_N$, respectively.

Correspondingly the turbulent shear stress that is given by the covariance of two orthogonal velocity components is calculated as

$$\overline{u'v'} = s_{uv} - \frac{a_u a_v}{12} (\varphi_N - \varphi_1)^2 \quad (11.39)$$

with

$$s_{uv} = \frac{1}{N} \sum_{i=1}^N (u_i - \bar{u})(v_i - \bar{v}) \quad (11.40)$$

Both a_u and a_v are constants that are obtained from calculating linear least squares fitting for velocity components u and v , respectively, see Eq. (11.30).

In an analogy to Sect. 11.2.2, the correlation coefficient that is calculated by Eq. (11.33) can be utilized to directly calculate the variance i.e. the turbulent normal stress. From Eqs. (11.23) and (11.24) regarding the velocity component u one obtains immediately

$$\overline{u'^2} = \frac{a^2}{12} \left(\frac{1}{R^2} - 1 \right) (\varphi_N - \varphi_1)^2 \quad (11.41)$$

$$\overline{u'^2} = \frac{1}{12} \left(\frac{1}{R^2} - 1 \right) (\hat{u}_N - \hat{u}_1)^2 \quad (11.42)$$

It should be mentioned again that in all above calculations the repeatability errors of mean velocity distribution from circle to circle in the periodic flow have been neglected. In addition, all calculations assumed the regular data distribution within the phase interval $\varphi_N - \varphi_1$, leading to the use of $\bar{\varphi} \approx (\varphi_N + \varphi_1)/2$. This condition could be more or less distorted when the measurement data is rearranged from the time to the phase domain under the condition of non-linearity between the time and the phase angle. This should only be considered when the associated effect is significantly large.

11.3.3 Phase-Dependent Flow Turbulences

More complex data processing is encountered when accounting for the periodic flows with complex velocity distribution and non-regular velocity fluctuations. Not only the mean velocities but also the turbulence quantities usually need to be resolved in the function of the phase angle. The method of linear least squares fitting presented in the last section appears to be not applicable, because it only applies to the phase interval $\varphi_N - \varphi_1$ with linear velocity distribution and almost consistent flow turbulence.

As in Sect. 11.2.3 of processing measurement data in the time domain by means of small sized time-averaging windows, periodic flows with complex velocity distribution and non-regular velocity fluctuations can be treated by specifying appropriate small sized phase-averaging windows. With sufficiently small phase angle window, both velocities and turbulence quantities within each window can be assumed to be constant and calculated by arithmetic average. In doing this, overlapping of the phase angle window can be arranged in order to smooth calculation results.

An example of calculating non-stationary turbulent flows by means of the window method named above has been shown in Fig. 11.4b, relying on the rearranged measurement data that had been shown in Fig. 11.4a. The mean velocity distribution was calculated by specifying a window size equal to $\Delta\varphi = 3^\circ$ without overlapping. The extent of velocity fluctuation has been shown as the time-dependent standard deviation in form of the root mean squares (*rms*).

In principle, calculations of mean velocity distributions will usually be less affected by the predefined phase-averaging window size. However, calculation results of the flow turbulence notably depend on the applied window size, if velocity gradients in these windows are significantly large. This is comparable with the data processing of time-dependent flow velocities (Sect. 11.2.3). The effect of velocity gradients on the data processing can only be neglected, when the window size is sufficiently small. Otherwise, the linear velocity distribution $\hat{u} = a\varphi + b$ within the phase angle window $\Delta\varphi$ should be assumed, so that

$$u(\varphi) = (a\varphi + b) + u'(\varphi) \quad (11.43)$$

Calculations performed in the last section based on linear least squares fitting in the phase interval $\varphi_N - \varphi_1$ can then be directly applied to the present case of using the small sized phase angle window $\Delta\varphi = \varphi_n - \varphi_1$, in which n velocity events are involved. From Eqs. (11.37) and (11.39) and by substituting $\Delta\varphi = \varphi_n - \varphi_1$ one immediately obtains the respective turbulence quantities representing Reynolds normal and shear stresses in the considered phase angle window as

$$\overline{u'^2} = \frac{1}{n} \sum_{i=1}^n (u_i - \bar{u})^2 - \frac{a_u^2}{12} \Delta\varphi^2 \quad (11.44)$$

$$\overline{u'v'} = \frac{1}{n} \sum_{i=1}^n (u_i - \bar{u})(v_i - \bar{v}) - \frac{a_u a_v}{12} \Delta\varphi^2 \quad (11.45)$$

They are comparable to Eqs. (11.27) and (11.28), respectively (Zhang et al. 1996, 1997). The temporal gradients of velocities inside the phase angle window are denoted by a_u and a_v , corresponding to velocity components u and v . In both equations, the second terms on the r.h.s. again behave as the correction terms. Correspondingly the arithmetic averages in the summation form of using $(u_i - \bar{u})$ and $(v_i - \bar{v})$ in above equations are called pseudo or apparent turbulent stresses. It is, however, evident that for sufficiently small window size both correction terms become negligible. The respective arithmetic average can then be directly applied to represent the actual turbulent stresses ($\overline{u^2}$ and $\overline{u'v'}$). On the other hand, the small window size usually also implies few or insufficient data that are included in each window for reliable statistical calculations. For this reason, each specified phase angle window should be sufficiently large and the related turbulence quantities should be determined by accounting for respective correction terms given in above equations. For a quasi-stationary turbulent flow inside the phase-averaging window there are $a_u = 0$ and $a_v = 0$.

As in Sect. 11.3.2, the repeatability errors of mean velocity distribution from circle to circle in the periodic flow have been neglected, while carrying out the above calculations.

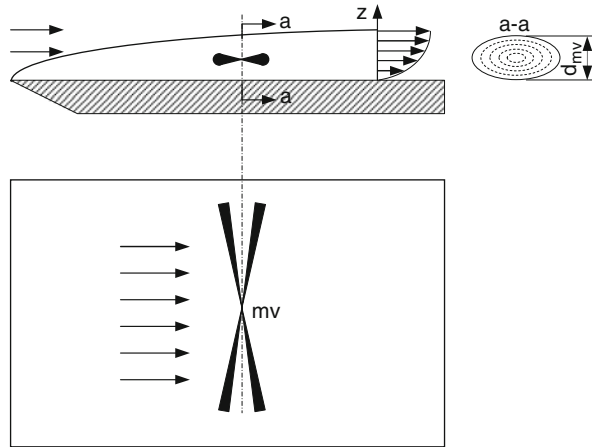
Chapter 12

Turbulent Flow with Spatial Velocity Gradient

In most applications, LDA measurements are considered as measurements of local flow velocities because of the small dimension of the measurement volume. Typically the LDA measurement volume possesses a thickness of about 0.1 mm and a finite length of about 0.3–3 mm, depending on the geometrical layout of LDA optics, see Sects. 3.8 and 4.2. This geometrical property of the measurement volume permits one to presume the uniform flow across the LDA measurement volume. On the side of instrumentations, the LDA unit is also commonly designed without being able to resolve the possible velocity distribution within the measurement volume. The assumption of the uniform flow within the LDA measurement volume is available, as long as the measurement volume is positioned sufficiently far away from the boundaries or in the flow where the spatial velocity gradient arising from eddy motions, for instance, is statistically negligible. In all these cases, no special care should be taken with regard to the measurement volume size. Because of the small dimension of the measurement volume, the LDA method has been acknowledged as being a method with high spatial resolutions in flow field measurements.

The high spatial resolution property of the LDA method can be made of use for special flow investigations. The well-known application is the measurement of the flow distribution in the near-wall region for instance in the turbulent boundary layers. Because of the large velocity gradient within the thin boundary layer the LDA measurement volume should be arranged so that the LDA optical plane is fairly parallel to the plane of the boundary layer (Fig. 12.1). By traversing the LDA head along the normal of the wall (z -axis) the velocity profile can be well measured. Such a measurement arrangement is generally able to resolve the velocity distribution within the near-wall region. Nevertheless, the measurement of velocity profiles in the viscous sub-layer region of a turbulent boundary layer could still be difficult because this viscous sub-layer has a thickness which is comparable to or even less than the thickness of the LDA measurement volume. In the practical application of flows with non-uniform velocity distribution and thus non-negligible influence on the measurement accuracy, the constant velocity gradient within the thickness of the thin measurement volume can be assumed. Naturally the arithmetic average of measurement data (velocity) has to be considered as existing at the centre of the measurement volume. While this can be sometimes accepted, the evaluation

Fig. 12.1 Optical arrangement of LDA for measurements of the velocity distribution in the near-wall region of a boundary layer

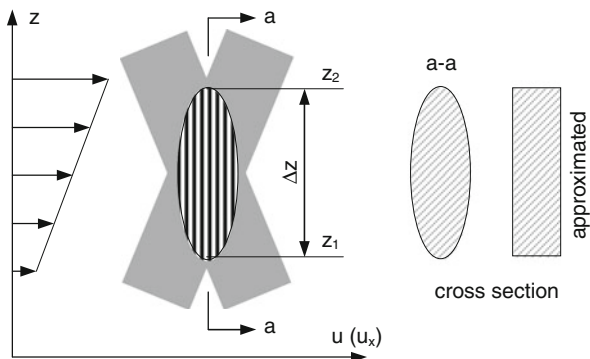


of measurement data to estimate the turbulence quantities requires the special process. This is comparable with the apparent turbulence intensity in the measurement of non-stationary turbulent flows, which has been treated in [Chap. 11](#). In particular, the same remains true that the turbulence intensity is always overestimated. The associated broadening effect in turbulence measurements becomes significant, if the non-uniform velocity distribution is along the length of the measurement volume. Corresponding descriptions of the associated phenomenon and the quantitative specifications can be found for instance by [Albrecht et al. \(2003\)](#) and [Durst et al. \(1998\)](#).

Although LDA method can be satisfactorily applied to flow measurements in the near-wall region according to the optical arrangement as shown in [Fig. 12.1](#), this LDA arrangement in the flow with velocity gradient, however, is not always available. This may be encountered for instance in the measurement of the flow in a circular pipe, at which the length scale of LDA measurement volume is usually aligned perpendicular to the pipe wall. Because the velocity gradient in this case lies along the length of the measurement volume, the apparent turbulence intensity becomes significant. For LDA measurements that are not restricted to the near-wall region of the turbulent boundary layer, however, the linear velocity distribution i.e. the constant velocity gradient along and within the length of the measurement volume can still be assumed in the first approximation. This applies to most complex engineering flows with velocity gradients and greatly contributes to the simplification of resolving the real from the apparent turbulence intensity.

Another phenomenon that is associated with the non-uniform velocity distribution in the measurement volume and affects the measurement accuracy is that the velocity sampling rate is proportional to the velocity itself, when homogeneous particle distribution in the flow is assumed. This phenomenon leads to some special features in calculating both the mean and turbulence velocities from the corresponding arithmetic average of measurement data. Because it is purely related to flow

Fig. 12.2 Optical arrangement for measurements of flows with velocity gradient along the LDA optical axis



velocities and is of the same mechanism as the flow instability in influencing the measurements, this phenomenon is also called velocity bias, which has been well known in measurements of non-stationary flows and the flows with high turbulence intensity (Chap. 17). In the case of large velocity gradient being present along the length of the measurement volume, the bias effect could be significant. It should be mentioned that the velocity bias, against the traditional viewpoint, could indeed not be simply categorized as being the measurement error. For details about this statement see Sect. 12.2 and Chap. 17.

It can be concluded that in dealing with flows that exhibit the velocity gradient within the area of LDA measurement volume, both the measurement and the related data processing suffer from two effects:

- the effect that leads to *apparent* turbulence intensity and
- the effect that leads to *velocity bias* in all flow quantities.

Two expressions have been used here to specify the two different effects. For LDA users it is helpful to know the quantitative outcomes of each and the combined effect. For simplicity and with respect to the practical engineering flows the linear velocity distribution in the LDA measurement volume will be supposed in the following analyses. In the related graphical illustrations, the non-uniform velocity distribution is assumed to be present along the length of the measurement volume (Fig. 12.2). The results are applicable to the velocity distribution along the thickness of the measurement volume. One needs only to make substitution for the respective length scale. For the purpose of comprehension, the case that results in the apparent turbulence intensity without the bias effect, will be considered first.

12.1 Apparent Turbulence Intensity and Related Quantities

The arrangement of LDA optics to the flow with velocity gradient has been illustrated in Fig. 12.2. In the applied coordinate system, the turbulent flow to be measured is considered as the superposition of the time-averaged linear velocity

distribution $\hat{u} = \bar{u}_1 + a(z - z_1)$ along the measurement volume and the random velocity fluctuations, as given by

$$u(z) = \bar{u}_1 + a(z - z_1) + u'(z) \quad (12.1)$$

The randomness of velocity fluctuations also implies that each velocity event is randomly ordered to a z -value. The linear velocity distribution is presented by the constant velocity gradient which is denoted by a and can be expressed by $a = (\bar{u}_2 - \bar{u}_1)/(z_2 - z_1)$. In assuming the unit thickness of the measurement volume in the direction perpendicular to the drawing plane, the volumetric mean velocity in the area of $\Delta z = z_2 - z_1$ is calculated as

$$\bar{u} = \frac{1}{z_2 - z_1} \int_{z_1}^{z_2} u dz = \frac{1}{2}(\bar{u}_1 + \bar{u}_2) \quad (12.2)$$

It is equal to the mean velocity that is found at the centre of the measurement volume. In this calculation, $u' dz = 0$ has been applied because of randomness of velocity fluctuations and their random distribution along the measurement volume length.

Combining the above equation with $a = (\bar{u}_2 - \bar{u}_1)/(z_2 - z_1)$ to eliminate \bar{u}_2 yields

$$\bar{u}_1 = \bar{u} - \frac{1}{2}a(z_2 - z_1) \quad (12.3)$$

Then Eq. (12.1) can be expressed as

$$u(z) = \bar{u} - \frac{1}{2}a(z_1 + z_2 - 2z) + u'(z) \quad (12.4)$$

To further calculate the turbulent normal stress, the fluctuation velocity in the above equation is resolved and then squared as

$$u'^2 = (u - \bar{u})^2 + a(u - \bar{u})(z_1 + z_2 - 2z) + \frac{1}{4}a^2(z_1 + z_2 - 2z)^2 \quad (12.5)$$

The velocity difference $u - \bar{u}$ in the second term on the r.h.s. of above equation will be interpreted by Eq. (12.4) in function of z , so that it yields, after a rearrangement,

$$u'^2 = (u - \bar{u})^2 - \frac{1}{4}a^2(z_1 + z_2 - 2z)^2 + a(z_1 + z_2 - 2z)u' \quad (12.6)$$

The averaged turbulent normal stress within the length of the LDA measurement volume can then be obtained by entirely averaging all three terms on the r.h.s. of the above equation. In reality, it deals with the arithmetic average of measurement data. To be expected is that the third term vanishes because of the randomness of velocity fluctuations and their random distribution along the z -axis. The corresponding

calculation of the second term can be transformed into an integral under the assumption of uniform distribution of velocity events along the LDA measurement volume (The case of non-uniform distribution of velocity events will be considered in the next section). The averaged turbulent normal stress in the area of the measurement volume is then calculated as

$$\overline{u'^2} = \frac{1}{N} \sum_{i=1}^N (u_i - \bar{u})^2 - \frac{1}{4} \frac{a^2}{z_2 - z_1} \int_{z_1}^{z_2} (z_1 + z_2 - 2z)^2 dz \quad (12.7)$$

The integral calculation can be performed easily. With $\Delta z = z_2 - z_1$ as the measurement volume length one obtains

$$\overline{u'^2} = \frac{1}{N} \sum_{i=1}^N (u_i - \bar{u})^2 - \frac{1}{12} a^2 (\Delta z)^2 \quad (12.8)$$

The first term on the r.h.s. of the above equation corresponds to the direct arithmetic average (sample mean). Because it does not represent the actual value of the related turbulence quantity it is called the pseudo or apparent normal stress. Using $a\Delta z = \Delta \bar{u}$, Eq. (12.8) is further written as

$$\overline{u'^2} = \overline{u'^2_{\text{app}}} - \frac{1}{12} (\Delta \bar{u})^2 \quad (12.9)$$

For the turbulent flow currently treated, the normal stress, which is calculated by the arithmetic average and thus is of apparent nature, needs to be corrected through a part that considers the spatial velocity difference $\Delta \bar{u} = \bar{u}_2 - \bar{u}_1$ i.e. the linear velocity distribution within the LDA measurement volume. The algorithm is similar to and comparable with that in Chap. 11 considering the non-stationary turbulent flows, see Eqs. (11.27) and (11.44). Only at flows with small spatial velocity gradient and comparably high turbulent velocities or at LDA with short measurement volumes, does the correction term become insufficient. The arithmetic average like in Eq. (12.8) can then be used, for convenience, to represent the actual value of the related turbulent normal stress.

Based on the same calculation procedure the turbulent shear stress is obtained in the form of the covariance of two orthogonal velocity components as

$$\overline{u'v'} = \frac{1}{N} \sum_{i=1}^N (u_i - \bar{u})(v_i - \bar{v}) - \frac{a_u a_v}{12} \Delta z^2 \quad (12.10)$$

It is comparable with Eq. (11.28) as well as Eq. (11.45).

The calculations given above have been performed with respect to the flow distribution along the LDA measurement volume that has a length equal to $\Delta z = z_2 - z_1$. The results can also be applied to the case of the flow distribution which is confirmed to be along the cross section of the measurement volume (Fig. 12.1). One needs only

to replace the length scale Δz in all above equations through the thickness d_{mv} of the LDA measurement volume. From Eq. (12.8) for instance, one obtains immediately

$$\overline{u'^2} = \overline{u_{app}^2} - \frac{1}{12} a^2 d_{mv}^2 \quad (12.11)$$

Because the thickness d_{mv} of the LDA measurement volume is usually very thin, the respective correction terms in both the normal and the shear stresses do behave as negligible.

It should be remembered that above calculations are based on the assumption of uniform distribution of velocity events along the LDA measurement volume. In reality, there are two factors that counteract this assumption. The first one is the velocity bias effect which implies that the high velocities will be more frequently detected by LDA optics than the low velocities. This effect will be considered in detail in the next section of this chapter. The second factor is related to the cross-section form of the LDA measurement volume. Because of the ellipsoidal form of the LDA measurement volume and hence non-constant width in its cross-section along the z -axis (Fig. 12.2), the assumption of uniform distribution of velocity events is not exact. The maximum probability of velocity events is obviously expected in the centre area of the measurement volume. This circumstance also applies to the case of LDA alignment as in Fig. 12.1, where along the thickness of LDA measurement volume the velocity gradient is present. With respect to the elliptic detection area of LDA measurement volume and in assuming the linear velocity distribution across the measurement volume thickness (d_{mv}), the averaged turbulent normal stress is calculated, according to Albrecht et al. (2003), as

$$\overline{u'^2} = \frac{1}{N} \sum_{i=1}^N (u_i - \bar{u})^2 - \frac{1}{16} a^2 d_{mv}^2 \quad (12.12)$$

In comparison with Eq. (12.11), only a small difference in the correction term is present.

At the end of this section, both the momentum and energy flow rates across the measurement volume should be considered. The mean velocity that is calculated in Eq. (12.2) is indeed the volumetric mean. In the practical application dealing with the flow with non-uniform velocity distribution, the mean velocities that are related to both the momentum and energy flow rates are all relevant flow quantities. The momentum flow rate as a vector quantity is calculated by the product of the velocity vector and the mass flow rate as $\dot{m} \cdot \vec{u}$. Its x -component is given by $\dot{m} \cdot u_x$. The corresponding component of the so-called momentum flux (momentum flow rate per unit area) is then given by $\dot{J}_x = (\rho u_x) u_x = \rho u_x^2$. Herein ρu_x represents the x -component of the mass flux. The related volumetric flux u_x in the unit of $m^3/(m^2s)$ is measured by LDA. In the case of Fig. 12.2, it is $u_x = u$. Furthermore the simplified rectangular cross-section with unit width is assumed. The averaged momentum flux component through the measurement volume is then calculated by

$$\bar{J}_x = \rho \frac{1}{\Delta z} \int_{z_1}^{z_2} u^2 dz \quad (12.13)$$

To the term u^2 in the integral, the linear velocity distribution according to Eq. (12.4) is applied. While calculating the integral, all terms with uneven power of velocity fluctuations (u') disappear. One obtains

$$\frac{\bar{J}_x}{\rho} = \bar{u}^2 + \frac{1}{12} a^2 (z_2 - z_1)^2 + \frac{1}{\Delta z} \int_{z_1}^{z_2} u'^2 dz \quad (12.14)$$

On the other side the interested momentum flux can also be written as $\bar{J}_x = \rho \bar{u}_J \bar{u}$, with \bar{u} as the mean of volumetric flux and \bar{u}_J as the mean velocity that is relevant for calculating the momentum flux. Eq. (12.14) then becomes

$$\bar{u}_J \bar{u} = \bar{u}^2 + \frac{1}{12} a^2 (\Delta z)^2 + \overline{u'^2} \quad (12.15)$$

Because of $a\Delta z = \bar{u}_2 - \bar{u}_1 = \Delta \bar{u}$ it is further written as

$$\bar{u}_J \bar{u} = \bar{u}^2 + \frac{1}{12} (\Delta \bar{u})^2 + \overline{u'^2} \quad (12.16)$$

As it will be shown in the next section, the mean velocity \bar{u}_J exactly corresponds to the sample mean undergoing the effect of velocity bias.

In practical applications, the momentum flux correction factor β has been used to represent the mean velocity \bar{u}_J through $\bar{u}_J = \beta \bar{u}$. From Eq. (12.16) it follows

$$\beta = \frac{\bar{u}_J}{\bar{u}} = 1 + \frac{1}{12} \frac{(\Delta \bar{u})^2}{\bar{u}^2} + \frac{\overline{u'^2}}{\bar{u}^2} \quad (12.17)$$

It represents a correction factor that is greater than unity.

For completeness, the mean velocity which is relevant for representing the energy flux is calculated by

$$\overline{u_E^2} \cdot \bar{u} = \frac{1}{\Delta z} \int_{z_1}^{z_2} u^3 dz \quad (12.18)$$

Following the similar calculations and by neglecting all terms with uneven power of velocity fluctuations (u') one finally obtains

$$\overline{u_E^2} = \bar{u}^2 + \frac{1}{4} (\Delta \bar{u})^2 + 3\overline{u'^2} \quad (12.19)$$

Correspondingly, the kinetic energy flux correction factor is calculated as

$$\alpha = \frac{\overline{u_E^2}}{\overline{u}^2} = 1 + \frac{1}{4} \frac{(\Delta\overline{u})^2}{\overline{u}^2} + 3 \frac{\overline{u'^2}}{\overline{u}^2} \quad (12.20)$$

It represents a value that is greater than unity.

12.2 Combined Velocity Bias Effect

It has been indicated that the velocity bias as a flow phenomenon is ascribed as the dependence of velocity sampling rate in LDA measurements on the velocity magnitude. Traditionally, the velocity bias has been acknowledged as being related to the non-stationary flows or the flows with velocity fluctuations (McLaughlin and Tiederman 1973). It is confirmed by that high velocities will be more frequently sampled than low velocities, if the homogeneous particle distribution in the flow is assumed. A great number of investigations aiming to estimate and correct the effect of velocity bias have been carried out. Detailed description and quantification of velocity bias in this traditional sense will be shown in Chap. 17.

As a matter of fact, the velocity bias in the similar form and of equal mechanism also exists in the flow with spatial velocity gradient. In this case, the non-uniform velocity distribution in the flow leads to non-uniform particle arrival rate and thus to non-uniform distribution of velocity events along the LDA measurement volume. To be expected is that more velocity events will be detected where the flow velocity is high. The arithmetic mean of velocities will be slightly shifted, if compared with the volumetric mean velocity, towards the upper value of the velocity.

The existence of velocity bias that is currently associated with the finite length of the LDA measurement volume and the spatially non-uniform velocity distribution will influence experimental determinations of both the mean velocity and all turbulent stresses. It is therefore reasonable to estimate the associated relationships in respective calculations. For simplicity, linear velocity distribution according to Eq. (12.4) as well as Fig. 12.2 is again assumed to be present along the measurement volume. In addition, further assumptions are specified as follows:

- (1) homogeneous particle distribution in the flow;
- (2) constant flow direction along the length of the measurement volume;
- (3) proportional dependence of velocity sampling rate on the magnitude of the measured velocity component.

Because of the second assumption the velocity bias which is hypothetically a function of the absolute velocity can be expressed in the proportional function of a velocity component.

Starting from the third assumption, the probability distribution of velocity sampling rate along the length of the measurement volume can be expressed by the probability density function

$$p_u = \frac{1}{N} \frac{dN}{dz} = ku \quad (12.21)$$

In this equation, the constant k must be determined from the condition that the probability of total velocity events sampled during a measurement is equal to unity. With the linear velocity distribution according to Eq. (12.4) one then obtains

$$\int_{z_1}^{z_2} p_u dz = k \int_{z_1}^{z_2} \left[\bar{u} - \frac{1}{2} a (z_1 + z_2 - 2z) + u' \right] dz = 1 \quad (12.22)$$

Without any difficulty the constant k can be resolved from this last equation. With $\Delta z = z_2 - z_1$ one obtains

$$k = \frac{1}{\bar{u} \Delta z} \quad (12.23)$$

12.2.1 Mean Velocity

From direct data processing of LDA measurements without any weighting form, the arithmetic mean velocity specifies the biased mean and is given as

$$\bar{u}_{\text{bias}} = \frac{1}{N} \sum_{i=1}^N u_i \quad (12.24)$$

On the other hand, the mean velocity that undergoes the bias effect is calculated with respect to the probability density function of velocity events as

$$\bar{u}_{\text{bias}} = \int_{z_1}^{z_2} p_u u dz = \frac{1}{\bar{u} \Delta z} \int_{z_1}^{z_2} u^2 dz \quad (12.25)$$

The integral in this equation has been already encountered at Eq. (12.13) and calculated at Eq. (12.14) in the last section. Thus, one immediately obtains

$$\bar{u}_{\text{bias}} \bar{u} = \bar{u}^2 + \frac{1}{12} (\Delta \bar{u})^2 + \overline{u'^2} \quad (12.26)$$

Obviously the mean velocity is shifted towards the upper value of the velocity ($\bar{u}_{\text{bias}} > \bar{u}$). The bias effect will disappear only when the second and the third terms on the r.h.s. of the above equation are negligible. For this reason it deals with a flow phenomenon and is therefore called velocity bias. The traditional aspect of velocity bias is related to the third term i.e. $\overline{u'^2}$.

As can be seen by comparing the above equation with Eq. (12.16), the biased mean velocity precisely represents the mean velocity that is used to calculate the mean momentum flow rate or the mean momentum flux across the measurement volume. In the field of flow dynamics as well as in related investigations, it is usual to distinguish between the volumetric mean velocity and mean velocities that are relevant for the momentum and the energy flux, respectively. While in applying the law of mass conservation the volumetric mean velocity is considered, the corresponding mean velocity should be accounted for when dealing with the momentum equations like Euler, Navier-Stokes or Reynolds equations (see Sect. 2.2). For this reason, the velocity bias represents an error only when the arithmetic mean velocity \bar{u}_{bias} according to Eq. (12.24) is used as the volumetric mean.

Correspondingly, the ratio of the biased to the volumetric mean velocities is equal to the momentum flux correction factor as $\beta = \bar{u}_{\text{bias}}/\bar{u}$.

For flows without velocity gradient ($a = 0$) as the special case, there is $\Delta\bar{u} = 0$ across the measurement volume. Eq. (12.26) is then simplified as

$$\bar{u}_{\text{bias}} = \bar{u} \left(1 + \frac{\overline{u'^2}}{\bar{u}^2} \right) = \bar{u} \left(1 + \text{Tu}^2 \right) \quad (12.27)$$

Here the use of turbulence intensity in the form $\text{Tu}^2 = \overline{u'^2}/\bar{u}^2$ is valid only when the velocity component u approximately represents the main flow. The fact that the biased velocity is simply related to the turbulence intensity agrees well with the approximation that was applied to estimate the bias effect in the traditional aspect of velocity bias (see Chap. 17). Because of this agreement it can be concluded that Eq. (12.26) concerns the effects of velocity bias in both the traditional aspect regarding the flow turbulence and the aspect that regards both the finite extent of LDA measurement volume and the non-uniform velocity distribution along the measurement volume.

As can be seen, Eq. (12.26) would basically also behave as the determination equation (polynomial of second order) for the volumetric mean velocity \bar{u} . While the biased mean velocity \bar{u}_{bias} is obtained by arithmetic mean of velocities according to Eq. (12.24), the actual turbulence quantity $\overline{u'^2}$, at the moment, remains unknown. Its determination will be presented in the next section, where it will be shown that the volumetric mean velocity \bar{u} can be rather more simply calculated than by using Eq. (12.26). The readers are kindly referred to Eq. (12.32).

12.2.2 Turbulent Normal Stress

More complex outcomes of non-uniform velocity distribution and thus non-uniform distribution of velocity events along the length of LDA measurement volume are found in determining actual values of turbulence quantities such as the turbulent normal stress. Firstly, the non-uniform velocity distribution results in the broadening of the turbulence scale, so that an *apparent* turbulent normal stress comes about. This

is comparable with the *apparent* turbulence that is resulted from the non-stationary flow and the related data processing. Secondly, both the non-uniformity of velocity events and the flow turbulence lead to *combined velocity bias*. To be noted is that the effect of this combined velocity bias on the mean velocity has been already treated in the last section.

With respect to these aspects the *biased apparent* turbulent normal stress in the velocity component u is calculated by direct data processing of LDA measurements as

$$\overline{u_{\text{app,bias}}^2} = \frac{1}{N} \sum_{i=1}^N (u_i - \bar{u}_{\text{bias}})^2 \quad (12.28)$$

It is called the apparent turbulent normal stress just because the velocity difference $u_i - \bar{u}_{\text{bias}}$ of each velocity event stands for the apparent velocity fluctuation. Like calculations of the biased mean velocity in the last section the *biased apparent* turbulent normal stress can be calculated by converting its summation form into the integral form. For this purpose the non-uniformity of velocity events along the measurement volume should be taken into account by again concerning the probability density function that is given in Eq. (12.21) with $k = 1/(\bar{u}\Delta z)$, so that

$$\overline{u_{\text{app,bias}}^2} = \int_{z_1}^{z_2} p_u (u - \bar{u}_{\text{bias}})^2 dz = \frac{1}{\bar{u}\Delta z} \int_{z_1}^{z_2} u (u - \bar{u}_{\text{bias}})^2 dz \quad (12.29)$$

The velocity component u in this equation is related to Eq. (12.4). It linearly changes along the measurement volume and further involves the flow fluctuations. In performing the integral calculation, all terms containing u' and u'^3 disappear because of the randomness of flow fluctuations. One obtains then from above equation

$$\overline{u_{\text{app,bias}}^2} = (\bar{u} - \bar{u}_{\text{bias}})^2 + \frac{1}{12} \left(3 - 2\frac{\bar{u}_{\text{bias}}}{\bar{u}} \right) (\Delta\bar{u})^2 + \left(3 - 2\frac{\bar{u}_{\text{bias}}}{\bar{u}} \right) \overline{u'^2} \quad (12.30)$$

Combining this equation with Eq. (12.26) to eliminate $\overline{u'^2}$ yields

$$\overline{u_{\text{app,bias}}^2} = (2\bar{u} - \bar{u}_{\text{bias}}) (\bar{u}_{\text{bias}} - \bar{u}) \quad (12.31)$$

The volumetric mean velocity is then resolved as

$$\bar{u} = \frac{1}{4} \left(3\bar{u}_{\text{bias}} + \sqrt{\bar{u}_{\text{bias}}^2 - 8\overline{u_{\text{app,bias}}^2}} \right) \quad (12.32)$$

This equation represents a simple method of determining the volumetric mean velocity \bar{u} directly from two arithmetic means. According to the context it actually belongs to the last section.

Equation (12.31) is further considered. The expression $(\bar{u}_{\text{bias}} - \bar{u})$ in it will be replaced by that from Eq. (12.26). It yields then

$$\overline{u_{\text{app,bias}}^2} = \left(2 - \frac{\bar{u}_{\text{bias}}}{\bar{u}}\right) \left(\frac{1}{12} (\Delta\bar{u})^2 + \overline{u'^2}\right) \quad (12.33)$$

or because of Eq. (12.9)

$$\overline{u_{\text{app,bias}}^2} = \left(2 - \frac{\bar{u}_{\text{bias}}}{\bar{u}}\right) \cdot \overline{u_{\text{app}}^2} \quad (12.34)$$

The biased apparent turbulent normal stress has been thus shown to be the apparent normal stress corrected by a factor which accounts for the bias effect. This relationship exactly represents the combination between the effect of velocity bias and the effect of non-uniform velocity distribution along the LDA measurement volume. In addition, comparing Eqs. (12.31) and (12.34) yields

$$\overline{u_{\text{app}}^2} = \bar{u} (\bar{u}_{\text{bias}} - \bar{u}) \quad (12.35)$$

For vanishing bias effect that is given only at laminar flows ($u' = 0$) with uniform velocity distribution along the LDA measurement volume, there is $\bar{u}_{\text{bias}} \approx \bar{u}$. Accordingly, there is $\overline{u_{\text{app,bias}}^2} \approx \overline{u_{\text{app}}^2} \approx \overline{u'^2} \approx 0$, as expected.

The actual turbulent normal stress can be calculated from Eq. (12.26) as

$$\overline{u'^2} = \left(\frac{\bar{u}_{\text{bias}}}{\bar{u}} - 1\right) \bar{u}^2 - \frac{1}{12} (\Delta\bar{u})^2 \quad (12.36)$$

and further with respect to $\Delta\bar{u} = a\Delta z$ as

$$\overline{u'^2} = \left(\frac{\bar{u}_{\text{bias}}}{\bar{u}} - 1\right) \bar{u}^2 - \frac{1}{12} a^2 (\Delta z)^2 \quad (12.37)$$

In this equation, the biased mean velocity \bar{u}_{bias} acts as known according to Eq. (12.24). The volumetric mean velocity has been already calculated in Eq. (12.32).

Based on all above calculations, additional simplifications are considered as follows:

12.2.2.1 Uniform Velocity Distribution

Because of $\Delta\bar{u} = 0$ along the LDA measurement volume, there is no apparent turbulence to be concerned, so that it comes about $\overline{u_{\text{app,bias}}^2} = \overline{u_{\text{bias}}^2}$ and $\overline{u_{\text{app}}^2} = \overline{u'^2}$. From Eq. (12.34) one obtains

$$\overline{u_{\text{bias}}^2} = \left(2 - \frac{\bar{u}_{\text{bias}}}{\bar{u}}\right) \cdot \overline{u'^2} \quad (12.38)$$

As can be confirmed from this relationship, the biased turbulent normal stress is less than its actual value because of $\bar{u}_{\text{bias}} > \bar{u}$ and hence $(2 - \bar{u}_{\text{bias}}/\bar{u}) < 1$. This circumstance has already been confirmed in earlier studies (Nobach 1998, Zhang 2002), see Chap. 17.

12.2.2.2 Negligible Turbulent Flow Fluctuations $\overline{u'^2} \approx 0$

This case can be considered to be comparable with measurements of laminar flows. From Eq. (12.33) one obtains

$$\overline{u_{\text{app,bias}}'^2} = \frac{1}{12} \left(2 - \frac{\bar{u}_{\text{bias}}}{\bar{u}} \right) (\Delta\bar{u})^2 \quad (12.39)$$

The term $\bar{u}_{\text{bias}}/\bar{u}$ in this equation is substituted by that from Eq. (12.26). It follows then with $\Delta\bar{u} = a\Delta z$

$$\overline{u_{\text{app,bias}}'^2} = \frac{1}{12} a^2 (\Delta z)^2 - \frac{a^4}{12^2} \frac{(\Delta z)^4}{\bar{u}^2} \quad (12.40)$$

Although the flow does not show any velocity fluctuations, a non-vanishing normal stress has been confirmed when using Eq. (12.28) to process LDA measurement data. The first term on the r.h.s. of above equation is the apparent part, as can be confirmed by comparing it with Eq. (12.9), and the second term of the part arising from the velocity bias, however, in negative effect. Obviously this second term represents a negligible part against the first term, especially at high velocity flow and the short measurement volume length. This indicates that for all practical flows with LDA measurements, when considering the turbulent normal stress, the velocity bias associated with non-uniform velocity distribution along the LDA measurement volume can be neglected. To be noted is that this conclusion is not applicable to the mean velocity according to Eq. (12.26).

12.3 Method of Resolving the Non-uniform Velocity Distribution

As shown above, the non-uniform velocity distribution for instance in the turbulent boundary layer complicates its accurate measurements. Neither the mean velocity nor the averaged turbulence quantities can be accurately located within the finite length of LDA measurement volume. Only when the LDA optics is arranged as in Fig. 12.1, the spatial distribution of the flow can be more accurately measured by a spatial resolution of about 0.1 mm.

In order to resolve both the mean velocity profile and the turbulence quantities within the finite length of the LDA measurement volume, separate receiving optics can be used, as shown in Fig. 12.3a for measurements of the velocity profile beneath a thin film of falling water. The transmitting optics is arranged to be perpendicular to the wall. The separate receiving optics is aligned with its focus to the measurement

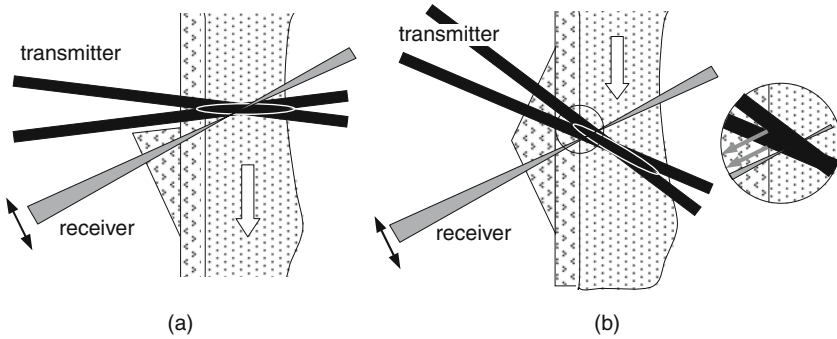


Fig. 12.3 LDA configuration to resolve the velocity profile beneath a thin water film

volume. In this case, a transparent wedge is applied to suppress all possible optical aberrations and hence to enhance the optical performance. Because of the small aperture of the receiving optics, only velocities at a local point along the length of the measurement volume will be measured each time. By traversing the receiving optics as shown in Fig. 12.3a, the velocity profile in the height of the thin water film can then be accurately resolved. Such an optical arrangement with the separate receiving optics has also been found by Wittig et al. (1996).

Another possible optical configuration is illustrated in Fig. 12.3b. This option, however, has a significant deficiency. Because of the symmetrical arrangement of transmitting and receiving optics the partial laser beams that are reflected on the window-water interface, will be directly guided to the receiving unit. This will lead to the rapid overloading of used photodetectors (e.g. photomultiplier) and to high noise in the opto-electronic signals. In addition, because of the non-regular refractions of two laser beams on the window-water interface, the optical performance of the measurement volume such as the fringe spacing and the fringe orientation will be affected.

Chapter 13

Flow Measurements Behind the Plane Window: On-axis

The non-intrusive property of the LDA method represents the greatest advantage against other methods using mechanical sensors for flow measurements. The LDA method thus has found its wide applications in measurements of internal flows such as the flows in ducts and machines. In such applications, both the ducts and the machines have to be configured to possess a window so that the flow is made optically accessible. It is well known by LDA users that the plane windows with parallel surfaces are always the first choice in practical applications, because the use of plane windows will significantly simplify calculations of laser beam transmissions through both the window and the test fluid. Another important advantage in using plane windows is that the fringe spacing in the LDA measurement volume remains constant i.e. independent of the optical properties both of the window and the test fluid, if the LDA optical axis is perpendicularly i.e. on-axis aligned to the window surface. This implies that in using plane windows no remarkable optical aberrations will occur. Refractions of laser beams do not have any remarkable influence on the measurements. These properties will be briefly revealed in this chapter.

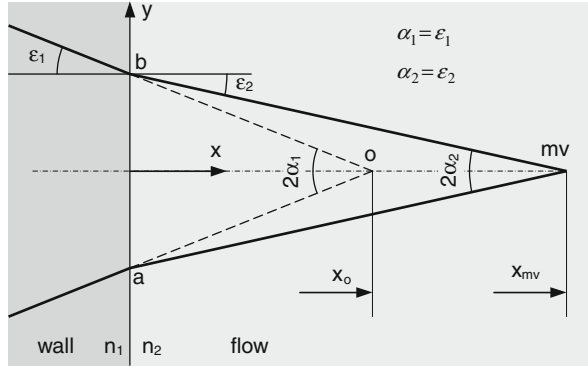
13.1 Fringe Spacing

The refraction of light waves on a medium interface follows the law of refraction according to Eq. (3.6). At the on-axis alignment of the LDA head to the plane of the medium interface, two laser beams of each laser beam pair in an LDA system undergo the symmetrical refraction. The half intersection angle between two refracted laser beams in the medium 2 is thus calculated according to Fig. 13.1

$$\sin \alpha_2 = \sin \varepsilon_2 = \frac{n_1}{n_2} \sin \varepsilon_1 \quad (13.1)$$

The speed of light in mediums 1 and 2, respectively, is given by $c_1 = \lambda_1 \nu$ and $c_2 = \lambda_2 \nu$ with λ as the wavelength and ν the frequency of the light wave. Firstly, the ratio of two light speeds is equal to the reciprocal of the corresponding refractive index ratio ($c_2/c_1 = n_1/n_2$). Secondly, the frequency of the light wave does not

Fig. 13.1 On-axis LDA alignment to the medium interface and the laser beam transmissions in the flow



change with the light ray refraction on the medium interface ($v_2 = v_1$). From these two conditions the wavelength of the light wave in the medium 2 is given by

$$\lambda_2 = \frac{n_1}{n_2} \lambda_1 \quad (13.2)$$

According to Eq. (3.46) for fringe model of LDA optics, the fringe spacing in the measurement volume, which is present in medium 2, should be calculated using the light wavelength λ_2 and the half intersection angle between two laser beams α_2 . With respect to Eqs. (13.1) and (13.2) the fringe spacing in the measurement volume is calculated as ($\alpha_1 = \epsilon_1$)

$$\Delta x = \frac{\lambda_2}{2 \sin \alpha_2} = \frac{\lambda_1}{2 \sin \alpha_1} \quad (13.3)$$

This equation signifies that at the on-axis i.e. perpendicular alignment of the LDA head to the medium interface, the fringe spacing in the measurement volume is independent of the fluid properties of the test flow. This is true even though both laser beams pass through a series of windows of different optical properties before reaching the flow.

13.2 Shift of the Measurement Volume

As a result of laser beam refractions on the medium interface, the intersection point of two laser beams, i.e. the measurement volume in the flow, shifts away from the virtual beam intersection point o (Fig. 13.1). The measurement volume as the actual intersection point of two laser beams is denoted by mv . Obviously the location of the measurement volume is a function of the location of the virtual beam intersection point. According to Fig. 13.1 this function can be easily established by considering the distance $y_b - y_a$ on the y-axis. By starting both from the virtual beam intersection

point and the measurement volume, respectively, this distance is given by

$$y_b - y_a = 2x_{mv} \tan \alpha_2 = 2x_o \tan \alpha_1 \quad (13.4)$$

Obviously the distance of the measurement volume from the medium interface is proportional to that distance of the virtual beam crossing point. The proportional constant is simply $\tan \alpha_1 / \tan \alpha_2$, as can be obtained from the above equation:

$$k_{mv} = \frac{dx_{mv}}{dx_o} = \frac{\tan \alpha_1}{\tan \alpha_2} \quad (13.5)$$

It also represents the ratio of the shift of the actual measurement volume to the shift of the virtual beam crossing point. The latter is equal to the shift of the LDA head, if the LDA head is positioned in the medium 1.

Although the calculation is achieved by considering two mediums, the ratio given in Eq. (13.5) also applies to the case of laser beam transmissions from air through a glass window into the test flow. It corresponds to the case of most available optical arrangement. The application of Eq. (13.5) is independent of the window used in between.

Because of small angles α_1 and α_2 in most LDA configurations, both $\tan \alpha_1$ and $\tan \alpha_2$ can be approximated by $\sin \alpha_1$ and $\sin \alpha_2$, respectively. With regard to Eq. (13.1), that represents the law of refraction, Eq. (13.5) then becomes

$$k_{mv} \approx \frac{\sin \alpha_1}{\sin \alpha_2} = \frac{n_2}{n_1} \quad (13.6)$$

The shift ratio of LDA measurement volume to the LDA head has been shown to be equal to the ratio of refractive indices of two mediums. It can be used to accurately position the LDA measurement volume in the flow by starting from a reference point of the measurement volume that lies, for instance, on the medium interface ($x = 0$).

Because of the simplest geometrical and optical behaviours in on-axis alignment of LDA optics, measurements of all types of internal flows behind a plane window can be well accomplished without having to pay any special attentions. In contrast to this, the optical condition and the measurement facilities will become much complex, when the LDA optical axis is aligned off-axis to the plane wall. This will be thoroughly described in Chap. 14.

13.3 Optical Dispersion and its Negligible Effect

A special phenomenon in the LDA optics with laser beams of different wavelengths should be mentioned. It is the optical dispersion which states that the refractive index of a dielectric medium fundamentally depends on the light wavelength. This phenomenon can be well demonstrated by using a dispersing prism to separate the white light that is composed of numerous wavelengths. The occurrence of the optical

dispersion in LDA measurements is confirmed by that the laser beams of different wavelengths, for instance $\lambda = 488$ and $\lambda = 514.5$ nm in a two-component LDA unit, will be differently refracted on the medium interface. As a result, both measurement volumes in the flow will no longer be found at the same point. The displacement between two measurement volumes, however, is usually negligible. This can be demonstrated by considering the laser beam refraction in water based on the following calculation example.

A two-component LDA system applies the laser light of wavelengths $\lambda = 488$ and $\lambda = 514.5$ nm. The half intersection angle between two laser beams in each laser beam pair is assumed to be equal to $\alpha_1 = 6.77^\circ$. The LDA head is assumed to be found in open air ($n_1 = 1$). Corresponding to both wavelengths of the laser light, the refractive index of water at a temperature of 20°C is given by $n_2 = 1.337$ for $\lambda = 488$ and $n_2 = 1.336$ for $\lambda = 514.5$. According to Eq. (13.6) the positions of both measurement volumes in the flow, corresponding to both laser beam pairs, are given by

$$x_{\text{mv},488} = n_2 x_0 = 1.337 x_0 \quad (13.7)$$

and

$$x_{\text{mv},514} = n_2 x_0 = 1.336 x_0 \quad (13.8)$$

respectively.

For example, the virtual beam crossing point is assumed to be given at $x_0 = 100$ mm, to which the corresponding measurement volumes are then found at about $x_{\text{mv}} = 134$ mm. The displacement between two measurement volumes is calculated to be

$$x_{\text{mv},488} - x_{\text{mv},514} = 0.001 x_0 = 0.1 \text{ (mm)} \quad (13.9)$$

In comparison to the measurement volume length of about 0.40 mm (Table 4.1) this displacement can usually be neglected.

Chapter 14

Flow Measurements Behind the Plane Window: Off-axis

The simplest case for internal flow measurements is the on-axis alignment of LDA optics, as this has been shown in the last chapter. There are other cases in which the LDA optics has to be aligned off-axis, i.e. the optical axis is no more perpendicular to the window plane. This situation indeed occurs very frequently, when for instance according to Fig. 14.1 the normal velocity component in the flow behind a plane window should be measured. The off-axis of LDA optics in this case is arranged within the plane containing two laser beams. Because of the asymmetrical beam refraction all geometrical specifications in both forming and shifting the measurement volume will change. This undesired and partly complex circumstance makes the flow measurements difficult. Every measurement result needs to be corrected.

In contrast to the on-axis alignment of LDA optics, the asymmetry of laser beam refractions in the off-axis case becomes a very serious matter when considered further in the aspect of entire optical performances. This is confirmed by the occurrence of optical aberrations in both the transmitting and the receiving optics. The situation with such optical aberrations may be so serious that no LDA measurements can be achieved. This corresponds to the case where both laser beams after the refractions do not intersect at all. The associated optical phenomenon has been recognized to be astigmatism (Zhang 1995, Zhang and Eisele 1995a, b). This phenomenon sensitively affects both the optical features of the LDA measurement volume and the signal quality in the receiving optics. Some LDA users may have probably encountered great difficulties of getting satisfactory optical signals while performing measurements by the LDA head at off-axis position. The cause is nothing other than the effect of astigmatism. In addition, the asymmetry of laser beam refractions leads to different deformation of beam waists on each individual laser beam and hence to the distortion of the LDA measurement volume. This again leads to fringe distortion in the measurement volume and further to measurement errors. Clearly a great deal of troubles in performing LDA measurements is related with the off-axis LDA alignment.

In the past, parallel to identifying all the influences of optical aberrations named above on LDA measurements, diverse measures have also been worked out to enhance the optical performances in the described complex situations. It should be mentioned that the passive method of matching refractive indices of test fluids does help reducing the optical aberration in LDA measurements. The method, however,

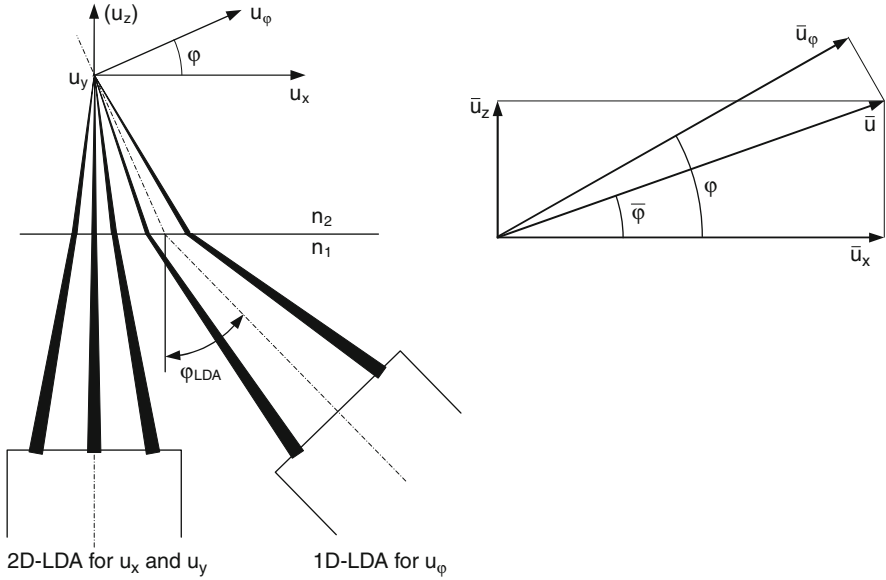


Fig. 14.1 Off-axis alignment of LDA optics for indirect measurements of velocity component u_z

is often not applicable where, for instance, field measurements out of the laboratory should be conducted.

A great deal of optical aspects related with the off-axis alignment of LDA optics will be presented in this chapter.

14.1 Off-axis Measurements and Velocity Transformation

As mentioned before, the off-axis alignment of the LDA head to the normal of the plane window usually aims to measure the velocity component out of the window plane. The optical arrangement according to Fig. 14.1 has found its broad applications, despite the measurement of the third velocity component not being coincident with the measurements of other two in-plane velocity components. In order to obtain the third velocity component u_z i.e. the component along the normal of the window surface, velocity transformation as described in Chap. 6 can be applied. The mean value of this velocity component is then obtained from Eq. (6.40)

$$\bar{u}_z = \frac{1}{\sin \phi} (\bar{u}_\phi - \bar{u}_x \cos \phi) \quad (14.1)$$

The main flow direction in the $x - z$ plane is calculated by

$$\tan \bar{\phi} = \frac{\bar{u}_z}{\bar{u}_x} \quad (14.2)$$

In order to determine the related turbulence quantities, the Zero-Correlation Method (ZCM) that is described in [Chap. 8](#) can be applied. From [Eq. \(8.18\)](#) one obtains

$$\overline{u_z^2} = \frac{\cos \varphi \cos (2\overline{\varphi} - \varphi) \cdot \overline{u_x^2} - \cos 2\overline{\varphi} \cdot \overline{u_\varphi^2}}{\sin \varphi \sin (2\overline{\varphi} - \varphi)} \quad (14.3)$$

Further according to [Eq. \(8.16\)](#) the turbulence quantity representing the Reynolds shear stress is obtained as

$$\overline{u_x' u_z'} = \frac{1}{2} \tan 2\overline{\varphi} \left(\overline{u_x^2} - \overline{u_z^2} \right) \quad (14.4)$$

Basically, when the off-axis alignment of the LDA head only aims to indirectly measure the on-axis velocity component according to [Eq. \(14.1\)](#), the measurement could be achieved at each off-axis position excluding $\varphi = 0$. Nevertheless, some special aspects associated with this LDA configuration have to be considered for high quality measurements and the maximum achievement from the measurements.

- Only one component measurement is possible. Otherwise two measurement volumes would separate from each other, see [Sect. 14.5](#) of this chapter.
- The angle φ used in above equations is the effective off-set angle of the LDA optical axis in the flow. This angle can be obtained approximately from φ_{LDA} by applying the law of refraction to the LDA optical axis. The velocity component which is measured is then approximately perpendicular to the refracted optical axis ([Sect. 14.3](#)).
- Because of different refractions of two laser beams the crossing angle between two laser beams in the fluid flow changes with the off-axis angle of the LDA head. This means that the fringe spacing in the measurement volume also depends on this angle. The measured velocity has thus to be corrected based on the fringe model of LDA optics, see [Sect. 14.2](#).
- The traversing path of the LDA measurement volume is generally two-dimensional, even though the LDA head is traversing along the normal of the window surface, see [Sect. 14.4](#)
- The LDA signal quality strongly depends on the off-axis angle of the LDA head, the focal length of used LDA optics and the depth of the measurement volume in the flow. Usually the deterioration of signal qualities is significant so that in worst cases no measurements could be accomplished at all. More to deteriorated signal qualities see [Sect. 14.8](#).

14.2 Fringe Spacing in Measurement Volume and Velocity Corrections

Depending on the off-axis alignment angle of the LDA head, the beam crossing angle in the flow changes. The fringe spacing in the measurement volume is then calculated by $\Delta x_{\text{off}} = \frac{1}{2} \lambda_n / \sin \alpha_{\text{off}}$ according to [Eq. \(3.46\)](#), with λ_n as the

wavelength of the laser light in the test medium (refractive index n) and α_{off} as the half intersection angle of two laser beams in the flow. Obviously this fringe spacing differs from that at the on-axis configuration $\Delta x_{\text{on}} = \frac{1}{2} \lambda_n / \sin \alpha_{\text{on}}$. A systematic error in velocity measurements then takes place as a result of this change in the fringe spacing. The ratio of the actual to the initial fringe spacing is obtained as

$$k_{\text{vel}} = \frac{\Delta x_{\text{off}}}{\Delta x_{\text{on}}} = \frac{\sin \alpha_{\text{on}}}{\sin \alpha_{\text{off}}} \quad (14.5)$$

To each off-axis angle φ_{LDA} in the LDA alignment according to Fig. 14.1, the half intersection angle of two laser beams in the flow α_{off} can be calculated by applying the law of refraction, given by Eq. (3.6), to each laser beam. Thus there is $\alpha_{\text{off}} = f(\varphi_{\text{LDA}})$ and naturally $\alpha_{\text{on}} = f(\varphi_{\text{LDA}} = 0)$.

Equation (14.5) represents, because of Eq. (3.47), a correction factor for each velocity that is measured at the off-axis LDA alignment:

$$u_{\varphi} = \Delta x_{\text{off}} \cdot \nu_D = k_{\text{vel}} \Delta x_{\text{on}} \nu_D = k_{\text{vel}} u_{\varphi, \text{measured}} \quad (14.6)$$

The correction of velocities is necessary because the specification of both the optical and geometrical parameters in a LDA-system is usually referred to the open air case. It is equivalent to the case of the on-axis alignment of the LDA head to the plane window (fringe spacing Δx_{on}), as has been shown in Chap. 13.

Figure 14.2 shows an example that represents the correction factor according to Eq. (14.5) as a function of the LDA off-axis angle φ_{LDA} for measurements of a water flow. As can be seen, velocity corrections up to 10% or even 15% are indispensable. The optical configuration at the LDA head, say the half intersection angle α_0 of two laser beams, has indeed the negligible influence on the velocity correction factor.

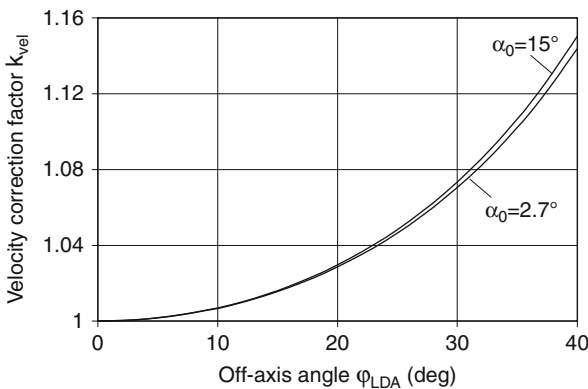


Fig. 14.2 Velocity correction factor for measurements of water flows ($n = 1.333$) by means of LDA in off-axis alignment; The half intersection angle α_0 between two laser beams is related to the design angle at the LDA head

14.3 Refraction of Optical Axis and Orientation of the Measurement Volume of the Measurement Volume

As in common applications of LDA method, the velocity component that is measured with the off-axis LDA is spatially perpendicular to the bisector of two laser beams in the test flow. As a result of optical aberrations the bisector of two refracted laser beams neither coincides with nor is parallel to the refracted optical axis. Such a disagreement is called comatic aberration. This phenomenon, however, does not have significant influence on LDA measurements. This can be demonstrated according to Fig. 14.3a with two laser beams that are refracted in a test medium. In applying the law of refraction according to Eq. (3.6) and because of $\varepsilon_{A1} = \varphi_{LDA} + \alpha_0$ and $\varepsilon_{B1} = \varphi_{LDA} - \alpha_0$, the refraction angles at two laser beams are calculated, respectively, as

$$\varepsilon_{A2} = \arcsin\left(\frac{n_1}{n_2} \sin(\varphi_{LDA} + \alpha_0)\right) \tag{14.7}$$

$$\varepsilon_{B2} = \arcsin\left(\frac{n_1}{n_2} \sin(\varphi_{LDA} - \alpha_0)\right) \tag{14.8}$$

The inclination angle of the bisector of two laser beams in the test medium is then given by

$$\varepsilon_b = \frac{1}{2}(\varepsilon_{A2} + \varepsilon_{B2}) \tag{14.9}$$

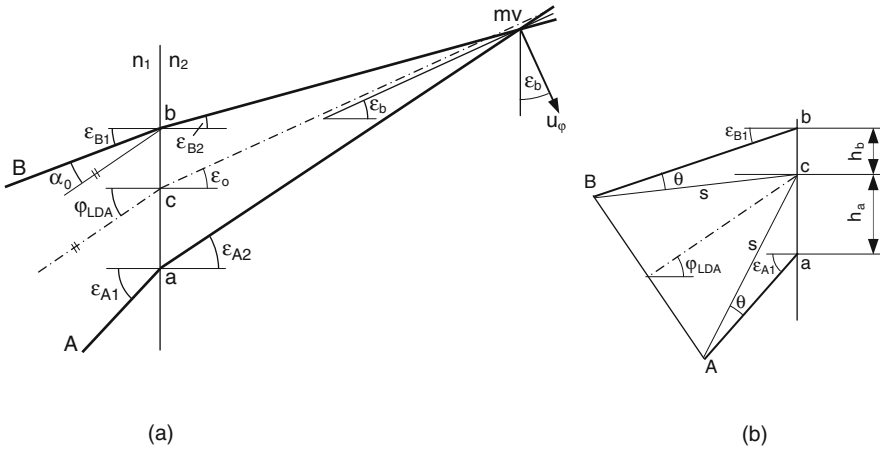


Fig. 14.3 Orientation of LDA measurement volume and the intersection of the LDA optical axis on the medium interface

Because the half intersection angle α_0 is usually small, this last equation can be approximated by considering the linear terms in the Taylor series of ε_{A2} and ε_{B2} , so that it becomes

$$\varepsilon_b = \arcsin\left(\frac{n_1}{n_2} \sin \varphi_{\text{LDA}}\right) \quad (14.10)$$

It is equal to the refraction angle of the optical axis ε_0 of the LDA head. For this reason, the refracted optical axis in the flow can be used to represent the measurement volume orientation. For water flow ($n_2/n_1 = 1.333$) and the LDA configuration with $\alpha_0 = 3^\circ$ and $\varphi_{\text{LDA}} = 30^\circ$, for instance, the uncertainty in ε_b arising from the above simplification is less than 0.02° . The comatic aberration is thus irrelevant. The velocity component measured by the off-axis LDA alignment corresponds to the component that is perpendicular to the refracted optical axis in the flow.

The intersection point of the optical axis on the medium interface is denoted by c , as shown in Fig. 14.3b. Sometimes one needs to know this intersection point, in order to further calculate and to track the laser beams with respect to the optical axis and its refraction on the interface. According to Fig. 14.3b the law of sines will be applied to triangles Aac and Bbc , respectively. Because of $\sin(90 - \varepsilon_{B1}) = \cos \varepsilon_{B1}$ and $\sin(90 + \varepsilon_{A1}) = \cos \varepsilon_{A1}$ there are accordingly

$$\frac{h_a}{\sin \theta} = \frac{s}{\cos \varepsilon_{A1}} \quad (14.11)$$

$$\frac{h_b}{\sin \theta} = \frac{s}{\cos \varepsilon_{B1}} \quad (14.12)$$

Eliminating s and $\sin \theta$ yields

$$\frac{h_a}{h_b} = \frac{\cos \varepsilon_{B1}}{\cos \varepsilon_{A1}} \quad (14.13)$$

With $h = h_a + h_b$ there are further

$$\frac{h_a}{h} = \frac{\cos \varepsilon_{B1}}{\cos \varepsilon_{A1} + \cos \varepsilon_{B1}} \quad (14.14)$$

$$\frac{h_b}{h} = \frac{\cos \varepsilon_{A1}}{\cos \varepsilon_{A1} + \cos \varepsilon_{B1}} \quad (14.15)$$

14.4 Two-Dimensional Shift of the Measurement Volume

In order to measure the flow distribution in an internal flow that is found behind an optical window, the measurement volume needs to be shifted through the flow field. An outstanding behaviour of the off-axis LDA setup is the two-dimensional shift of the measurement volume when the LDA head moves one-dimensionally parallel to the normal of the medium interface. This feature of the measurement volume

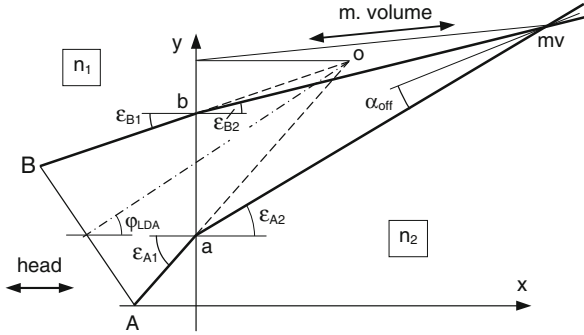


Fig. 14.4 Two-dimensional shift of the LDA measurement volume

shift can be specified by accounting for the geometrical relations between two laser beams, as shown in Fig. 14.4. The virtual and actual intersection points of two laser beams (A and B) are marked by o and mv , respectively. Herein mv stands for the measurement volume. Corresponding incident and refraction angles of both laser beams are denoted by ε_{A1} , ε_{B1} , ε_{A2} and ε_{B2} . Both laser beams A and B intersect the y-axis at y_a and y_b , respectively. The distance between intersection points a and b can be calculated respectively from the virtual and actual intersection points of two laser beams, as given by

$$x_{mv} (\tan \varepsilon_{A2} - \tan \varepsilon_{B2}) = x_o (\tan \varepsilon_{A1} - \tan \varepsilon_{B1}) = y_b - y_a \quad (14.16)$$

From this equation the following differentiation is obtained

$$k_{mv} = \frac{dx_{mv}}{dx_o} = \frac{\tan \varepsilon_{A1} - \tan \varepsilon_{B1}}{\tan \varepsilon_{A2} - \tan \varepsilon_{B2}} \quad (14.17)$$

This equation represents the x-component of the shift ratio between the actual and virtual crossing points of two laser beams. Because the virtual crossing point moves with the LDA head, the ratio k_{mv} given in above equation simply represents the ratio of the measurement volume shift to the shift of the LDA head. Like in the case of on-axis alignment that has been treated in Chap. 13, the shift ratio in the present case is also independent of the glass window which is found between the LDA head and the flow.

In Fig. 14.4, it has also shown that the shift of the measurement volumes mv does not follow a path that is parallel to the x-axis, even though the LDA head is merely shifting in the x-direction. Such a two-dimensional feature of the measurement volume shift can be well quantified. According to Fig. 14.4 the y-coordinate of the measurement volume is given as

$$y_{mv} = y_a + x_{mv} \tan \varepsilon_{A2} \quad (14.18)$$

and because of $y_a = y_o - x_o \tan \varepsilon_{A1}$ as

$$y_{mv} = y_o - x_o \tan \varepsilon_{A1} + x_{mv} \tan \varepsilon_{A2} \quad (14.19)$$

It is of concern that the shift of the LDA head along the x -axis means that the y -coordinate of the virtual crossing point remains constant. Thus differentiation of above equation with respect to $y_o = \text{const}$ and $k_{mv} = dx_{mv}/dx_o$ yields

$$\frac{dy_{mv}}{dx_{mv}} = \tan \varepsilon_{A2} - \frac{dx_o}{dx_{mv}} \tan \varepsilon_{A1} = \tan \varepsilon_{A2} - \frac{1}{k_{mv}} \tan \varepsilon_{A1} \quad (14.20)$$

This equation describes the path that the measurement volume follows when the LDA head is moving parallel to the x -direction. In general, the lateral shift of the measurement volume dy_{mv}/dx_{mv} does not disappear, except for the special cases of the on-axis alignment, the off-axis alignment with one laser beam perpendicular to the plane of the medium interface, or the flow medium that is the same as the medium in which the LDA head is present. Figure 14.5 as an example shows the two-dimensional shift rate of the measurement volume in water, calculated from Eqs. (14.17) and (14.20) for an LDA optics with $\alpha_0 = 2.75^\circ$.

The results presented here are of special importance for cases where simultaneous three-component velocity measurements would be carried out by using two LDA heads. When trying to shift measurement volumes in the flow, all three measurement volumes will separate from each other, so that both LDA heads need to be realigned, see also Thiele and Eckelmann (1994).

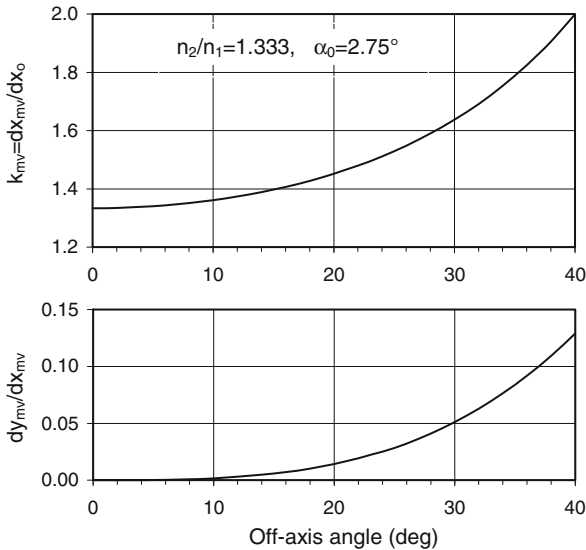


Fig. 14.5 Two-dimensional shift rate of LDA measurement volume in water

14.5 Astigmatism and its Presence in Transmitting Optics

Astigmatism is an optical aberration which refers to the loss of the unique focal point of a light bundle after the refraction through a non-perpendicular interface (Fig. 14.6). While the meridian plane (also called the tangential plane) of the light bundle focuses on the point m after the refraction, the sagittal plane focuses on the point s . The distance between these two focal points is known as the astigmatic difference. Obviously this astigmatic difference depends on both the off-axis angle φ of the light bundle against the normal of the interface and the focusing angle i.e. the thickness of the incident light bundle. In addition, it also depends on the distance of the virtual focal point from the plane interface.

In the context of LDA applications, the focused light bundle that is shown in Fig. 14.6 can be considered as being constructed by four laser beams of a two-component LDA system. One pair of laser beams forms the meridian plane and another pair the sagittal plane. Correspondingly two measurement volumes are obtained, respectively, at the meridian and the sagittal focal point. Because of the remarkable separation between two measurement volumes, two-component coincident LDA measurements become impossible. Also other optical features such as signal qualities and the fringe distortion in the measurement volume are related to the effect of astigmatism aberration. This will be separately shown in following sections.

The occurrence of astigmatism at off-axis LDA alignment and the related effect on measurements are always inevitable, even if only one-component measurements by using two laser beams in the meridian plane will be carried out. Besides the fringe distortion in the measurement volume the astigmatism effect is additionally confirmed in the backward propagation of scattered laser lights from the measurement volume to the receiving optics, which is integrated in the LDA head. As a result,

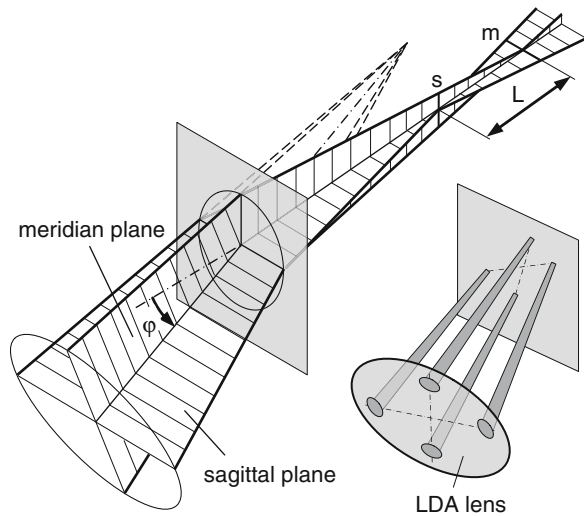


Fig. 14.6 Astigmatism

the existence of astigmatism in the receiving optics directly influences the signal strength and qualities. To quantify such an influence, the astigmatic difference as a quantitative measure of the phenomenon should be considered. It is represented in the present case with two pairs of laser beams (Fig. 14.6) by the distance between two focal points i.e. the available (m) and unavailable (s) measurement volumes.

For practical LDA applications in internal flow measurements, astigmatism takes place twice: in the transparent optical window of thickness d and in the fluid flow, as illustrated in Fig. 14.7 showing the laser beam refractions in the meridian plane. The crossing point of two in-plane laser beams (A and B) is denoted by m . Because of symmetrical refraction of two other laser beams in the sagittal plane, the corresponding crossing point s is also found in the meridian plane. According to the detailed calculations, as shown in Appendix A using the theory of ray optics (Zhang 1995), the displacement between two measurement volumes (m and s) along the x -axis is given by

$$\Delta x_{m,s} = \frac{1}{T_{20}} (\Psi_1 d + \Psi_2 d_s) \quad (14.21)$$

Herein

$$\Psi_1 = \frac{\cos \alpha_0 \cos \varphi_{LDA}}{\sqrt{\frac{n_1^2}{n_0^2} - (1 - \cos^2 \alpha_0 \cos^2 \varphi_{LDA})}} - T_{10} \quad (14.22)$$

$$\Psi_2 = \frac{\cos \alpha_0 \cos \varphi_{LDA}}{\sqrt{\frac{n_2^2}{n_0^2} - (1 - \cos^2 \alpha_0 \cos^2 \varphi_{LDA})}} - T_{20} \quad (14.23)$$

$$T_{10} = \frac{\tan \varepsilon_{A1} - \tan \varepsilon_{B1}}{\tan \varepsilon_{A0} - \tan \varepsilon_{B0}} \quad (14.24)$$

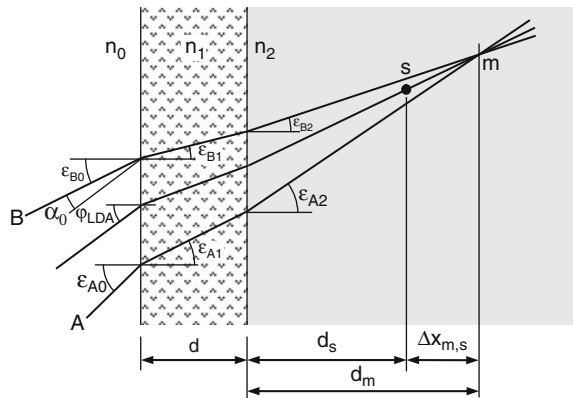


Fig. 14.7 Calculation of the distance between the available (m) and the unavailable (s) measurement volumes in the test flow

$$T_{20} = \frac{\tan \varepsilon_{A2} - \tan \varepsilon_{B2}}{\tan \varepsilon_{A0} - \tan \varepsilon_{B0}} \tag{14.25}$$

with ε_{A1} , ε_{A2} , ε_{B1} and ε_{B2} as the refraction angles of laser beams (A and B) in the medium 1 and 2, respectively. They can be calculated from corresponding incident angles in the form of $\varepsilon_{A0} = \varphi_{LDA} + \alpha_0$ and $\varepsilon_{B0} = \varphi_{LDA} - \alpha_0$ by applying the law of refraction. The half intersection angle between two laser beams in air is designated by α_0 . Also worth mentioning is that at small off-axis angles there may be $\varepsilon_{B0} < 0$ according to Fig. 14.7 with given parameter notations. The parameters Ψ_1 and Ψ_2 refer to the window and the test fluid, respectively.

The above equations are obtained based on the assumption that in the medium 0 all four laser beams intersect at a unique point. This medium is denoted as the reference medium. Usually it is the air in that the LDA head is found. The special case with water as the reference medium will be shown in Sect. 14.10.

Figure 14.8 represents an example of calculated displacements between two measurement volumes (m and s) at the off-axis LDA alignment. The calculations are referred to an air-glass-water system with a glass thickness of $d = 20$ mm. The displacement i.e. the distance between two measurement volumes is enormous, especially at large off-axis angles. It linearly increases with the depth of the measurement volume in the test flow and is also dominated by this depth. The effect of the glass window on the extent of astigmatism can be read out at $d_s = 0$ in Fig. 14.8. Usually it deals with a relatively small effect because of the small thickness of the used window.

Because of the great distance between two measurement volumes the two-component LDA measurements become impossible. In the practical applications, the LDA off-axis alignment is indeed initially required for separate one-component velocity measurement, as already shown in Fig. 14.1. The two laser beams used for

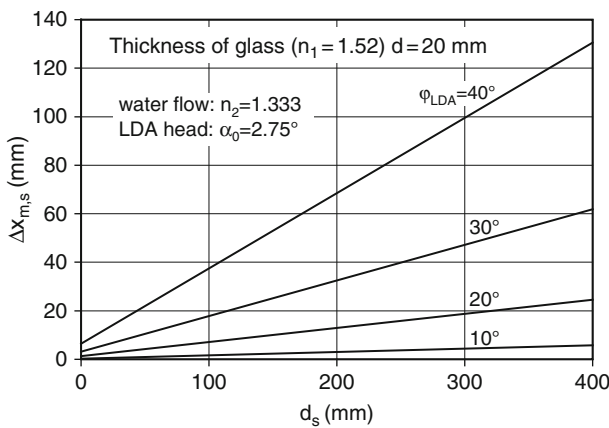


Fig. 14.8 Distance between the available (m) and the unavailable (s) measurement volumes in water as a result of the off-axis alignment of the LDA head

measurements lie in the meridian plane and form the measurement volume at d_m . This measurement volume is therefore called available measurement volume, while the measurement volume at d_s is unavailable. For using d_m as the parameter to express the distance between two measurement volumes, Eq. (14.21) is rearranged by substituting $d_s = d_m - \Delta x_{m,s}$ as

$$\Delta x_{m,s} = \frac{1}{T_{20} + \Psi_2} (\Psi_1 d + \Psi_2 d_m) \quad (14.26)$$

For $d = 0$ there is simply

$$\frac{\Delta x_{m,s}}{d_m} = \frac{\Psi_2}{T_{20} + \Psi_2} \quad (14.27)$$

These two expressions are sometimes preferred because of the use of the available and hence visible measurement volume at the distance d_m . Also worth mentioning is that for small values of the distance d_m the unavailable measurement volume may be found virtually within the window because of $d_s < 0$.

Based on Eq. (14.27) for negligible window thickness, Fig. 14.9 shows the related displacement between the available and unavailable measurement volumes in function of the LDA off-axis angle, as for the medium with $n = 1.333$.

A special case will be considered in which the test medium is equal to the reference medium. For measurements of air flows behind the window, which implies an arrangement of air-glass-air, all related equations can be simplified. Because of $n_2 = n_0 = 1$ there is $T_{20} = 1$. From Eq. (14.23) one obtains

$$\Psi_2 = 0 \quad (14.28)$$

Eq. (14.26) then becomes

$$\Delta x_{m,s} = \Psi_1 d \quad (14.29)$$

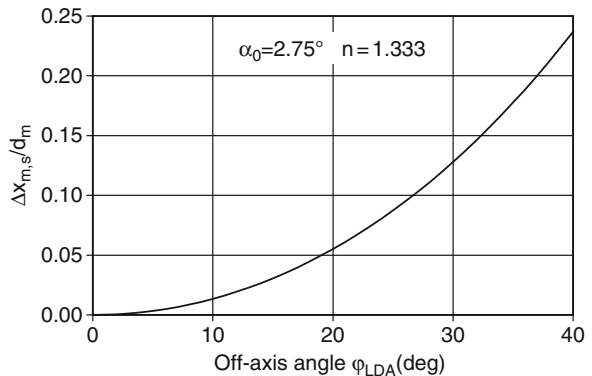


Fig. 14.9 Related displacement between the available and the unavailable measurement volumes in water in function of the LDA off-axis angle (window thickness $d = 0$)

The astigmatism and the associated displacement between two measurement volumes have been thus related to the thickness and the refractive index of the used glass window. They are independent of the depth of the measurement volumes in the air flow. In reality, this is always the case as long as the test medium is equal to the reference medium. See also Sect. 14.10 dealing with the method of suppressing the astigmatism effect.

At the end of this section, it should be emphasized that the LDA off-axis alignment should be performed strictly in the optical plane i.e. the plane containing two laser beams. Deviations from this requirement will lead to separation of two laser beams and thus to failure in forming the measurement volume. More about this aspect will be given in Sect. 14.9.

In the following sections, some other related optical aspects in LDA measurements will be further accounted for.

14.6 Astigmatism at the Focused Laser Beam Bundle

As is known, astigmatism represents an optical aberration and refers in the present context to the loss of the unique focal point of a light bundle after the refraction through a non-perpendicular interface (Fig. 14.6). Since each individual laser beam in an LDA-system is precisely a focused light bundle, its refraction on the medium interface then leads to the occurrence of astigmatism. As a result each refracted laser beam exhibits two characteristic focal points: one in the meridian plane and another in the sagittal plane. Because these two focal points in a laser beam do not coincide, the wave front of the laser beam is thus nowhere of the plane form. The intersection of two such laser beams obviously leads to fringe distortion in the measurement volume. This type of the fringe distortion, however, cannot be simply described as the well-known fringe distortions caused by the improper crossing of two regular laser beams (Chap. 16). The attempt by Li and Tieu (1998) to get the insight into the measurement volume that is distorted by reasons of astigmatism did not refer to the astigmatism associated with the off-axis LDA as presented here.

The extent of the fringe distortion caused by astigmatism in the present case clearly depends on the relative positions of the measurement volume and the respective meridian and sagittal focal points of two laser beams. It depends therefore on the off-axis angle in the individual LDA arrangement. For this reason, the laser beams that suffer from astigmatism should be characterized in function of LDA off-axis angle. Corresponding detailed investigations have been performed by Zhang and Eisele (1996b).

14.6.1 One-time Refraction of a Focused Beam Bundle

A spatially focused beam bundle is considered which is refracted at the interface of mediums 1 and 2 (Fig. 14.10). For this configuration, a coordinate system is chosen

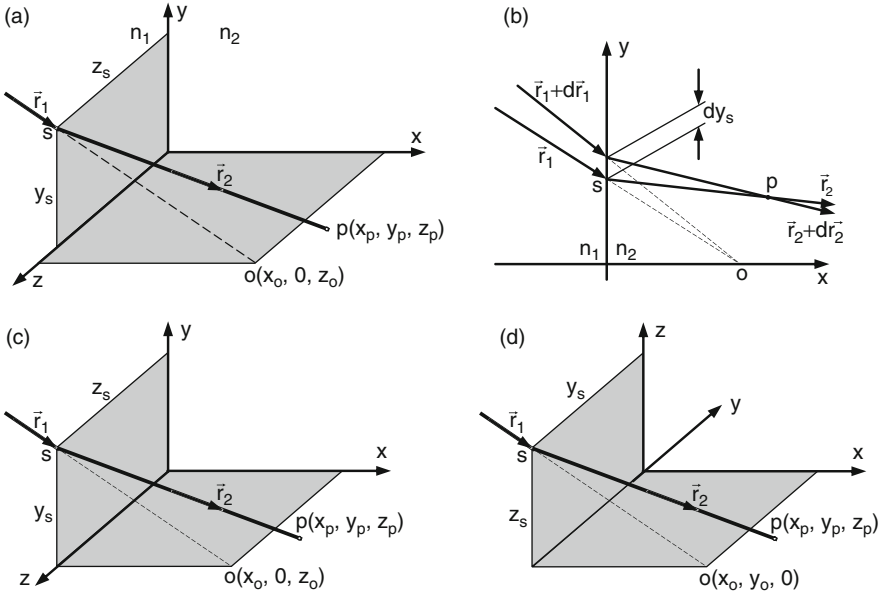


Fig. 14.10 Ray optics to calculate the astigmatism in a focused light bundle

with the $y - z$ plane on the interface between two mediums. The x -axis is then directed from medium 1 to medium 2. The virtual focal point of the incident beam bundle lies on the $x - z$ plane and is thus given at $o = (x_o, 0, z_o)$. In accordance with definitions of astigmatism parameters, two characteristic planes related to the incident beam should be noted: the plane containing the beam axis and the normal of the interface is called the meridian plane; the plane perpendicular to this and through the beam axis is called the sagittal plane.

To simplify the geometric optical calculations the beam bundle will be firstly considered as a single ray which may be described by a straight line with the parallel unit vector $\vec{r}_1 (r_{1x}, r_{1y}, r_{1z})$ as follows

$$\frac{x - 0}{r_{1x}} = \frac{y - y_s}{r_{1y}} = \frac{z - z_s}{r_{1z}} \tag{14.30}$$

with $s(0, y_s, z_s)$ as the intersection point of the straight line on the interface.

The coordinates of the intersection point s can be determined by inserting the coordinates of the known virtual focal point of the incident beam $o = (x_o, 0, z_o)$ into Eq. (14.30). For y_s for instance one obtains

$$y_s = -\frac{r_{1y}}{r_{1x}}x_o \tag{14.31}$$

Analogous to Eq. (14.30) the refracted ray that departs from the intersection point s can be represented by a straight line with $\vec{r}_2 (r_{2x}, r_{2y}, r_{2z})$ as a parallel unit vector

$$\frac{x - 0}{r_{2x}} = \frac{y - y_s}{r_{2y}} = \frac{z - z_s}{r_{2z}} \quad (14.32)$$

The unit vector \vec{r}_2 depends on the unit vector \vec{r}_1 and can be determined by use of the law of refraction according to Eqs. (3.8) and (3.9):

$$r_{2y} = \frac{n_1}{n_2} \cdot r_{1y} \quad (14.33)$$

$$r_{2z} = \frac{n_1}{n_2} \cdot r_{1z} \quad (14.34)$$

with n_1 and n_2 as the refractive index of respective mediums.

The objective of the following calculations is to find out the focal points of the refracted beam for a given incident beam bundle that is focused at $o = (x_o, 0, z_o)$. The form of the considered focused beam bundle can be imagined to be created by infinitesimally turning the incident ray \vec{r}_1 around the virtual focal point o , so that in the plane of the medium interface ($y - z$ plane) the intersection point s shifts. A certain infinitesimal change $d\vec{r}_1$ in the incident ray will thus cause an infinitesimal change $d\vec{r}_2$ in the refracted ray \vec{r}_2 and an infinitesimal shift of the intersection point s in the plane of the medium interface. Usually both the ray \vec{r}_2 and $\vec{r}_2 + d\vec{r}_2$ propagate spatially and thus do not meet each other. By projecting the rays onto the $x - y$ plane, the intersection between two refracted rays can be confirmed, as shown in Fig. 14.10b. The related infinitesimal shift of the intersection point s in the plane of the medium interface is identified by the component dy_s .

In reality, the intersection of the projected rays \vec{r}_2 and $\vec{r}_2 + d\vec{r}_2$ just represents a focal point of the simulated beam bundle after the refraction, however, conditionally for the given change $d\vec{r}_1$ in the incident ray and in the section plane that is parallel to the $x - y$ plane. Because the rays \vec{r}_2 and $\vec{r}_2 + d\vec{r}_2$ generally do not spatially intersect, the observed intersection between them obviously depends on the orientation of the projection plane. This means that no unique focal point could be expected. This phenomenon with the loss of the unique focal point in the refracted beam bundle, as outlined, is known as astigmatism. In order to mathematically specify this type of optical aberrations, the intersection point of \vec{r}_2 and $\vec{r}_2 + d\vec{r}_2$ is mathematically interpreted as to be found at the coordinate x_p , at which the refracted ray \vec{r}_2 does not show any change in the y -coordinate for instance in the projected $x - y$ plane (Fig. 14.10b), despite the infinitesimal change $d\vec{r}_1$ in the incident ray. For simplicity, the change in the incident ray is firstly assumed to be dr_{1y} i.e. in the y -component of the unit vector \vec{r}_1 . The corresponding focal point at x_p on the refracted beam, considered in the projected $x - y$ plane, then has to fulfil the condition

$$\frac{\partial y_p}{\partial r_{1y}} = 0 \quad (14.35)$$

In further derivations, the z -component of the unit vector \vec{r}_1 will be assumed to be constant. The change in r_{1y} will then cause a simultaneous change in r_{1x} . On the side of the refracted ray which is described by Eq. (14.32) there will be both a change in the unit vector \vec{r}_2 and a displacement of the ray because of the displacement of the intersection point s in the plane of the medium interface. With regard to this behaviour of ray optics the corresponding relation $y = f(x)$ from Eq. (14.32) is inserted into Eq. (14.35), which leads to

$$\frac{\partial y_s}{\partial r_{1y}} + x_p \frac{\partial}{\partial r_{1y}} \left(\frac{r_{2y}}{r_{2x}} \right) = 0 \quad (14.36)$$

The differentiation $\partial y_s / \partial r_{1y}$ can be calculated from Eq. (14.31) which applies to the incident ray. With regard to $r_{1z} = \text{const}$ it follows then

$$\frac{\partial y_s}{\partial r_{1y}} = -x_o \frac{\partial}{\partial r_{1y}} \left(\frac{r_{1y}}{\sqrt{1 - r_{1y}^2 - r_{1z}^2}} \right) = -x_o \frac{1 - r_{1z}^2}{r_{1x}^3} \quad (14.37)$$

Regarding the second term in Eq. (14.36) the following expression with regard to Eq. (14.33) is considered first

$$\frac{r_{2y}}{r_{2x}} = \frac{n_1}{n_2} \frac{r_{1y}}{\sqrt{1 - (n_1/n_2)^2 r_{1y}^2 - (n_1/n_2)^2 r_{1z}^2}} \quad (14.38)$$

Its differentiation leads to

$$\frac{\partial}{\partial r_{1y}} \left(\frac{r_{2y}}{r_{2x}} \right) = \frac{n_1}{n_2} \frac{1 - r_{1z}^2}{r_{2x}^3} \quad (14.39)$$

Both Eqs. (14.37) and (14.39) are inserted into Eq. (14.36). Then the x -coordinate, at which the geometrical condition given by Eq. (14.35) is fulfilled, is resolved as

$$x_p = x_o \frac{n_2}{n_1} \frac{r_{2x}^3}{r_{1x}^3} \frac{1 - r_{1z}^2}{1 - r_{2z}^2} \quad (14.40)$$

This is the position on the refracted ray, within which there is no change in y -coordinate despite the given change in the incident ray. The related point at x_p can thus be seen as a focal point of the refracted laser beam bundle, however, conditionally in the section plane which is parallel to $x - y$ plane because of Eq. (14.35).

As can also be seen from Eq. (14.40), x_p obviously depends on the spatial orientation of the incident beam bundle, or in other words, in the specification of used coordinate system. For the case where the meridian plane of the incident beam i.e. the plane containing the unit vector \vec{r}_1 and a parallel of x -axis, coincides with or is parallel to the $x - y$ plane (Fig. 14.10c), then there is simply $r_{1z} = r_{2z} = 0$.

Equation (14.35) represents the condition of a focal point in the meridian plane of the refracted beam bundle. From Eq. (14.40) the corresponding focal point on the refracted beam bundle is then given as

$$x_m = x_o \frac{n_2 r_{2x}^3}{n_1 r_{1x}^3} \quad (14.41)$$

A second case will be considered when departing from the first case the coordinate system is rotated around the x -axis by 90° (Fig. 14.10d). Then Eq. (14.35) represents a focusing condition in the sagittal plane of the refracted beam bundle. Calculations given above are hence available for the ray optics in the sagittal plane. Because of $r_{1y} = r_{2y} = 0$ i.e. $1 - r_{1z}^2 = r_{1x}^2$ and $1 - r_{2z}^2 = r_{2x}^2$ one obtains from Eq. (14.40) the corresponding sagittal focal point on the refracted beam bundle as

$$x_s = x_o \frac{n_2 r_{2x}}{n_1 r_{1x}} \quad (14.42)$$

Obviously the meridian and sagittal focal points are found at different positions on the refracted beam bundle. The distance between them is given by

$$\Delta x_{m,s} = x_m - x_s = x_o \frac{n_2}{n_1} \left(\frac{r_{2x}^2}{r_{1x}^2} - 1 \right) \frac{r_{2x}}{r_{1x}} \quad (14.43)$$

In the conventional specification of astigmatism, the spatial distance between both focal points is called astigmatic difference. With r_{2x} as the projection of the unit vector \vec{r}_2 on the x -axis the astigmatic difference is calculated as

$$\Delta s_{m,s} = \frac{x_m - x_s}{r_{2x}} = x_o \frac{n_2}{n_1} \frac{r_{2x}^2 - r_{1x}^2}{r_{1x}^3} \quad (14.44)$$

The unit vector components r_{1x} and r_{2x} in this equation can be expressed by $r_{1x} = \cos \varepsilon_1$ and $r_{2x} = \cos \varepsilon_2$, respectively, with ε_1 and ε_2 as the incident and the refraction angles of the beam bundle. Equation (14.43) then becomes

$$\Delta x_{m,s} = x_o \frac{n_2}{n_1} \left(\frac{\cos^2 \varepsilon_2}{\cos^2 \varepsilon_1} - 1 \right) \frac{\cos \varepsilon_2}{\cos \varepsilon_1} \quad (14.45)$$

Because the two focal points respectively on the meridian and sagittal planes no longer occur at the same place, there exists at each focal point indeed a focal line. This focal line changes its orientation as observed from one focal point (x_m) to another (x_s). For a finite beam bundle like a laser beam in an LDA-system, the elliptical cross section of the beam between x_m and x_s should be observed. The existence of an elliptical cross section, instead of the single focal line, arises from the coma effect (see Sect. 14.3) and other third-order aberrations. The comatic aberration, however, is much smaller than that caused by astigmatism.

The results presented above are relevant for LDA measurements and measurement accuracies. The change in the cross section of each refracted laser beam from one to another focal point influences the uniformity of the fringe spacing in the measurement volume that is created by intersection of two laser beams. The extent of the fringe distortion in the measurement volume clearly depends on deviations of all focal points (x_m and x_s) from the measurement volume. Detailed calculations of such deviations will be presented in Sect. 14.7.

Equation (14.43) will be further considered. Substituting x_o from Eq. (14.42) yields

$$\Delta x_{m,s} = x_s \left(\frac{r_{2x}^2}{r_{1x}^2} - 1 \right) \quad (14.46)$$

Because of Eq. (3.12) this can also be written as

$$\Delta x_{m,s} = x_s \left(1 - \frac{n_1^2}{n_2^2} \right) \tan^2 \varepsilon_1 \quad (14.47)$$

The astigmatic difference has thus been shown to depend on both the incident angle of the light bundle and the position of the sagittal focal point in the medium 2. Sometimes it would be necessary to relate the astigmatic difference to the position of the meridian focal point. For this reason $x_s = x_m - \Delta x_{m,s}$ is inserted in above equation:

$$\Delta x_{m,s} = (x_m - \Delta x_{m,s}) \left(1 - \frac{n_1^2}{n_2^2} \right) \tan^2 \varepsilon_1 \quad (14.48)$$

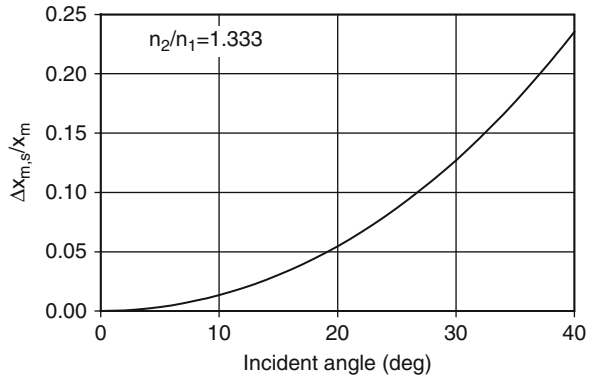
Then the astigmatic difference, related to x_m , is resolved as

$$\frac{\Delta x_{m,s}}{x_m} = \frac{\left(1 - \frac{n_1^2}{n_2^2} \right) \tan^2 \varepsilon_1}{1 + \left(1 - \frac{n_1^2}{n_2^2} \right) \tan^2 \varepsilon_1} \quad (14.49)$$

For the given two mediums, the related astigmatic difference is thus only a function of the incident angle of the light bundle, as this dependence has been shown in Fig. 14.11 for $n_2/n_1 = 1.333$. At large incident angles of the beam bundle, the astigmatic difference becomes significant. If compared with Fig. 14.9, which stands for a macro light bundle comprising four laser beams and being aligned off-axis at angle φ_{LDA} , it is evident that the displacement or the astigmatic difference does not much depend on the light bundle thickness.

It should be mentioned that Eq. (14.47) and hence Eq. (14.49) can also be obtained from Eq. (14.21) through corresponding simplifications. In the present case with two mediums, one needs to set $d = 0$. In addition, it deals here with a thin beam

Fig. 14.11 Astigmatism difference in function of the incident angle of a focused light bundle



bundle, so that to the beam crossing angle in Eq. (14.21) the condition $\alpha_0 \ll 1$ has to be put to use. Corresponding verification calculations have been performed by Zhang (1995).

14.6.2 Multiple Refraction of a Focused Beam Bundle

Multiple refraction of a focused beam bundle is often encountered in LDA measurements of internal flows, at which all laser beams have always to pass through at least one glass window of thickness d . In this case, both focal points corresponding to the meridian and the sagittal planes of a beam bundle will be calculated in line with Fig. 14.12. In order to simplify the presentation, only the meridian plane of the beam bundle is sketched in Fig. 14.12. The initial i.e. virtual focal point of the incident beam is again found at $o(x_0, y_0)$. To calculate the focal point o_2 of the refracted beam bundle in the medium 2, the focal point o_1 of the refracted beam bundle in medium 1 has to be calculated first.

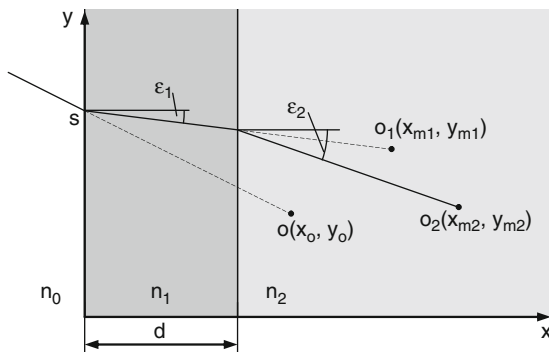


Fig. 14.12 Meridian plane of a focused light bundle with refractions in the medium 1 and 2

The first beam refraction takes place on the interface between mediums 0 and 1. From Eqs. (14.41) and (14.42) the meridian and sagittal focal points of the beam bundle in medium 1 are given at

$$x_{m1} = x_o \frac{n_1 r_{1x}^3}{n_0 r_{0x}^3} \quad (14.50)$$

$$x_{s1} = x_o \frac{n_1 r_{1x}}{n_0 r_{0x}} \quad (14.51)$$

In Fig. 14.12, only the focal point in the meridian plane has been shown by o_1 . Both this point and the related sagittal focal point are virtual. They will be utilized to further calculate the focal points of the refracted beam bundle in the medium 2.

Equations (14.41) and (14.42) will again be applied to the beam that is refracted on the interface between mediums 1 and 2. With regard to the thickness d of the medium 1 one obtains

$$x_{m2} = (x_{m1} - d) \frac{n_2 r_{2x}^3}{n_1 r_{1x}^3} + d \quad (14.52)$$

$$x_{s2} = (x_{s1} - d) \frac{n_2 r_{2x}}{n_1 r_{1x}} + d \quad (14.53)$$

The displacement between two focal points in medium 2 is then given by

$$\begin{aligned} \Delta x_{m,s} &= x_{m2} - x_{s2} = (x_{m1} - d) \frac{n_2 r_{2x}^3}{n_1 r_{1x}^3} - (x_{s1} - d) \frac{n_2 r_{2x}}{n_1 r_{1x}} \\ &= x_o \frac{n_2}{n_0} \left(\frac{r_{2x}^2}{r_{0x}^2} - 1 \right) \frac{r_{2x}}{r_{0x}} - d \frac{n_2}{n_1} \left(\frac{r_{2x}^2}{r_{1x}^2} - 1 \right) \frac{r_{2x}}{r_{1x}} \end{aligned} \quad (14.54)$$

Corresponding components of unit vectors in this equation can be substituted by respective refraction angles for instance $r_{2x} = \cos \varepsilon_2$.

The same calculation procedure will be given, if a beam bundle is refracted more than two times. In particular, if $d = 0$, Eq. (14.54) takes the form of Eq. (14.43) for the one-time refraction of a focused beam bundle.

14.7 Measurement Volume and Its Distortion

In LDA measurements there are at least two laser beams that create the measurement volume through their intersection. Each laser beam will suffer from astigmatism, if it has to be refracted for measuring the internal flow. The existence of astigmatism results in spatial deviations of beam focal points (meridian and sagittal) from the measurement volume. These deviations act as the main reason for the distortion and the non-uniformity of interference fringes in the measurement volume. The

possibility of calculating these deviations is therefore of great relevance for further investigations of optical properties of the measurement volume. The fringe distortion in the measurement volume in association with astigmatism indeed represents a new type that has not been widely investigated. Conventional fringe distortions in LDA measurement volume have been concerned to be merely caused by improper intersection of two normal laser beams (see Chap. 16).

In order to quantify the separations of diverse focal points as well as deviations of them from the measurement volume, calculation results in the last section dealing with the characterizations of astigmatism will be needed. For practical reasons a one-component LDA system with two laser beams at off-axis alignment will be considered. In order to ensure the intersection of two laser beams after refractions, the off-axis alignment of the LDA head has to be taken exactly in the plane containing both laser beams, as shown in Fig. 14.13. For the general case two-time refractions of laser beams will be firstly considered. The refracted laser beams in the first medium (often a glass window) are denoted by A_1 and B_1 , while they are denoted in the test medium by A_2 and B_2 , respectively.

Deviations of diverse focal points on the refracted laser beams from the measurement volume can be specified by firstly determining the measurement volume in the test medium. From the first interface (0–1) to the measurement volume in the medium 2, both laser beams (A and B) converge themselves by a lateral distance equal to t (Fig. 14.13a). With respect to this distance the following relation can be established

$$x_o (\tan \varepsilon_{A0} - \tan \varepsilon_{B0}) = [d \tan \varepsilon_{A1} + (x_{mv} - d) \tan \varepsilon_{A2}] - [d \tan \varepsilon_{B1} + (x_{mv} - d) \tan \varepsilon_{B2}] = t \tag{14.55}$$

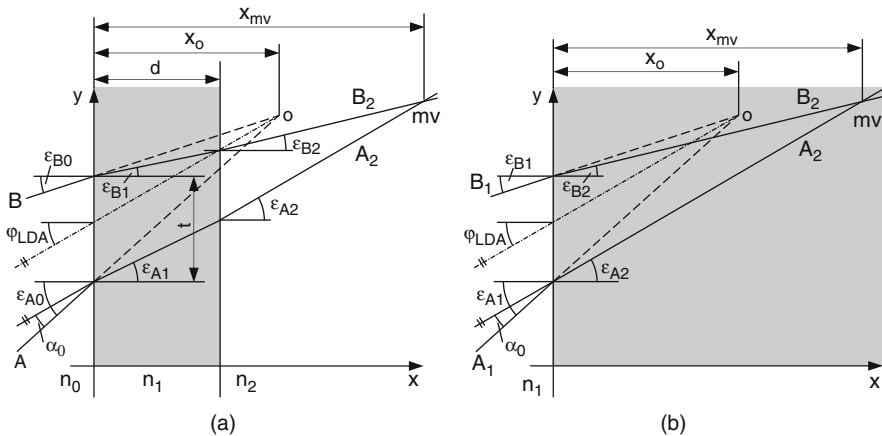


Fig. 14.13 Laser beam transmissions and the formation of the measurement volume (a) Two-time refractions as the general case (medium indices 0, 1, 2) (b) One-time refraction as a special case (medium indices 1, 2)

In relying on this basic equation, calculations will be given by taking into account the single and the multiple refractions of laser beams, respectively.

14.7.1 Single Refraction of Laser Beams

The occurrence of single or one-time refraction of laser beams, as shown in Fig. 14.13b, is encountered for instance in measuring an open channel flow or an internal flow whose refractive index is matched to that of the optical window. In such cases, Eq. (14.55) is simplified for $d = 0$ as

$$\frac{x_{mv}}{x_o} = \frac{\tan \varepsilon_{A1} - \tan \varepsilon_{B1}}{\tan \varepsilon_{A2} - \tan \varepsilon_{B2}} \quad (14.56)$$

Herein the order of two mediums is rearranged by using the subscripts 1 and 2.

For a given off-axis LDA alignment, the distance ratio x_{mv}/x_o in the above equation is a constant. This implies that it also represents the ratio of the measurement volume shift to the shift of the virtual beam intersection, given by dx_{mv}/dx_o . This is equal to Eq. (14.17), as expected.

The above equation is, to eliminate x_o , combined with Eqs. (14.41) and (14.42), respectively. This leads to respective deviations of the meridian and sagittal focal points of a laser beam from the measurement volume as

$$\Delta x_{m,mv}^* = \frac{x_m - x_{mv}}{x_{mv}} = \frac{n_2 r_{2x}^3 \tan \varepsilon_{A2} - \tan \varepsilon_{B2}}{n_1 r_{1x}^3 \tan \varepsilon_{A1} - \tan \varepsilon_{B1}} - 1 \quad (14.57)$$

$$\Delta x_{s,mv}^* = \frac{x_s - x_{mv}}{x_{mv}} = \frac{n_2 r_{2x} \tan \varepsilon_{A2} - \tan \varepsilon_{B2}}{n_1 r_{1x} \tan \varepsilon_{A1} - \tan \varepsilon_{B1}} - 1 \quad (14.58)$$

Both deviations are referred to a single laser beam that is specified by the unit vector components r_{1x} in medium 1 and r_{2x} in medium 2. For two laser beams (*A* and *B*) of a beam pair forming the measurement volume there are four focal points in total to be considered. Their deviations from the measurement volume can be calculated from the above two equations, as quantitatively shown in Fig. 14.14a for a concrete LDA configuration and demonstratively in Fig. 14.14b. As can be seen, the sagittal focal points of both laser beams are further away from the measurement volume than the meridian focal points. Because of such deviations, the measurement volume and the interference fringes in it will clearly be distorted. At least the form of the measurement volume is no longer an exact ellipsoid. It remains, however, still unknown, how the fringes in the measurement volume will be distorted and how the measurement accuracies will be affected.

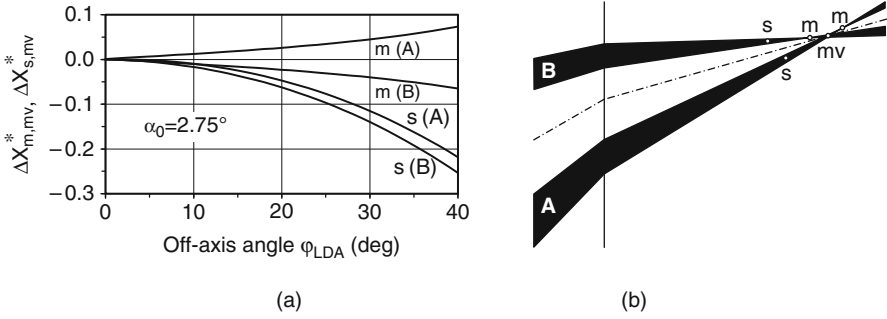


Fig. 14.14 Displacements of all four focal points on two laser beams (A and B) from the measurement volume (one-time refraction) (a) Quantitative calculations (b) Illustrations

14.7.2 Multiple Refractions of Laser Beams

Multiple refractions of laser beams are found in measuring internal flows where at least one glass window is present, as shown in Fig. 14.13a. Following the similar calculation procedure as that in Sect. 14.7.1, however, with the window thickness $d \neq 0$, Eq. (14.55) is combined with Eqs. (14.50) and (14.51) aiming to eliminate the initial focal point x_0 . This leads to

$$x_{m1} = \frac{n_1 r_{1x}^3 (\tan \varepsilon_{A1} - \tan \varepsilon_{B1}) d - (\tan \varepsilon_{B2} - \tan \varepsilon_{A2}) (x_{mv} - d)}{n_0 r_{0x}^3 \tan \varepsilon_{A0} - \tan \varepsilon_{B0}} \quad (14.59)$$

$$x_{s1} = \frac{n_1 r_{1x} (\tan \varepsilon_{A1} - \tan \varepsilon_{B1}) d - (\tan \varepsilon_{B2} - \tan \varepsilon_{A2}) (x_{mv} - d)}{n_0 r_{0x} \tan \varepsilon_{A0} - \tan \varepsilon_{B0}} \quad (14.60)$$

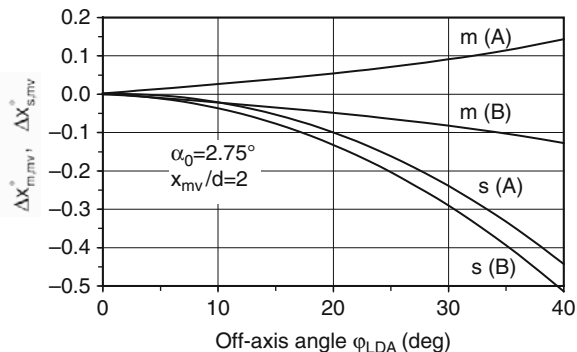
Then from Eq. (14.52) as well as Eq. (14.53) the relative deviations of respective focal points from the measurement volume can be derived to be

$$\begin{aligned} \Delta x_{m,mv}^* &= \frac{x_{m2} - x_{mv}}{x_{mv} - d} \\ &= \frac{n_2 r_{2x}^3 \tan \varepsilon_{A2} - \tan \varepsilon_{B2}}{n_0 r_{0x}^3 \tan \varepsilon_{A0} - \tan \varepsilon_{B0}} - 1 + \left(\frac{n_2 r_{2x}^3 \tan \varepsilon_{A1} - \tan \varepsilon_{B1}}{n_0 r_{0x}^3 \tan \varepsilon_{A0} - \tan \varepsilon_{B0}} - \frac{n_2 r_{2x}^3}{n_1 r_{1x}^3} \right) \frac{d}{x_{mv} - d} \end{aligned} \quad (14.61)$$

$$\begin{aligned} \Delta x_{s,mv}^* &= \frac{x_{s2} - x_{mv}}{x_{mv} - d} \\ &= \frac{n_2 r_{2x} \tan \varepsilon_{A2} - \tan \varepsilon_{B2}}{n_0 r_{0x} \tan \varepsilon_{A0} - \tan \varepsilon_{B0}} - 1 + \left[\frac{n_2 r_{2x} \tan \varepsilon_{A1} - \tan \varepsilon_{B1}}{n_0 r_{0x} \tan \varepsilon_{A0} - \tan \varepsilon_{B0}} - \frac{n_2 r_{2x}}{n_1 r_{1x}} \right] \frac{d}{x_{mv} - d} \end{aligned} \quad (14.62)$$

with $x_{mv} - d$ as the depth of the measurement volume in the test medium.

Fig. 14.15 Displacements of all four focal points on two laser beams (A and B) from the measurement volume (two-time refractions)



All deviations calculated in the current case of multiple beam refractions depend on the off-axis angle of the LDA head as well as on the depth of the measurement volume in the test fluid. In the case of very small window thickness ($d/x_{mv} \ll 1$), Eqs. (14.61) and (14.62) can be simplified, leading to Eqs. (14.57) and (14.58), respectively, for one-time refractions.

Taking into account both laser beams forming the measurement volume, the deviations of all four focal points from the measurement volume are presented in Fig. 14.15 for a concrete LDA configuration with $\alpha_0 = 2.75^\circ$ and $x_{mv}/d = 2$. They are similar to those in Fig. 14.14. In particular, it has been again confirmed that the sagittal focal points of both laser beams are further away from the measurement volume than the meridian focal points. For the same reason the distortion of the measurement volume will be expected.

14.7.3 Astigmatism at the On-axis LDA Alignment

In most cases of practical applications, LDA measurements of channel flows are carried out with on-axis alignment of the LDA head ($\phi_{LDA} = 0$). Both laser beams suffers from the same effect of astigmatism, however, only in relation to the small beam crossing angle ($2\alpha_0$). Corresponding deviations of laser focal points from the measurement volume can be calculated for instance for the case of $d/x_{mv} \ll 1$ by Eqs. (14.57) and (14.58) with respective incident and refraction angles of two laser beams. In assuming $\alpha_0 = 2.75^\circ$ and the refractive index ratio $n_1/n_0 = 1.333$, one obtains

$$\Delta x_{m,mv}^* = 0.001 \quad (14.63)$$

$$\Delta x_{s,mv}^* = 0 \quad (14.64)$$

This result signifies that no distortion of the measurement volume takes place. The best optical condition for LDA measurements is reached in this way (see [Chap. 13](#)).

14.8 Signal Qualities and the Lens Dependence

14.8.1 Deterioration of Signal Qualities and Strengths

It can be inferred from Fig. 14.6 that in the case of occurring astigmatism, each elementary segment on the front lens of the LDA head has its individual focal point in the medium. The measurement volume that is formed by two laser beams in the meridian plane obviously coincides with the focal points of only a few such elementary segments and thus cannot be seen by others. The scattered laser light from the measurement volume therefore cannot be efficiently detected by the receiving unit. The direct consequence is that the velocity signal rate rapidly decreases with the LDA off-axis angle. In this respect, the influence of astigmatism on the signal quality is rooted in the receiving optics rather than in the transmitting optics, as this is illustrated in Fig. 14.16. The light scattered from the measurement volume backward propagates along the optical axis through the medium interface. It is initially a beam bundle with a unique focal point at mv i.e. the measurement volume. After passing through the medium interface the light in the meridian plane has its virtual focal point at o_m , which is the same as that of the transmitting optics. The light in the sagittal plane, however, shows its virtual focal point o_s which does not coincide with o_m . This phenomenon exactly demonstrates the existence of astigmatism in the receiving optics. The distance between two virtual focal points is again called the astigmatic difference. Because the scattered light after passing through the medium interface is no longer a beam bundle with unique focal point, it cannot be efficiently collected to the detector for further signal processing. Both the signal

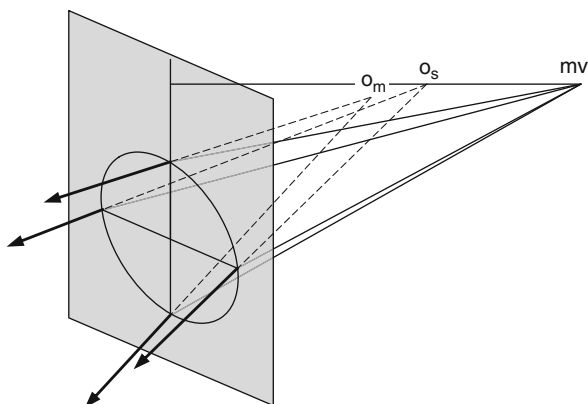


Fig. 14.16 Astigmatism in the receiving optics

quality and the strength will thus be considerably affected. As a result the reduction of the signal rate will come about.

14.8.2 Lens Dependence of Signal Qualities and Strengths

The existence of astigmatism in receiving optics deteriorates both the qualities and the strengths of light signals and hence leads to a reduction of the sampling rate in measurements. In a detailed investigation carried out by Zhang and Eisele (1996a, 1998b), it has been demonstrated that the reduction of the sampling rate in off-axis LDA measurements additionally and sensitively depends on the lens focal length specified at the LDA-head.

As known and explained in Sect. 4.2, the use of an LDA front lens with short focal length (f) will enhance the brightness of the measurement volume and consequently the strength of the scattered laser light. It is also known that this front lens as the receiving optics in turn has a large aperture to the measurement volume (proportional to $1/f^2$). For these two reasons the light signal received is then much stronger than that received by using a lens with a long focal length. A much high sampling rate in LDA measurements may usually be expected. This advantage of receiving optics with short focal length is lost, however, if the receiving optics is aligned off-axis, as in the case treated here. This can be demonstrated by employing the ray optics with respect to two lenses with different focal lengths ($f_1 < f_2$).

In order to model the astigmatism in LDA measurements, it is assumed, according to Fig. 14.7a, that the measurement volume (mv) is located at the distance s to the left of the lens and does not coincide with the focus of the lens. This modelling of astigmatism is based on the demonstration in the last section that hardly any elementary segments on the receiving lens have their focal points being coincident with the measurement volume. Because of the distance s the scattered laser light from the measurement volume will not be parallel to the lens axis after passing the lens. The slopes of the light rays before and after the lens are denoted by m and m' , respectively. From the geometric optics the relationship between oncoming and departing light rays is given by

$$m' = m - h/f \quad (14.65)$$

With $m = h/s$ as the slope of the oncoming ray and $d = s - f$ as the deviation of the measurement volume from the lens focus, the above equation is rearranged to

$$f \cdot (f + d) m' = -h \cdot d \quad (14.66)$$

For the purpose of comparing the effectiveness of two changeable receiving lenses with different focal lengths, the deviation d in above equation should be considered. In the first instance, the approximation $f + d \approx f$ can be made because of $d \ll f_1$ and $d \ll f_2$ in both cases of lenses. In the second instance, the deviation d can

be assumed to be constant i.e. $d_1 \approx d_2$. This assumption relies on the fact that the astigmatic difference is nearby independent of the light bundle thickness, as this can be verified by comparing Fig. 14.11 as being calculated for a thin light bundle with Fig. 14.9 as being calculated for a thick light bundle which comprises four laser beams. The nearby constant astigmatic difference points out that the same astigmatic difference will be given when using a lens with another focal length. With respect to these two aspects of the distance d Eq. (14.66) can be applied in comparison of optical effectiveness of two receiving lenses with different focal lengths. It yields then from Eq. (14.66) with $h = \text{const}$

$$f_1^2 m'_1 = f_2^2 m'_2 = -d \cdot h \tag{14.67}$$

This equation is available for comparison between corresponding segments (condition $h_1 = h_2 = h$) on both lenses. As known, the non-zero slope of the light ray after a lens segment implies that this light will not be efficiently collimated to the small aperture in the receiving optics and the corresponding segment on the lens behaves as blind to the measurement volume. Obviously the lens with short focal length ($f_1 < f_2$) behaves as more blind ($m'_1 > m'_2$) to the measurement volume than the lens with long focal length, as shown in Fig. 14.17b. For achieving better optical conditions in off-axis LDA measurements, the applying of the lenses with long focal lengths is therefore suggested.

Analogous to Eq. (14.67) another comparison with regard to the slopes of both departing rays for equal oncoming rays ($m_1 = m_2 = m$) can be made. Combining

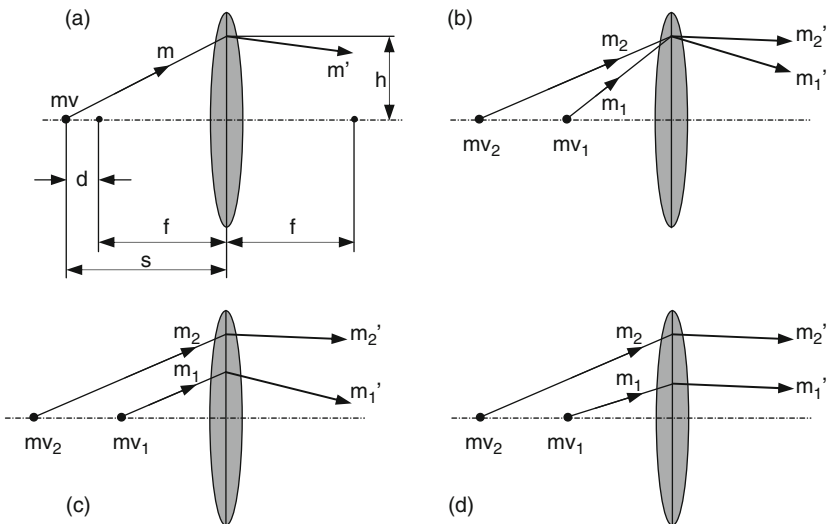


Fig. 14.17 Effects of the lens focal length on the signal transmission performance (quality and strength of signals) in the receiving optics

$m = h/s$ and $d = s - f$ yields $h = (d + f)m$ which is again inserted into Eq. (14.65). One obtains then

$$f_1 m'_1 = f_2 m'_2 = -md \quad (14.68)$$

Since $m_1 = m_2$ represents the same aperture of the lens segments to the measurement volume, Eq. (14.68) implies that for the same amount of incident light and thus of incident light energy (Fig. 14.17c) the inclination of departure rays is inversely proportional to the lens focal length. The lens with the short focal length ($f_1 < f_2$) is thus comparatively inefficient ($m'_1 > m'_2$) to conduct the scattered laser light from the measurement volume to be received by the receiving optics. It again suggests applying the lenses with long focal length.

A third comparison between lenses with different focal lengths can be made from Eq. (14.65) if equal slopes of departure rays from the lenses ($m'_1 = m'_2 = m'$) are considered. Combining $m = h/s$ and $d = s - f$ yields $m = h/(d + f)$ which is again inserted into Eq. (14.65). One obtains then with $f + d \approx f$

$$\frac{h_1}{f_1^2} = \frac{h_2}{f_2^2} = -\frac{m'}{d} \quad (14.69)$$

This equation shows that for detecting the departure lights whose inclinations are below a given value $|m'|$ the available lens height (h) is proportional to the square of the lens focal length. This means that the lens with a longer focal length ($f_2 > f_1$) also has a large available lens surface ($h_2 > h_1$) and thus a large aperture to the measurement volume, as shown in Fig. 14.17d. This circumstance again suggests the use of the lenses with long focal length.

Based on above analyses it can be concluded that at a given off-axis angle of an LDA head and for the given position of the measurement volume in the test medium, an LDA receiving lens with longer focal length is preferred in use instead of the lenses with short focal length. This ensures the effective conduction of scattered laser light from the measurement volume to the receiving optics and consequently the obtaining of signals of better qualities. The rapid reduction of velocity sampling rate because of the occurrence of astigmatism can then be successfully suppressed.

Figure 14.18 shows an experimental verification concerning the velocity sampling rate as a function of the off-axis angle of an LDA head with two different focal lengths. The appearance of astigmatism has been here realized by means of a plane window of Plexiglas (40 mm of thickness) between the LDA head and the flow. The orientation of the plane window to the optical axis was changed, so that a great number of cases with astigmatism could be obtained. It can be clearly seen from Fig. 14.18 that the data sampling rate by using the lens with the long focal length ($f = 400$ mm) has hardly changed with the LDA off-axis angle up to 20° . In contrast to this, the data sampling rate by using the lens with the short focal length ($f = 160$ mm) rapidly decreases, as the LDA off-axis angle increases.

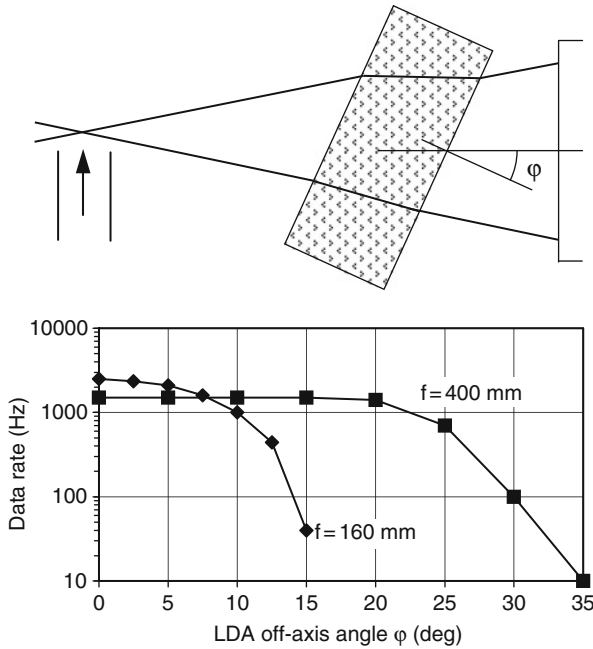


Fig. 14.18 Data rate reduction at off-axis LDA measurements and the dependence on the lens focal length

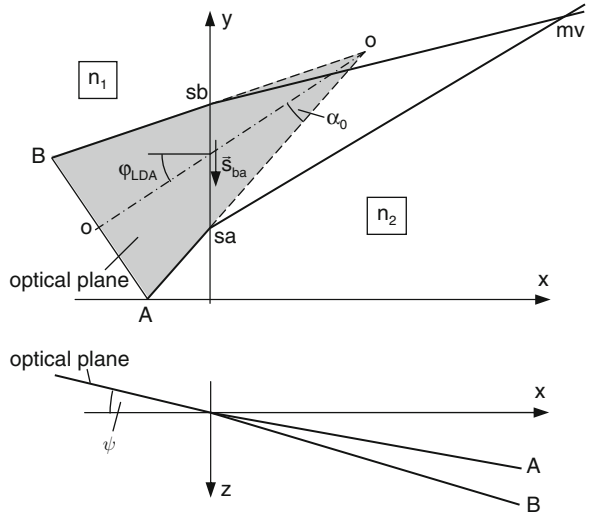
Another possibility to compensate for astigmatism and its influence on the signal strength and qualities is to use a water-filled prism if water flow is measured. Details in use of such a prism and its calculation will be given in Sect. 14.10.

14.9 Error Sensitivities in Forming the Measurement Volume

14.9.1 Beam Separation in the Test Medium

In the foregoing sections, the LDA off-axis alignment against the plane wall (i.e. the medium interface) is assumed to be within the optical plane containing two laser beams. This is the way that ensures the laser beam propagation, after being refracted, within the same plane and thus leads to perfect laser beam intersection. Any deviation in arranging the off-axis LDA from this requirement, as the consequence of inaccurate mechanical support of LDA for instance, will cause the imperfect laser beam intersection or laser beam separation. This undesired outcome comes about because two refracted laser beams after being refracted do not propagate in a unique plane (Fig. 14.19). For the practical use as well as for the reference purpose, the possible beam separations arising from errors and inaccuracy in LDA off-axis alignment will be presented based on investigations carried out by Zhang and Eisele (1998b).

Fig. 14.19 Bias angle ψ and the separation of two laser beams after the refraction in the medium 2



The desired off-axis LDA alignment is given by arranging the LDA off-axis in the LDA optical plane. It can also be said that the normal of the medium interface lies in the optical plane. Any inaccurate LDA off-axis alignment can be considered as the combined outcome of the accurate off-axis alignment in the optical plane followed by

- tilting this plane by ψ (Fig. 14.19) and/or by
- rotating the optical plane about the optical axis by δ (Fig. 14.20).

These two bias angles are independent and represent two possible sources leading to separation between the normal of the medium interface and the LDA optical plane. As a result, no or an imperfect measurement volume can be formed. In fact,

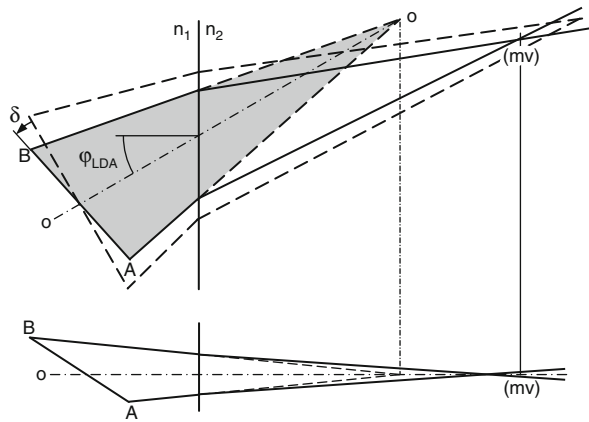


Fig. 14.20 Bias angle δ and the separation of two laser beams after the refraction in the medium 2

any improper LDA off-axis alignment can be expressed to be the additive effect of these two bias angles.

To simulate the improper off-axis LDA alignment for internal flow measurements, a one-component LDA head with two laser beams is assumed to generally have an arbitrary spatial orientation against the normal of the medium interface. In order to calculate the beam separation explicitly, both laser beams that are denoted by A and B, respectively, will be expressed by unit vectors \vec{a}_1 and \vec{b}_1 before and \vec{a}_2 and \vec{b}_2 after the refractions. As in the geometric optics, the unit vectors \vec{a}_2 and \vec{b}_2 can be determined from the unit vectors \vec{a}_1 and \vec{b}_1 by applying the law of refraction in the vector form according to Eqs. (3.8) and (3.9). For this reason, a coordinate system will be fixed at which the $y - z$ plane agrees with the medium interface (Fig. 14.19).

Two laser beams will be assumed to have their initial (i.e. virtual) focal point at $o(x_o, y_o, z_o)$. The intersection of laser beams with the medium interface ($y - z$ plane) at points sa and sb , respectively, is determined as follows:

$$x_{sa} = 0, \quad y_{sa} = y_o - \frac{a_{1y}}{a_{1x}}x_o, \quad z_{sa} = z_o - \frac{a_{1z}}{a_{1x}}x_o \quad (14.70)$$

$$x_{sb} = 0, \quad y_{sb} = y_o - \frac{b_{1y}}{b_{1x}}x_o, \quad z_{sb} = z_o - \frac{b_{1z}}{b_{1x}}x_o \quad (14.71)$$

Combining these two intersection points yields a new vector (from B to A) as

$$\vec{s}_{ba} = (0, y_{sa} - y_{sb}, z_{sa} - z_{sb}) \quad (14.72)$$

The arbitrary spatial orientation of the LDA head to the medium interface implies that the normal of the medium interface may not lie in the plane containing two laser beams (LDA optical plane). If this occurs, both refracted laser beams then no longer propagate in a common plane, so that no or imperfect intersection of two laser beams will be given. The separation between these two spatial laser beams is represented by the minimum distance in the direction perpendicular to both beam axes. The direction perpendicular to both laser beams is given by the unit vector $(\vec{a}_2 \times \vec{b}_2) / |\vec{a}_2 \times \vec{b}_2|$. The projection of the separation vector \vec{s}_{ba} in this direction then gives the definite distance between both laser beams (plus and minus are available):

$$s = \frac{\vec{a}_2 \times \vec{b}_2}{|\vec{a}_2 \times \vec{b}_2|} \cdot \vec{s}_{ba} = \frac{n_1}{n_2} x_o \frac{a_{1y}b_{1z} - a_{1z}b_{1y}}{|\vec{a}_2 \times \vec{b}_2|} \cdot \left(\frac{a_{2x}}{a_{1x}} - \frac{b_{2x}}{b_{1x}} \right) \quad (14.73)$$

Because the expression $|\vec{a}_2 \times \vec{b}_2|$ represents the sine value of the angle between both laser beams with \vec{a}_2 and \vec{b}_2 as unit vectors, it can be found by

$$|\vec{a}_2 \times \vec{b}_2| = \sqrt{1 - (\vec{a}_2 \cdot \vec{b}_2)^2} = \sqrt{1 - (a_{2x}b_{2x} + a_{2y}b_{2y} + a_{2z}b_{2z})^2} \quad (14.74)$$

The desired i.e. accurate off-axis LDA alignment is regarded to occur in the LDA optical plane. This means that, according to Fig. 14.19 with chosen coordinate system and $\psi = 0$, the LDA optical plane coincides with the $x - y$ plane. Because of $a_{1z} = 0$ and $b_{1z} = 0$ the distance s from Eq. (14.73) is zero. This corresponds to the case with perfect intersection of axes of two laser beams after being refracted in the medium 2. Deviations from this desired off-axis LDA alignment may be caused by inaccurate manipulation or the inaccurate mechanical support. As explained before, any deviation can be considered as the combined and additive effect of two bias angles ψ and δ . Because these two parameters are independent of each other, the beam separations respectively caused by these two bias angles can be separately calculated.

14.9.1.1 Beam Separation Due to the Bias Angle ψ

This case with the bias angle ψ as an error parameter corresponds to the case that has been shown in Fig. 14.19. Both incident laser beams can be represented by the unit vector \vec{a}_1 and \vec{b}_1 , respectively, that are given by the following components:

$$a_{1x} = \cos(\varphi_{\text{LDA}} + \alpha_0) \cdot \cos \psi \quad (14.75)$$

$$a_{1y} = \sin(\varphi_{\text{LDA}} + \alpha_0) \quad (14.76)$$

$$a_{1z} = \cos(\varphi_{\text{LDA}} + \alpha_0) \cdot \sin \psi \quad (14.77)$$

$$b_{1x} = \cos(\varphi_{\text{LDA}} - \alpha_0) \cdot \cos \psi \quad (14.78)$$

$$b_{1y} = \sin(\varphi_{\text{LDA}} - \alpha_0) \quad (14.79)$$

$$b_{1z} = \cos(\varphi_{\text{LDA}} - \alpha_0) \cdot \sin \psi \quad (14.80)$$

In these equations, the constant α_0 denotes the half intersection angle between two laser beams.

With available incident beams given in above equations the spatial separation between two laser beams after refraction in the medium 2 can be calculated from Eq. (14.73). For the reason of compact writing form, only the expression $a_{1y}b_{1z} - a_{1z}b_{1y}$ in Eq. (14.73) is replaced by respective components listed above, leading to

$$\frac{s}{x_0} = \frac{n_1}{n_2} \frac{\sin \psi \sin 2\alpha_0}{\sqrt{1 - (a_{2x}b_{2x} + a_{2y}b_{2y} + a_{2z}b_{2z})^2}} \left(\frac{a_{2x}}{a_{1x}} - \frac{b_{2x}}{b_{1x}} \right) \quad (14.81)$$

In this equation, all components of unit vectors representing the refracted laser beams in medium 2 can be calculated by applying the law of refraction that has already been presented by Eqs. (3.8) and (3.9). One then obtains

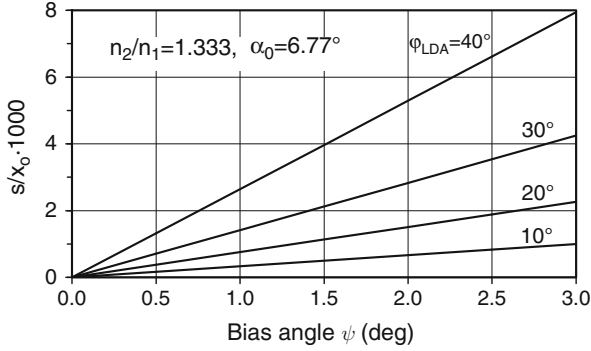


Fig. 14.21 Beam separation caused by the bias angle ψ

$$a_{2y} = \frac{n_1}{n_2} a_{1y}, \quad a_{2z} = \frac{n_1}{n_2} a_{1z}, \quad a_{2x} = \sqrt{1 - a_{2y}^2 - a_{2z}^2} \quad (14.82)$$

$$b_{2y} = \frac{n_1}{n_2} b_{1y}, \quad b_{2z} = \frac{n_1}{n_2} b_{1z}, \quad b_{2x} = \sqrt{1 - b_{2y}^2 - b_{2z}^2} \quad (14.83)$$

According to Eq. (14.81) the related separation between two refracted laser beams has been shown as a function of the off-axis angle of the LDA head φ_{LDA} and the bias angle ψ . For an example of calculations, Fig. 14.21 shows the beam separation in medium 2 (water) in an air-water system. This simplified system can be applied when the window thickness of an air-window-water system is negligible. The half intersection angle between two laser beams is taken as $\alpha_0 = 6.77^\circ$. As it can be read out for instance with $\varphi_{LDA} = 30^\circ$ and $\psi = 1^\circ$, the resultant beam separation is given by $s/x_0 = 1.4 \cdot 10^{-3}$. If the initial focal point is positioned by $x_0 = 100$ mm, to which the measurement volume in the medium 2 is found at about $1.65x_0$ (Fig. 14.5), then the beam separation takes $s = 0.14$ mm. It should be mentioned that this beam separation may no longer be neglected in the practical LDA measurements because the thickness of the measurement volume itself is only in the order of 0.1 mm. The undesired outcome of the beam separation is the drop of velocity sampling rate and in the worst case the total loss of LDA signals.

14.9.1.2 Beam Separation Due to the Bias Angle δ

This case with the bias angle δ corresponds to the case that has been shown in Fig. 14.20. According to Appendix B, both incident laser beams can be again represented by the unit vector \vec{a}_1 and \vec{b}_1 , respectively, that are given by the following components:

$$a_{1x} = \cos \varphi_{LDA} \cos \alpha_0 + \sin \varphi_{LDA} \sin \alpha_0 \cos \delta \quad (14.84)$$

$$a_{1y} = \sin \varphi_{LDA} \cos \alpha_0 - \cos \varphi_{LDA} \sin \alpha_0 \cos \delta \quad (14.85)$$

$$a_{1z} = \sin \alpha_0 \sin \delta \quad (14.86)$$

$$b_{1x} = \cos \varphi_{\text{LDA}} \cos \alpha_0 - \sin \varphi_{\text{LDA}} \sin \alpha_0 \cos \delta \quad (14.87)$$

$$b_{1y} = \sin \varphi_{\text{LDA}} \cos \alpha_0 + \cos \varphi_{\text{LDA}} \sin \alpha_0 \cos \delta \quad (14.88)$$

$$b_{1z} = -\sin \alpha_0 \sin \delta \quad (14.89)$$

Substituting respective expressions in Eq. (14.73) yields

$$\frac{s}{x_0} = -\frac{n_1}{n_2} \frac{\sin \varphi_{\text{LDA}} \sin 2\alpha_0 \sin \delta}{\sqrt{1 - (a_{2x}b_{2x} + a_{2y}b_{2y} + a_{2z}b_{2z})^2}} \left(\frac{a_{2x}}{a_{1x}} - \frac{b_{2x}}{b_{1x}} \right) \quad (14.90)$$

In this equation, all components of unit vectors representing the refracted laser beams in medium 2 can be calculated by Eqs. (14.82) and (14.83).

From the above equation the resultant separation between both refracted laser beams has been shown as a function of the off-axis angle of the LDA head φ_{LDA} and the bias angle δ . For an example of calculations, Fig. 14.22 shows the beam separation in medium 2 (water) in a simplified air-water system. The half intersection angle between two laser beams is again taken as $\alpha_0 = 6.77^\circ$. As it can be read out for instance with $\varphi_{\text{LDA}} = 30^\circ$ and $\delta = 1^\circ$ typically, the resultant beam separation is $s/x_0 = 0.7 \cdot 10^{-3}$. If the initial focal point is positioned by $x_0 = 100$ mm, to which the measurement volume in the medium 2 is found at about $1.65x_0$, then the beam separation takes $s = 0.07$ mm. This value has also to be considered as sufficiently large if compared with the measurement volume whose thickness is only about 0.1 mm. As said before, the undesired outcome of the beam separation is the drop of velocity sampling rate or the total loss of LDA signals.

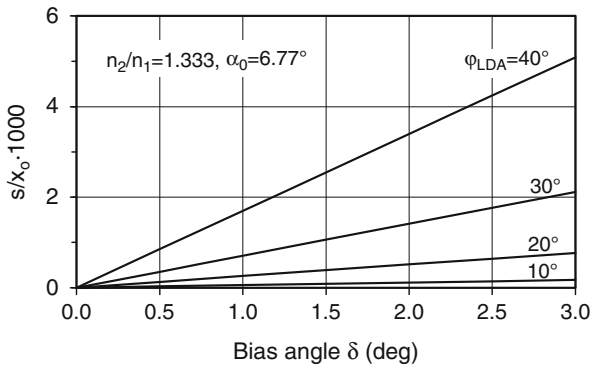


Fig. 14.22 Beam separation caused by the bias angle δ

14.9.1.3 Statement Regarding the Inaccurate Laser Beam Alignment

Calculations made above and shown in Figs. 14.21 and 14.22 clearly pointed out that the uncertainty in forming the measurement volume is very sensitive to the imperfect off-axis LDA alignment, especially at large off-axis angles. The resultant beam separation implies that either no measurement is possible (for large beam separation) or the geometrical size of the measurement volume decreases. The signal rate will thus be much affected. This knowledge undoubtedly suggests that the off-axis LDA alignment has to be accurately accomplished, so that the laser beams after refractions do propagate in the same optical plane containing two incident beams. It is, however, usually not necessary to exactly know the error i.e. the beam separation s while forming the measurement volume. In addition, both bias angles (ψ and δ) are usually not available.

If possible, LDA alignment at large off-axis angles should be avoided. This is recommended also in concerning the rapid reduction of the signal rate because of astigmatism, as already treated in Sect. 14.8.

In dealing with multiple refractions e.g. in an air-window-water system, calculations of the beam separation will be given in the next section.

14.9.2 Beam Separation After Multiple Refractions

Most LDA applications to internal flow measurements are characterized by at least two-time refraction of each laser beam, for instance at medium interface air-glass and glass-water. Analogous to the derivation of Eq. (14.73) the beam separation after passing through a plane layer, say a glass window of thickness d , can be calculated as (Zhang and Eisele 1998b)

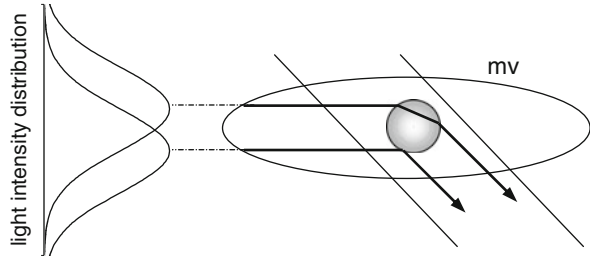
$$\frac{s}{x_0} = \frac{n_0}{n_2} \frac{a_{0y}b_{0z} - a_{0z}b_{0y}}{\sqrt{1 - (a_{2x}b_{2x} + a_{2y}b_{2y} + a_{2z}b_{2z})^2}} \left[\left(\frac{a_{2x}}{a_{0x}} - \frac{b_{2x}}{b_{0x}} \right) - \frac{d}{x_0} \frac{n_0}{n_1} \left(\frac{a_{2x}}{a_{1x}} - \frac{b_{2x}}{b_{1x}} \right) \right] \quad (14.91)$$

Herein the indices 0, 1 and 2 are commonly rearranged to the medium air, glass and water. x_0 indicates the location of the virtual focal point of laser beams. The origin of x -axis lies on the first refraction surface.

14.9.3 Possible Impact on PDA Measurements

As stated, LDA is a method for flow velocity measurements. It operates on the wave theory and makes use of the Doppler effect in the light that is scattered by a moving particle in the flow. Based on the LDA principle, the LDA method has also been extended to measure the particle size. The extended method makes use of the phase difference in the scattered laser lights that are detected from two spatially different directions. Because this phase difference is proportional to the size

Fig. 14.23 Gaussian beam effect in PDA measurements as the consequence of the imperfect laser beam intersection



of the particle that scatters the laser light, the particle size can be calculated from the measured phase difference. It again deals with a method that does not need any calibration. This extended LDA for particle size measurements is known as the Phase Doppler Anemometry (PDA). It contains a transmitting optics that is the same as that in the LDA method and a separate receiving optics. Detailed descriptions of the functionality of the PDA method can be found for instance by Albrecht et al. (2003).

The analyses of the outcome of errors in LDA alignment, as described above with regard to the LDA off-axis angle ϕ_{LDA} and two bias angles ψ and δ , also apply to the transmitting optics of the PDA method in measuring the particle size in the flow. Because of the beam separation, the Gaussian distributions of the light intensity in both laser beams may no longer be coincident in the measurement volume, as illustrated in Fig. 14.23. It is then quite possible that the light of one laser beam is mainly reflected by a particle, whereas the light of another laser beam is mainly refracted by the same particle. The superposition and detection of two such different types of scattered laser light will lead to erroneous interpretation of the particle size. In addition, only large particles have a high probability of simultaneously scattering both laser beams. This again leads to mistaken interpretation of the size distribution of particles in the flow. Furthermore, because the effective flow area in the measurement volume could not be clearly specified, accurate measurements of both the concentration and the mass flux of particles in the flow could not be achieved. This will in turn largely limit the fundamental evaluations of related physical and engineering processes with particle flows (Zhang et al. 1998, Zhang and Eisele 1999, Zhang and Ziada 2000).

14.10 Method for Compensation of Astigmatism

The astigmatism in LDA measurements has been confirmed to greatly influence the measurement accuracy. In worst cases, no measurement can be carried out at all because of the separation between two laser beams. To compensate for the astigmatism, for instance in measuring the internal water flow, a water-filled prism according to Fig. 14.24, with or without the air gap, can be applied. Such an optical arrangement has already found its practical applications (Booij and Tukker 1994).

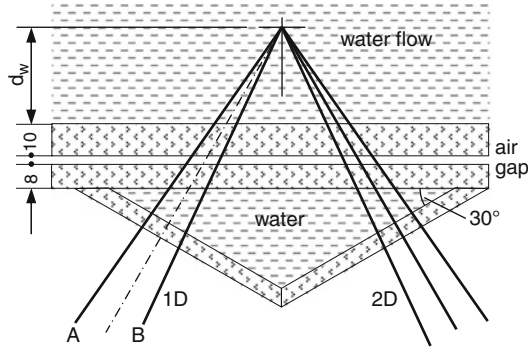


Fig. 14.24 Application example of using a water-filled prism to reduce and compensate for the optical aberration (astigmatism) in LDA measurements of water flows

The air gap serves to cause a “negative” astigmatism so that a complete compensation of astigmatism in both the transmitting and the receiving optics can be achieved. Because the perpendicular entry of laser beams into the prism does not cause any significant optical aberrations (see Chap. 13 and especially Sect. 14.7.3), the use of a water-filled prism acts as to submerge the LDA head into the same water. The occurrence of astigmatism on the side of transmitting optics thus changes from the case of air-glass-water to the case of water-glass-air-water. This is meaningful not only because of the possibility of completely suppressing the astigmatism, but also because of the simplicity of doing this, as will be shown below.

With the help of the water-filled prism the LDA head acts as to be submerged in water. This ensures that all four laser beams within the water of the water-filled prism are free of the optical aberrations and would intersect at a unique virtual focal point. The water in the prism should thus be considered as the reference medium for calculating the astigmatic difference in relying on calculation fundamentals in Sect. 14.5. The first non-perpendicular refraction of the optical axis occurs at $\varphi_0 = 30^\circ$, while the optical axis intersects the next medium interface. The same optical property of transparent walls on both sides of the air gap is assumed. Hence for further calculations an equivalent wall thickness to the sum of both can be used.

The half intersection angle between two laser beams in the reference medium α_w should be used in place of α_0 . Between α_w and α_0 it applies the law of refraction with $n_0 = 1$

$$\sin \alpha_w = \frac{n_0}{n_w} \sin \alpha_0 \tag{14.92}$$

The two laser beams in the meridian plane are designated by A and B. There are generally three distances that cause astigmatism and contribute to the astigmatic difference: the glass thickness (d_g), the air gap (d_a) and the depth of the measurement volume in the water flow (d_w). Against the reference medium the air gap causes a negative astigmatic difference. In order to achieve the complete

compensation of astigmatism, the necessary thickness of the air gap can be calculated from Eq. (14.26) by setting $\Delta x_{m,s} = 0$:

$$\Psi_g d_g + \Psi_a d_a + \Psi_w d_w = 0 \quad (14.93)$$

Herein

$$\Psi_g = \frac{\cos \alpha_w \cos \varphi_o}{\sqrt{\frac{n_g^2}{n_w^2} - (1 - \cos^2 \alpha_w \cos^2 \varphi_o)}} - T_{g,w} \quad (14.94)$$

$$\Psi_a = \frac{\cos \alpha_w \cos \varphi_o}{\sqrt{\frac{n_a^2}{n_w^2} - (1 - \cos^2 \alpha_w \cos^2 \varphi_o)}} - T_{a,w} \quad (14.95)$$

$$\Psi_w = 0 \quad (14.96)$$

$$T_{g,w} = \frac{\tan \varepsilon_{Ag} - \tan \varepsilon_{Bg}}{\tan \varepsilon_{Aw} - \tan \varepsilon_{Bw}} \quad (14.97)$$

$$T_{a,w} = \frac{\tan \varepsilon_{Aa} - \tan \varepsilon_{Ba}}{\tan \varepsilon_{Aw} - \tan \varepsilon_{Bw}} \quad (14.98)$$

The result $\Psi_w = 0$ has been automatically obtained as expected since the test medium is equal to the reference medium (see Sect. 14.5). This just represents the advantage of using a water-filled prism for water flow measurements, because the astigmatism and thus the optical aberration become independent of the depth of the measurement volume in the flow. From Eq. (14.93) the necessary thickness of the air gap is calculated as

$$d_a = -\frac{\Psi_g}{\Psi_a} d_g \quad (14.99)$$

A calculation example of using the water-filled prism should be demonstrated here. The LDA head is specified by the laser beams with a half intersection angle equal to $\alpha_0 = 5.5^\circ$. The water-filled prism is designed with $\varphi_o = 30^\circ$. Table 14.1 shows the calculation results, from which the thickness of the air gap is calculated as 1.9 mm.

As shown in Table 14.1, the parameter Ψ_a is negative. This means that the used air gap leads to a negative astigmatic difference which enables the total astigmatism to be compensated for. If no air gap is used, then an astigmatic difference, caused by the glass wall of the thickness $d_g = 18$ mm, is calculated from Eq. (14.29) again with $\Psi_w = 0$ to

$$\Delta x_{m,s} = \Psi_g d_g = 1.1 \text{ (mm)} \quad (14.100)$$

This astigmatic difference which in effect represents a displacement between two measurement volumes appears to be too large for the 2D LDA optics in Fig. 14.24. For two component measurements, therefore, it is indispensable to use an air gap

Table 14.1 Calculation example of using a water-filled prism and the air gap to completely compensate for the astigmatism

Parameter specifications:		
Refractive index of water	n_w	1.333
Refractive index of transparent glass window	n_g	1.52
Half intersection angle of two laser beams at LDA head	α_0	5.5
Geometrical angle of the water-filled prism	φ_0	30
Glass window thickness total (mm)	d_g	18
Calculations:		
Half intersection angle of two laser beams in water	α_w	4.1
Refraction angle of beam A in glass	ε_{Ag}	29.5
Refraction angle of beam B in glass	ε_{Bg}	22.5
Refraction angle of beam A in air	ε_{Aa}	48.4
Refraction angle of beam B in air	ε_{Ba}	35.6
Refraction angle of beam A in water	ε_{Aw}	34.1
Refraction angle of beam B in water	ε_{Bw}	25.9
Parameter (glass – water)	$T_{g,w}$	0.78
Parameter (air – water)	$T_{a,w}$	2.13
Parameter (glass)	Ψ_g	0.061
Parameter (air gap)	Ψ_a	-0.58
Air gap needed (mm)	d_a	1.9

to completely compensate for the astigmatism. For 1D LDA optics in Fig. 14.24, however, the astigmatic difference $\Delta x_{m,s} = 1.1$ mm is irrelevant. This means that measurements of using the 1D LDA head can be performed without any significant difficulties and inaccuracies.

For the purposes of comparison, the case of off-axis LDA alignment without using the prism should be considered. Because the reference medium in this case is air (index 0), the parameter Ψ_1 (for glass), Ψ_2 (for water) and T_{20} are recalculated to be $\Psi_1 = 0.098$, $\Psi_2 = 0.091$ and $T_{20} = 0.608$, respectively. The astigmatic difference that is caused by the glass wall of the thickness $d = 10$ (Fig. 14.24) is calculated to $\Delta x_{m,s(\text{glass})} = 1.4$, by concerning the first part in Eq. (14.26). Also worth being mentioned is that in this case the depth of the measurement volume in the flow additionally contributes to the astigmatic difference. Because of this a water-filled prism should always be applied when the LDA optics has to be aligned off-axis.

It should be further mentioned that in the case of Fig. 14.24 with full compensation of astigmatism, the shift of each measurement volume is generally two-dimensional, even though the LDA head outside of the flow merely moves along the normal direction of the plane wall. This leads to undesirable separation between the measurement volumes of one- and two-component LDA units. This two-dimensional shift of each measurement volume is similar to that considered in Sect. 14.4. The flow field behind the wall could only be measured, provided that the optical realignment would take place for each new measurement point in the flow.

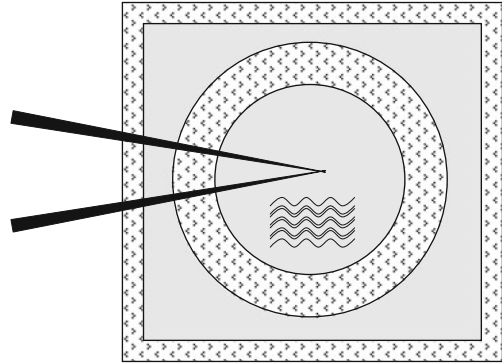
Chapter 15

Flow Measurements in Circular Pipes

Fluid flows in circular pipes belong to the most familiar and most broadly investigated flows. But the measurement of such flows by means of laser Doppler anemometry is not at all straightforward because of the surface curvatures on both the inside and the outside of the pipe. As is well known, simultaneous two-component velocity measurements, that are taken by using two pairs of laser beams, cannot be carried out, as the four laser beams do not intersect at a unique point in the flow because of optical aberrations. One of these optical aberrations is comparable with the astigmatism that occurs when the LDA optical axis is aligned off-axis against the normal of a plane wall, as treated in the last chapter. Nearly all the optical features and the effects of astigmatism in the case of plane windows also exist in a similar but often more complex form in the measurement of the circular pipe flow. Laser beam refractions on the curved interfaces of a circular pipe, for instance, complicate the calculation of beam propagations with regard to both the location of the measurement volume and the intersection angle between two laser beams (Boadway and Karahan 1981). In order to avoid the difficulty of calculating complex laser beam refractions on the curved flow interface, the method of matching the refractive index of the test fluid to that of the pipe wall has often been applied in small-scaled laboratory measurements. The method, however, is not applicable to the flows in most industrial applications where the refractive index matching is impossible or the gaseous flows are in use.

The problems that are related with direct measurements of flows in circular pipes have been additionally recognized in the signal strengths and qualities. Experiences show that in traversing the velocity profile across a circular pipe, the available signal qualities and thus the signal rate could be achieved only within a depth of about 1/3 of the pipe diameter. Beyond this depth both the signal strengths and qualities briskly drop down so that no measurements can be further carried out. The reason for such a disturbance in the respective measurement is the optical aberration in the receiving optics. This means, in concrete terms, that only a few elementary segments on the LDA receiving lens can see the measurement volume, while majorities are blind. This circumstance is comparable with that in flow measurements behind a plane wall by means of an off-axis LDA head, as already treated in Sect. 14.8. It appears that the flow in the centre area of a circular pipe could hardly be directly measured without matching the refractive index of the flow to that of the pipe wall.

Fig. 15.1 Method to improve the optical condition in LDA measurements of flows in the circular pipe, effective but not quite convenient



Because of this, some LDA users applied the method of putting the circular pipe with flows into a rectangular water tank with plane walls (Fig. 15.1). In using such a measurement facility, the optical performance on the side of receiving optics can be significantly enhanced, so that better qualities of signals can be obtained. The problem of calculating the measurement volume, however, remains because each laser beam still suffers from two-time refraction on the curved interfaces.

In dealing with flow measurements in a circular pipe by means of the LDA method without matching the refractive index, the optical performance can be considerably improved if the outside of the pipe is cut off and made plane, as illustrated in Fig. 15.2 from an industrial application (Zhang and Casey 2007, Zhang and Parkinson 2002). This approach was initially considered to simplify calculations of laser beam transmissions, as each laser beam undergoes only one time refraction on the curved interface and the formation of the measurement volume is independent of the thickness of the pipe wall. The approach indeed additionally contributes to a lot of reductions of diverse optical aberrations, since the main optical aberration is then only restricted to the beam refraction on the internal surface of the circular pipe. Therefore high quality signals can be obtained even at a distance of about $2/3$ of pipe diameters from the pipe wall. To get the complete distribution of each

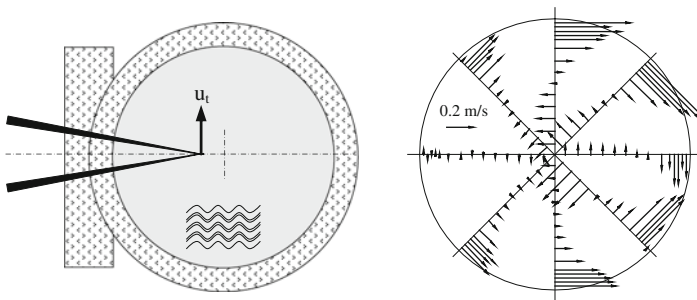


Fig. 15.2 Plane wall configuration on the outside of a circular pipe and measurements of the tangential velocity component (Zhang and Parkinson 2002)

velocity component across the pipe, additional measurements need to be performed from the opposite side by rotating the LDA head 180° around the pipe axis. The use of a moveable prism according to Fig. 15.2 creates a comparable plane cut-off on the outside of the pipe and enables the free alignment of the LDA head to the pipe and around the pipe axis. With this method both the main and the secondary flow distributions in the cross section of the respective pipe flow could be well measured. Clearly, measurements of all three velocity components in a pipe flow could only be achieved one after another.

As a matter of fact, a great number of flow measurements in circular pipes have been restricted to axial and tangential velocity components. The measurement of the tangential velocity component (secondary flow) does require some more calculations for tracking the laser beam in the flow. It actually does not represent a highly difficult task. In contrast, the measurement of the radial velocity component is obviously very restricted by complexities and intricacies of tracking the laser beams in the flow. It is in any case true that almost no such measurements have ever been carried out or can be referred to. Based on detailed analyses a fundamental guideline of measuring the radial velocity component of the flow in a circular pipe has been worked out by Zhang (2004a, b).

Another serious aspect associated with the laser beam refraction on the curved interface is the dislocation of all laser beam waists from the measurement volume. At large displacement between the measurement volume and the laser beam waists, the laser light intensity in the measurement volume decreases so that velocity signals will become too weak to be detected. This incident states an additional reason for the measurement limitation within a depth at about $2/3$ of the pipe diameter. Furthermore, the dislocation of laser beam waists inevitably leads to the fringe distortion in the measurement volume and hence to measurement errors.

In the following sections, essential calculations of tracking the laser beams in the flow will be presented with respect to the shift and optical properties of the measurement volume. All three velocity components will be considered. In that case, possible influences on both the signal quality and the measurement accuracy will be revealed and quantified. Because the plane outside of the circular pipe, as shown in Fig. 15.2, has been confirmed to be very effective and helpful in improving the optical conditions, all calculations will be referred to in this optical configuration. Correspondingly, the LDA head is assumed to be perpendicularly aligned to this plane surface.

15.1 Measurements of Axial Velocities

The measurements of axial velocities require that the two laser beams lie in a plane parallel to the pipe axis. The plane containing two laser beams is called the optical plane. By arranging the optical plane to go through the pipe axis (Fig. 15.3b), the laser beam refraction on the inside of the circular pipe is comparable with that on a perpendicular plane surface. Both laser beams propagate in the same plane as the

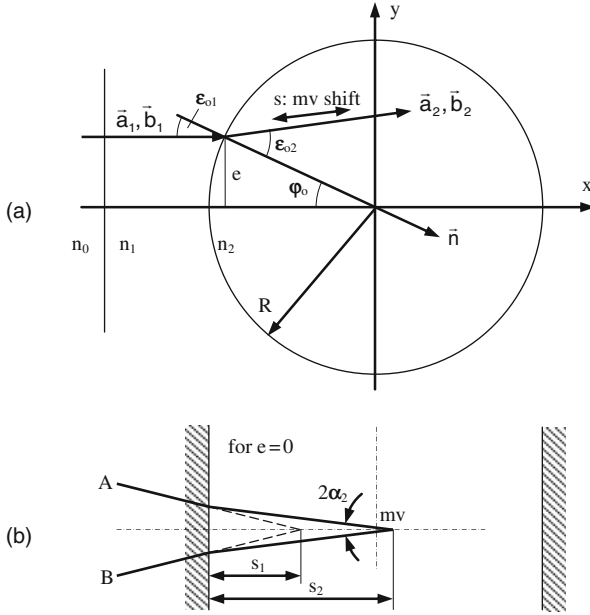


Fig. 15.3 Deviation of the optical plane from the pipe axis and its effect on the measurements of the axial velocity component

optical plane prior to refractions. The optical aberration in the transmitting optics remains at a minimum so that the best available optical condition is ensured.

The position of the measurement volume, measured from the pipe wall, can be directly written out from Eq. (13.6) in proportion to the position of the virtual measurement volume as

$$s_2 = \frac{n_2}{n_1} s_1 \tag{15.1}$$

with s_1 as the coordinate of the virtual intersection point of two laser beams.

A particular property of the optical layout for measurements of axial velocities should be highlighted here for future reference. As long as the optical plane is kept parallel to the pipe axis, without having to go through it, the intersection angle between the two refracted laser beams remains unchanged. This can be confirmed according to Fig. 15.3a which shows a deviation e of the optical plane from the pipe axis. With regard to the laser beam A for instance, the laser beam is denoted by the unit vector \vec{a}_1 in the medium 1 and \vec{a}_2 after the refraction in the medium 2. For the applied coordinate system the corresponding z -component of the unit vector \vec{a}_2 is given, according to Eq. (3.9), as $a_{2z} = n_1 n_2 \cdot a_{1z}$. The intersection angle $2\alpha_2$ between the two refracted laser beams A and B can then be calculated by

$$\cos 2\alpha_2 = \vec{a}_2 \cdot \vec{b}_2 \tag{15.2}$$

Because of the symmetry condition between two laser beams there are $a_{2x} = b_{2x}$, $a_{2y} = b_{2y}$ and $a_{2z} = -b_{2z}$ as well as $a_{2x}^2 + a_{2y}^2 = 1 - a_{2z}^2$ for the unit vector \vec{a}_2 . From Eq. (15.2) it then follows

$$\cos 2\alpha_2 = 1 - 2a_{2z}^2 = 1 - 2\left(\frac{n_1}{n_2}a_{1z}\right)^2 \quad (15.3)$$

With respect to the trigonometric identity $\cos 2\alpha_2 = 1 - 2\sin^2 \alpha_2$ and $a_{1z} = \sin \alpha_1$ for the incident laser beam A it further follows from the above equation

$$\sin \alpha_2 = \frac{n_1}{n_2}a_{1z} = \frac{n_1}{n_2} \sin \alpha_1 \quad (15.4)$$

The intersection angle of the two laser beams and thus the optical properties of the measurement volume in the test fluid remain the same as that on the pipe axis. This result indicates that the deviation in aligning the optical plane from going through the pipe axis does not lead to any error in velocity measurements. The analysis made here can be easily demonstrated by a table-top experiment when a scaled rule is inserted into a circular pipe with or without water (Fig. 15.4). Observation from the outside verifies that there is no longitudinal distortion in the rule scale along the pipe axis. The distortion only occurs in the radial direction.

Although a certain deviation of the optical plane from the pipe axis does not lead to any change in the beam intersection angle, there are, however, some other aspects that should be accounted for:

- With the displacement of the LDA head in the x -direction, the measurement volume in the test fluid gets moved along the bisector of two refracted laser beams i.e. along a path which is not parallel to the x -axis. Because of the comatic aberration, similar to that in Fig. 14.3a, the bisector of the two refracted laser

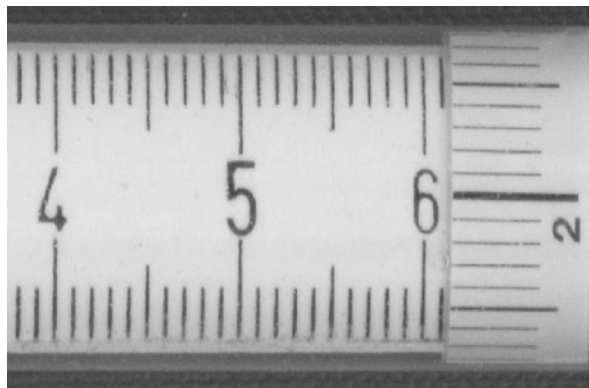


Fig. 15.4 A table-top experiment showing no any longitudinal distortion in the rule scale along the pipe axis

beams does not precisely coincide with the refracted optical axis. The difference between them can, however, be left to a first approximation. The refracted optical axis in the test fluid is calculated by using the law of refraction as

$$\sin \varepsilon_{02} = \frac{n_1}{n_2} \sin \varepsilon_{01} = \frac{n_1}{n_2} \frac{e}{R} \quad (15.5)$$

As an example, the beam refraction with $n_1/n_2 = 1.52/1.33$ is assumed. For $e/R = 0.5$ which means $\varepsilon_{01} = 30^\circ$ there is $\varepsilon_{02} = 34.8^\circ$. The inclination angle of the refracted optical axis in the flow against the x -axis is 4.8° .

- Because the intersection angle between two refracted laser beams in the flow is entirely a constant and thus independent of the position of the measurement volume, the shift of the measurement volume along the bisector (s) of two laser beams is proportional to the displacement of the LDA head along the x -axis. The corresponding shift ratio is for $\alpha_0 \ll 1$ and $\alpha_2 \ll 1$ simply

$$k_{mv} = \frac{\Delta s_{mv}}{\Delta x_{LDA}} = \frac{\tan \alpha_0}{\tan \alpha_2} \approx \frac{\sin \alpha_0}{\sin \alpha_2} = \frac{n_2}{n_0} \quad (15.6)$$

The LDA head is assumed to be positioned in air ($n_0 = 1$).

The x -component of the above shift ratio is calculated, according to Fig. 15.3, by

$$k_{mv,x} = k_{mv} \cos(\varepsilon_{02} - \varphi_0) \quad (15.7)$$

Usually the inclination angle of the refracted optical axis in the flow is small. For instance for $e/R < 0.5$ there is almost $\varepsilon_{02} - \varphi_0 < 5^\circ$, so that $k_{mv,x} \approx k_{mv}$ can be applied.

- At large deviations of the optical plane from the pipe axis ($e/R > 0.5$), which might be desired in some cases, the LDA optical axis tends to largely deviate from the normal \vec{n} of the interface. This situation is comparable with large off-axis angles of the LDA head against the normal of a plane wall (see Chap. 14). As a result the optical aberration related to the LDA optics, or accurately speaking, the effect of astigmatism becomes significant and the quality of optical signals will be considerably deteriorated. This optical aberration can also be visualized with the table-top experiment mentioned above, at which the scale on the rule in the pipe becomes continuously more unclear along the pipe radius (Fig. 15.4).

Since the deviation of the LDA optical plane from the pipe axis causes undesirable features, large deviations should be avoided. For moderate deviations (say $e/R < 0.5$), as long as the signal rate is sufficiently high, no particular attention needs to be paid. The fringe distortion in the measurement volume, which results from the dislocation of laser beam waists, is not significant and can be neglected.

15.2 Measurements of Tangential Velocities

For measurements of tangential velocities the LDA head is aligned, so that the optical plane is perpendicular to the pipe axis (Fig. 15.2). With regard to the laser beam refractions on the circular surface, two main aspects need to be considered:

- The shift of the measurement volume in the flow is no longer proportional to the shift of the LDA head.
- The intersection angle between the two refracted laser beams and thus both the geometrical and optical properties of the measurement volume depend on the local position of the measurement volume in the flow.

Detailed calculations of tracking the laser beams in the flow should therefore be conducted to ensure correct LDA measurements.

15.2.1 Basic Geometrical Relationships

The laser beams are again considered as they are present in the transparent pipe wall (index 1). Owing to the symmetrical layout between two laser beams, only one beam will be considered. The measurement volume is then formed on the symmetrical axis i.e. the x -axis in Fig. 15.5. For clarity, the crossing angle between two laser beams has been shown exaggerated. The laser beam is assumed to have its start position 1, when the measurement volume is positioned on the inside of the circular pipe. The shift of the laser beam to the position 2 is given by a distance s_1 with which the virtual measurement volume is moved to m' . The distance s_1 is about n_1 -times the movement of the LDA head in air. Because of the laser beam refraction the real measurement volume is found at m . The application of the law of sines to the triangles ocm' and ocm , respectively, yields

$$\frac{R - s_1}{\sin(\alpha_1 - \varphi)} = \frac{R}{\sin \alpha_1} \quad (15.8)$$

$$\frac{R - s_2}{\sin(\alpha_2 - \varphi)} = \frac{R}{\sin \alpha_2} \quad (15.9)$$

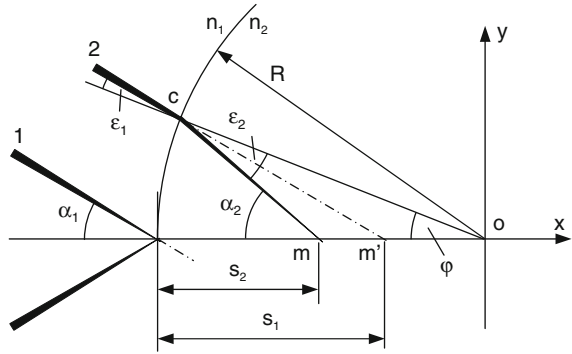
The law of refraction in such a case is given by

$$n_1 \sin(\alpha_1 - \varphi) = n_2 \sin(\alpha_2 - \varphi) \quad (15.10)$$

These three equations form the basic solutions for both the new position (s_2) and the geometrical parameter ($2\alpha_2$) of the measurement volume in the flow. For a given movement s_1 the following calculation process can be performed

$$s_1 \xrightarrow{(15.8)} \varphi \xrightarrow{(15.10)} \alpha_2 \xrightarrow{(15.9)} s_2 \quad (15.11)$$

Fig. 15.5 Formation of the measurement volume in the flow for measurements of the tangential velocity component



An application example of the presented technique has already been shown in Fig. 15.2.

15.2.2 Simplifications of Calculations

In the above calculation, Eq. (15.11) represents the way of indirectly calculating the relevant parameters α_2 and s_2 that are related to the measurement volume. This process seems to be somewhat inconvenient. With respect to the configuration of common LDA systems, at which the half intersection angle of laser beams is usually not more than 10° , the half intersection angle of laser beams in the transparent pipe wall is then not more than 7° and the angle φ seldom exceeds 14° . For this reason all the angles under the symbol of sine functions (α_1 , α_2 , $\alpha_1 - \varphi$ and $\alpha_2 - \varphi$) in the basic equations from Eq. (15.8) to Eq. (15.10) can be considered as small angles. All three equations can then be simplified by using the approximation $\sin x = x$ for paraxial rays. The characteristic parameters for the measurement volume can then be directly interpreted as the function of the virtual position of the measurement volume as follows:

$$\frac{s_2}{R} = \frac{1}{1 + \frac{n_1}{n_2} \left(\frac{R}{s_1} - 1 \right)} \tag{15.12}$$

$$\frac{\alpha_2}{\alpha_1} = \frac{n_1}{n_2} - \left(\frac{n_1}{n_2} - 1 \right) \frac{s_1}{R} \tag{15.13}$$

$$\frac{\varphi}{\alpha_1} = \frac{s_1}{R} \tag{15.14}$$

At present, Eq. (15.14) is only written for completeness. It will not be applied to quantify the measurement volume.

The inaccuracy arising from the approximations made above should be estimated. An LDA system is assumed to have a half intersection angle $\alpha_1 = 4.45^\circ$

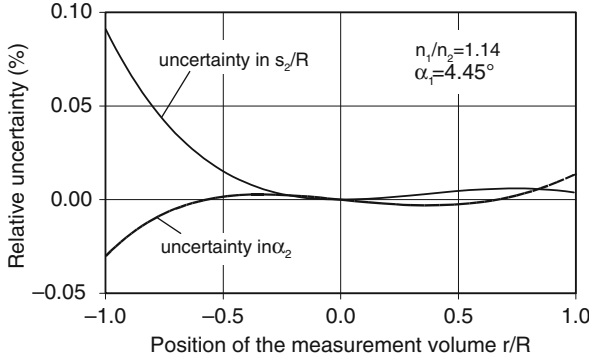


Fig. 15.6 Relative uncertainties in calculating the measurement volume in the water flow by using the simplified relations

between laser beams in the pipe wall ($n_1 = 1.52$). It is further assumed that the measurement volume traverses the pipe section for the case of water flows ($n_2 = 1.33$). From Eqs. (15.12) and (15.13), respectively, both the parameter s_2 and α_2 are calculated in the function of s_1 . Their relative deviations from those as calculated from Eq. (15.11) can then be determined, as shown in Fig. 15.6. As can be seen, the maximum error arising from the approximations leading to Eqs. (15.12) to (15.14) is below 0.1% and really negligible. The same calculation can also be made for air flow ($n_2 = 1$). The maximum error embedded in Eq. (15.12) is 0.4%, while in Eq. (15.13) is only 0.1%.

15.2.3 Fringe Spacing and Velocity Corrections

By using the laser beam intersection angle in the fluid, the fringe spacing in the measurement volume is calculated as

$$\Delta x = \frac{\lambda_2}{2 \sin \alpha_2} \tag{15.15}$$

Because of $\lambda_1/\lambda_2 = n_2/n_1$ this equation is rewritten as

$$\Delta x = \frac{n_1 \sin \alpha_1}{n_2 \sin \alpha_2} \frac{\lambda_1}{2 \sin \alpha_1} = \frac{n_1 \sin \alpha_1}{n_2 \sin \alpha_2} \Delta x_0 \tag{15.16}$$

Herein Δx_0 represents the predefined fringe spacing in the LDA optics i.e. the reference fringe spacing, when the measurement volume is found in the open air or in the pipe wall.

Equation (15.16) points out that the tangential velocities that are measured have to be corrected by a factor equal to

$$k_{\text{vel}} = \frac{u_t}{u_{t,\text{measured}}} = \frac{\Delta x}{\Delta x_0} = \frac{n_1 \sin \alpha_1}{n_2 \sin \alpha_2} \quad (15.17)$$

or with respect to Eqs. (15.8), (15.9) and (15.10) to

$$k_{\text{vel}} = \frac{R - s_2}{R - s_1} \quad (15.18)$$

In applying Eq. (15.12), this is again reformed as

$$k_{\text{vel}} = 1 + \left(\frac{n_1}{n_2} - 1 \right) \frac{s_2}{R} \quad (15.19)$$

It linearly depends on the depth of the measurement volume in the pipe flow. While in the near region to the pipe wall the correction factor is equal to unity, it takes n_1/n_2 on the pipe axis. For $n_1 = 1.52$ (glass) and $n_2 = 1.33$ (water) there is $k_{\text{vel}} = 1.14$.

15.3 Measurements of Radial Velocities

The measurements of radial velocities in circular pipes represent a highly complex process, if no index matching method is applied. In positioning the LDA head for radial velocity measurements according to Fig. 15.7, the following problems have to be solved:

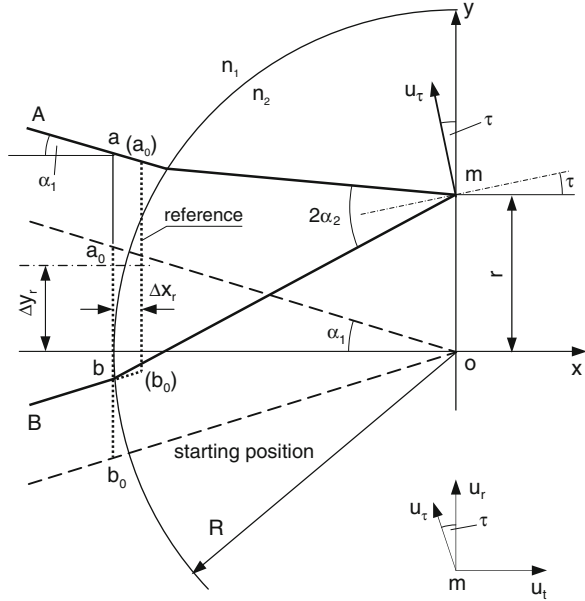
- How can the measurement volume (m) be accurately positioned?
- How can the beam intersection angle ($2\alpha_2$) be calculated?
- What about the orientation (τ) of the measurement volume?

The beam intersection angle and the measurement volume orientation have to be known in order to correct systematic measurement errors. In reality, because of $\tau \neq 0$ each measured velocity does not exactly represent the radial velocity component.

15.3.1 Accurate Positioning of the Measurement Volume

In principle, each LDA head position determines a position of the measurement volume in the flow. With the shift of the LDA head parallel to the y -axis, the measurement volume would generally travel along a two-dimensional path. This will considerably complicate the profile measurements of the radial velocity component. A relatively easy method is to calculate the necessary movement of the LDA

Fig. 15.7 Off-axis alignment of laser beams for measurements of the radial velocity component along the y-axis



head for the given path of the measurement volume along the y-axis, as shown in Fig. 15.7. The starting point is the LDA head position at which the measurement volume is positioned on the pipe axis (as the starting position). This can be achieved from the method described in the last section for measurement of the tangential velocity component. For each new position of the measurement volume (m) on the y-axis at r , the necessary movement of the beam pair in medium 1 from the starting position is assumed to be Δx_r and Δy_r . These are measured by shifting the reference line a_0b_0 (denoted by a fine dotted line) from the starting position to the new position. Then the following relationships can be obtained:

$$\Delta x_r = \frac{(y_a - y_b) - (y_{a0} - y_{b0})}{2 \tan \alpha_1} \tag{15.20}$$

$$\Delta y_r = \frac{1}{2} (y_a + y_b) \tag{15.21}$$

In these two equations, a_0 , b_0 , a and b are intersections between laser beams and the tangent of the circular pipe at $x = -R$. The basic intersection coordinates y_{a0} and y_{b0} are given by

$$y_{a0} = R \cdot \tan \alpha_1 \tag{15.22}$$

and

$$y_{b0} = -R \cdot \tan \alpha_1 \tag{15.23}$$

The intersection points a and b represent positions which the laser beams A and B at the new position of the beam pair must pass through. Clearly detailed calculations of y_a and y_b for a given measurement volume position have to be completed.

15.3.1.1 Determination of Intersection Points y_a and y_b

The purpose of present calculations is to establish the functions of both $y_a = f(r)$ and $y_b = f(r)$ for the given measurement volume along the y -axis. Because it deals with the same calculations both for y_a and y_b , only detailed calculations of $y_a = f(r)$ for the laser beam A will be presented below.

According to Fig. 15.8 the function $y_a = f(r)$ can be obtained if the function $\varphi_a = f(r)$ is known. For this reason the function $\varphi_a = f(r)$ or equivalently $r = f(\varphi_a)$ will be established first. The position of the measurement volume on the y -axis can be expressed by

$$r = R \sin \varphi_a - R \cos \varphi_a \tan \alpha_{2a} \tag{15.24}$$

or related to R as

$$\frac{r}{R} = \sin \varphi_a - \cos \varphi_a \tan \alpha_{2a} \tag{15.25}$$

Here $\tan \alpha_{2a}$ needs to be expressed as a function of φ_a .

With respect to $\alpha_{2a} = \varphi_a - \varepsilon_2$ and the law of refraction in the form of $n_2 \sin \varepsilon_2 = n_1 \sin \varepsilon_1$ the following relationship can be obtained:

$$\tan \alpha_{2a} = \frac{\sqrt{T_a - 1} \tan \varphi_a - 1}{\sqrt{T_a - 1} + \tan \varphi_a} \tag{15.26}$$

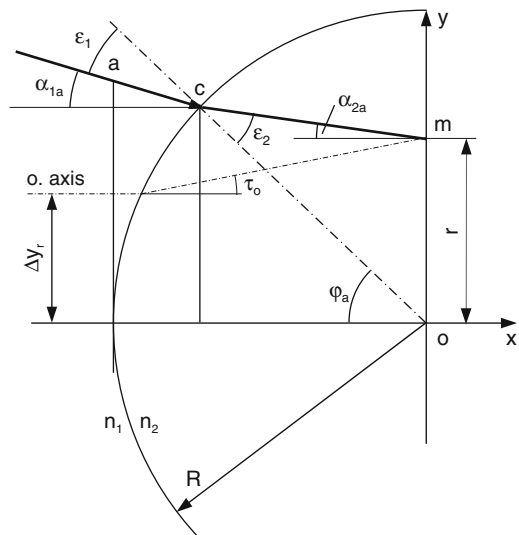


Fig. 15.8 Calculation of the laser beam transmission for the measurement volume located on the y -axis

Herein T_a is given by

$$T_a = \left(\frac{n_2}{n_1}\right)^2 \frac{1}{\sin^2 \varepsilon_1} = \left(\frac{n_2}{n_1}\right)^2 \frac{1}{\sin^2 (\varphi_a - \alpha_{1a})} \quad (15.27)$$

According to Eq. (15.26) there has to be $T_a \geq 1$. In fact, $T_a = 1$ just represents the beginning of the total reflection, as given in Eq. (15.27).

Together with Eq. (15.25), the position of the measurement volume on the y -axis is now expressed as a function of the angle φ_a :

$$\frac{r}{R} = \frac{1}{\sqrt{T_a - 1} + \tan \varphi_a} \frac{1}{\cos \varphi_a} = f(\varphi_a) \quad (15.28)$$

According to Figs. 15.7 and 15.8 the angle φ_a begins at $\varphi_a = \alpha_{1a}$, at which the measurement volume is positioned in the pipe centre.

In a similar way, the same function for the laser beam B could be found. As a matter of fact, the subscript a in Eq. (15.28) needs only to be replaced by the subscript b . However, attention should be paid to the fact that both the angle α_{1b} and α_{2b} are negative for the laser beam B. Correspondingly the angle φ_b begins at $\varphi_b = \alpha_{1b}$.

The intersection between laser beam A and the tangent at $x = -R$ is calculated according to Fig. 15.8 as

$$y_a = R \cdot \sin \varphi_a + R(1 - \cos \varphi_a) \tan \alpha_{1a} = f(r) \quad (15.29)$$

Similarly there is for the laser beam B

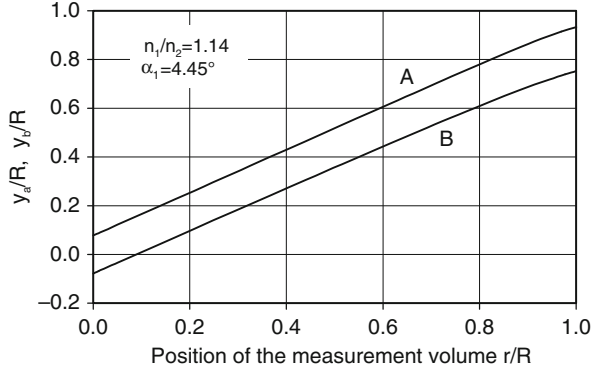
$$y_b = R \cdot \sin \varphi_b + R(1 - \cos \varphi_b) \tan \alpha_{1b} = f(r) \quad (15.30)$$

They are both functions of r because of Eq. (15.28) for the laser beam A and the corresponding equation for the laser beam B. Together with Eqs. (15.20) and (15.21) the necessary movements of the laser beam pair in the medium 1 for a given measurement volume at r can be determined.

15.3.1.2 Simplifications of Calculations

Both functions given in Eqs. (15.29) and (15.30) are not explicit, because according to Eq. (15.28) the polar angle φ_a cannot be expressed to be an explicit function of r/R . For a series of angles φ_a being assumed to be given, however, corresponding y_a/R and r/R can be calculated and related to each other, as these have been shown in Fig. 15.9 as an example. In this figure, the corresponding function for the laser beam B has also been shown. It can be concluded that below $r/R = 0.8$ there exist linear functions of both $y_a = f(r)$ and $y_b = f(r)$. For $r = 0$ there are $y_{a0} = R \tan \alpha_{1a}$ and $y_{b0} = R \tan \alpha_{1b}$ according to Fig. 15.7. To calculate these linear functions, one

Fig. 15.9 Coordinates of intersections between the laser beams (A and B) and the circle tangent at $x = -R$



needs to further calculate the respective gradients at $r = 0$. From Eq. (15.29), for instance, for the laser beam A one obtains

$$\frac{dy_a}{dr} = \frac{dy_a}{d\varphi_a} \frac{d\varphi_a}{dr} = R (\cos \varphi_a + \tan \alpha_{1a} \sin \varphi_a) \frac{d\varphi_a}{dr} \quad (15.31)$$

It is known that at $r = 0$ there is $\varphi_a = \alpha_{1a}$. Furthermore it results from Eq. (15.28) $T_a \rightarrow \infty$ and then from Eq. (15.27) $\sqrt{T_a} \sin(\varphi_a - \alpha_{1a}) = n_2/n_1$. With respect to these conditions it can be calculated from Eq. (15.28)

$$\frac{1}{R} \frac{dr}{d\varphi_a} \Big|_{r=0} = \frac{1}{\cos \alpha_{1a}} \frac{n_1}{n_2} \quad (15.32)$$

Hence it follows from Eq. (15.31) for $r = 0$

$$\frac{dy_a}{dr} = \frac{n_2}{n_1} \quad (15.33)$$

From similar calculations or immediately from Fig. 15.9 the same gradient is obtained for the laser beam B at $r = 0$.

The linear functions of both $y_a = f(r)$ and $y_b = f(r)$ are thus obtained as

$$\frac{y_a}{R} = \tan \alpha_{1a} + \frac{n_2}{n_1} \frac{r}{R} \quad (15.34)$$

$$\frac{y_b}{R} = \tan \alpha_{1b} + \frac{n_2}{n_1} \frac{r}{R} \quad (15.35)$$

To be mentioned again is $\alpha_{1b} < 0$ and thus $\tan \alpha_{1b} < 0$.

15.3.1.3 Necessary Movement Δx_r and Δy_r of Laser Beam Pair

The intersection coordinates shown in Eqs. (15.34) and (15.35) are now used to calculate the necessary movements of the laser beam pair in medium 1, when the measurement volume is shifted from the pipe centre ($r = 0$) to a given radius r on the y -axis. With respect to $\alpha_{1a} = -\alpha_{1b} = \alpha_1$ Eqs. (15.20) and (15.21) are calculated respectively to

$$\frac{\Delta x_r}{R} = 0 \quad (15.36)$$

$$\frac{\Delta y_r}{R} = \frac{n_2}{n_1} \frac{r}{R} \quad (15.37)$$

These beautiful results point out that for measurements along the y -axis the LDA head needs only to be moved in the parallel direction. The ratio between the LDA movement and the shift of the measurement volume is equal to the ratio of respective refractive indices. It deals with a simple way which enables the LDA measurement volume to be easily positioned in the flow. Measurements of radial velocities thus become possible.

15.3.2 Laser Beam Intersection Angle

It is generally the case that the results of velocity measurements must be corrected because of systematic errors arising from the change in the fringe spacing in the measurement volume. Related to this change is, in the first place, the intersection angle between two laser beams refracted in the flow. For this reason Eqs. (15.34) and (15.35) are again considered for further calculations. Combining these two equations with Eqs. (15.29) and (15.30), respectively, yields

$$\sin(\varphi_a - \alpha_{1a}) = \frac{n_2}{n_1} \frac{r}{R} \cos \alpha_{1a} \quad (15.38)$$

$$\sin(\varphi_b - \alpha_{1b}) = \frac{n_2}{n_1} \frac{r}{R} \cos \alpha_{1b} \quad (15.39)$$

Due to $\alpha_{1a} = -\alpha_{1b} = \alpha_1$ the r.h.s. of these two equations are equal to each other, so that it yields from equality of both terms on the l.h.s. of the two equations

$$\varphi_a - \varphi_b = \alpha_{1a} - \alpha_{1b} = 2\alpha_1 \quad (15.40)$$

With regard to Eq. (15.10) that represents the law of refraction Eqs. (15.38) and (15.39) are further written as

$$\sin(\varphi_a - \alpha_{2a}) = \frac{r}{R} \cos \alpha_1 \quad (15.41)$$

$$\sin(\varphi_b - \alpha_{2b}) = \frac{r}{R} \cos \alpha_1 \quad (15.42)$$

These two equations straightforwardly indicate

$$\varphi_a - \varphi_b = \alpha_{2a} - \alpha_{2b} \quad (15.43)$$

Because of Eq. (15.40) there is then

$$\alpha_{2a} - \alpha_{2b} = 2\alpha_1 \quad (15.44)$$

That is to say

$$\alpha_2 = \alpha_1 \quad (15.45)$$

This beautiful result indicates that the beam intersection angle remains constant and is the same as that in the medium 1 (pipe wall). This angle will be used to correct the measurement results which involve systematic errors.

15.3.3 Fringe Spacing and Velocity Corrections

In using the laser beam intersection angle in the fluid, the fringe spacing in the measurement volume is calculated to be:

$$\Delta x = \frac{\lambda_2}{2 \sin \alpha_2} \quad (15.46)$$

Due to $\alpha_2 = \alpha_1$ and $\lambda_1/\lambda_2 = n_2/n_1$ this equation is rewritten as

$$\Delta x = \frac{n_1}{n_2} \frac{\lambda_1}{2 \sin \alpha_1} = \frac{n_1}{n_2} \Delta x_0 \quad (15.47)$$

Herein Δx_0 represents the initial fringe spacing in the LDA optics i.e. the reference fringe spacing, when the measurement volume is found in the open air or in the pipe wall.

Equation (15.47) points out that the measured velocities must be corrected by a factor equal to $k_{\text{vel}} = n_1/n_2$:

$$u_\tau = \frac{n_1}{n_2} u_{\text{measured}} \quad (15.48)$$

It must be mentioned, however, that the measured velocity corresponds to the velocity component that is perpendicular to the bisector of two laser beams (Fig. 15.7). It should not be considered to be the radial velocity component.

15.3.4 Orientation of the Measurement Volume

The orientation of the measurement volume i.e. the bisector of two refracted laser beams determines the measured velocity component that generally differs from the radial velocity. The deviation angle τ of the bisector, as shown in Fig. 15.7, is considered positive and given by

$$\tau = \alpha_2 - \alpha_{2a} = \alpha_1 - \alpha_{2a} \tag{15.49}$$

For α_{2a} see Fig. 15.8.

In order to express the deviation angle of the measurement volume as a function of the radial position r of the measurement volume, Eqs. (15.38) and (15.41) are taken into account, respectively, so that

$$\tau = (\varphi_a - \alpha_{2a}) - (\varphi_a - \alpha_1) = \arcsin\left(\frac{r}{R} \cos \alpha_1\right) - \arcsin\left(\frac{n_2}{n_1} \frac{r}{R} \cos \alpha_1\right) \tag{15.50}$$

Clearly both the optical layout (α_1) and the medium properties (n_2/n_1) additionally influence the deviation angle of the measurement volume. Figure 15.10 for example shows the calculated deviation angle of the measurement volume in the function of the radial position r/R for a given optical configuration. For the measurement volume that is positioned within $r/R = 0.8$, the corresponding deviation angle slowly increases up to 10° .

The optical axis and its refraction should now be considered. In reality, the situation of the optical axis in the present case is equal to the situation that was shown in Fig. 15.3 concerning the measurement of the axial velocity component. The inclination angle of the refracted optical axis in the flow against the x -axis is thus

$$\tau_o = \varepsilon_{o2} - \varphi_o \tag{15.51}$$

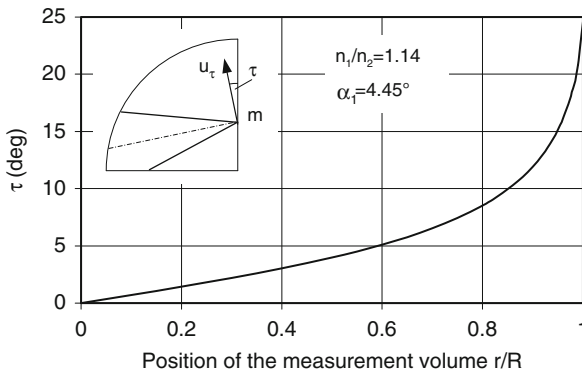


Fig. 15.10 Deviation angle of the bisector of the two refracted laser beams in the fluid

For the angle φ_o it applies that $\sin \varphi_o = \Delta y_r/R$. Because of Eq. (15.37) this is further written as

$$\sin \varphi_o = \frac{n_2}{n_1} \frac{r}{R} \quad (15.52)$$

The refraction angle of the optical axis in the present case is obtained directly from Eq. (15.5) as given by

$$\sin \varepsilon_{o2} = \frac{n_1}{n_2} \frac{\Delta y_r}{R} = \frac{r}{R} \quad (15.53)$$

Herein Δy_r , as the displacement of the optical axis from the x -axis, is applied according to Fig. 15.8 and Eq. (15.37).

Equation (15.51) then becomes

$$\tau_o = \arcsin\left(\frac{r}{R}\right) - \arcsin\left(\frac{n_2}{n_1} \frac{r}{R}\right) \quad (15.54)$$

This equation represents an approximation of Eq. (15.50) by assuming $\cos \alpha_1 \approx 1$ for small laser beam intersection angles. The difference between Eqs. (15.50) and (15.54) is less than 0.4% for the case considered in Fig. 15.10 for $r/R < 0.5$. Because of this Eq. (15.54) can be applied to specify the deviation angle of the measurement volume in the flow.

15.3.5 Determination of Radial Velocities

Because of $\tau \neq 0$, the measured velocity u_τ does not directly represent the radial velocity component. In principle, the radial velocity component can be obtained if the tangential velocity at the given measurement point on the y -axis is known. By assuming that the positive tangential velocity agrees with the x -direction, the radial velocity component can be resolved according to Fig. 15.7 from

$$u_\tau = u_r \cos \tau - u_t \sin \tau \quad (15.55)$$

For measurements of tangential velocities, refer to Sect. 15.2.

15.3.6 Remarks on the Method

The entire treatments shown above are based on the linearization according to Eqs. (15.34) and (15.35) for $r/R < 0.8$. This is in any case available because measurements beyond $r/R = 0.5$ rapidly become impossible, just as a result of the optical aberrations (e.g. astigmatism) and the growth of the beam thickness. The latter straightforwardly leads to the drop of laser light intensity in the measurement

volume (total reflection occurs at $T = 1$). Calculations have shown that within $r/R = 0$ to $r/R = 0.5$ the maximum error in u_τ arising from the linearization is less than 1% (at $r/R = 0.5$). In most engineering flows, this error is well acceptable. The error in the deviation angle τ of the measurement volume, if Eq. (15.54) is applied, is less than 0.4%.

The optical aberration is related to the off-axis positioning of the measurement volume by r/R and can be represented, according to Eq. (15.52), by the off-axis angle φ_o of the optical axis. At large values of r/R , the off-axis angle becomes large. The entire optical properties then are comparable with those related with the off-axis LDA alignment to a plane wall, as thoroughly treated in Chap. 14. In the example of $n_1/n_2 = 1.14$ and $r/R = 0.6$ there is $\varphi_o = 32^\circ$. This off-axis angle is associated with huge astigmatism effects, so that the effective aperture of the receiving lens and consequently the signal rate would be radically reduced, for reference see Fig. 14.9 as well as Fig. 14.18. Another serious problem at the large off-axis angle is the increased probability that due to a small inaccuracy in the optical layout both laser beams after refractions could no longer intersect at all. For this reason, it could be concluded that at positions of the measurement volume beyond $r/R = 0.5$, measurements would become impossible. This optical behaviour, in fact, also applies to the case for measurements of axial velocities with a deviation limit at $e/R < 0.5$, as already discussed in Sect. 15.1.

15.4 Optical Aberrations and Measurement Volume Distortion

Generally the optical condition of measurements continuously deteriorates as the depth of the measurement volume in the test fluid increases, for instance in measurements of both axial and tangential velocity distributions. From experience, as mentioned at the beginning of this chapter, flow measurements can be achieved at the most up to a depth of about $2/3$ of the pipe diameter. The worsening of the optical condition, while positioning the measurement volume in the upper depth, is related to the increased optical aberration and the enlarged dislocation of laser beam waists. In measurements of radial velocities, the worsening of signal qualities becomes more and more significant with the shift of the measurement volume away from the pipe centre. This phenomenon as related to the optical aberration has already been discussed at the end of the last section.

The optical aberration and the beam waist dislocation will be quantified in the following sections. In particular, the analysis should comprehensibly reveal why the measurements of axial and tangential velocities will become impossible if the measurement volume is located in the pipe at a distance beyond $2/3$ of the pipe diameter. To be mentioned is that analyses that will be made below are rather complex. They should mainly serve as the references and fundamentals for further extended investigations. For most LDA users it would be sufficient to correctly make measurements and afterwards to properly correct measurement results. They are therefore mostly referred to foregoing sections. In the case where the measurements do not run or

both signal strengths and qualities are not satisfactory, the LDA users should know the reason that is often ascribed to the optical aberrations i.e. to the existence of astigmatism.

15.4.1 Optical Aberrations in Transmitting and Receiving Optics

The significance of using the plane cut-off on the outside of a circular pipe and aligning the LDA head perpendicular to this plane is to ensure laser beams in the pipe wall to be free of any optical aberrations. This is confirmed in that all four laser beams of a two-component LDA system intersect at an actual or a virtual unique point. The optical aberration then originates only at the internal surface of the circular pipe, leading to separations of two measurement volumes. In the case where the LDA optical axis goes through the pipe centre, these two measurement volumes correspond to those for measurements of axial and tangential velocities. To describe the optical aberration associated with the non-regular laser beam refractions on the curved pipe surface, the displacement between two measurement volumes for axial and tangential velocities, for the given LDA head position, can be applied. This is indeed the common case of using such a displacement as the astigmatic difference to represent the extent of the present optical aberration i.e. astigmatism, see [Chap. 14](#).

The displacement between the two measurement volumes can be easily obtained from the calculation results that have already been obtained in Sects. [15.1](#) and [15.2](#). In using Eqs. (15.1) and (15.12), the displacement between two measurement volumes is obtained in function of the position of the virtual beam crossing point as

$$\Delta s_R = \frac{s_{2,t} - s_{2,a}}{R} = \frac{1}{1 + \frac{n_1}{n_2} \left(\frac{R}{s_1} - 1 \right)} - \frac{n_2 s_1}{n_1 R} \quad (15.56)$$

This distance can also be shown in the function of the measurement volume position for tangent velocity component. The first term on the r.h.s. of the above equation is simply $s_{2,t}/R$. The second term with s_1/R should be replaced by respective value from Eq. (15.12), so that

$$\Delta s_R = \frac{s_{2,t}}{R} - \frac{1}{\left(\frac{R}{s_{2,t}} - 1 \right) + \frac{n_1}{n_2}} \quad (15.57)$$

Figure [15.11](#) shows the calculated displacements between two measurement volumes in function of the position of the measurement volume for tangential velocity component. As can be seen, both measurement volumes get separated from each other, as the depth of the measurement volume in the flow increases. In other words, the optical aberration related to the LDA optics increases with the distance of the measurement volume from the pipe wall. This phenomenon significantly influences

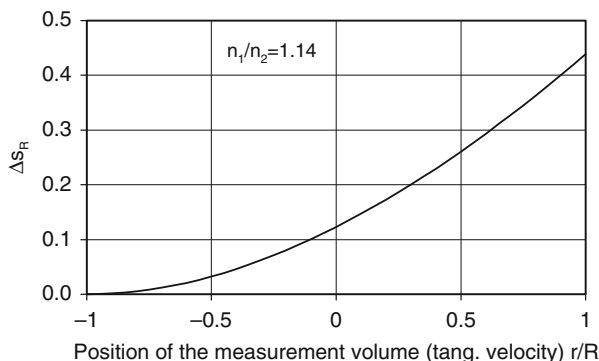


Fig. 15.11 Relative displacement between the tangential and the axial measurement volumes in function of the position of the measurement volume for the tangential velocity component

the measurements of both the axial and the tangential velocities. The influence mechanism is again found in the receiving optics.

Like in the case of astigmatism associated with the off-axis LDA against a plane medium interface (Chap. 14), the optical aberration in the current case implies that the larger the depth of the measurement volume in the flow, the fewer are the effective elementary segments on the receiving lens, that can see the measurement volume. Because the majority of elementary segments on the receiving lens behave as blind to the measurement volume, the signal strength diminishes and consequently the signal rate in data acquisition decreases. For this reason it is almost impossible to get optical signals of sufficiently high strengths and qualities in the flow area of a depth beyond $2/3$ of the pipe diameter. Because of this the entire flow distribution through the pipe section could only be achieved, if an additional measurement is completed from the opposite side by rotating the LDA head for 180° around the pipe axis. This two-measurement feature applies to measurements of both the axial and tangential velocities. It provides, however, just an opportunity for utilizing the so-called Dual Measurement Method (DMM) with which the distribution of the very weak tangential velocity component can be exactly resolved from two measurements (see Chap. 9).

15.4.2 Dislocation of Laser Beam Waists from the Measurement Volume

Another undesirable outcome of the optical aberration related to measurements of tangential and radial velocities in a circular pipe is the dislocation i.e. the separation of laser beam waists from the measurement volume. This feature leads, on one hand, to the well-known fringe distortion in the measurement volume and, on the other hand, to the decrease of laser light intensity in the measurement volume and successively to the reduction of signal qualities. This type of signal disturbances

additionally contributes to a reduction of signal qualities on account of the optical aberration just treated before.

To quantify the beam waist dislocation, the laser beams in the medium 1 prior to the test fluid are considered as focused light bundle and thus to be free of any optical aberration. Both cases of respectively measuring the tangential and the radial velocity components are separately considered.

15.4.2.1 Laser Beam Waists in Measuring the Tangential Velocities

With regard to the symmetrical refraction of two laser beams, only one laser beam is considered which is found in the $x - y$ plane (Fig. 15.12). Associated with the laser beam refraction on the internal surface of the pipe, the laser beam suffers from astigmatism effect. As a result there exist two particular focal points that are confirmed in the meridian and sagittal planes of the laser beam and denoted by p_m and p_s , respectively. The distance between these two focal points is called astigmatic difference. It is a measure of the extent of the associated optical aberration. To calculate the respective locations of these two focal points and to directly apply the analysis results in Sect. 14.6, a new coordinate ξ will be inserted that begins at the beam intersection point c and runs along the normal of the circular pipe i.e. goes through the pipe axis. The laser beam considered is represented here by the unit vector \vec{r} . Its corresponding ξ -coordinates prior to and after the refraction are represented by $r_{1\xi} = \cos \varepsilon_1$ and $r_{2\xi} = \cos \varepsilon_2$, respectively.

Because the laser beam is thin, the intersection area on the cylindrical surface is assumed as the plane surface. This assumption contributes to the simplification of beam refraction calculations. The respective meridian and sagittal focal points of the refracted laser beam in the test fluid have their ξ -coordinates which, according to Eqs. (14.41) and (14.42) for the plane interface, are given by

$$\xi_m = \xi_0 \frac{n_2}{n_1} \frac{r_{2\xi}^3}{r_{1\xi}^3} \tag{15.58}$$

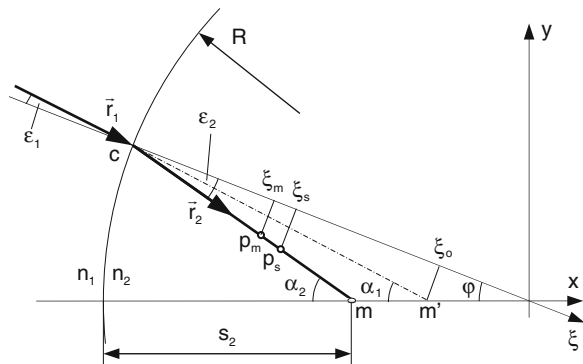


Fig. 15.12 Calculations of the laser beam waists and the measurement volume

and

$$\xi_s = \xi_o \frac{n_2 r_{2\xi}}{n_1 r_{1\xi}} \quad (15.59)$$

Herein ξ_o denotes the ξ -coordinate of the virtual focal point m' , as given by

$$\xi_o = cm' \cdot \cos \varepsilon_1 = \frac{R \sin \varphi}{\sin \alpha_1} r_{1\xi} \quad (15.60)$$

In the case of water flow in the circular pipe, it can be verified that $(r_{1\xi} - r_{2\xi})/r_{1\xi} < 0.1\%$ is nearly always satisfied, so that $r_{2\xi} \approx r_{1\xi}$ can be assumed. This shows that there is no need to differ from the meridian and sagittal focal points and the refracted laser beam can still be considered as a focused light bundle with a unique beam waist. For the sake of getting the simple form of the results, however, Eq. (15.59) is applied to represent the ξ -coordinate of the approximated unique laser beam waist:

$$\xi_w = \xi_s = \xi_o \frac{n_2 r_{2\xi}}{n_1 r_{1\xi}} \quad (15.61)$$

On the refracted laser beam in the test fluid, this beam waist lies at a distance from the intersection point c :

$$\ell_w = \xi_w / \cos \varepsilon_2 = \xi_w / r_{2\xi} \quad (15.62)$$

Because of the symmetrical refraction at two laser beams the measurement volume lies on the x -axis at m and has a distance from the intersection point c :

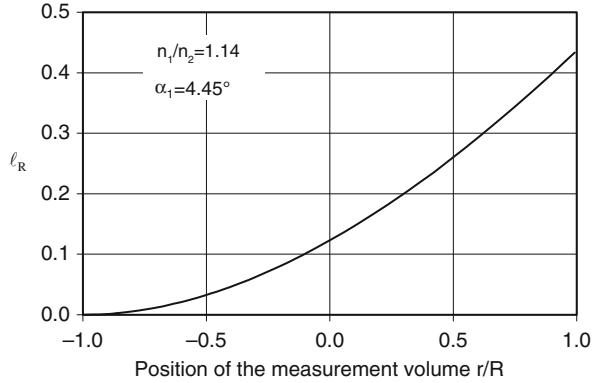
$$\ell_{mv} = \frac{R \sin \varphi}{\sin \alpha_2} \quad (15.63)$$

The distance between the measurement volume and the waist of the laser beam is then given by $\ell_{mv} - \ell_w$ or in dimensionless form by

$$\ell_R = \frac{\ell_{mv} - \ell_w}{R} = \frac{\sin \varphi}{\sin \alpha_2} - \frac{n_2}{n_1} \frac{\sin \varphi}{\sin \alpha_1} \quad (15.64)$$

Clearly this distance depends on the local position of the measurement volume in the flow. Both the angle φ and α_2 in function of the position s_2 of the measurement volume can be obtained by Eq. (15.11). Figure 15.13 shows a calculation example, in which the position parameter s_2 is replaced by the radial position $r = R - s_2$. Evidently, there exists a largely extended dislocation of the beam waist from the measurement volume, when the measurement volume is located beyond the pipe centre. Such a dislocation of the beam waist doubtless implies the low brightness of the measurement volume and the undesirable fringe distortion in it. These two features related to the measurement volume on the side of LDA transmitting optics

Fig. 15.13 Relative dislocation of the laser beam waists from the measurement volume at the measurements of the tangential velocity component



again signify that the measurement of tangential velocity components is more critical than that of axial velocities. In addition, it can be concluded from the values shown in Fig. 15.13 in dimensionless form that the absolute beam waist dislocation ($\ell_{mv} - \ell_w$) will be bigger, if circular pipes of large diameter are encountered in use. On the pipe axis for instance, the distance between the beam waist and the measurement volume is about $0.12R$, which will be 12 mm when $R = 100$ mm.

In comparing Fig. 15.13 with Fig. 15.11, it is evident that two curves are rather identical. This identity can be confirmed by applying the approximation for paraxial rays as in the form of $\sin \varphi \approx \varphi$, $\sin \alpha_1 \approx \alpha_1$ and $\sin \alpha_2 \approx \alpha_2$. Equation (15.64) can then be conducted to a form equal to Eq. (15.57).

The fringe distortion in the measurement volume in the current case is caused by the dislocation of beam waists in two symmetrical laser beams. It exactly represents the well-known type of fringe distortions at which the measurement volume is found prior to or after their respective waists located at equal distance from the beam intersection point. The optical occurrence in the present case is illustrated in Fig. 15.14. The fringe spacing in the measurement volume then linearly varies along the measurement volume. Corresponding errors involved in measurements of both the mean velocity and the flow turbulence have already been exactly analyzed by Zhang and Eisele (1997, 1998c). The apparent i.e. the affected mean velocity and its standard deviation are given as

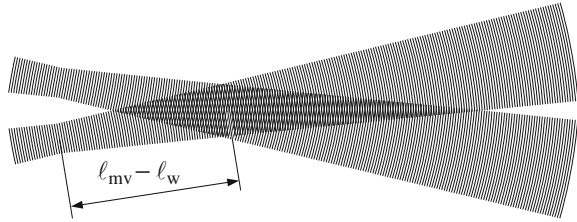
$$\frac{\bar{u}_{app}}{\bar{u}} = 1 + \frac{1}{3}\gamma^2 \quad (15.65)$$

$$\frac{\sigma_{app}^2 - \sigma^2}{\bar{u}^2} = \gamma^2 \left(\frac{\sigma^2}{\bar{u}^2} + \frac{1}{3} \right) \quad (15.66)$$

The exact derivation of these two equations will be presented in Chap. 16.

In these two equations, the fringe distortion number γ is a geometrical parameter that represents the relative change in the fringe spacing at the end of the measurement volume to the initial fringe spacing and is usually below 0.02. Because it deals

Fig. 15.14 Existence of the first type of the fringe distortion in the measurement volume at the measurement of the tangential velocity component in the circular pipe



with a quite small number, the fringe distortion in the LDA measurement volume usually does not appreciably influence the measurement accuracies.

15.4.2.2 Laser Beam Waists in Measuring the Radial Velocities

In Sect. 15.3, it has been indicated that for measurements of radial velocity components the measurement volume should be located on the y -axis, as shown in Fig. 15.7. It has also been indicated, relying on Eq. (15.36), that for shifting the measurement volume along the y -axis the laser beam pair in the medium 1 needs only to be shifted in the parallel direction. This implies that the virtual beam crossing point has also to lie on the y -axis, as it is so when the measurement volume is positioned at the pipe centre ($y = 0$). Corresponding locations of both the actual and virtual measurement volumes have been shown in Fig. 15.15, in which for simplicity only one laser beam has been illustrated. To be expected is that the dislocation of laser beam waists from the measurement volume also exists in this case. For calculations the laser beam is again represented by the unit vector \vec{r}_1 in the medium 1 and \vec{r}_2 in the medium 2.

Like in the above calculations, a new coordinate ξ will be inserted which begins at the beam intersection point c and runs along the normal of the circular pipe. Both unit vectors then have their components $r_{1\xi} = \cos \varepsilon_1$ and $r_{2\xi} = \cos \varepsilon_2$, respectively.

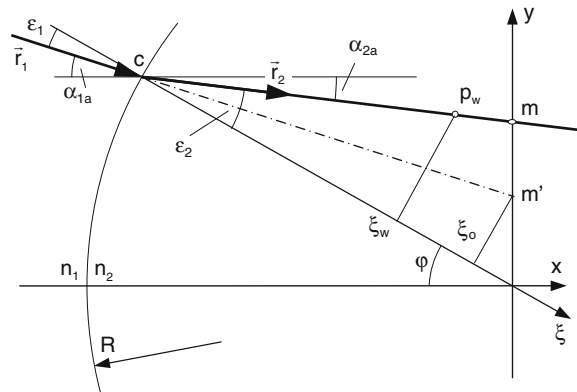


Fig. 15.15 Calculations of the laser beam waist (p_w) and the measurement volume (m)

For simplicity only the sagittal focal point of the refracted laser beam in the test fluid is considered as the beam waist p_w . Similarly there is

$$\xi_w = \xi_o \frac{n_2 r_{2\xi}}{n_1 r_{1\xi}} \quad (15.67)$$

with

$$\xi_o = cm' \cos \varepsilon_1 = \frac{R \cos \varphi}{\cos \alpha_{1a}} r_{1\xi} \quad (15.68)$$

On the refracted laser beam in the test fluid, the beam waist lies at p_w with a distance from the intersection point c

$$\ell_w = \frac{\xi_w}{\cos \varepsilon_2} = \frac{\xi_w}{r_{2\xi}} \quad (15.69)$$

The measurement volume m has a distance from the same intersection point c

$$\ell_{mv} = \frac{R \cos \varphi}{\cos \alpha_{2a}} \quad (15.70)$$

The distance between the measurement volume (m) and the laser beam waist (p_w) is then given by $\ell_{mv} - \ell_w$. In dimensionless form and with subscripts a and b for laser beam A and B, respectively, there are

$$\ell_{R,a} = \frac{\cos \varphi_a}{\cos \alpha_{2a}} - \frac{n_2 \cos \varphi_a}{n_1 \cos \alpha_{1a}} \quad (15.71)$$

$$\ell_{R,b} = \frac{\cos \varphi_b}{\cos \alpha_{2b}} - \frac{n_2 \cos \varphi_b}{n_1 \cos \alpha_{1b}} \quad (15.72)$$

Clearly both of these distances depend on the local position r/R of the measurement volume in the flow. Angles φ_a , φ_b , α_{2a} and α_{2b} and their dependences on r/R

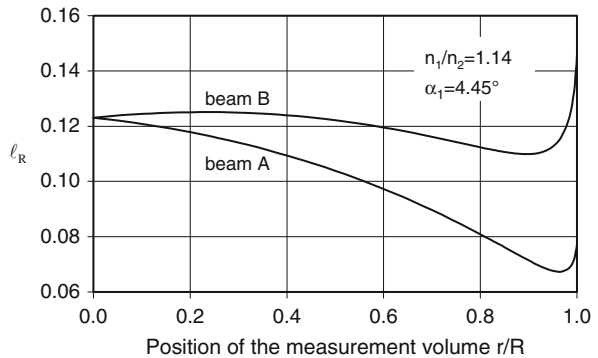


Fig. 15.16 Relative dislocation of the laser beam waists from the measurement volume at the measurement of the radial velocity component

have already been found to be given by Eqs. (15.38), (15.39), (15.40), (15.41), and (15.42).

Figure 15.16 shows the results calculated from Eqs. (15.71) and (15.72) for laser beam A and B, respectively. Because in the available area of $r/R < 0.6$ both beam waists are on the same side of the measurement volume and show no large differences in the distance to the measurement volume, it can be assumed that the fringe distortion in the manner according to Fig. 15.14 occurs. Like in the case of beam waist dislocation at measurements of tangential velocity components, the beam waist dislocation ($\ell_{mv} - \ell_w$) in the current case of measuring the radial velocities will also be large, if circular pipes of large diameter are encountered to use. On the pipe axis same values are obtained as in Fig. 15.13.

Chapter 16

Fringe Distortion Effects

From the LDA principle described in [Chap. 3](#), the necessary condition for accurate LDA measurements is the uniformity of the fringe spacing in the measurement volume. The uniform fringe spacing can be achieved if the measurement volume that is formed by two laser beams coincides with two beam waists. Each deviation from this requirement will lead to fringe distortion in the measurement volume and hence to measurement errors. Because of the non-uniformity of the fringe spacing along the measurement volume a uniform constant laminar flow for instance will then be measured as a flow with velocity fluctuations. Measurements of both the mean velocity and the turbulence quantities thus suffer from systematic errors.

Fringe distortions in LDA measurement volumes have been historically considered as the consequence of improper optical layout. Two most well-known forms of the optical layout causing the fringe distortion have been shown in [Fig. 16.1](#). The visible non-uniformity of the fringe spacing in these two cases is either along or across the measurement volume. Corresponding detailed investigations to characterize the non-uniformity of two such different fringe patterns have been performed for instance by [Hanson \(1973, 1975\)](#), [Durst and Stevenson \(1975\)](#) and [Miles and Witze \(1994, 1996\)](#). According to [Hanson \(1973, 1975\)](#) linear distributions of the fringe spacing exist in both longitudinally ([Fig. 16.1a](#)) and laterally ([Fig. 16.1b](#)) distorted measurement volumes. The influence of the fringe distortion on the measurement accuracy has been investigated by [Zhang and Eisele \(1997, 1998c\)](#) with respect to the longitudinal fringe distortion. As it has already been shown in [Fig. 15.14](#), the first type of the fringe distortion in the measurement volume is confirmed as exactly taking place, when the tangential velocity of the flow in a circular pipe is measured without matching the refractive index of the fluid. It is obviously the most representative fringe distortion encountered in the practical applications. The second type of fringe distortion across the measurement volume ([Fig. 16.1b](#)), however, is still considered as merely a matter of the improper optical layout.

Another type or the third type of possible fringe distortions in the LDA measurement volume, as shown in [Fig. 14.14b](#) for a special case, is related to the astigmatism due to the laser beam refractions. Because of the irregular distribution of the beam waists around the LDA measurement volume and hence the complexity of the form of respective wave front of two laser beams, this type of fringe distortion may not yet

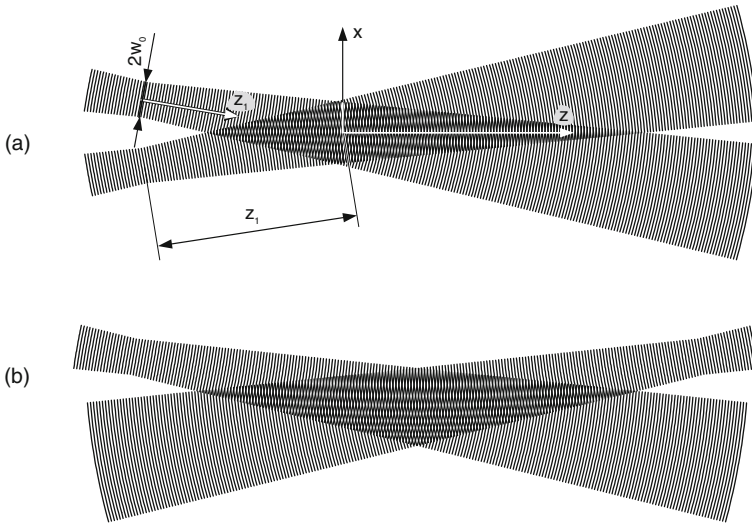


Fig. 16.1 Fringe distortions (first and second types) in the measurement volume; The third type of the possible fringe distortion is referred to [Fig. 14.14b](#)

be well characterized. A further type of fringe distortions in the measurement volume is known as the local fringe distortion which is caused by laser light diffraction through particles in the transmission path of the laser beams (Ruck 1991).

The outcome of the fringe distortion in the LDA measurement volume is the systematic measurement error in both the mean velocity and the turbulence quantities. In all cases of measuring the flow turbulence, the fringe distortion results in the broadening of the Doppler frequency and hence the overestimation of the turbulence intensity. This overestimation obviously depends on both the form and the scale of the complex fringe distortion. As an LDA user one is indeed interested in knowing the extent of respective measurement errors and the possibility of correcting them. For this purpose, the influence of the most representative fringe distortion in form of [Fig. 16.1a](#) on the flow measurement is considered here, in order to give a reference as well as to make a criterion for error estimations. The analysis assumes the linear distribution of the fringe spacing along the measurement volume length.

16.1 Linear Longitudinal Distribution of the Fringe Spacing

According to [Fig. 16.1a](#) the crossing of two Gaussian beams takes place after their respective waists located at equal distance from the beam intersection point. The same fringe distortion with the same consequence in LDA flow measurements will be given when the beam crossing is found prior to both beam waists. The assumption of linear distribution of the fringe spacing in the LDA measurement volume is

based on earlier investigations of this type of fringe distortion and contributes to the simplification of calculations.

The uniform velocity distribution within the measurement volume length is assumed. From its measurement by $u = \Delta x \cdot \nu_D$ with non-uniform fringe spacing, one obtains the related non-uniform Doppler frequency as

$$\frac{1}{\nu_D} \frac{d(\nu_D)}{dz} = - \frac{1}{\Delta x} \frac{d(\Delta x)}{dz} \quad (16.1)$$

According to Hanson (1973, 1975) from accounting for the relative shift in Doppler frequency, the fringe spacing gradient is expressed as

$$\frac{1}{\Delta x} \frac{d(\Delta x)}{dz} = \frac{1}{R} \quad (16.2)$$

Herein R is the radius of curvature of two Gaussian beam wave fronts at the beam crossing point. It is calculated, according to Eq. (3.63), with the spot size (radius w_0) at the beam waist and the distance (z_1) of the beam waist from the beam crossing point as follows

$$R = z_1 \left[1 + \left(\frac{\pi w_0^2}{\lambda z_1} \right)^2 \right] = z_1 \left[1 + \left(\frac{z_R}{z_1} \right)^2 \right] \quad (16.3)$$

In this equation, z_R represents the Rayleigh length, as given in Eq. (3.66).

From Eq. (16.2) it can be shown that, by assuming $|z/R| \ll 1$ within the region of the measurement volume, the longitudinal fringe spacing varies linearly over the length of the measurement volume. That is with $k = \Delta x_0/R$

$$\Delta x = kz + \Delta x_0 \quad (16.4)$$

In this equation, Δx_0 is the fringe spacing at the centre of the measurement volume ($z = 0$). According to Hanson (1973), this value of fringe spacing is equal to that in the undistorted measurement volume ($\lambda/2 \sin \alpha$).

16.2 Fringe Distortion Number and the Apparent Mean Velocity

It should be mentioned that the fringe distortion in the measurement volume also influences the measurement of mean velocities. Indeed, the error in the mean velocity will not disappear, even if linear fringe distortion according to Eq. (16.4) takes place. This can be easily demonstrated by assuming the uniform flow of velocity u_0 through the measurement volume. From the measured Doppler frequency and the specified constant fringe spacing in the software, the flow velocity is calculated as follows:

$$u = \Delta x_0 v_D = \Delta x_0 \frac{u_0}{\Delta x} \quad (16.5)$$

It is inversely related to the fringe spacing which linearly changes along the measurement volume. For this reason the ensemble average of velocities u from measurements is in no cases equal to the actual flow velocity u_0 and is therefore denoted as the apparent mean. For the general case a turbulent flow with random velocity fluctuations is considered to have a mean velocity equal to \bar{u} . The apparent mean velocity is calculated by the arithmetic average as

$$\bar{u}_{\text{app}} = \Delta x_0 \frac{1}{N} \sum_{i=1}^N \frac{u_i}{\Delta x_i} \quad (16.6)$$

On the side of the measurement volume, the measurement volume will longitudinally be divided into m partial volumes of equal distance. In each partial volume, the fringe spacing can be considered to be constant. On the side of the flow, the same and constant statistical flow properties are assumed to exist among all partial volumes. This also includes the assumption that particles have equal probability in passing through every partial volume. With respect to $N = m \cdot n$ and the mean velocity equal to \bar{u} Eq. (16.6) is then written as

$$\bar{u}_{\text{app}} = \Delta x_0 \frac{1}{N} \sum_{j=1}^m \left(\frac{1}{\Delta x_j} \sum_{i=1}^n u_i \right) = \Delta x_0 \bar{u} \frac{1}{m} \sum_{j=1}^m \frac{1}{\Delta x_j} \quad (16.7)$$

By extending m to infinity and with substitution of Δx_j by Eq. (16.4) the summation in the above equation can be presented by the corresponding integral calculation, so that with $\Delta z/2$ as the half length of the measurement volume

$$\bar{u}_{\text{app}} = \bar{u} \frac{\Delta x_0}{\Delta z} \int_{-\Delta z/2}^{\Delta z/2} \frac{dz}{kz + \Delta x_0} \quad (16.8)$$

To simplify the calculation results, the fringe distortion number is introduced as defined by

$$\gamma = \frac{k \Delta z/2}{\Delta x_0} = \frac{\Delta z/2}{R} \quad (16.9)$$

It represents the relative change of the fringe spacing at the end of the measurement volume. Usually it is a small value because of $\Delta z \ll R$.

Equation (16.8) is then calculated as

$$\frac{\bar{u}_{\text{app}}}{\bar{u}} = \frac{1}{2\gamma} \ln \frac{1+\gamma}{1-\gamma} \approx 1 + \frac{1}{3}\gamma^2 \quad (16.10)$$

Herein the approximation has been made because of $\gamma \ll 1$.

This calculation result demonstrates that the measurement of the mean flow velocity will also be affected by the fringe distortion in the measurement volume, even though the linear fringe spacing distribution is assumed. The relative error, however, is mostly negligible because of $\gamma \ll 1$.

The fringe distortion number has been defined in Eq. (16.9) as a pure function of geometric parameters of the measurement volume. Since it specifies the relative change in the fringe spacing at the end of the measurement volume ($z = \Delta z/2$) against that at the measurement volume centre ($z = 0$), it also represents the frequency broadening $\Delta\nu_D/\nu_D$ at $z = \Delta z/2$.

According to Eq. (16.9) the fringe distortion number has also been shown to be a function of the radius of wave front curvature of two Gaussian beams at the beam crossing point. Substituting this curvature radius by Eq. (16.3) then yields

$$\gamma = \frac{\Delta z/2}{z_1 [1 + (z_R/z_1)^2]} \tag{16.11}$$

For laser beams with given beam waist thickness $2w_0$ and hence given Raleigh length z_R the fringe distortion number has been shown as the function of the distance z_1 between the beam waist and the measurement volume centre. This functionality is illustrated in Fig. 16.2 for a given LDA optical set-up. The radius of the curvature of the Gaussian beam wave front has also been shown in function of the distance. At the Rayleigh length which is equal to $z_R = 30$ mm in this example, the fringe distortion number reaches its maximum.

Based on parameter quantifications in this example the fringe distortion number has been confirmed to be in the range of usually not exceeding 0.02. In applying this limit to Eq. (16.10), the error in the mean velocity is practically very small. By the way, the minimum radius of the curvature of the Gaussian beam wave front reads $R = 60$ mm. Compared with this value, the half length of the measurement volume ($\Delta z/2 = 1$ mm) is negligible. The assumption of $|z/R| \ll 1$ that leads to Eq. (16.4) is thus validated.

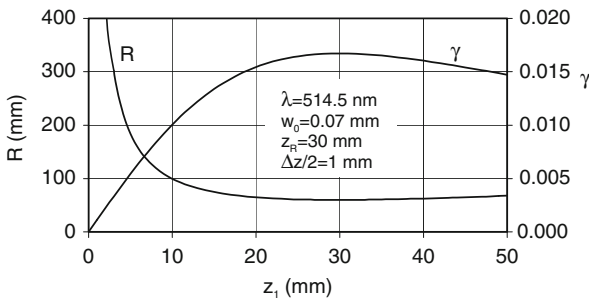


Fig. 16.2 Radius of the curvature of the Gaussian beam wave front and the fringe distortion number

16.3 Overestimation of the Flow Turbulence

As is well-known, the most significant outcome of the fringe distortion in LDA measurements is the Overestimation of the turbulence intensity. This is also called the broadening effect in turbulence measurements. In order to quantify this effect, a stationary turbulent flow is considered which is specified by a mean velocity \bar{u} and a fluctuation velocity σ (standard deviation). From the viewpoint of statistics, the connection between the mean velocity and the standard deviation is given, according to Eq. (5.5), as

$$\sigma^2 = \overline{u^2} - \bar{u}^2 \quad (16.12)$$

with $\overline{u^2}$ as the mean square of velocity component u .

This relationship also applies in the case of velocity data from measurements undergoing the effect of fringe distortion in the measurement volume. Corresponding velocities are thus apparent, as given by

$$\sigma_{\text{app}}^2 = \overline{u_{\text{app}}^2} - \bar{u}_{\text{app}}^2 \quad (16.13)$$

The overestimation of the turbulence intensity and the related quantities as a result of the fringe distortion in the measurement volume is then determined by

$$\sigma_{\text{app}}^2 - \sigma^2 = \left(\overline{u_{\text{app}}^2} - \bar{u}^2 \right) - \left(\bar{u}_{\text{app}}^2 - \bar{u}^2 \right) \quad (16.14)$$

While the second term on the r.h.s. of this equation can be calculated by using Eq. (16.10) or simply set to zero, the first term requires similar calculations as those in Sect. 16.2. In response to each velocity event the Doppler frequency is again $u_i/\Delta x_i$. The apparent mean square of velocities in the above equation is basically calculated, in analogy to Eq. (16.6), by

$$\overline{u_{\text{app}}^2} = (\Delta x_0)^2 \frac{1}{N} \sum_{i=1}^N \left(\frac{u_i}{\Delta x_i} \right)^2 \quad (16.15)$$

By dividing the measurement volume into m partial volumes of equal distance and based on same assumptions that led to Eq. (16.7), the above equation is converted into

$$\overline{u_{\text{app}}^2} = (\Delta x_0)^2 \bar{u}^2 \frac{1}{m} \sum_{j=1}^m \frac{1}{(\Delta x_j)^2} \quad (16.16)$$

The linear fringe spacing distribution according Eq. (16.4) is applied. By extending m to infinity, the summation in the above equation can be presented by the corresponding integral calculation, so that

$$\overline{u_{\text{app}}^2} = (\Delta x_0)^2 \overline{u^2} \frac{1}{\Delta z} \int_{-\Delta z/2}^{\Delta z/2} \frac{dz}{(kz + \Delta x_0)^2} \quad (16.17)$$

In using the fringe distortion number as defined by Eq. (16.9), one obtains

$$\overline{u_{\text{app}}^2} = \frac{1}{1 - \gamma^2} \overline{u^2} \approx (1 + \gamma^2) \overline{u^2} \quad (16.18)$$

Substitution of Eqs. (16.10) and (16.18) in Eq. (16.14) and with respect to $\overline{u^2} = \sigma^2 + \bar{u}^2$ yields

$$\frac{\sigma_{\text{app}}^2 - \sigma^2}{\bar{u}^2} = \gamma^2 \left(\frac{\sigma^2}{\bar{u}^2} + \frac{1}{3} \right) \quad (16.19)$$

Because of $\sigma_{\text{app}} + \sigma \approx 2\sigma$ (not for $\sigma = 0$) this equation can also be written as

$$\frac{\Delta\sigma}{\bar{u}} = \frac{1}{2} \gamma^2 \frac{\bar{u}}{\sigma} \left(\frac{\sigma^2}{\bar{u}^2} + \frac{1}{3} \right) \quad (16.20)$$

with $\Delta\sigma = \sigma_{\text{app}} - \sigma$ as the overestimation of the standard deviation of the mean flow velocity.

The overestimation of the turbulence intensity obviously depends on both the real flow turbulence to be measured and the extent of the fringe distortion that is specified by the fringe distortion number. In regards Eq. (16.20), the overestimation of the flow turbulence is illustrated in Fig. 16.3 in the function of the real turbulence intensity for different fringe distortion numbers. For typical fringe distortions ($\gamma < 0.02$) the overestimation of the flow turbulence has been found to be not significant, especially in the measurement of flows with high turbulence intensity.

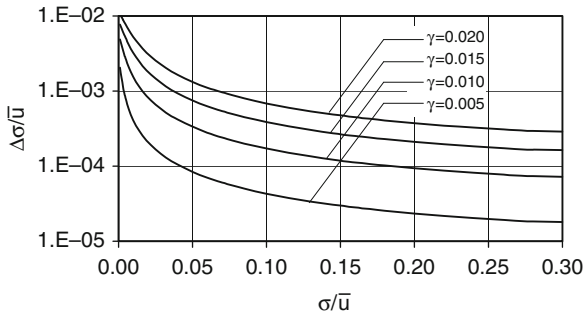


Fig. 16.3 Overestimations of the standard deviation in function of the real flow turbulence and the fringe distortion number γ

For a uniform laminar flow with $\sigma = 0$ the apparent turbulence intensity is calculated from Eq. (16.19) as

$$\frac{\sigma_{\text{app}}}{\bar{u}} = \sqrt{1/3} \cdot \gamma \quad (16.21)$$

Calculations made in this chapter basically refer to the fringe distortion with linear longitudinal variation in the fringe spacing (Fig. 16.1a). The calculation results can be used as the reference, if other types of fringe distortions and the respective influences on measurements should be accounted for. In general, the influence of the second type of fringe distortions (Fig. 16.1b) on turbulence measurements is rather smaller than that treated above, as this influence was already considered by Hanson (1975) in the earlier time to be negligible. The same might also be true for the case accounting for the third type of fringe distortions that is caused by the optical aberration i.e. astigmatism according to Fig. 14.14.

Chapter 17

Velocity Bias Effects

17.1 Velocity Bias as a Flow Phenomenon

Flow velocity measurements by means of LDA method are based on random sampling of velocity events which occur when particles pass through the measurement volume. The available velocity sampling rate depends on particle concentration, particle size, flow velocity and other flow and optical parameters. The dependence on the velocity magnitude in the turbulent flow becomes significant, if the sampling rate is considerably larger than the mean frequency of flow fluctuations. This type of dependence is generally characterized by the fact that velocities of large magnitudes will be more frequently sampled than velocities of small magnitudes. Accordingly, the time between two subsequent velocity samples is not equidistant. The sample mean of velocities according to Eq. (5.1) is then higher than that from velocities with equidistant time intervals. The shift of the sample mean of velocities towards the high value has been called the velocity bias and was first recognised by McLaughlin and Tiederman (1973). From the mechanism of velocity bias it is expected that not only the mean velocity but also other statistical parameters like the standard deviation show the difference to those from measurements with equidistant time intervals. Because of its dependence purely on velocity fluctuations, the velocity bias indeed represents a flow phenomenon. In the LDA terminology, the velocity bias i.e. the related difference in mean velocities has been categorized as being the measurement error. Corresponding investigations are generally restricted to two aspects: estimation and correction of effects of velocity bias.

In assuming homogeneous particle distribution in the flow, the particle arrival rate across the measurement volume and thus the velocity sampling rate are theoretically proportional to the velocity magnitude. From this viewpoint, considerable efforts have been made to estimate and correct the effect of velocity bias (Buchhave 1975, Buchhave et al. 1979, Lehmann 1986, Nobach 1998, Owen and Rogers 1975). An empirical estimation of the biased mean velocity has been given for instance by Edwards (1987) as a function of the turbulence intensity $\bar{u}_b/\bar{u} = 1 + Tu^2$. In applying the numerical method, Nobach (1998) investigated bias effects which are included in both the mean velocity and the standard deviations in all three velocity components of a complex three-dimensional turbulent flow. Exact analytical quantifications of

the bias effects have been carried out by Zhang (2002), considering all three components of velocity fluctuations from zero to infinity. The analysis serves as a reference to estimate the extent of the bias effects.

One of the well-known effects of velocity bias on measurements of turbulent flows is the distortion of the symmetrical distribution of velocity fluctuations around the corresponding mean. Another effect is the misinterpretation of an isotropic turbulence as an apparent anisotropic one. In addition, the bias errors in all three velocity components obviously differ from each other.

Concerning the matter of correcting for the bias effect, different methods have been developed and applied in data processing of LDA measurements. The most common method uses the reciprocal velocity or the residence time of particles in the measurement volume as a weighting factor in the calculations for arithmetic averages, as these have been shown at Eqs. (5.13), (5.14), and (5.15). The method of using the reciprocal value of each velocity vector as the weighting factor is obviously very limited, because this value must be known from measurement. In addition, the result is only true if the flow fluctuation is one-dimensional. The method of using the residence time or the transit time as the weighting factor is based on the assumption of statistically uniform flow through the measurement volume (no velocity gradient within the measurement volume). This method indeed has been recognised to be able to account for both the three-dimensionality of flow fluctuations and the measurement volume shape (Buchhave et al. 1979). The transit time can be theoretically attained by measuring the burst lengths. Another correction method to be mentioned is the method of using controlled processors to externally impose a constant sampling frequency (Edwards 1987, Erdmann and Tropea 1981). Such processors are basically only recommended for measurements with high data densities. In reality, the constant sampling frequency that is externally imposed can also be obtained by the post data processing.

As it states, the velocity bias has been historically considered to affect the measurement accuracy. This viewpoint, however, has to be partially declined. According to Chap. 12, the velocity bias does represent a measurement error if the volumetric flow rate (or volumetric flux) is to be calculated without any correction. The velocity bias, however, precisely ensures correct velocity measurements and data processing if the momentum flux is interesting. This will be required when dealing with the momentum equations like Euler, Navier-Stokes or Reynolds equations. Concerning the matter of flow turbulence, the relevant physical turbulence quantities are generally turbulent Reynolds stresses according to Eqs. (2.7), (2.8), and (2.9). Because they all represent the momentum quantities (or in terms of the specific kinetic energy), the occurrence of velocity bias in LDA measurements does not mean any measurement errors. For this reason, it is generally necessary to basically clarify the physical significance of each flow parameter that needs to be obtained from measurements.

For the historical reason, nevertheless, the word “velocity bias” will still be applied to denote the related flow phenomenon.

For LDA users in engineering applications, it is rather more interesting to know about the extent of velocity bias and its influences than to correct it. In general, it

is the responsibility of researchers and engineers to decide whether the associated measurement inaccuracy is acceptable or not, based on requirements of each related flow process. It is therefore reasonable to make distinctions between mean velocities and other flow parameters with and without the effect of velocity bias. The analysis made by Zhang (2002) will be referred to as the main content of this chapter.

It should be mentioned that in measurements of turbulent flows by the LDA method, another type of bias, the so-called angular bias, exists. This bias arises from the fact that the cross sectional area of the measurement volume and thus the particle arrival rate changes with the flow direction. It differs from the velocity bias physically in that the angular bias is not simply a flow phenomenon. Due to the three-dimensionality of flow fluctuations, it is usually impossible to distinguish between the velocity bias and the angular bias in the measurements.

17.2 Velocity Bias and the Momentum Flow Rate

It has been indicated that the velocity bias is in effect a flow phenomenon. This gives rise to basically clarifying its related flow dynamic properties. In Chap. 12 with regard to the non-uniform velocity distribution along the LDA measurement volume, it has been demonstrated that the related biased mean velocity precisely represents the mean velocity which is relevant for the momentum flow rate across the measurement volume. The ratio of the biased to the unbiased mean velocity simply stands for the so-called momentum flux correction factor. Because the velocity bias is traditionally referred to the turbulent flow with time-dependent velocity fluctuations, it is naturally of interest whether the same relation exists. The following analysis will demonstrate that this is true.

As known, the momentum flow rate is a vector quantity that is determined by the velocity vector (\vec{u}) and the normal vector (\vec{n}_A) of the related cross-sectional area in the flow. The so-called momentum flux (momentum flow rate per unit area) is then given by $\vec{J} = \rho \vec{u} \cdot (\vec{n}_A \cdot \vec{u})$. In this equation, the product in brackets represents the volumetric flux in unit of $\text{m}^3/(\text{m}^2\text{s})$. For further discussion a one-dimensional stationary turbulent flow of velocity u_x is considered. The volumetric flux through the unit area perpendicular to x -axis is then simply equal to u_x . The mean momentum flux during a time interval Δt is calculated by

$$\bar{J}_x = \rho \frac{1}{\Delta t} \int_0^{\Delta t} u_x^2 \cdot dt \quad (17.1)$$

For large time intervals, the averaged momentum flux represents a statistical constant of the flow. Based on the ergodic hypothesis the average of such a process parameter over time is equal to the average over the statistical ensemble. In order to convert the above calculation into the ensemble average, the statistical distribution of fluctuation velocity, as the ensemble from measurements, is considered as being described by an existing probability density function (pdf) p . The most

well-known pdf is obviously the Gaussian function (see Figs. 2.1 and 2.2). The ensemble averaged momentum flux can then be calculated by the corresponding integral

$$\bar{J}_x = \rho \int_{-\infty}^{\infty} p u_x^2 du_x \quad (17.2)$$

On the other side, the averaged momentum flux is usually represented by the product of an appropriate mean velocity and the mean of the volumetric flux \bar{u}_x as

$$\bar{J}_x = \rho \bar{u}_{x,J} \bar{u}_x \quad (17.3)$$

With respect to Eq. (17.2) the mean velocity $\bar{u}_{x,J}$ that represents a significant parameter for the momentum flow rate or likewise for the momentum flux is calculated by

$$\bar{u}_{x,J} = \frac{1}{\bar{u}_x} \int_{-\infty}^{\infty} p u_x^2 du_x \quad (17.4)$$

In dealing with stationary laminar flows there is simply $\bar{u}_{x,J} = \bar{u}_x$.

For practical applications and in likeness to dealing with flows with non-uniform velocity distributions, the momentum flux correction factor β can be applied to the concerns of the effect of velocity fluctuations in each interested turbulent flow, as given in the form

$$\bar{u}_{x,J} = \beta \bar{u}_x \quad (17.5)$$

The momentum flux given in Eq. (17.3) is then expressed as

$$\bar{J}_x = \beta \cdot \rho \bar{u}_x^2 \quad (17.6)$$

The velocity bias involved in LDA measurements will be again considered. As a result of velocity bias the probability density function p of the fluctuation velocity distribution will be distorted when calculated from measurements. In assuming the linear dependence of velocity sampling rate on the magnitude of velocities, the distorted i.e. biased probability density function then takes the form as given by

$$p_b = k |u_x| p \quad (17.7)$$

The constant k in this equation must fulfil the condition

$$\int_{-\infty}^{\infty} p_b du_x = 1 \quad (17.8)$$

from which one obtains

$$k = \frac{1}{\int_{-\infty}^{\infty} p |u_x| du_x} \quad (17.9)$$

Like at Eq. (5.2), the sample mean of velocities based on Eq. (5.1) can be calculated equivalently by the following integral with respect to the biased probability density function

$$\bar{u}_{x,b} = \int_{-\infty}^{\infty} p_b u_x du_x = k \int_{-\infty}^{\infty} p u_x |u_x| du_x \quad (17.10)$$

In all low turbulent flows, the velocity fluctuations ($u'_x = u_x - \bar{u}_x$) are always small compared to the mean velocity so that the occurrence of the back flow is negligible and $u_x > 0$ at all times is satisfied. From Eq. (17.9) with respect to $u_x > 0$ it follows $k = 1/\bar{u}_x$ directly from the mean velocity definition. Consequently Eq. (17.10) becomes

$$\bar{u}_{x,b} = \frac{1}{\bar{u}_x} \int_0^{\infty} p u_x^2 du_x \quad (17.11)$$

Because for $u_x < 0$ there is $p = 0$ this equation is equal to Eq. (17.4). It can then be pronounced that the biased mean velocity actually stands for the mean velocity that is applied to the momentum flow rate or similarly to the momentum flux at a local point in the flow. It can thus be directly applied in all momentum equations like the Euler, Navier-Stokes as well as Reynolds equations. On the other hand, both the use of the continuity equation and the calculation of the momentum flux according to Eq. (17.3) suppose the knowledge of the volumetric flux (\bar{u}_x). Thus the objective in dealing with the velocity bias is to estimate the difference between the mean for volumetric flux and its biased value for momentum flux. In other words, it is intended to determine the momentum flux correction factor according to Eq. (17.5).

17.3 Velocity Bias in One-Dimensional Flow Fluctuations

Although the flow fluctuation in a turbulent flow is always three-dimensional, the assumption of one-dimensional flow fluctuations contributes to the significant simplification of theoretical analyses of velocity bias. Since velocity fluctuations in the turbulent flow are of random nature, the fluctuations can then be approximated by the Gaussian probability distribution given by

$$p = \frac{1}{\sqrt{2\pi}\sigma} e^{-\frac{(u-\bar{u})^2}{2\sigma^2}} \quad (17.12)$$

Herein \bar{u} and σ are the volumetric mean velocity and its standard deviation, respectively. Clearly, the probability distribution of fluctuation velocity is symmetrical.

The symmetrical probability density function according to Eq. (17.12) will be distorted by the velocity bias in LDA measurements. As in the common case with the assumption of homogeneous particle distribution in the flow, the linear dependence of velocity sampling rate on the magnitude of velocities can be further assumed. The biased probability density function then must be written as

$$p_b = k |u| p = \frac{k |u|}{\sqrt{2\pi}\sigma} e^{-\frac{(u-\bar{u})^2}{2\sigma^2}} \tag{17.13}$$

As it states, the probability of negative velocity occurrence (back flow) because of velocity fluctuations has also been accounted for. From the same condition as given in Eq. (17.8) the constant k is determined as

$$\frac{1}{k\sigma} = \sqrt{\frac{2}{\pi}} \cdot e^{-\frac{\bar{u}^2}{2\sigma^2}} + \frac{\bar{u}}{\sigma} \operatorname{erf}\left(\frac{\bar{u}}{\sqrt{2}\sigma}\right) \tag{17.14}$$

In this equation, the error function is defined by

$$\operatorname{erf}(x) = \frac{2}{\sqrt{\pi}} \int_0^x e^{-u^2} du \tag{17.15}$$

The product of $k\sigma$ is given here as a function of relative flow fluctuations i.e. of the turbulence intensity σ/\bar{u} . Since the constant k appears always in the product form with σ , the product $k\sigma$ is designated here to be the bias product. It represents a measure of the distortion of the symmetrical probability distribution of the turbulent flow velocity. This has been demonstrated in Fig. 17.1 with two calculation examples.

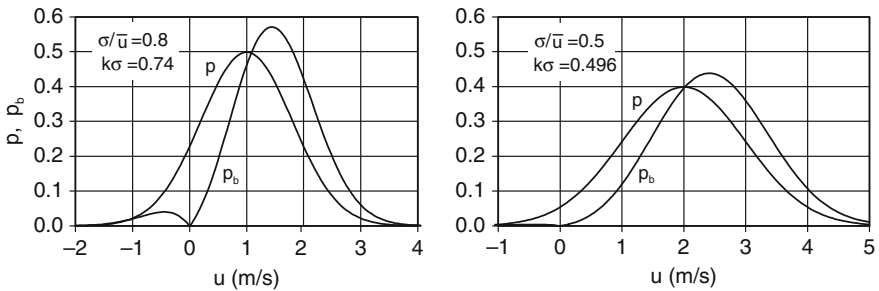


Fig. 17.1 Distortion of the distributions of the fluctuation velocity due to the effect of velocity bias in turbulent flows

For large turbulence i.e. $\bar{u} / \sigma \ll 1$ and due to the error function $\text{erf}(0) = 0$, the bias product is calculated from Eq. (17.14) as

$$k\sigma = \sqrt{\pi / 2} \quad (17.16)$$

On the other hand, the bias product becomes zero if laminar flows ($\sigma / \bar{u} = 0$) are measured:

$$k\sigma = \sigma / \bar{u} = 0 \quad (17.17)$$

As shown in Fig. 17.1, there is $k\sigma \approx \sigma / \bar{u}$ i.e. $k \approx 1 / \bar{u}$ already for $\sigma / \bar{u} \leq 0.5$. Actually, for low turbulent flow at which $u > 0$ can be assumed, $k = 1 / \bar{u}$ is available as it has been already applied to Eq. (17.10), leading to Eq. (17.11).

In applying the biased probability density function and like in Eq. (17.10), the biased mean velocity is calculated by the integral

$$\bar{u}_b = \int_{-\infty}^{\infty} p_b u du \quad (17.18)$$

With respect to Eq. (17.13) for p_b the integral in above equation is calculated as

$$\frac{\bar{u}_b}{\bar{u}} = 1 + k\sigma \frac{\sigma}{\bar{u}} \text{erf}\left(\frac{\bar{u}}{\sqrt{2}\sigma}\right) \quad (17.19)$$

Like the bias product, the ratio of the biased to the initial mean velocity is again a function of the turbulence intensity σ / \bar{u} .

Similarly, the biased standard deviation because of the distortion of the probability distribution of velocities is calculated as

$$\begin{aligned} \frac{\sigma_b^2}{\sigma^2} &= \frac{1}{\sigma^2} \int_{-\infty}^{\infty} p_b (u - \bar{u}_b)^2 du \\ &= 2 + \left(\frac{\bar{u}}{\sigma}\right)^2 \left(1 - \frac{\bar{u}_b}{\bar{u}}\right)^2 + k\sigma \left(\frac{\bar{u}}{\sigma} - 2\frac{\bar{u}_b}{\sigma}\right) \text{erf}\left(\frac{\bar{u}}{\sqrt{2}\sigma}\right) \end{aligned} \quad (17.20)$$

or with Eq. (17.19) to replace \bar{u}_b as

$$\frac{\sigma_b^2}{\sigma^2} = 2 - (k\sigma)^2 \left[\text{erf}\left(\frac{\bar{u}}{\sqrt{2}\sigma}\right)\right]^2 - k\sigma \frac{\bar{u}}{\sigma} \text{erf}\left(\frac{\bar{u}}{\sqrt{2}\sigma}\right) \quad (17.21)$$

For flows with turbulence intensities $\sigma / \bar{u} < 0.5$, the error function tends to unity ($\text{erf}(\bar{u} / \sqrt{2}\sigma) > 0.95$). Since this again leads to $k\sigma \approx \sigma / \bar{u}$ i.e. $k \approx 1 / \bar{u}$, Eqs. (17.19) and (17.21) are then simplified to

$$\frac{\bar{u}_b}{\bar{u}} \approx 1 + \frac{\sigma^2}{\bar{u}^2} \tag{17.22}$$

and

$$\frac{\sigma_b^2}{\sigma^2} \approx 1 - \frac{\sigma^2}{\bar{u}^2} \tag{17.23}$$

respectively.

Equation (17.22) agrees exactly with the empirical estimation given by Edwards (1987), as mentioned in Sect. 17.1.

In Fig. 17.2, both the biased mean velocity and its standard deviation according to Eqs. (17.19), (17.21), (17.22) and (17.23), respectively, are shown in the function of turbulence intensity ($Tu = \sigma/\bar{u}$). The turbulence intensities applied in Fig. 17.2 are restricted in the range between 0.01 and 10. This range, however, is sufficient to show the related effect of velocity bias for turbulence intensities varying from zero to infinity. As can be seen from the figure, the volumetric mean velocity is always overestimated because of the effect of velocity bias, while its standard deviation is underestimated at low and overestimated at high turbulence intensities. The approximations leading to Eqs. (17.22) and (17.23) are obviously valid for turbulence intensities below 50%. Again worth mentioning is that at low turbulent flows, at which $u_i > 0$ applies to all velocity samples, the overestimated mean velocity exactly agrees with the mean velocity that is relevant for the momentum flux. This means that the biased mean velocity given in Eq. (17.22) can be directly applied to the momentum flux.

At flows with very high turbulence intensities, the biased mean velocity and its standard deviation become

$$\bar{u}_b / \bar{u} = 2 \tag{17.24}$$

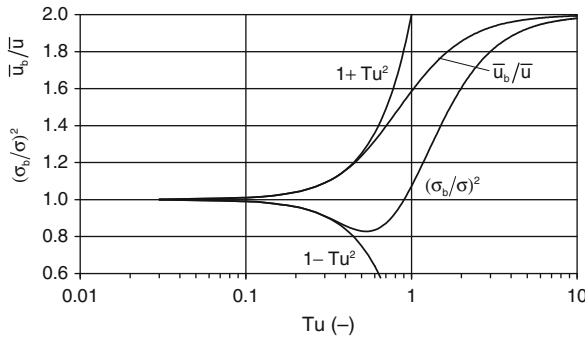


Fig. 17.2 Velocity bias in turbulent flow with one-dimensional flow fluctuations

and

$$\sigma_b^2 / \sigma^2 = 2 \tag{17.25}$$

respectively.

For measurements of flows with low turbulence intensities ($\sigma / \bar{u} \approx 0$), the velocity bias becomes negligible ($\bar{u}_b \approx \bar{u}$, $\sigma_b \approx \sigma$).

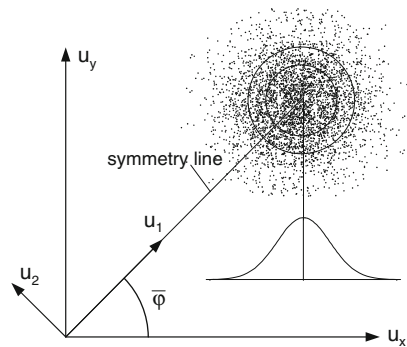
17.4 Velocity Bias in Two- and Three-Dimensional Flow Fluctuations

In reality, turbulent flow fluctuations are always three-dimensional and consist of fluctuations in both the velocity magnitude and the flow direction. LDA measurements of such turbulent flows undergo the velocity bias in each measured velocity component. It is therefore reasonable to establish the relationship between biased velocity components. In the case of isotropic or mostly anisotropic turbulence, the mean velocity vector can be considered to be the value which is surrounded symmetrically by velocities with fluctuations (Fig. 17.3). It can then be assumed that to each velocity event existing on one side of the symmetry line, there is always a conjugate one on the opposite side. For this type of flow turbulence, the velocity bias does not result in any change in the main flow direction. The ratio of the biased and the unbiased velocity component (for instance u_x) is then

$$\frac{\bar{u}_{x,b}}{\bar{u}_x} = \frac{\bar{u}_b \cos \bar{\varphi}}{\bar{u} \cos \bar{\varphi}} = \frac{\bar{u}_b}{\bar{u}} \tag{17.26}$$

The relative bias in the velocity component u_x is thus independent of the mean flow angle $\bar{\varphi}$. This signifies that the relative bias in the mean velocity is constant amongst all the velocity components. This is obviously also true if one-dimensional velocity fluctuations are assumed, as considered in Sect. 17.3.

Fig. 17.3 Velocity fluctuations symmetrically around the mean velocity vector



17.4.1 Velocity Bias in Mean Velocities

With respect to Eq. (17.26) it is sufficient to estimate the velocity bias in the velocity component that corresponds to the main flow direction. For the sake of simplicity, an isotropic turbulent flow is considered as having a unique standard deviation σ of velocities. The coordinate system has been chosen, such that the first axis coincides with the main flow direction (Fig. 17.3).

17.4.1.1 Two-Dimensional Flow Fluctuations

In the case of two-dimensional flow fluctuations, the velocity components on the coordinates axis are denoted by u_1 and u_2 , respectively. The Gaussian probability distribution of fluctuation velocity is given by

$$p = \frac{1}{2\pi\sigma^2} e^{-\frac{(u_1 - \bar{u}_1)^2 + u_2^2}{2\sigma^2}} \quad (17.27)$$

Because of the effect of velocity bias, this distribution is distorted, as this can be formulated by multiplying it with the factor $k\sqrt{u_1^2 + u_2^2}$

$$p_b = k\sqrt{u_1^2 + u_2^2} \frac{1}{2\pi\sigma^2} e^{-\frac{(u_1 - \bar{u}_1)^2 + u_2^2}{2\sigma^2}} \quad (17.28)$$

The bias constant $k\sigma$ can be determined from the similar condition as that in Eq. (17.8), so that

$$\frac{1}{k\sigma} = \frac{1}{2\pi} \int_{-\infty}^{\infty} X\left(\frac{u_2}{\sigma}\right) d\left(\frac{u_2}{\sigma}\right) \quad (17.29)$$

In this equation, the expression X is given by

$$X\left(\frac{u_2}{\sigma}\right) = \int_{-\infty}^{\infty} \sqrt{\left(\frac{u_1}{\sigma}\right)^2 + \left(\frac{u_2}{\sigma}\right)^2} \cdot e^{-\frac{1}{2}\left[\left(\frac{u_1}{\sigma} - \frac{\bar{u}_1}{\sigma}\right)^2 + \left(\frac{u_2}{\sigma}\right)^2\right]} d\left(\frac{u_1}{\sigma}\right) \quad (17.30)$$

The biased mean of velocity component u_1 is then calculated as

$$\frac{\bar{u}_{1,b}}{\bar{u}_1} = \frac{1}{\bar{u}_1} \int_{-\infty}^{\infty} \int_{-\infty}^{\infty} p_b u_1 du_1 du_2 = \frac{k\sigma}{2\pi} \frac{\sigma}{\bar{u}_1} \frac{1}{\sigma^4} \int_{-\infty}^{\infty} \int_{-\infty}^{\infty} u_1 \sqrt{u_1^2 + u_2^2} e^{-\frac{(u_1 - \bar{u}_1)^2 + u_2^2}{2\sigma^2}} du_1 du_2 \quad (17.31)$$

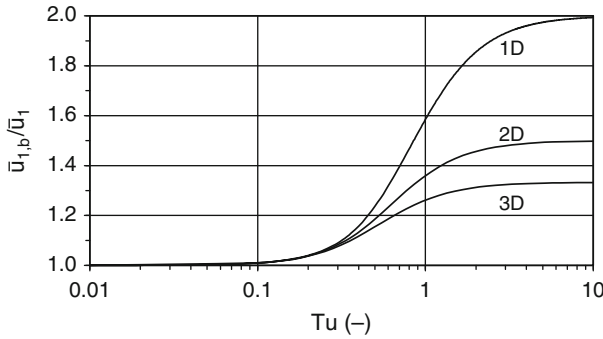


Fig. 17.4 Velocity bias in the mean velocity of the turbulent flow, respectively, with one-, two- and three-dimensional flow fluctuations

It is evident that the biased velocity component is again only a function of the turbulence intensity ($Tu = \sigma/\bar{u}_1$). Because the integrations in both Eqs. (17.29) and (17.31) could not be analytically performed, the finite numerical method has to be applied. Figure 17.4 shows corresponding calculation results regarding the biased velocity component $\bar{u}_{1,b} / \bar{u}_1$ in the function of the turbulence intensity (curve 2D). For the purposes of comparison, the biased mean velocity in the case of one-dimensional flow fluctuations, calculated from Eq. (17.19), has also been shown (curve 1D).

17.4.1.2 Three-Dimensional Flow Fluctuations

Similar calculation procedures can be applied to the flows with three-dimensional flow fluctuations. In place of Eq. (17.27), the Gaussian probability distribution of velocities takes the following form:

$$p = \frac{1}{\sqrt{8\pi}\pi\sigma^3} e^{-\frac{(u_1 - \bar{u}_1)^2 + u_2^2 + u_3^2}{2\sigma^2}} \tag{17.32}$$

Because of the effect of velocity bias this distribution is distorted, as this can be similarly formulated by multiplying it with the factor $k\sqrt{u_1^2 + u_2^2 + u_3^2}$, so that

$$p_b = \frac{k\sqrt{u_1^2 + u_2^2 + u_3^2}}{\sqrt{8\pi}\pi\sigma^3} e^{-\frac{(u_1 - \bar{u}_1)^2 + u_2^2 + u_3^2}{2\sigma^2}} \tag{17.33}$$

The bias constant $k\sigma$ can be again determined from the similar condition as that in Eq. (17.8). The biased mean of velocity component u_1 is then calculated as

$$\begin{aligned}
\frac{\bar{u}_{1,b}}{\bar{u}_1} &= \frac{1}{\bar{u}_1} \int_{-\infty}^{\infty} \int_{-\infty}^{\infty} \int_{-\infty}^{\infty} p_b u_1 du_1 du_2 du_3 \\
&= \frac{k\sigma}{\sqrt{8\pi\pi}} \frac{\sigma}{\bar{u}_1} \frac{1}{\sigma^5} \int_{-\infty}^{\infty} \int_{-\infty}^{\infty} \int_{-\infty}^{\infty} u_1 \sqrt{u_1^2 + u_2^2 + u_3^2} e^{-\frac{(u_1 - \bar{u}_1)^2 + u_2^2 + u_3^2}{2\sigma^2}} du_1 du_2 du_3
\end{aligned} \tag{17.34}$$

The integration must be again performed by the finite numerical method. Corresponding calculation results have been shown in Fig. 17.4 (curve 3D) in the function of the turbulence intensity. Obviously the effect of velocity bias in the velocity component is lowest if the flow fluctuation is three-dimensional.

The above calculations for three cases of flow fluctuations (1D, 2D and 3D) help to understand the extent of influences of velocity bias in LDA measurements. The flow fluctuations in turbulent flows, in fact, are always three-dimensional. For this reason and by comparing Figs. 17.2 and 17.4 it can be concluded that the approximation $\bar{u}_b / \bar{u} = 1 + Tu^2$ is only applicable for real flows with turbulence intensities up to 30%.

17.4.2 Velocity Bias in Turbulent Normal Stresses

The influence of velocity bias on measurements of turbulence quantities is identified, for instance, in that the velocity bias will cause the actual isotropic turbulence to be measured and presented as an apparent anisotropic one. For simplicity, turbulent flows that show the symmetrical velocity fluctuations around the main flow direction are considered here. According to Chap. 8 and in considering a two-dimensional section in the flow field (Fig. 17.3), the turbulent normal stress in the velocity component u_x for instance is calculated by Eq. (8.7). Obviously, Eq. (8.7) also applies to the biased normal stress, so that

$$\sigma_{x,b}^2 = \sigma_{1,b}^2 \cos^2 \bar{\varphi} + \sigma_{2,b}^2 \sin^2 \bar{\varphi} \tag{17.35}$$

For this reason, one needs only to determine the effects of velocity bias on the turbulence quantities $\sigma_{1,b}^2$, $\sigma_{2,b}^2$ and $\sigma_{3,b}^2$ in a general turbulent flow. The simplest case would be again the turbulent flow with isotropic turbulence ($\sigma_1 = \sigma_2 = \sigma_3 = \sigma$) that is described by the turbulence intensity $Tu = \sigma / \bar{u}_1$ and undergoes the velocity bias with $\sigma_{2,b} \neq \sigma_{1,b}$ and $\sigma_{2,b} = \sigma_{3,b}$. For this reason and because of Eq. (17.35) it is proposed that one only calculates the biased quantities $\sigma_{1,b}$ and $\sigma_{2,b}$, respectively. From the viewpoint of statistics leading to Eq. (5.5), the following relationship between the statistical quantities, as applied to the velocity component u_1 for instance, is available

$$\sigma_{1,b}^2 = \overline{u_{1,b}^2} - \bar{u}_{1,b}^2 \tag{17.36}$$

As the biased mean velocity has been obtained in Sect. 17.4.1, only the first term on the r.h.s. of above equation needs to be calculated. For the purpose of again making a comparison between flows with two- and three-dimensional turbulence, respective flows will be separately considered, as presented below.

17.4.2.1 Two-Dimensional Turbulence

For an assumed flow with two-dimensional and isotropic velocity fluctuations, Eq. (17.36) is rewritten in detail

$$\frac{\sigma_{1,b}^2}{\sigma^2} = \frac{1}{\sigma^2} \int_{-\infty}^{\infty} \int_{-\infty}^{\infty} u_1^2 p_b du_1 du_2 - \frac{\bar{u}_{1,b}^2}{\sigma^2} \tag{17.37}$$

The biased probability distribution p_b is the same as that which is given by Eq. (17.28) and has been used in Eq. (17.31). Equation (17.37) is expected to be a function of the turbulence intensity ($Tu = \sigma/\bar{u}_1$) only.

Similarly, the biased standard deviation in the second velocity component i.e. the component perpendicular to the flow direction is given by

$$\frac{\sigma_{2,b}^2}{\sigma^2} = \frac{1}{\sigma^2} \int_{-\infty}^{\infty} \int_{-\infty}^{\infty} u_2^2 p_b du_1 du_2 \tag{17.38}$$

with $\bar{u}_2 = \bar{u}_{2,b} = 0$.

Figure 17.5 shows corresponding calculation results in the function of the turbulence intensity. In the velocity component u_1 , the related turbulent normal stress is underestimated for flows of the turbulence intensity below 65%. At the flows of the turbulence intensity $Tu < 30\%$, the over- and underestimation of the turbulent stress in the velocity component u_1 and u_2 , respectively, are of the same order.

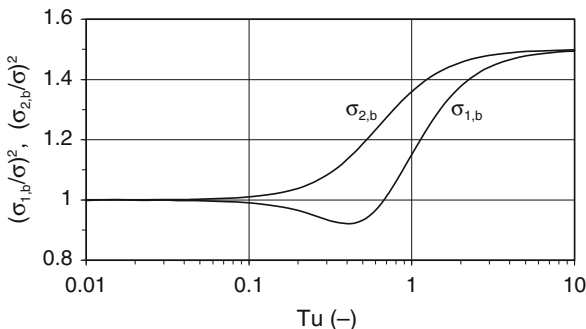


Fig. 17.5 Velocity bias in the turbulent stresses of the turbulent flow with two-dimensional flow fluctuations

17.4.2.2 Three-Dimensional Turbulence

Under the assumption of isotropic turbulence in a turbulent flow with three-dimensional velocity fluctuations, measurements of velocity components perpendicular to the main flow direction then undergo the same effect of velocity bias. This simply means $\sigma_{2,b}^2 = \sigma_{3,b}^2$. Because of this equality one needs to only estimate the biased quantities $\sigma_{1,b}^2$ and $\sigma_{2,b}^2$. The biased turbulence quantities in other velocity components can be generally calculated through the coordinate transformation of the related Reynolds stress matrix with $\sigma_{2,b}^2 = \sigma_{3,b}^2$. For the turbulent normal stress $\sigma_{x,b}^2$ for instance, it applies (Appendix C)

$$\sigma_{x,b}^2 = \sigma_{1,b}^2 \cos^2 \alpha_1 + \sigma_{2,b}^2 \sin^2 \alpha_1 \tag{17.39}$$

Herein α_1 is the angle between the main flow direction (axis with σ_1) and the x -axis (see also Fig. 6.1). The above equation is formally equal to Eq. (17.35). It applies, however, also to the flow in which the main flow direction does not lie in the $x - y$ plane.

Following the same calculation procedures, as presented above with respect to the two-dimensional flow fluctuations, the biased turbulence quantities $\sigma_{1,b}^2$ and $\sigma_{2,b}^2$ in the current case are calculated as

$$\frac{\sigma_{1,b}^2}{\sigma^2} = \frac{1}{\sigma^2} \int_{-\infty}^{\infty} \int_{-\infty}^{\infty} \int_{-\infty}^{\infty} u_1^2 p_b du_1 du_2 du_3 - \frac{\bar{u}_{1,b}^2}{\sigma^2} \tag{17.40}$$

$$\frac{\sigma_{2,b}^2}{\sigma^2} = \frac{1}{\sigma^2} \int_{-\infty}^{\infty} \int_{-\infty}^{\infty} \int_{-\infty}^{\infty} u_2^2 p_b du_1 du_2 du_3 \tag{17.41}$$

In these two equations, the biased probability density function p_b is the same as that given by Eq. (17.33) which has been applied in Eq. (17.34).

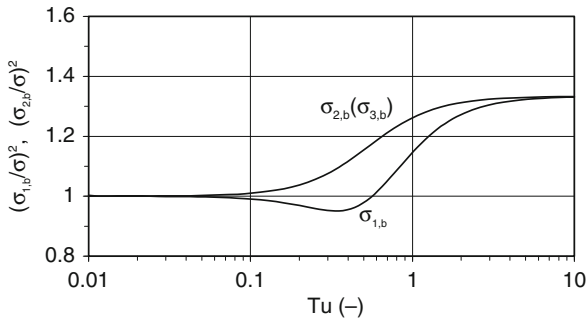


Fig. 17.6 Velocity bias in the turbulent stresses of the turbulent flow with three-dimensional flow fluctuations (The unbiased flow turbulence is isotropic)

Corresponding calculation results have been shown in Fig. 17.6. The effect of velocity bias in this case, if compared with Fig. 17.5 regarding two-dimensional flow fluctuations, has further diminished.

17.4.3 Velocity Bias in Turbulent Shear Stresses

Based on calculations of velocity bias in turbulent normal stresses in the last section, the velocity bias in the respective turbulent shear stress can be determined by means of the coordinate transformation of the related second order tensor i.e. the Reynolds stress matrix with $\sigma_{2,b}^2 = \sigma_{3,b}^2$. In interest of biased turbulent shear stress $\left(\overline{u'_x u'_y}\right)_b$ for instance, it applies (Appendix C)

$$\left(\overline{u'_x u'_y}\right)_b = \left(\sigma_{1,b}^2 - \sigma_{2,b}^2\right) \cos \alpha_1 \cos \beta_1 \quad (17.42)$$

In this equation, α_1 stands for the angle between the velocity components u_1 and u_x , as in Eq. (17.39). The angle β_1 conventionally denotes the angle between velocity components u_1 and u_y .

A special case is obtained when all four velocity components (u_1, u_2, u_x and u_y) are found in a plane. It is assumed that it deals with the $x - y$ plane, as shown in Fig. 17.3. Because of $\alpha_1 = \bar{\varphi}$ and $\beta_1 = \pi/2 - \alpha_1 = \pi/2 - \bar{\varphi}$ it follows from Eq. (17.42)

$$\left(\overline{u'_x u'_y}\right)_b = \frac{1}{2} \left(\sigma_{1,b}^2 - \sigma_{2,b}^2\right) \sin 2\bar{\varphi} \quad (17.43)$$

It completely agrees with Eq. (8.9) in Chap. 8.

Chapter 18

LDA Application Examples

18.1 High Speed Water Jet Flow in a Pelton Turbine

One of the most successful applications of the LDA method in flow measurements is the measurement of the high speed jet in a Pelton turbine. Such an application has been partly shown in Chap. 9 while describing the Dual Measurement Method (DMM). The high speed jet flow in a Pelton turbine represents a very important component which influences the entire hydraulic performance of the turbine system (Zhang 2009). For a long time, jet measurements were carried out by means of the pressure tubes and the photography with very limited accuracies. The first application of the LDA method to the high speed jet flow was conducted by Zhang et al. (2000a, b) in using a model injector of a Pelton turbine. In performing such measurements, the first step that must be completed is to bring the laser beams through the rough jet surface into the jet. This can be realized by using a transparent plane piece to slightly contact the jet, as illustrated in Fig. 18.1. The resulted disturbance on the jet flow is restricted within the boundary layer thickness on the rigid surface of the plane piece. Because this thickness is in the order of only about 0.1 mm, the flow disturbance can be neglected. In addition, the use of the plane piece as an optical window ensures the perfect optical conditions for LDA measurements.

It has been confirmed from measurements that the jet flow and the flow properties significantly depend on the flow condition ahead of the injector. The flow presented in Sect. 9.2 (see Fig. 9.2) corresponds to the condition of the inlet flow passing through a 90° bend. The secondary flow has been thus generated. Because it represents swirling flows, it persists while passing through the injector and thus also remains in the jet.

The simplest case of the jet flow is the jet flow without any secondary flow structure in it. This almost ideal flow can be generated by connecting the injector to a long straight pipe with uniform inlet flow. Corresponding measurements of flow distributions in such a high speed jet could be well carried out by means of the LDA method, as demonstrated in Fig. 18.2. At four different sections along the jet, the axial jet speeds are measured and normalized by the theoretical maximum jet speed $c_0 = \sqrt{2gh_0}$, with $h_0 = 30$ meters as the hydraulic head that is available at the

Fig. 18.1 High speed jet flow in a Pelton turbine and the LDA arrangement for flow measurements

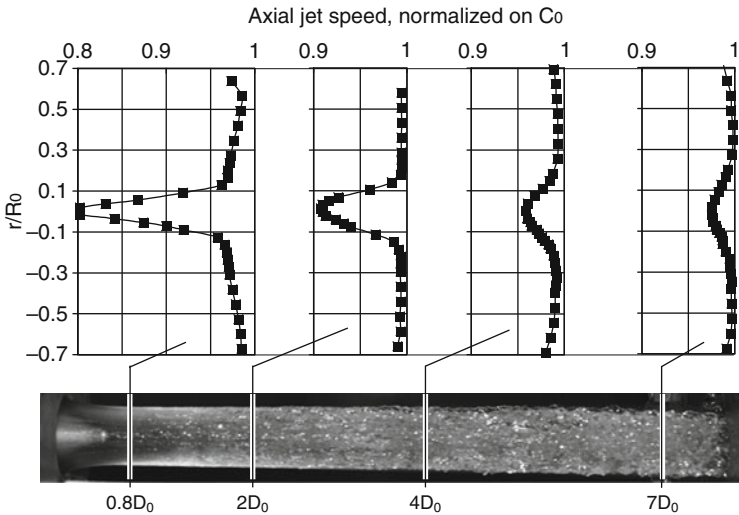
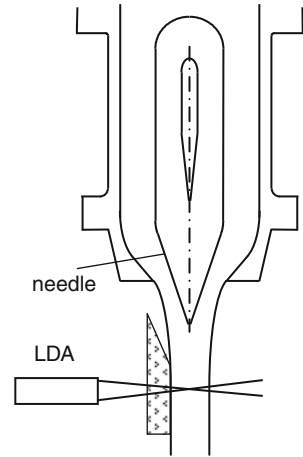


Fig. 18.2 Velocity distributions in the high speed jet flow measured by LDA

injector. Based on these accurate measurements, the following statements can be additionally made with regard to the flow dynamics.

A Flow deficit in the jet core

A significant flow deficit is confirmed in the jet core while the jet flow is formed at the nozzle exit. This is the wake arising from the viscous boundary layers on the needle surface. The boundary layer and its spatial limitation could thus be clearly identified.

B Streamline curvature

At the jet section $0.8D_0$ downstream of the nozzle, the flow velocity distribution across the jet and out of the jet core is non-uniform. The highest flow velocity is found near the edge of the jet. Such a velocity distribution indicates that the flow at this distance exhibits the streamline curvature in the length plane. This streamline curvature leads to the increase of the static pressure along the curvature radius towards the jet core and in a flow with constant total pressure, the velocity has to decrease. This appearance signifies that the slope of such a velocity distribution is simply a measure of the streamline curvature and thus of the pressure distribution, as this can be demonstrated here.

To calculate the streamline curvature in the jet near to the nozzle outlet, the jet flow is considered in the cylindrical coordinate system to have no circumferential velocity component. The streamline of the flow is then given by

$$r' = \frac{dr}{dz} = \frac{u_r}{u_z} \quad (18.1)$$

For the general case of $dr/dz = f(r, z)$, it is further differentiated as

$$r'' = \frac{d^2r}{dz^2} = \frac{1}{u_z^2} \left[u_z \left(\frac{\partial u_r}{\partial z} + \frac{\partial u_r}{\partial r} \frac{dr}{dz} \right) - u_r \left(\frac{\partial u_z}{\partial z} + \frac{\partial u_z}{\partial r} \frac{dr}{dz} \right) \right] \quad (18.2)$$

The jet flow out of the jet core can be considered to be the potential flow because a short distance downstream of the considered flow section, the flow with uniform and straight streamlines exhibits no vorticity. With respect to $dr/dz = u_r/u_z$ and $u_r/u_z \ll 1$ as well as $\partial u_r/\partial z = \partial u_z/\partial r$ for potential flow the above equation is simplified to

$$r'' = \frac{1}{u_z} \frac{\partial u_z}{\partial r} \quad (18.3)$$

The curvature radius of a streamline is calculated by

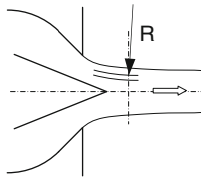
$$\frac{1}{R} = \frac{r''}{(1 + r'^2)^{3/2}} \approx r'' = \frac{1}{u_z} \frac{\partial u_z}{\partial r} \quad (18.4)$$

The streamline curvature is thus directly related to the velocity gradient in the area out of the jet core. In the first approximation, the velocity distribution out of the jet core can be considered to be a linear function of the radial coordinate, so that the velocity gradient $\partial u_z/\partial r$ is a constant. Based on calculations in Eq. (18.4) an abstract of calculated radii of streamline curvatures from a series of measurements with different hydraulic heads is shown in Table 18.1.

As can be seen, the calculated radii of streamline curvatures are nearly independent of the available hydraulic head. This indicates that the jet flows operating at three different hydraulic heads are hydraulically similar.

Table 18.1 Streamline curvature radii in the near region to the nozzle exit for a constant needle stroke (Zhang and Casey 2007)

Hydraulic head h_0	Needle stroke $s=16$ mm	
	$\partial u_z/\partial r$	Curvature radius R (m)
10 m	37.7	0.37
20 m	54.0	0.37
30 m	61.1	0.39



Streamline curvatures in the jet flow lead to pressure increase toward the jet core. This pressure increase can be calculated by applying the Euler momentum equation for the radial component as

$$-\frac{1}{\rho} \frac{dp}{dr} = u_r \frac{\partial u_r}{\partial r} + u_z \frac{\partial u_r}{\partial z} \tag{18.5}$$

As mentioned above the jet flow is considered to be the potential flow to which the irrotational flow condition $\partial u_r/\partial z - \partial u_z/\partial r = 0$ is satisfied. Combining this condition with $\partial u_z/\partial r = u_z/R$ from Eq. (18.4) leading to

$$\frac{\partial u_r}{\partial z} = \frac{u_z}{R} \tag{18.6}$$

With respect to $u_r \approx 0$ the pressure gradient in the jet at the considered jet section is then calculated as

$$\frac{1}{\rho} \frac{dp}{dr} = -u_z \frac{\partial u_r}{\partial z} = -\frac{u_z^2}{R} \tag{18.7}$$

The non-uniform flow distribution due to the streamline curvature clearly shows that the flow velocity in the considered section has not reached its maximum and the jet flow still undergoes acceleration. The mean velocity across this jet section is thus smaller than the mean velocity downstream at other sections. This first section was initially localized for detailed measurements as it was taken as the jet waist from photographic estimation. According to the presented LDA measurements, it is evident that the true jet waist is found further downstream. This also signifies that the LDA method is much more accurate than the photographic method even though for the purpose of localizing the jet waist.

It is worth mentioning here that because of the non-uniform static pressure distribution across the jet, the flow in the considered section could not be accurately measured by a conventional Pitot tube, which in reality only measures the total pressure. In assuming the constant static pressure, the Pitot tube measurement would then provide a uniform velocity distribution across the jet, which is clearly not true.

C *Limitation of measuring the jet diameter*

The use of the small wedge shaped Perspex window, as shown in Fig. 18.1, means that the jet surface position on the side of the jet adjacent to the wedge cannot be estimated. On the opposite side of the jet, the rough jet surface scatters so much laser light that the LDA optics rapidly reaches its limitation. For this reason it is impossible to accurately estimate the location of the edge of the jet, i.e. the jet thickness, from LDA measurements.

D *Negligible energy loss in the jet flow*

The mean velocity in the jet remains nearly constant along the jet, at least up to the section of a distance that is measured seven times of the nozzle exit diameter. This indicates that the jet is highly compact and the loss of the kinetic energy is negligible.

Measurements shown above were carried out at the hydraulic head up to 30 meters, as shown in Table 18.1. Successful LDA measurements of the jet flows at the hydraulic head of 90 meters have been carried out by Zhang et al. (2003). More about the measurements including those with a 90° bend ahead of the injector as well as at the hydraulic head of 90 meters can be found in Zhang and Casey (2007) that summarized the most relevant jet flow measurements by the LDA method.

18.2 Measurements of Warp Yarn Speed in a Weaving Machine

LDA method has been generally recognized to be a technique for flow measurements. In reality, it can also be applied to measurements of other object motions instead of small particle motions in the flow. One needs only to position the LDA measurement volume on the surface of the moving object of finite dimensions. The possible problem associated with the positioning of the measurement volume is obviously the light scattering that is very strong and will lead to rapid overloading of used photodetectors like the photomultiplier. In addition, the visibility of signals will considerably decrease, like in the case of large particles passing through the measurement volume. The high quality burst like that in Fig. 3.6 could not be achieved. Instead, continuous signals with highly diminished signal to noise ratio (SNR) will be obtained. Although the signal quality is largely deteriorated by the low SNR, signals can still be successfully evaluated by the powerful signal processor like the burst spectrum analyzer (BSA) that is based on the spectrum analysis using FFT and corresponds to the current state of the art LDA technologies. Because of this performance, the application area of the LDA method has been significantly extended, as it can be found for instance in measurements of mechanical vibrations at machines or machine components.

Figure 18.3 shows an example of extended LDA applications in the weaving machine. It represents the measurements of the time-dependent moving speed of a warp yarn with the purpose of checking and controlling the yarn tension in the

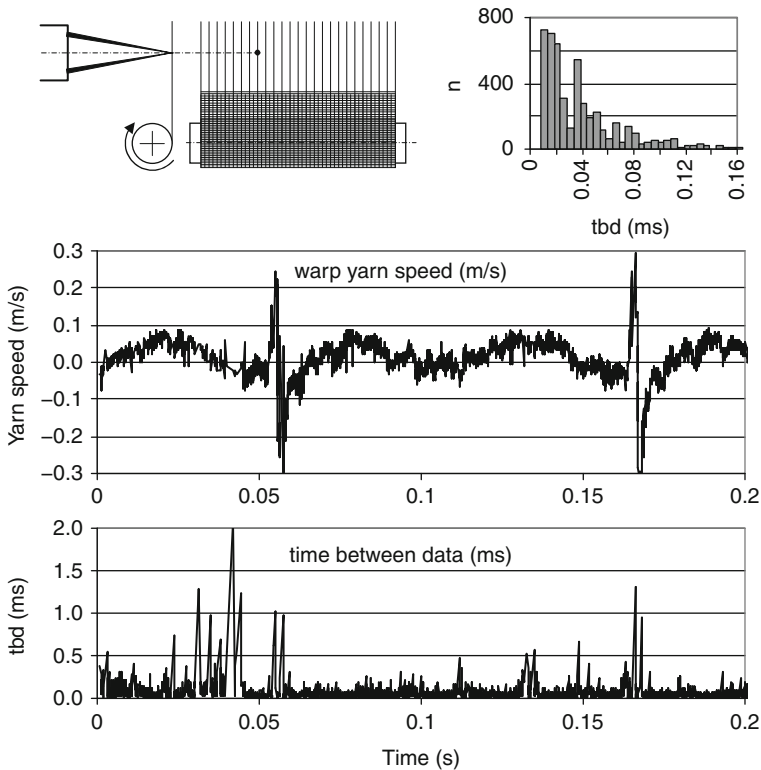


Fig. 18.3 LDA application to measurements of the warp yarn speed in a weaving machine

weaving machine. In the example given, the LDA measurement volume was directly positioned on the moving yarn. The measurement could be conducted with a very high data rate of about 30 kHz. This enables the highly dynamical motion of the yarn to be highly resolved.

In principle, the mean speed of the yarn movement can be calculated from the arithmetic average of measurement data. The calculation, however, has shown that this mean speed mostly does not agree with the actual mean speed of yarns while the machine is operating. The reason for this discrepancy is simply the non-constant data sampling rate. Worth remembering is that the non-constant data sampling rate as a result of the velocity bias in flow measurements (Chap. 17) usually does not significantly influence the determination of the mean velocity. In the present case, the non-constant data sampling rate arises from the non-constant light scattering on the moving yarn of about 0.1 mm in diameter. Such a non-constant data sampling rate can be shown by the time-dependent time-between-data ($tbd = t_{i+1} - t_i$), as also shown in Fig. 18.3 together with the corresponding probability distribution in form of the histogram. Obviously the measurements were carried out with a wide spectrum of the time-between-data i.e. data sampling rate. Because of the highly

dynamical motion and comparably very low mean speed of yarns the non-constant data sampling rate will considerably sensitively influence the measurement of the mean speed of the moving yarn. In the example shown in Fig. 18.3, the relative fluctuation speed is measured at about $\sigma/\bar{u} \approx 100 = 10000\%$, with σ as the standard deviation of the mean speed. Worth mentioning is that in the measurement of a turbulent flow with comparable turbulence intensity the biased mean velocity is equal to two times of the unbiased mean, see Fig. 17.2.

It has been shown that in the present case the mean speed of the moving yarn could not be accurately determined. In reality, the most significant meaning of the current LDA measurements is in showing the dynamic behaviours of moving yarns in a weaving machine. The mean speed of the moving yarns could be accurately measured by simply using a meter and a stop watch.

The measurement shown in Fig. 18.3 clearly demonstrates the excellent applicability of the LDA method in areas other than the fluid flow mechanics.

18.3 Verification of the Shift Frequency in the Laser Beam

For purposes of resolving the flow direction in LDA measurements, the frequency of one laser beam in each laser beam pair is usually shifted, as described in Sect. 3.6. Sometimes it is necessary to verify the accuracy of the shift frequency, in order to estimate the system accuracy of the LDA unit and to identify the possible systematic error in LDA measurements. Direct measurements of the shift frequency as an optical quantity by using the interferometer, for instance, are not always available or usually very time-consuming. The simplest way to verify the shift frequency is probably to measure a non-moving object with the present LDA optics. For the correct setup and specification of shift frequency in LDA optics, zero velocity should be obtained. Any deviation of measured velocities from zero indicates the error in the shift frequency specifications.

The method of measuring the non-moving object seems to be somewhat inadequate, because it does not deal with the direct measurement of velocities. In addition, the object might likely be burned down at the place where the laser beams are focused. The strong laser light scattering at the object also leads to continuous overloading of the photodetectors such as the photomultiplier. For this reason it would be very helpful to use a rotating object such as a variable frequency optical chopper. Either the object surface, or better a thin wire on it, can be utilized to scatter the laser light in the configured LDA test.

For the purpose of merely verifying the shift frequency in the transmitting laser light, one doesn't need to compare the measured velocities with the actual velocity of the rotating object. The measurements can be quite easy and accurately performed, if the motor of the used optical chopper can be switched to rotate in both directions at equal rotational speed. The LDA measurement volume will be simply positioned on the rotating object without having to know where it is and which velocity component will be measured. One needs to only compare two velocities

which are measured while the motor rotates, respectively, in two different directions at the same speed. Theoretically both velocities with different signs should exhibit the same absolute value when the specification of the shift frequency in the transmitting laser light is exact. Each difference in the absolute values of both velocities straightforwardly indicates that there is a difference between the shift frequency that is specified in the software and the actual shift frequency that is achieved by means of the Bragg cell, for instance. In reality, the error in the specification of the shift frequency can not only be confirmed, but also quantified. For this purpose, the error in the shift frequency is considered to result in an error in the shift speed of fringes in the measurement volume according to Eq. (3.60). This shift speed error is constantly involved in the verification measurements by means of the rotating object. As the motor rotates in two different directions, the measured velocity components are

$$u_+ = u_0 + \Delta u_{sh} \tag{18.8}$$

and

$$u_- = -u_0 + \Delta u_{sh} \tag{18.9}$$

respectively. Herein the actual velocity component is assumed to be u_0 . By eliminating this actual velocity from above two equations, the error that is involved in the measurements is determined as

$$\Delta u_{sh} = \frac{u_+ + u_-}{2} \tag{18.10}$$

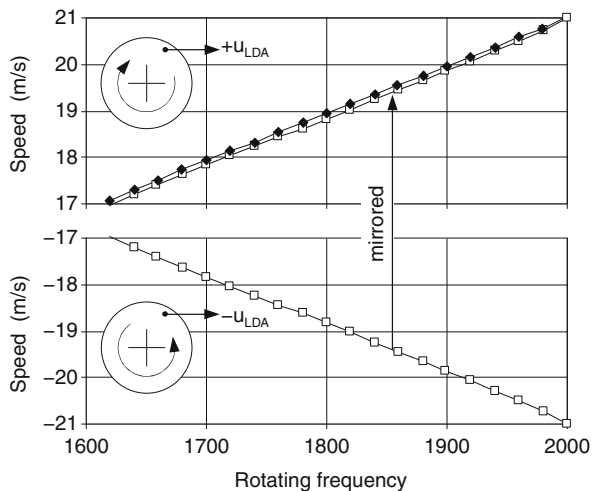


Fig. 18.4 Method of verifying the shift frequency accuracy in an LDA system

This error should remain constant, when the verification measurement is carried out at other rotational speeds of the motor. Figure 18.4 shows an example of the outlined verification measurement by using a variable frequency optical chopper that can be accurately set at each constant value of rotational speeds. As can be seen, the error in the outlined velocity measurements is highly constant. It indeed represents an error which is negligibly small. In the example shown in Fig. 18.4, the error in the shift speed takes $\Delta u_{sh} = 0.047$. It corresponds to an additive amount to the velocity component that is positive in the LDA coordinate system. With respect to the fringe spacing $\Delta x = 2.18 \mu\text{m}$, the error in the shift frequency is calculated from Eq. (3.60) to be 22 kHz. If related to the applied shift frequency of 40 MHz, the error takes about 0.05%.

The method of rotating the object in two different directions represents an accurate method to examine any negligible difference between the actual and the specified shift frequency in an LDA unit. It is accurate because it is founded on the natural law and is occasionally called the two-step method. The most famous application example of this method might be the Michelson-Morley experiment (Hecht 1991) that was conducted to find out whether the light speed is different in different spatial directions. The same principle has also been applied in Chap. 9 to derive the Dual Measurement Method (DMM) which enables the very small secondary flow structures in the high speed jet flow to be accurately measured.

Appendix A

Off-axis LDA Alignment and Measurement Volume Displacement

For measurements of internal flows or flows behind a plane wall by means of the LDA method, it is sometimes necessary to align the LDA head off-axis against the normal of the plane wall. Such an arrangement of LDA optics requires a special concern that the LDA head should be off-axis aligned strictly in the plane containing two laser beams. This ensures the laser beams in both the window and the flow to propagate within the same plane and thus to intersect (Fig. A.1). One of the most significant outcomes of such an arrangement of a two-component LDA head with two pairs of laser beams is that the two measurement volumes (m and s) do not meet together. This phenomenon is known as astigmatism as a special form of optical aberrations. The distance between two intersection points, i.e. measurement volumes, is denoted as the astigmatic difference. Details about this form of optical aberrations have been described in Chap. 14, see Fig. 14.6.

To specify and evaluate the optical performance of an LDA system at the off-axis alignment, the distance between two separate measurement volumes has been considered to be a measure of the related optical aberration. It can be applied even in the case of using a one-component LDA with two laser beams. As a reference, this distance will be calculated in this appendix.

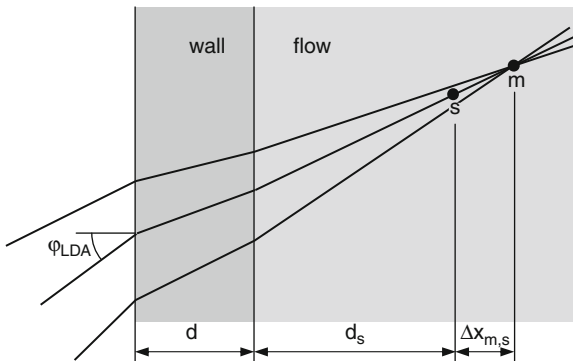
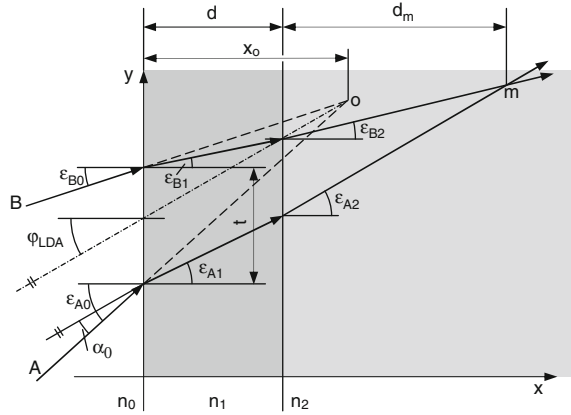


Fig. A.1 Off-axis alignment of a two-component LDA head and the separation of two measurement volumes (astigmatic difference)

Fig. A.2 Propagation of two laser beams in the meridian plane



For the common purpose of regarding the astigmatism, the plane in which the off-axis alignment takes place is denoted as the meridian plane. The plane that is perpendicular to the meridian plane is denoted as the sagittal plane. For an LDA head with four laser beams then each plane contains two laser beams. The way to calculate the distance between two measurement volumes is to firstly calculate the intersection point of two laser beams in each laser beam pair.

The medium 0, in which all four laser beams intersect at a unique point, is denoted as the reference medium. Usually it refers to the air in which the LDA head is present.

A.1 Laser Beams in the Meridian Plane

The two laser beams in the meridian plane will be considered according to Fig. A.2 first. The initial i.e. virtual intersection point of two laser beams is found at o that is measured by x_o in the used coordinate system. Obviously both laser beams propagate in the same two-dimensional plane from the medium 0 to the medium 2. For the calculation purpose both laser beams A and B in the medium 0 are represented by the unit vector \vec{a}_0 and \vec{b}_0 , respectively. In the used x - y coordinate system, these two unit vectors are expressed as

$$\vec{a}_0 = [\cos(\varphi_{LDA} + \alpha_0), \sin(\varphi_{LDA} + \alpha_0)] = (\cos \varepsilon_{A0}, \sin \varepsilon_{A0}) \quad (A.1)$$

$$\vec{b}_0 = [\cos(\varphi_{LDA} - \alpha_0), \sin(\varphi_{LDA} - \alpha_0)] = (\cos \varepsilon_{B0}, \sin \varepsilon_{B0}) \quad (A.2)$$

In the medium 1 and 2, the corresponding laser beams are represented by respective unit vectors as

$$\vec{a}_1 = (\cos \varepsilon_{A1}, \sin \varepsilon_{A1}) \quad (\text{A.3})$$

$$\vec{b}_1 = (\cos \varepsilon_{B1}, \sin \varepsilon_{B1}) \quad (\text{A.4})$$

$$\vec{a}_2 = (\cos \varepsilon_{A2}, \sin \varepsilon_{A2}) \quad (\text{A.5})$$

$$\vec{b}_2 = (\cos \varepsilon_{B2}, \sin \varepsilon_{B2}) \quad (\text{A.6})$$

Both laser beams intersect with the y -axis. The distance between two intersection points, as shown by t , can be calculated from either the virtual intersection point o or the actual point m , as given by

$$t = (\tan \varepsilon_{A0} - \tan \varepsilon_{B0}) x_o = (d \tan \varepsilon_{A1} + d_m \tan \varepsilon_{A2}) - (d \tan \varepsilon_{B1} + d_m \tan \varepsilon_{B2}) \quad (\text{A.7})$$

from which one obtains

$$x_o = \frac{\tan \varepsilon_{A1} - \tan \varepsilon_{B1}}{\tan \varepsilon_{A0} - \tan \varepsilon_{B0}} d + \frac{\tan \varepsilon_{A2} - \tan \varepsilon_{B2}}{\tan \varepsilon_{A0} - \tan \varepsilon_{B0}} d_m \quad (\text{A.8})$$

This equation relates the actual and virtual intersection points of two laser beams which lie in the meridian plane

A.2 Laser Beams in the Sagittal Plane

The two laser beams in the sagittal plane will be considered according to Fig. A.3. The virtual intersection point of two laser beams is again given by o and located at x_o . Obviously both laser beams propagate in the medium 1 and 2 in other two-dimensional planes than that in medium 0. The optical axis lies in the x - y plane and is inclined by φ_{LDA} . Two laser beams are denoted by C and D, respectively. Because of the symmetry condition only the beam C will be further considered.

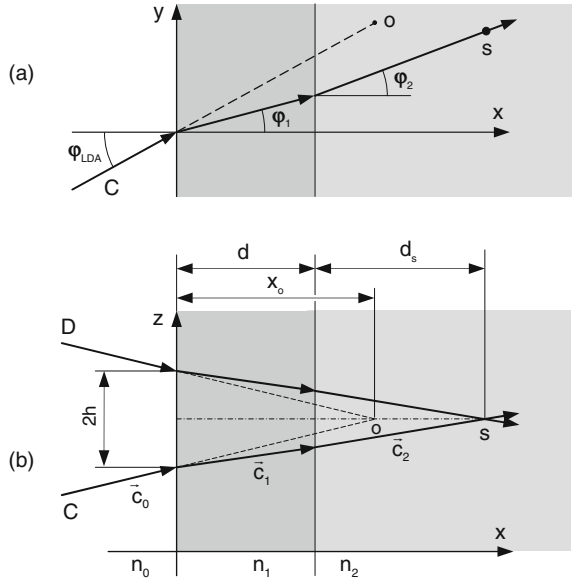
The laser beam C in the medium 0 is represented by the unit vector \vec{c}_0 . Because the projection of this unit vector on the optical axis in the x - y plane leads to $\cos \alpha_0$ and this in turn has its x - and y -components $\cos \alpha_0 \cos \varphi_{\text{LDA}}$ and $\cos \alpha_0 \sin \varphi_{\text{LDA}}$, respectively, the unit vector \vec{c}_0 is expressed by

$$\vec{c}_0 = (\cos \alpha_0 \cos \varphi_{\text{LDA}}, \cos \alpha_0 \sin \varphi_{\text{LDA}}, \sin \alpha_0) \quad (\text{A.9})$$

The projection of this unit vector in the x - z plane (Fig. A.3b) has a slope that is given by

$$\frac{c_{0z}}{c_{0x}} = \frac{\sin \alpha_0}{\cos \alpha_0 \cos \varphi_{\text{LDA}}} = \frac{\tan \alpha_0}{\cos \varphi_{\text{LDA}}} \quad (\text{A.10})$$

Fig. A.3 Propagation of two laser beams in the sagittal plane



According to Eqs. (3.8) and (3.9) the unit vector after the first refraction i.e. in the medium 1 is expressed as

$$\vec{c}_1 = \left(c_{1x}, \frac{n_0}{n_1} \cos \alpha_0 \sin \varphi_{LDA}, \frac{n_0}{n_1} \sin \alpha_0 \right) \quad (A.11)$$

Herein

$$c_{1x} = \sqrt{1 - c_{1y}^2 - c_{1z}^2} = \sqrt{1 - \frac{n_0^2}{n_1^2} (1 - \cos^2 \alpha_0 \cos^2 \varphi_{LDA})} \quad (A.12)$$

The projection of the unit vector \vec{c}_1 in the $x-z$ plane has a slope that is calculated as

$$\frac{c_{1z}}{c_{1x}} = \frac{n_0 \sin \alpha_0}{n_1 c_{1x}} \quad (A.13)$$

In a similar way, the unit vector after the second refraction i.e. in the medium 2 is expressed as

$$\vec{c}_2 = \left(c_{2x}, \frac{n_0}{n_2} \cos \alpha_0 \sin \varphi_{LDA}, \frac{n_0}{n_2} \sin \alpha_0 \right) \quad (A.14)$$

with

$$c_{2x} = \sqrt{1 - c_{2y}^2 - c_{2z}^2} = \sqrt{1 - \frac{n_0^2}{n_2^2} (1 - \cos^2 \alpha_0 \cos^2 \varphi_{LDA})} \quad (A.15)$$

The projection of the unit vector \vec{c}_2 in the $x-z$ plane exhibits a slope confirmed by

$$\frac{c_{2z}}{c_{2x}} = \frac{n_0 \sin \alpha_0}{n_2 c_{2x}} \quad (\text{A.16})$$

Two laser beams in the medium 2 intersect at point s which is located at d_s . In order to find out the relation between x_o and d_s , two intersection points of two laser beams on the first medium interface ($y-z$ plane) are considered. Half of the distance $2h$ between two intersection points can be calculated from either the virtual intersection point o or the actual point s , as given by

$$h = \frac{c_{0z}}{c_{0x}} x_o = \frac{c_{1z}}{c_{1x}} d + \frac{c_{2z}}{c_{2x}} d_s \quad (\text{A.17})$$

With respect to the slopes of respective unit vectors in the $x-z$ plane (Fig. A.3b), as calculated above, the following relationship can be found:

$$x_o = \left(\frac{n_0}{n_1} \frac{1}{c_{1x}} d + \frac{n_0}{n_2} \frac{1}{c_{2x}} d_s \right) \cos \alpha_0 \cos \varphi_{\text{LDA}} \quad (\text{A.18})$$

This equation relates the actual and virtual intersection point of two laser beams which lie in the sagittal plane.

A.3 Combination

Combining Eqs. (A.8) and (A.18) to eliminate x_o yields

$$\begin{aligned} & \frac{\tan \varepsilon_{A1} - \tan \varepsilon_{B1}}{\tan \varepsilon_{A0} - \tan \varepsilon_{B0}} d + \frac{\tan \varepsilon_{A2} - \tan \varepsilon_{B2}}{\tan \varepsilon_{A0} - \tan \varepsilon_{B0}} d_m \\ &= \left(\frac{n_0}{n_1} \frac{1}{c_{1x}} d + \frac{n_0}{n_2} \frac{1}{c_{2x}} d_s \right) \cos \alpha_0 \cos \varphi_{\text{LDA}} \end{aligned} \quad (\text{A.19})$$

With $d_m = d_s + \Delta x_{m,s}$ then the distance between the meridian and sagittal focal points $\Delta x_{m,s}$ (Fig. A.1) is resolved as

$$\Delta x_{m,s} = \frac{1}{T_{20}} (\Psi_1 d + \Psi_2 d_s) \quad (\text{A.20})$$

Herein

$$\Psi_1 = \frac{n_0}{n_1} \frac{1}{c_{1x}} \cos \alpha_0 \cos \varphi_{\text{LDA}} - T_{10} \quad (\text{A.21})$$

$$\Psi_2 = \frac{n_0}{n_2} \frac{1}{c_{2x}} \cos \alpha_0 \cos \varphi_{\text{LDA}} - T_{20} \quad (\text{A.22})$$

$$T_{10} = \frac{\tan \varepsilon_{A1} - \tan \varepsilon_{B1}}{\tan \varepsilon_{A0} - \tan \varepsilon_{B0}} \quad (\text{A.23})$$

$$T_{20} = \frac{\tan \varepsilon_{A2} - \tan \varepsilon_{B2}}{\tan \varepsilon_{A0} - \tan \varepsilon_{B0}} \quad (\text{A.24})$$

In these equations, all refraction angles (ε_{A1} , ε_{A2} , ε_{B1} , ε_{B2}) can be calculated from incident angles ε_{A0} and ε_{B0} in the form of $\varepsilon_{A0} = \varphi_{\text{LDA}} + \alpha_0$ and $\varepsilon_{B0} = \varphi_{\text{LDA}} - \alpha_0$ by applying the law of refraction. Both c_{1x} and c_{2x} can be determined from Eqs. (A.12) and (A.15), respectively.

A special case will be considered in that the flow medium to be measured is equal to the reference medium. Then because of $n_2 = n_0$ it yields from Eqs. (A.15) and (A.24)

$$c_{2x} = \cos \alpha_0 \cos \varphi_{\text{LDA}} \quad (\text{A.25})$$

$$T_{20} = 1 \quad (\text{A.26})$$

These values are inserted into Eq. (A.22), yielding

$$\psi_2 = 0 \quad (\text{A.27})$$

The distance between two measurement volumes, as given in Eq. (A.20), is then reduced to

$$\Delta x_{m,s} = \psi_1 d \quad (\text{A.28})$$

It is independent of the location of the measurement volume in the flow. This also means that the depth of the measurement volume in the flow does not contribute to the astigmatic difference.

Appendix B

Laser Beam Orientation Under the Effect of the Bias Angle δ

This appendix refers to [Sect. 14.9.1](#).

One reason that leads to inaccurate off-axis LDA alignment is confirmed by the off-axis alignment angle φ_{LDA} followed by the bias angle δ , at which the LDA head has turned around its own axis i.e. the optical axis. This type of imperfect off-axis LDA alignment indicates that the unit vector \vec{n} that represents the normal of the plane containing two laser beams (known as the optical plane) deviates from z-axis by δ (Fig. B.1). Thus the normal vector \vec{n} of the optical plane generally

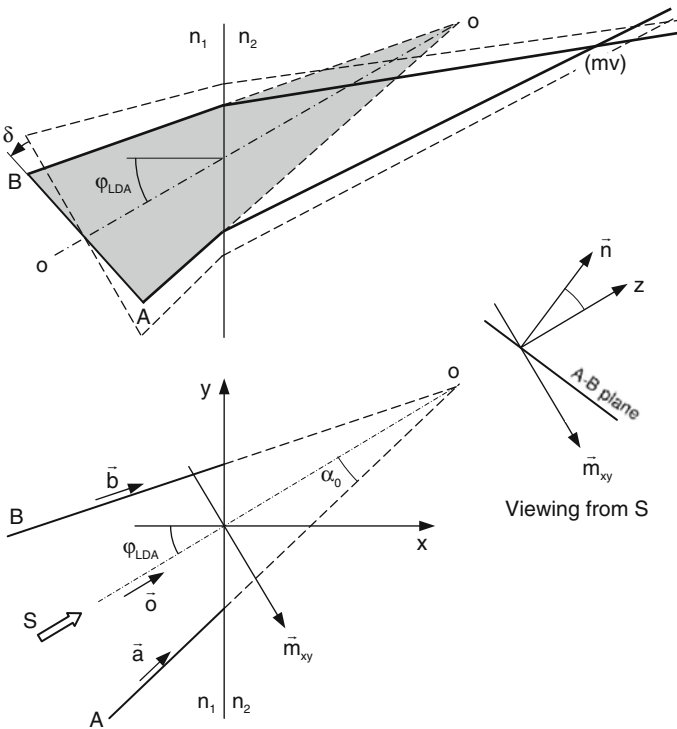


Fig. B.1 Laser beam orientation after rotating the LDA head by φ_{LDA} followed by the bias angle δ

has its spatial orientation. In order to determine the spatial direction of this normal vector, an auxiliary unit vector \vec{m}_{xy} is introduced which lies in the $x - y$ plane and is perpendicular to the optical axis. Because the optical axis is represented by $\vec{o} = (\cos \varphi_{LDA}, \sin \varphi_{LDA}, 0)$, it yields for the unit vector \vec{m}_{xy}

$$\vec{m}_{xy} = (\sin \varphi_{LDA}, -\cos \varphi_{LDA}, 0) \quad (\text{B.1})$$

Then, the following equations are used to derive the spatial direction of the normal vector \vec{n} :

$$\vec{n} \cdot \vec{z} = \cos \delta \quad (\text{B.2})$$

$$(\vec{n} \times \vec{m}_{xy}) \cdot \vec{z} = 0 \quad (\text{B.3})$$

In these equations, the z -axis has been considered as a unit vector $\vec{z} = (0, 0, 1)$. The triple product in Eq. (B.3) is zero because all three vectors lie in the same plane. From these two equations and with respect to $|\vec{n}| = 1$ the normal vector \vec{n} can be solved as

$$n_x = -\sin \varphi_{LDA} \sin \delta \quad (\text{B.4})$$

$$n_y = \cos \varphi_{LDA} \sin \delta \quad (\text{B.5})$$

$$n_z = \cos \delta \quad (\text{B.6})$$

In using these calculation results, the spatial orientations of both laser beams A and B can be calculated. According to Fig. B.1 following equations can be immediately obtained:

$$\vec{a} \cdot \vec{o} = \cos \alpha_0 \quad (\text{B.7})$$

$$\vec{b} \cdot \vec{o} = \cos \alpha_0 \quad (\text{B.8})$$

$$(\vec{a} \times \vec{o}) \cdot \vec{n} = \sin \alpha_0 \quad (\text{B.9})$$

$$(\vec{b} \times \vec{o}) \cdot \vec{n} = -\sin \alpha_0 \quad (\text{B.10})$$

Equations (B.9) and (B.10) are derived from the knowledge that the vectors in the respective parentheses have the magnitude of $\sin \alpha_0$ and the directions parallel to \vec{n} and $-\vec{n}$, respectively.

From Eqs. (B.7) and (B.9) it results for the laser beam A

$$a_x = \cos \varphi_{LDA} \cos \alpha_0 + \sin \varphi_{LDA} \sin \alpha_0 \cos \delta \quad (\text{B.11})$$

$$a_y = \sin \varphi_{LDA} \cos \alpha_0 - \cos \varphi_{LDA} \sin \alpha_0 \cos \delta \quad (\text{B.12})$$

$$a_z = \sin \alpha_0 \sin \delta \quad (\text{B.13})$$

Analogous to the related calculations one obtains from Eqs. (B.8) and (B.10) for the laser beam B:

$$b_x = \cos \varphi_{\text{LDA}} \cos \alpha_0 - \sin \varphi_{\text{LDA}} \sin \alpha_0 \cos \delta \quad (\text{B.14})$$

$$b_y = \sin \varphi_{\text{LDA}} \cos \alpha_0 + \cos \varphi_{\text{LDA}} \sin \alpha_0 \cos \delta \quad (\text{B.15})$$

$$b_z = -\sin \alpha_0 \sin \delta \quad (\text{B.16})$$

As can be seen, the bias angle $\delta \neq 0$ leads to $a_z \neq 0$ and $b_z \neq 0$. This means that both laser beams A and B, after refractions in the medium 2, do not lie in the same plane as in the medium 1. They will obviously propagate in different directions which indeed do not lie in a two-dimensional plane at all. Because of this, two laser beams will not intersect in the medium 2 to form the measurement volume. Corresponding calculations of using the above results have been performed in [Sect. 14.9.1](#).

Appendix C

Coordinate Transformation of the Reynolds Stress Matrix

In representing the flow velocities and the velocity fluctuations, the method of using coordinate transformation has often been applied. In [Chap. 6](#), transformations of both velocities and turbulence quantities in the two-dimensional $x - y$ plane have been presented. For reference purposes, as required for instance by [Sect. 17.4.2](#), the velocity transformation in three-dimensional orthogonal coordinate systems should be shown in this appendix.

According to [Fig. C.1](#), the Cartesian coordinate system is shown to represent the velocity vector \vec{u} with components u_x, u_y and u_z . This coordinate system is usually directly related to the flow system. Another orthogonal coordinate system is also drawn to represent the same velocity vector, however in components of u_1, u_2 and u_3 . The relative position between two coordinate systems is specified by angles α_i, β_i and γ_i . For instance, the coordinate axis for velocity component u_1 is given by angles α_1, β_1 and γ_1 in the $x - y - z$ coordinate system. The components of the velocity vector \vec{u} in both coordinate systems are related by (see also [Sect. 6.1.1](#))

$$\begin{bmatrix} u_1 \\ u_2 \\ u_3 \end{bmatrix} = \begin{bmatrix} \cos \alpha_1 & \cos \beta_1 & \cos \gamma_1 \\ \cos \alpha_2 & \cos \beta_2 & \cos \gamma_2 \\ \cos \alpha_3 & \cos \beta_3 & \cos \gamma_3 \end{bmatrix} \begin{bmatrix} u_x \\ u_y \\ u_z \end{bmatrix} = R \begin{bmatrix} u_x \\ u_y \\ u_z \end{bmatrix} \quad (C.1)$$

Herein R represents the orthogonal transformation matrix. As an orthogonal matrix its inverse is simply equal to its transpose, as given by $R^{-1} = R^t$.

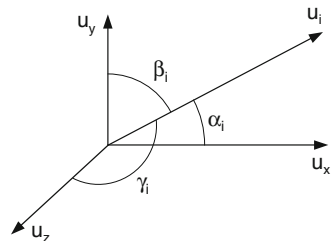


Fig. C.1 Relative position between two coordinate systems for velocity transformations

In order to transform the turbulent Reynolds stresses, the following matrix calculation is applied

$$\sigma_{mn} = R' \sigma_{ij} R \quad (\text{C.2})$$

that is in concrete form

$$\begin{bmatrix} \sigma_{xx} & \tau_{xy} & \tau_{xz} \\ \tau_{yx} & \sigma_{yy} & \tau_{yz} \\ \tau_{zx} & \tau_{zy} & \sigma_{zz} \end{bmatrix} = R' \begin{bmatrix} \sigma_{11} & \tau_{12} & \tau_{13} \\ \tau_{21} & \sigma_{22} & \tau_{23} \\ \tau_{31} & \tau_{32} & \sigma_{33} \end{bmatrix} R \quad (\text{C.3})$$

A special case will be considered in which the velocity component u_1 coincides with the main flow direction. Based on the zero correlation principle that has been presented in [Chap. 8](#) for conducting the Zero Correlation Method (ZCM), the main flow direction also corresponds to the orientation of the principal normal stress. Because all turbulent shear stresses vanish in the related coordinate system it remains

$$\sigma_{ij} = \begin{bmatrix} \sigma_{11} & 0 & 0 \\ 0 & \sigma_{22} & 0 \\ 0 & 0 & \sigma_{33} \end{bmatrix} \quad (\text{C.4})$$

Starting from this state of turbulent stresses, all turbulent stresses in the $x - y - z$ coordinate system are then calculated from Eq. (C.2) as follows:

$$\sigma_{xx} = \sigma_{11} \cos^2 \alpha_1 + \sigma_{22} \cos^2 \alpha_2 + \sigma_{33} \cos^2 \alpha_3 \quad (\text{C.5})$$

$$\sigma_{yy} = \sigma_{11} \cos^2 \beta_1 + \sigma_{22} \cos^2 \beta_2 + \sigma_{33} \cos^2 \beta_3 \quad (\text{C.6})$$

$$\sigma_{zz} = \sigma_{11} \cos^2 \gamma_1 + \sigma_{22} \cos^2 \gamma_2 + \sigma_{33} \cos^2 \gamma_3 \quad (\text{C.7})$$

$$\tau_{xy} = \sigma_{11} \cos \alpha_1 \cos \beta_1 + \sigma_{22} \cos \alpha_2 \cos \beta_2 + \sigma_{33} \cos \alpha_3 \cos \beta_3 \quad (\text{C.8})$$

$$\tau_{zy} = \sigma_{11} \cos \beta_1 \cos \gamma_1 + \sigma_{22} \cos \beta_2 \cos \gamma_2 + \sigma_{33} \cos \beta_3 \cos \gamma_3 \quad (\text{C.9})$$

$$\tau_{xz} = \sigma_{11} \cos \alpha_1 \cos \gamma_1 + \sigma_{22} \cos \alpha_2 \cos \gamma_2 + \sigma_{33} \cos \alpha_3 \cos \gamma_3 \quad (\text{C.10})$$

A further special case will be considered. It is assumed that in the plane perpendicular to the main flow direction, i.e. in the plane of velocity components u_2 and u_3 , isotropic turbulence is present. This simply means $\sigma_{22} = \sigma_{33}$. Then, with respect to $\cos^2 \alpha_1 + \cos^2 \alpha_2 + \cos^2 \alpha_3 = 1$ and the corresponding trigonometric identities for both the angle β and γ , one obtains

$$\sigma_{xx} = \sigma_{11} \cos^2 \alpha_1 + \sigma_{22} \sin^2 \alpha_1 \quad (\text{C.11})$$

$$\sigma_{yy} = \sigma_{11} \cos^2 \beta_1 + \sigma_{22} \sin^2 \beta_1 \quad (\text{C.12})$$

$$\sigma_{zz} = \sigma_{11} \cos^2 \gamma_1 + \sigma_{22} \sin^2 \gamma_1 \quad (\text{C.13})$$

$$\tau_{xy} = \sigma_{11} \cos \alpha_1 \cos \beta_1 + \sigma_{22} (\cos \alpha_2 \cos \beta_2 + \cos \alpha_3 \cos \beta_3) \quad (\text{C.14})$$

The last equation for τ_{xy} can be further simplified. Both the x - and the y -coordinate in the $x - y - z$ system will be represented by the respective unit vectors $\vec{x} = (\cos \alpha_1, \cos \alpha_2, \cos \alpha_3)$ and $\vec{y} = (\cos \beta_1, \cos \beta_2, \cos \beta_3)$ in the u_i -coordinate system. Because of $\vec{x} \perp \vec{y}$ there is $\vec{x} \cdot \vec{y} = 0$. This leads to

$$\cos \alpha_2 \cos \beta_2 + \cos \alpha_3 \cos \beta_3 = -\cos \alpha_1 \cos \beta_1 \quad (\text{C.15})$$

By substituting this expression into Eq. (C.14) it then follows

$$\tau_{xy} = (\sigma_{11} - \sigma_{22}) \cos \alpha_1 \cos \beta_1 \quad (\text{C.16})$$

This equation has been referred to in Sect. 17.4.2 by Eq. (17.42).

References

- Albrecht H, Borys M, Damaschke N, Tropea C (2003) Laser Doppler and phase Doppler measurement techniques. Springer, Berlin
- Boadway J, Karahan E (1981) Correction of laser Doppler anemometer readings for refraction at cylindrical interfaces. *DISA Inf* 26:4–6
- Booij R, Tukker J (1994) 3-Dimensional laser Doppler measurements in a curved flume. 7th int. Symposium on Applications of Laser Techniques to Fluid Mechanics, Lisbon, Portugal, p 28.5
- Bradshaw P (1978) Turbulence. Topics in applied physics, vol. 12. Springer, Berlin
- Buchhave P (1975) Biasing errors in individual particle measurements with the LDA-counter signal processor. The Accuracy of Flow Measurements by Laser Doppler Methods, Proceedings of the LDA-Symposium, Copenhagen, Denmark, pp 258–278
- Buchhave P, George WK, Lumley JL (1979) The measurement of turbulence with the laser-Doppler anemometer. *Ann Rev Fluid Mech* 11:443–503
- Carter J, Martin K, Campbell W, Hall N, Ezekoye O (2001) Design of an oscillating flow apparatus for the study of low Reynolds number particle dynamics. *J Exp Fluids* 30:578–583
- Durst F, Fischer M, Jovanovic J, Kikura H (1998) Methods to set up and investigate low Reynolds number, fully developed turbulent plane channel flows. *ASME J Fluid Eng* 120:496–503
- Durst F, Kikura H, Lekakis I, Jovanovic J, Ye Q (1996) Wall shear stress determination from near-wall mean velocity data in turbulent pipe and channel flows. *J Exp Fluids* 20:417–428
- Durst F, Martinuzzi R, Sender J, Thevenin D (1992) LDA-measurements of mean velocity, RMS-values and higher order moments of turbulence intensity fluctuations in flow fields with strong velocity gradients. 6th int. Symposium on Applications of Laser Techniques to Fluid Mechanics, Lisbon, Portugal, p 5.1
- Durst F, Melling A, Whitelaw JH (1981) Principles and practice of laser-Doppler anemometry. 2nd edn, Academic Press, London
- Durst F, Stevenson WH (1975): Moiré patterns to visually model laser-Doppler signals. The Accuracy of Flow Measurements by Laser Doppler Methods, Proceedings of the LDA-Symposium, Copenhagen, Denmark, pp 183–205
- Edwards RV (1987) Report of the special panel on statistical particle bias problems in laser anemometry. *Trans ASME, J Fluids Eng* 109:89–93
- Erdmann JC, Tropea C (1981) Turbulence induced statistical bias in laser anemometry. Proceedings of the 7th Symposium on Turbulence, University of Missouri-Rolla, USA
- Hanson S (1973) Broadening of the measured frequency spectrum in a differential laser anemometer due to interference plane gradients. *J Phys D Appl Phys* 6:164–171
- Hanson S (1975) Visualization of alignment errors and heterodyning constraints in laser Doppler velocimeters. The Accuracy of Flow Measurements by Laser Doppler Methods, Proceedings of the LDA-Symposium, Copenhagen, Denmark, pp 176–182
- Hecht E (1990) Optics. 2nd edn, Addison-Wesley, Reading, MA
- Hinze JO (1975) Turbulence. 2nd edn, McGraw-Hill, New York, NY

- Hirt F, Jud E, Zhang Zh (1994) Investigation of the local flow topology in the vicinity of a prosthetic heart valve using particle image velocimetry. 7th. Int. Symposium on Applications of Laser Techniques to Fluid Mechanics, Lisbon, Portugal, p 37.3
- Hüttmann F, Leder A, Michael M, Majohr D (2007) Wechselwirkungen runder Düsenfreistrahlen mit ebenen Wänden bei verschiedenen Auftreffwinkeln. 15. GALA-Fachtagung, Lasermethoden in der Strömungsmesstechnik, Rostock, Deutschland, pp 7.1–7.6
- Jakoby R, Willmann M, Kim S, Dullenkopf K, Wittig S (1996) LDA-Messungen in rotierenden Bezugssystemen: Einfluss von Geschwindigkeitsgradienten auf die Bestimmung des Turbulenzgrads. 5. GALA-Fachtagung, Berlin, Deutschland, pp 41.1–41.10
- Lehmann B (1986) Laser-Doppler-Messungen in einem turbulenten Freistrahle. DFVLR Forschungsbericht, DFVLR-FB 86–55
- Li EB, Tieu AK (1998) Analysis of the three-dimensional fringe patterns formed by the interference of ideal and astigmatic Gaussian beams. 9th int. Symposium on Applications of Laser Techniques to Fluid Mechanics, Lisbon, Portugal, p 15.5
- Lumley J, Acrivos A, Leal L, Leibovich S (1996) Research trends in fluid dynamics. American Institute of Physics, Woodbury, New York, NY
- McLaughlin DK, Tiederman WG (1973) Biasing correction for individual realization of laser anemometer measurements in turbulent flows. *Phys Fluids* 16(12):2082–2088
- Miles PC, Witze PO (1994): Fringe field quantification in an LDA probe volume by use of a magnified image. *J Exp Fluids* 16:330–335
- Miles PC, Witze PO (1996): Evaluation of the Gaussian beam model for prediction of LDV fringe fields. 8th int. Symposium on Applications of Laser Techniques to Fluid Mechanics, Lisbon, Portugal, p 40.1
- Nobach H (1998) Verarbeitung stochastisch abgetasteter Signale – Anwendung in der Laser-Doppler-Anemometrie. Diss., Univ. Rostock, Shaker Verlag, Aachen
- Owen J, Rogers R (1975) Velocity biasing in laser Doppler anemometers. The Accuracy of Flow Measurements by Laser Doppler Methods, Proceedings of the LDA-Symposium, Copenhagen, Denmark, pp 89–114
- Richter F, Leder A (2006) Wechselwirkungen runder Düsenfreistrahlen mit ebenen Wänden. 14. GALA-Fachtagung, Lasermethoden in der Strömungsmesstechnik. Braunschweig, Deutschland, pp 13.1–13.7
- Ruck B. (1991) Distortion of LDA fringe pattern by tracer particles. *J Exp Fluids* 10:349–354
- Thiele B, Eckelmann H (1994) Application of a partly submerged two component laser-Doppler anemometer in a turbulent flow. *J Exp Fluids* 17:390–396
- Tropea C (1983) A note concerning the use of a one-component LDA to measure shear stress terms. Technical Notes, *J Exp Fluids* 1:209–210
- Wittig S, Elsässer A, Samenfink W, Ebner J, Dullenkopf K (1996) Velocity profiles in shear-driven liquid films: LDV-measurements. 8th Int. Symposium on Applications of Laser Techniques to Fluid Mechanics, Lisbon, Portugal, p 25.2
- Yeh H, Cummins H (1964) Localized flow measurements with an He-Ne laser spectrometer. *App Phys Lett* 4:176
- Zhang Zh (1995) Einfluss des Astigmatismus auf Laser Doppler Messungen. Sulzer Innotec Bericht, Nr. STT. TB95.022, Winterthur, Schweiz
- Zhang Zh (1999) Null-Korrelationsmethode zur Bestimmung der anisotropen Strömungsturbulenz. Lasermethoden in der Strömungsmesstechnik. 7. GALA-Fachtagung, Lasermethoden in der Strömungsmesstechnik, St-Louis, Frankreich, pp 7.1–7.6
- Zhang Zh (2000) Zur Bestimmung des “Biasing Error” in LDA-Messungen von komplexen turbulenten Strömungen. 8. GALA-Fachtagung, Lasermethoden in der Strömungsmesstechnik, Freising/München, Deutschland, pp 16.1–16.8
- Zhang Zh (2002) Velocity bias in LDA measurements and its dependence on the flow turbulence. *J Flow Meas Instrum* 13:63–68
- Zhang Zh (2004a) Optical guidelines and signal quality for LDA applications in circular pipes. *J Exp Fluids* 37:29–39

- Zhang Zh (2004b) LDA-Methoden in Messungen aller drei Geschwindigkeitskomponenten in Rohrströmungen. 12. GALA-Fachtagung, Lasermethoden in der Strömungsmesstechnik, Karlsruhe, Deutschland, pp 8.1–8.8
- Zhang Zh (2005) Dual-Measurement-Method and its extension for accurately resolving the secondary flows in LDA applications. *J Flow Meas Instrum* 16:57–62
- Zhang Zh (2009) Freistrahlturbinen, Hydromechanik und Auslegung. Springer, Berlin
- Zhang Zh, Bissel C, Parkinson E (2003) LDA-Anwendung zu Freistrahlmessungen bei einem Pelton-Turbine-Modell mit der Fallhöhe von 90 Metern. 11. GALA-Fachtagung, Lasermethoden in der Strömungsmesstechnik, Braunschweig, Deutschland, pp 13.1–13.6
- Zhang Zh, Casey M (2007) Experimental studies of the jet of a Pelton turbine. *Proc. IMechE Vol. 221 Part A: J Power Energy*, 1181–1192
- Zhang Zh, Eisele K (1995a) Off-axis alignment of an LDA-probe and the effect of astigmatism on the measurements. *J Exp Fluids* 19:89–94
- Zhang Zh, Eisele K (1995b) Einfluss des Astigmatismus auf LDA-Messungen. 4. GALA-Fachtagung, Lasermethoden in der Strömungsmesstechnik, Rostock, Deutschland, pp 45.1–45.6
- Zhang Zh, Eisele K (1996a) Neue Erkenntnisse über den Einfluss des Astigmatismus auf LDA-Messungen. 5. GALA-Fachtagung, Lasermethoden in der Strömungsmesstechnik, Berlin, Deutschland, pp 54.1–54.7
- Zhang Zh, Eisele K (1996b) The effect of astigmatism due to beam refractions in the formation of the measurement volume in LDA measurements. *J Exp Fluids* 20:466–471
- Zhang Zh, Eisele K (1997) On the broadening of the flow turbulence due to fringe distortion in LDA measurement volumes. *Proceedings of the 7th Int. Conference Laser Anemometry, Advances and Applications*, Karlsruhe, Germany, pp 351–357
- Zhang Zh, Eisele K (1998a) On the directional dependence of turbulence properties in anisotropic turbulent flows. *J Exp Fluids* 24:77–82
- Zhang Zh, Eisele K (1998b) Further considerations of the astigmatism error associated with off-axis alignment of an LDA-probe. *J Exp Fluids* 24:83–89
- Zhang Zh, Eisele K (1998c) On the overestimation of the flow turbulence due to fringe distortion in LDA measurement volumes. *J Exp Fluids* 25:371–374
- Zhang Zh, Eisele K (1998d) Zur Bestimmung des “Biasing Error” bei LDA-Messungen. 6. GALA-Fachtagung, Lasermethoden in der Strömungsmesstechnik, Essen, Deutschland, pp 37.1–37.37.7
- Zhang Zh, Eisele K (1999) Mass flux measurements by PDA method. *Proceedings of the 8th Int. Conference Laser Anemometry, Advances and Applications*, Rome, Italy, pp 97–104
- Zhang Zh, Eisele K, Geppert L (2000a) Untersuchungen am Freistrahls aus einer Modeldüse von Pelton-Turbinen mittels LDA. 8. GALA-Fachtagung, Lasermethoden in der Strömungsmesstechnik, Freising/München, Deutschland, pp 15.1–15.6
- Zhang Zh, Eisele K, Hirt F (1996) Methode zur Bestimmung der Turbulenzgrößen in instationären Strömungen aus LDA-Messungen. 5. GALA-Fachtagung, Lasermethoden in der Strömungsmesstechnik, Berlin, Deutschland, pp 10.1–10.4
- Zhang Zh, Eisele K, Hirt F (1997) The influence of phase-averaging window size on the determination of turbulence quantities in unsteady turbulent flows. *J Exp Fluids* 22: 265–267
- Zhang Zh, Eisele K, Ziada S, Kälin R (1998) PDA measurements of water jet break-up in air cross-flow. *Proceedings of the 7th European Symposium Particle Characterisation*, Nürnberg, Germany, pp 131–140
- Zhang Zh, Muggli F, Parkinson E, Schärer C (2000b) Experimental investigation of a low head jet flow at a model nozzle of a Pelton turbine. 11th int. Seminar on Hydropower Plants, Vienna, Austria, pp 181–188
- Zhang Zh, Parkinson E (2001) Strömungsuntersuchungen am Freistrahls der Pelton-Turbine und Anpassen des LDA-Verfahrens. 9. GALA-Fachtagung, Lasermethoden in der Strömungsmesstechnik, Winterthur, Schweiz, pp 43.1–43.7

- Zhang Zh, Parkinson E (2002) LDA application and the dual-measurement-method in experimental investigations of the free surface jet at a model nozzle of a Pelton turbine. 11th. Int. Symposium on Applications of Laser Techniques to Fluid Mechanics, Lisbon, Portugal, p 2
- Zhang Zh, Zhang Ch (2002) Null-Korrelations-Methode und die Abweichungen in Turbulenzmessungen. 10. GALA-Fachtagung, Lasermethoden in der Strömungsmesstechnik, Rostock, Deutschland, pp 40.1–40.8
- Zhang Zh, Ziada S (2000) PDA measurements of droplet size and mass flux in the three-dimensional atomisation region of water jet in air cross-flow. *J Exp Fluids* 28:29–35

Index

A

- Added mass, 71, 73–76, 87–88
- Air bubbles in water, 88
- Angular bias, 229
- Apparent mean velocity, 221–223
- Apparent turbulence intensity, 134–140, 226
- Apparent turbulent stresses, 125, 131
- Astigmatic difference, 159–160, 167–168, 253
 - negative, 187–188
- Astigmatism, 5–6, 151, 159–171, 174–176, 178–179, 253
 - compensation, 186–189

B

- Beam separation, 179–186
- Beam waist, 36–40, 44–45
 - dislocation, 209, 212, 214, 217
 - thickness, 36, 38, 40, 44
- Beat frequency, 27–28
- Bernoulli equation, 72–73
- Bias angle, 97–98, 100–104, 106, 108, 110, 180–186
- Bias product, 232–233
- Bragg cell, 29, 32, 35, 41, 250
- Burst spectrum analyzer, 247

C

- Coma effect, 167
- Comatic aberration, 155–156, 167, 195
- Correlation coefficient, 120, 122–123, 128–129

D

- Detection volume, 40, 52
- Diffuser flow, 76–82
- Dispersion, 20, 149–150
- Doppler burst, 31–32
- Doppler effect, 22–24, 27
- Doppler frequency, 28–29, 31–33
- Drag coefficient, 70–71

- Drag force, 69–76, 79, 86–88
- Dual measurement method (DMM), 97–111

E

- Ellipse form of the turbulence distribution, 65–66
- Energy flux, 139–140, 142
 - correction factor, 139–140
- Ergodic hypothesis, 229
- Euler momentum equation, 246

F

- Flatness, 50–51
- Fringe distortion, 4–6, 211, 213–215, 217, 219–226
- Fringe distortion number, 214, 221–223, 225
- Fringe model, 29–31, 33
- Fringe number, 39, 45
- Fringe shift speed, 33–35
- Fringe spacing, 31, 35, 39–40, 44–45

G

- Gaussian beam, 35–38
 - divergence angle, 37–38
- Gaussian probability density function, 12–13, 49

I

- Isotropic and anisotropic turbulences, 13–15

J

- Jet flow, 97–103, 243–247

K

- Kurtosis factor, 51

L

- Linear least squares fitting, 119–123, 127–130

M

- Measurement volume, 27–29, 31–33, 35–36, 39–41, 43–45
 - available, 162
 - length, 40, 44–45
 - size, 39–40, 44
 - thickness, 39–40, 44–45
- Meridian focal points, 168, 172, 174
- Michelson-Morley experiment, 98, 251
- Modulation frequency, 25–26, 28
- Modulation wavenumber, 26
- Mohr's stress circle, 60, 66–67
- Momentum flow rate, 138, 142, 229–231
- Momentum flux, 138–139, 142, 228–231
 - correction factor, 139, 142, 229–231

N

- Non-orthogonal transformation, 61–65
- Nozzle flow, 77–80

O

- Optical chopper, 249, 251
- Oscillation flow model, 85

P

- Particle motion equation, 69–88
- Phase Doppler Anemometry (PDA), 40, 113, 185–186
- Photodetector, 28–29, 41–42
- Photomultiplier tubes, 27
- Plane of incidence, 20–21
- Potential flow, 73–74, 245–246
- Pressure force, 69–74, 76, 82, 87–88
- Principal normal stresses, 16, 56–57, 60–61
- Probability density function, 12–13, 48–49, 140–141, 143
 - biased, 230–233, 240

R

- Rayleigh length, 36–38, 44, 221, 223
- Receiving unit, 33, 41–43
- Reference medium, 161–163, 187–189
- Refraction, 19–21
 - law of refraction, 20–21
- Refractive index, 20
- Relaxation time, 75–77, 80, 84, 87
- Reynolds equations, 15–16
- Reynolds stress, 15–17
 - matrix, 16–17, 240–241, 263–264

- normal, 15

- shear, 16, 153

- Root mean square, 48–49, 66, 130
- Rotary encoder, 127

S

- Sagittal focal point, 159, 163, 167–168, 170, 172, 174
- Shift frequency, 33–35, 249–251
- Signal to noise ratio (SNR), 247
- Skewness, 50
- Special theory of relativity, 22–23
- Standard deviation, 12–14, 16, 48–51
- Stokes drag force, *see* Drag force
- Stokes law, 70–71
- Stokes number, 83–88
- Streamline curvature, 69–70, 245–246
- Superposition of two light waves, 24–25, 27

T

- Time-between-data, 248
- Table-top experiment, 195–196
- Total reflection, 203, 209
- Transformation matrix, 54, 63, 263
- Transit time, 52, 228
- Transmitter, 41–42
- Turbulence intensity, 14, 17, 49
- Turbulent kinetic energy, 16–17, 51
- Turbulent stresses, *see* Reynolds stress
- Two-step method, 98, 251

V

- Velocity bias, 47–49, 51–52, 135, 138–145, 227–241
- Velocity shift (DMM), 101–106, 108–110
- Viscous drag force, *see* Drag force
- Volumetric flow rate, 228
- Volumetric flux, 52, 138–139, 228–231

W

- Water-filled prism, 179, 186–189
- Wavenumber, 19–20, 26, 29–30
- Weaving machine, 247–249
- Weighting factor, 51–52, 120, 228

Z

- Zero correlation method (ZCM), 7–8, 64, 89–96, 153